



HAL
open science

Biosenseurs reposant sur l'AMPK et le FRET pour l'analyse du métabolisme énergétique: AMPFret

Martin Pelosse

► **To cite this version:**

Martin Pelosse. Biosenseurs reposant sur l'AMPK et le FRET pour l'analyse du métabolisme énergétique: AMPFret. Biologie cellulaire. Université Grenoble Alpes, 2015. Français. NNT: 2015GREAV057. tel-01686340

HAL Id: tel-01686340

<https://theses.hal.science/tel-01686340>

Submitted on 17 Jan 2018

HAL is a multi-disciplinary open access archive for the deposit and dissemination of scientific research documents, whether they are published or not. The documents may come from teaching and research institutions in France or abroad, or from public or private research centers.

L'archive ouverte pluridisciplinaire **HAL**, est destinée au dépôt et à la diffusion de documents scientifiques de niveau recherche, publiés ou non, émanant des établissements d'enseignement et de recherche français ou étrangers, des laboratoires publics ou privés.

UNIVERSITÉ DE GRENOBLE



THÈSE

Pour obtenir le grade de

DOCTEUR DE L'UNIVERSITÉ DE GRENOBLE

Spécialité : **Biologie Moléculaire & Cellulaire**

Arrêté ministériel : 7 août 2006

Présentée par

Martin PELOSSE

Thèse dirigée par **Prof. Uwe SCHLATTNER**

Thèse préparée au sein du
Laboratoire de Bioénergétique Fondamentale et Appliquée
dans l'**École Doctorale de Chimie et Sciences du Vivant**

AMPK- and FRET-based biosensors for energy metabolism: AMPfret

Thèse soutenue publiquement le **19 juin 2015**,

Devant le jury composé de :

Benoit VIOLLET	Examineur, Président
Directeur de recherche, Institut Cochin, Paris, France	
Pascual SANZ	Rapporteur
Professeur, Instituto de Biomedicina de Valencia (CSIC), Valence Espagne	
Theo WALLIMANN	Rapporteur
Professeur émérite, ETH Zürich, Zürich, Suisse	

Uwe SCHLATTNER	Directeur de thèse
Professeur, Université Joseph Fourier, Grenoble, France	

Imre BERGER	Co-encadrant
Professeur, EMBL, Grenoble, France, and University of Bristol, Bristol, UK	



Acknowledgements

Avant d'aborder le travail scientifique qui fait l'objet de mon doctorat, je voudrais remercier ceux qui ont participé, de prêt ou de loin, à sa maturation.

Je tiens tout d'abord à remercier Uwe Schlattner pour son accompagnement, sa confiance, la pertinence de ses conseils et la liberté qu'il m'a accordée tout au long de mon travail.

Aussi, je tiens tout particulièrement à remercier Imre Berger pour m'avoir accueilli au sein de son équipe. C'est aussi grâce à sa collaboration que les résultats présents dans ce manuscrit ont pu être obtenus.

Mes remerciements vont également aux membres du jury, Pascual Sanz, Theo Wallimann ainsi que Benoit Viollet pour avoir donné de leur temps et de leurs compétences afin de juger ce travail.

Ces années passées au sein de deux laboratoires aux thématiques différentes m'ont permis d'élargir mon horizon scientifique. Cela n'aurait pu être possible sans le soutien et l'affection de mes proches.

Pour leur savoir et leur appui, Merci à: Sarah, Matthias, Clovis, Yan, Simon, Rafaela, Kapil, Arthur, Adeline, Etienne, Fred G., Fred L., Maxime, Camille, Charline, Fayçal, Isai, Mathieu, Hervé, Aurélien, Christoph, Céline, Marine, Denis, Stéphane, Ottilie, Deepak, Guillaume, Evangelia, Marie, Petra, Alice, Lahari, Malgorzata, Christiane, Cristina, Jelger, Catarina, Philippe, Amédé, Gerard, Tanya, Qiyang, Sarah, Taiana, Itxaso, Régis, Laurence, Pietro, Karine, Emily, Mani, Cécile, Adam, Éric, Damien, Sylvie, Benoit, Cléo, Rémi, Julien, Romain, Léna, Hugo, Barbara, Flora, Sylvain, Pascale, Cyrille, Laurent, Basile, Momo, Gilles, Nicolas, Justine, Perrine, Aurore, Julien, Emma, Angéline, Nicolas, Marlène, Jacky, Valentine, Benjamin, Jonathan, Lulu, Karine, Alexandre, Jérôme, Louise, Béline, Vincent, Mahrez, Charly, Jonathan, Sarah, Mélanie, Clémentine, Romane, Isabelle, Coline, Adrien, Aymeric, Camille etc...

Je tiens à associer à ces remerciements la Région Rhône-Alpes pour le financement de mon doctorat.

Je ne pourrais finir sans remercier Laura, pour son amour qui m'accompagne chaque jour.

Abstract. AMP-activated protein kinase (AMPK) is a heterotrimeric protein complex (130kDa), conserved from yeast to plants and mammals, and functions as a central signaling hub and master regulator of energy metabolism and beyond. AMPK emerged as a suitable target to develop novel drugs for various metabolic pathologies (e.g. type II diabetes). Once activated AMPK restores the energy homeostasis, among others by down-regulating ATP-demanding pathways (anabolism) and up-regulating ATP-producing ones (catabolism). *In vivo*, the AMPK activity is finely regulated by incompletely understood complex mechanisms. First, AMPK activity is systemically modulated via activating phosphorylation at the α -subunit which is increased upon AMP and ADP binding to the γ -subunit. Second, AMPK is allosterically activated by AMP binding to the γ -subunit when the ATP/AMP ratio is falling. All these mechanisms require close communication between the γ - and α subunits, but a complete consensus model for AMPK activation is still lacking. We and others have proposed an AMP-induced conformational switch within the full-length heterotrimeric AMPK complex based on different, complementary structural studies. In this work, we have exploited the conformational switch for designing and engineering an AMPK complex that allows a direct, real-time readout of the AMPK conformational state by fluorescence resonance energy transfer (FRET). A definite bottleneck is engineering and expression of such multiprotein complexes, which could be achieved by using site-specific and homologous recombination techniques within the ACEMBL technology. From an array of engineered constructs, those with AMP-sensitive FRET changes were selected and named AMPfret. The sensor can report conformational changes within the AMPK heterotrimer, independent of its phosphorylation state, that are induced by AMP or ADP binding, and the monitored FRET signal correlates with AMPK allosteric activation or protection of AMPK dephosphorylation, respectively. AMPfret responds to physiologically low, micromolar concentrations of AMP and ADP, provides final proof for the exclusive ability of ATP, but not Mg-ATP, to compete with AMP for binding to the γ -subunit, and allows novel insight into the role of CBS domains for allosteric AMPK activation. Proof of principle experiments are provided for using AMPfret as a tool for AMPK-targeted drug screening and for reporting the intracellular energy state.

Résumé. La protéine kinase activée par AMP (AMPK) est un complexe hétérotrimérique (130kDa), ubiquitaire chez les eucaryotes, fonctionnant comme un hub central de la signalisation cellulaire et un régulateur du métabolisme énergétique et au-delà. L'AMPK émerge comme étant une cible de choix pour développer de nouveaux médicaments contre de nombreuses maladies métaboliques (ex: diabète de type 2). Une fois activée, l'AMPK va restaurer l'homéostasie énergétique, notamment en diminuant le métabolisme demandeur d'ATP (anabolisme) et en stimulant le métabolisme produisant l'ATP (catabolisme). *In vivo*, l'activité de l'AMPK est finement régulée par des mécanismes complexes encore partiellement inconnus. Premièrement, l'activité de l'AMPK est modulée de manière systémique par phosphorylation de la sous unité α , elle-même augmentée par l'attachement d'AMP et d'ADP à la sous unité γ . Deuxièmement, l'AMPK est activée de manière allostérique par liaison de l'AMP à la sous unité γ lors de chutes du ratio ATP/AMP. Tous ces mécanismes requièrent une communication étroite entre les sous unités α et γ , mais un modèle consensus complet de l'activation de l'AMPK est toujours manquant. Se basant sur différentes études structurales, d'autres et nous-mêmes avons proposé un changement de conformation induit par AMP au sein de l'hétérotrimère AMPK. Lors de ce travail, nous avons exploité ces changements conformationnels pour imaginer et créer un hétérotrimère d'AMPK permettant de suivre directement et en temps réel l'état de conformation de l'AMPK par FRET. La création et la production de tels complexes multi protéiques sont de réelles difficultés, qui ont pu être réalisées par l'utilisation de la technologie ACEMBL qui exploite notamment, des techniques de recombinaisons homologues. A partir d'un éventail de constructions, celles présentant des changements de FRET induit par AMP ont été sélectionnées et renommées AMPfret. Indépendamment de son degré de phosphorylation, le senseur a la propriété de rapporter les changements de conformation de l'AMPK étant induits par l'AMP ou l'ADP et ces changements de signal FRET corrélerent respectivement avec l'activation allostérique de l'AMPK ou sa protection contre la dephosphorylation. Le senseur répond à des concentrations physiologiques en AMP et ADP (micromolaire) et a finalement démontré la capacité exclusive qu'a l'ATP, et non l'ATP-Mg, à concurrencer l'AMP. De plus, son utilisation a permis une meilleure compréhension du rôle des sites CBS lors de l'activation allostérique. Des preuves qu'AMPfret peut aussi être considéré comme un outil de choix pour le criblage de molécules ciblant l'AMPK, et pour le monitoring de l'état énergétique intracellulaire sont aussi présentées.

Table of contents

• Introduction 1: AMP-activated protein kinase: a metabolic stress sensor	3
• Introduction 2: Genetically encoded fluorescent biosensors to explore energy metabolism in single cells in space and time	3
• Materials and Methods	93
• Aim of the work	127
• Results	129
• Discussion	219
• Annexes	243
• Abbreviations	261
• Side project	263

Introduction 1

AMP-activated protein kinase: a metabolic stress sensor

1.	Evolving physiological roles.....	6
2.	Molecular structure	7
3.	Localization	10
4.	Activation.....	13
5.	Regulation	25
6.	Pharmacological activation	29
7.	References.....	33

Abstract. AMP-activated protein kinase (AMPK) is a central cellular signaling hub that senses and responds to different kinds of stress, mainly those triggered by impaired cellular energy homeostasis. Since this is of major importance for the whole organism functioning, the kinase plays important roles in human health and disease. Here we review recent progress on the molecular structure and roles of AMPK, and summarize regulation and biological actions of the AMPK pathway. Activation of the kinase is involved in many metabolic diseases such as type 2 diabetes and metabolic syndrome. Pharmacological activation of AMPK may prove to be a useful therapeutic strategy in the treatment of these pathologies.

Résumé. La protéine kinase activée par AMP (AMPK) constitue un hub central de la signalisation cellulaire qui détecte et répond à différents types de stress, et plus particulièrement ceux induits par un dérèglement de l'homéostasie énergétique cellulaire. Cette dernière étant d'une importance cruciale pour le bon fonctionnement d'un organisme vivant, l'AMPK tient une place importante aux vues de la santé et des pathologies humaines. Dans ce chapitre, sont présentés les récentes données concernant la structure moléculaire de l'AMPK ainsi que son rôle; sont aussi résumés la régulation et les actions biologiques des voies de signalisation liées à l'AMPK. L'activation de la kinase est impliquée dans de nombreuses pathologies métaboliques comme le diabète de type 2 et le syndrome métabolique. L'activation pharmacologique de l'AMPK s'inscrit comme une stratégie prometteuse dans le traitement de ces pathologies.

Parts of this review have been published in part in:

Ehler, Elisabeth (Ed.) Cardiac Cytoarchitecture - How to Maintain a Working Heart. Springer (Heidelberg), 2015, pp 187-225. ISBN 978-3-319-15262-2.

AMP-Activated Protein Kinase: A Metabolic Stress Sensor in the Heart. Martin Pelosse, Malgorzata Tokarska-Schlattner, Uwe Schlattner.

Aon, Miguel A., Saks, Valdur, Schlattner, Uwe (Eds.) Systems Biology of Metabolic and Signaling Networks - Energy, Mass and Information Transfer. Series: Springer Series in Biophysics, Vol. 16. Springer (Heidelberg), 2013, pp 261-320. ISBN 978-3-642-38505-6.

Systems Level Regulation of Cardiac Energy Fluxes Via Metabolic Cycles: Role of Creatine, Phosphotransfer Pathways, and AMPK Signaling. Valdur Saks, Uwe Schlattner, Malgorzata Tokarska-Schlattner, Theo Wallimann, Rafaela Bagur, Sarah Zorman, Martin Pelosse, Pierre Dos Santos, François Boucher, Tuuli Kaambre, Rita Guzun.

A living organism is an energy-requiring system and it needs a perfect match of energy supply with energy demand to maintain its continuous being. The most relevant protein kinase in the context of metabolic stability and energy homeostasis is the AMP-activated protein kinase (AMPK). Many studies have confirmed the importance of AMPK signaling for a correct energy metabolism functioning (reviewed in (Hardie et al., 2012a; Arad et al., 2007; Dyck and Lopaschuk, 2006; Kim et al., 2009; Young, 2008; Zaha and Young, 2012)).

AMPK can be characterized as gatekeeper of cellular energy homeostasis and key regulator of energy metabolism, since it plays a central role in sensing and regulating energy state at the cellular, organ and whole-body level (Winder and Hardie, 1999; Hardie and Carling, 1997). It is an evolutionary conserved and ubiquitously expressed protein kinase (Hardie, 2007; Hardie, 2011) which is thought to have evolved as one of the first kinase signaling pathways in unicellular eukaryotes in response to starvation for a carbon source. It only later during evolution developed into a more general metabolic and energy stress sensor (Hardie, 2011; Hardie and Ashford, 2014; Hardie, 2014b).

Activation of AMPK is triggered by a diverse array of signals linked to limited energy availability in physiological and pathological situations, including extracellular (e.g. hormones, cytokines, nutrients) and intracellular stimuli (e.g. AMP, ADP, Ca^{2+}) (Hardie et al., 2012b). AMPK activation occurs in the context of metabolic stress that decreases ATP and increases intracellular AMP, ADP or Ca^{2+} concentrations. These include nutrient starvation, hypoxia (Hardie et al., 1999; Marsin et al., 2002), metabolic poisons (e.g. that inhibiting mitochondrial ATP production), or muscle contraction (Winder and Hardie, 1996). AMPK activation involves covalent phosphorylation and allosteric effects of AMP, ADP, and possibly other metabolites (Calabrese et al., 2014). Generally, these activation mechanisms cooperate in a very complex manner, even though new findings suggest they may also occur independently (Scott et al., 2014). They are coordinated to activate AMPK in situations of energy deficit and aim at compensating ATP loss, mostly via accelerated catabolism and inhibited anabolism. However, AMPK exerts pleiotropic control not only of metabolic pathways but also of other physiological functions more indirectly linked to cell energetics. These include cell growth, proliferation, shape and motility of cells, autophagy and apoptosis, and even central, systemic control of appetite in the hypothalamus (reviewed in (Steinberg and Kemp, 2009)). In all these cases, AMPK mediates fast (acute) effects by

regulating the activity of metabolic key enzymes and others, and slow (chronic) effects by tuning gene expression of these proteins. The downstream targets of AMPK have made this kinase also a prime pharmacological target for treating type II diabetes, cancer, and other pathologies (Hardie, 2008a); Zhang et al., 2009; Inoki et al., 2012; Srivastava et al., 2012).

It is to note that the majority of our knowledge on AMPK comes from various organs a cell type, and part of it may not be applicable to all situations. For example, this may concern the nature of activating stimuli and/or the threshold of activation (Zaha and Young, 2012), especially in the heart which is a quite unique organ in several aspects, in particular in the context of its energy metabolism characterized by an unusual stability. Depending on the considered organ, energy homeostasis is maintained by multiple regulatory mechanisms having various influence and controlling cellular ATP production, utilization and transfer, including allosteric regulations and feedback loops, micro-compartmentation, and metabolic channeling with concerted action of several metabolic and signaling kinases (Neumann et al., 2007; Saks et al., 2006). Globally AMPK functions as a metabolic master regulator, orchestrating the response to various stress-related stimuli. Importantly, pharmacological activation of AMPK also holds promise as a therapeutic strategy for treating different metabolic diseases (Calvert et al., 2008; Sasaki et al., 2009; Shinmura et al., 2007).

Here we briefly review AMPK structure, the way the kinase is activated, the regulated metabolic pathways and cellular functions, as well as available AMPK-targeted drugs. For any more extensive information on these or other issues of AMPK signaling, the reader is referred to the many excellent general reviews (Hardie, 2014; Hardie et al., 2012a; Mihaylova and Shaw, 2011; Hardie, 2014a, 2014c; Steinberg and Kemp, 2009).

1. Evolving physiological roles

AMP-activated protein kinase (AMPK) was first described in studies on the regulation of lipid metabolism, where an enzyme activity was identified that is responsible for phosphorylation and inhibition of acetyl-CoA carboxylase (ACC) and 3-hydroxy-3-methylglutaryl-CoA reductase (HMG-CoA reductase, HMGR) (Beg et al., 1980), and which was activated by AMP

(Ferrer et al., 1985). Since both phosphorylations are inhibitory, AMPK was first perceived as a down-regulator of lipid synthesis.

However, it then became evident that AMPK more generally functions as a cellular “fuel gauge” and can regulate many metabolic processes related to the cellular energy state. With the discovery that both AMP and ADP are activators (Oakhill et al., 2011; Xiao et al., 2011), AMPK regulation became quite similar to what has been described already 50 years ago by Atkinson as the so-called energy charge regulation of cell metabolism (Atkinson, 1968). In fact, AMPK is able to respond to low energy charge by reorganizing energy and metabolic fluxes towards a non-stressed state. It thus represents a true control point for maintaining energy and metabolic homeostasis.

The role of AMPK has been even further extended, with AMPK activity also depending on physiological stimuli independent of the cellular energy charge like hormones and nutrients (Minokoshi et al., 2002; Minokoshi et al., 2004). As mentioned above, more recently identified AMPK substrates reveal that AMPK signaling acts far beyond the control of primary metabolism, as e.g. in proliferation, autophagy and central appetite control. Thus, AMPK can now be defined as a “metabolic sensor” or “metabolic master switch”. However, also in these cases, AMPK signaling somehow acts to prevent a low energy state of cells, tissues or the entire organism, by preventing ATP-consuming processes (growth, motility), or favoring potentially ATP-generating processes (autophagy, appetite).

2. Molecular structure

The AMPK family consists of evolutionary conserved and ubiquitously expressed serine/threonine kinases that present complex structural and functional features. Structurally, AMPK occurs in vertebrates exclusively as an obligatory heterotrimeric protein complex composed of a catalytic subunit, α , and two regulatory subunits, β and γ . As a first layer of complexity, in vertebrates, each subunit occurs as different isoforms ($\alpha 1$, $\alpha 2$, $\beta 1$, $\beta 2$, $\gamma 1$, $\gamma 2$ and $\gamma 3$) encoded by distinct genes (Carling, 2004; Hardie et al., 2003), including some splice variants (of $\gamma 2$ and $\gamma 3$), generating a large variety of heterotrimeric complexes.

Alternative promoters can further increase this complexity (Kahn et al., 2005). The precise physiological significance of all these isoforms is not yet entirely clear.

Much has been learned about the molecular structure of AMPK by crystallographic studies on AMPK domains and heterotrimeric core complexes (carrying larger truncations) (Townley and Shapiro, 2007; Amodeo et al., 2007; Chen et al., 2009, 2012, 2013; Oakhill et al., 2011; Xiao et al., 2007, 2011, 2013a), and most of all by the most recently published structures of AMPK holo-complexes (Chen et al., 2009, 2012, 2013; Oakhill et al., 2011; Xiao et al., 2007, 2011, 2013a; Calabrese et al., 2014; Li et al., 2014). The so far most complete X-ray structure covers the entire α 2-subunit (with some internal truncations), the β 1-subunit (lacking only the flexible N-terminal portion), and the entire γ 1-subunit (Xiao et al., 2013) (Figure 1). This work, stimulated by a growing interest in AMPK as a putative drug target, revealed the overall topology of the heterotrimer, the conserved global fold of large parts of the subunits, and suggested putative activation mechanisms. However, a high resolution structure of full-length heterotrimeric complex in both active and inactive states is still lacking.

α -subunit. The α -subunit contains a typical Ser/Thr protein kinase catalytic domain in its N-terminal part, with features conserved throughout the entire protein kinase superfamily (Hanks et al., 1988). It harbors a typical activation loop carrying the critical Thr172 residue which is phosphorylated for activation by AMPK upstream kinases like liver kinase B1 (LKB1) or Ca^{2+} -calmodulin-dependent protein kinase kinase beta (CamKK β ; see chapter 4) (Hawley et al., 2003, 2005; Woods et al., 2003, 2005). This phosphorylation is considered as essential for AMPK activity (Hawley et al., 1996), although this has been recently challenged (Scott et al., 2014). Thr172 phosphorylation is also often used as a readout for AMPK activity, although this may not always be correct (see chapter 4). The C-terminal part of the α -subunit carries different and important functionalities. Immediately downstream of the catalytic domain follows the auto-inhibitory domain (AID) (Crute et al., 1998), which when fused to the kinase domain reduces AMPK activity as compared to kinase domain alone (Chen et al., 2009; Pang et al., 2007). In the further C-terminal sequence follows the so-called linker peptide, and finally the very C-terminal region (~150 amino acids) which is required for association with the β -subunit. The latter also contains a long Ser/Thr-rich loop (not resolved in X-ray structures), as well as a nuclear export sequence (known to be functional in α 2 (Kazgan et al., 2010)).

Of particular importance is the linker peptide, since it wraps around the γ -subunit like in a close embrace. A part of this linker peptide, first identified as α -hook, closely contacts γ -subunit (Xiao et al., 2011). Chen and colleagues (Chen et al., 2013) more recently corrected the amino acid register for the electron density in this region, revealing the true γ -interacting sequence termed α -regulatory subunit interacting motif (α -RIM), interacting with CBS site 3 (see below) and with a pocket formed by a newly observed β -subunit loop. More recent structures of the near full-length heterotrimers confirmed these interactions of α -linker with β - and γ -subunits (Xiao et al., 2013), and its role in moving AID away from the kinase domain in the activated state (Li et al., 2014). In addition to Thr172, the α -subunit can be phosphorylated on several other residues both *in vitro* and *in vivo*. Most of these phosphorylations occur in the Ser/Thr-rich loop and seem to inhibit the activating Thr172 phosphorylation (see chapter 4). Further structural studies will be necessary to delineate covalent and non-covalent activation of the kinase domain in molecular detail.

β -subunit. The regulatory β -subunit represents the core of the heterotrimeric complex, since it provides a scaffold for binding of catalytic α - and regulatory γ -subunits. The N-terminal domain of the β -subunit carries an additional regulatory element, the conserved carbohydrate binding module (CBM; also called glycogen binding domain, GBD). Its structure complexed to beta-cyclodextrin has been solved (Polekhina et al., 2005), and it was shown that glucose α 1-6-branched glycogen can behave as allosteric inhibitor, negatively regulating AMPK phosphorylation by its upstream kinases (McBride et al., 2009). In addition, CBM may serve to recruit AMPK to glycogen-bound downstream targets such as glycogen synthase (Hardie and Sakamoto, 2006). The recent near full-length AMPK structures confirmed that glycogen binding moves CBM away from the α -kinase domain, while binding of pharmacological activators 991 and A769662 and autophosphorylation of β -S108, both at the α/β -interface (see chapter 4), closely attach CBM to the kinase domain (Xiao et al., 2013; Li et al., 2014). The former conformation seems to be rather inhibitory, while the latter strongly activates AMPK. Thus, CBM is part of an allosteric regulatory site, which may also sense cellular energy reserves in the form of glycogen, and mediate effects of certain pharmacological activators. The large very N-terminal portion of the β -subunit is not resolved in the known X-ray structures, and its function is not entirely clear. An N-terminal myristoylation affects activation (Oakhill et al., 2010) and could mediate membrane

interaction. The sequence could also be involved in the interaction of AMPK with other proteins (Klaus et al., 2013).

γ -subunit. All γ -subunits contain in their C-terminal part four tandem cystathionine β -synthase (CBS) repeats, a motif named by analogy to the cystathionine β -synthase in which it was first identified (Bateman, 1997). In AMPK γ -subunits, the four CBS sites (numbered CBS 1 to CBS 4 according to their occurrence in the sequence) constitute a flattened disk with one CBS repeat in each quadrant, and two pairs of CBS motifs assembling into a so-called Bateman domain. Four potential binding sites for adenylates (AMP, ADP, ATP) are created in the cleft between the CBS motifs, numbered according to the CBS motif that provides the conserved Asp for adenine ribose interaction (Kemp, 2004). According to several crystal structures of the mammalian γ 1-subunit in presence of various nucleotides (Chen et al., 2012, 2013; Xiao et al., 2007, 2011, 2013a), it appears that only CBS sites 1, 3 and 4 are functional, while the site 2 is different and always empty. The γ 2- and γ 3-isoforms contain long N-terminal extensions, which can be subject to truncation by RNA splicing, and whose molecular structure and function are currently unknown. The different γ -subunits isoforms and splice variants may be involved in protein/protein interaction, and confer different cellular localization and function (Pinter et al., 2012).

3. Localization

Tissue-specificity. AMPK isoforms show some differences in their tissue- and developmental-specific expression patterns, although the physiological significance is still uncertain. There is no strict tissue specificity of AMPK isoforms, but increasing evidence suggests that a given tissue expresses a specific subset of AMPK heterotrimers which may be linked to particular signaling pathways in this tissue (Table 1). Studies with transgenic mice lacking specific α - and β -subunits have contributed to progress in this field (Viollet et al., 2009). While the α 1 β 1 γ 1 complex is probably the most abundant in a vast majority of cell types, differences seem to occur in the amount of additional isoforms in a given tissue. For example, the heart contains high levels of the α 2 isoform, which is much less expressed in skeletal muscle and liver, and almost absent in brain. The β 2 isoform is abundant in heart, in muscle and brain. In addition to the γ 1 isoform, heart expresses a specific intermediate length γ 2 splice variant

(γ 2-3B), while γ 3 seem to be quite specifically expressed only in skeletal muscle (Stapleton et al., 1996; Thornton et al., 1998; Pinter et al., 2012). There are also pathological and developmental changes in AMPK expression. The α 2, β 2, and γ 2 isoforms are all up-regulated by pressure overload or heart failure in rodents, although in patients rather the content of α 1, β 1, and γ 2 (an intermediate form) increases with different forms of cardiomyopathy (Tian et al., 2001, (Kim et al., 2012b). During embryonic development in rodents, γ 1 increases while high levels of γ 3 disappear, and the embryonically predominant full length γ 2 form is replaced by γ 2-3B in heart, but by short γ 2b in other tissues (Pinter et al., 2012). These developmental and tissue particularities may also explain why γ 2 gene mutations in the CBS domains cause hereditary hypertrophic cardiomyopathy but no other pathological symptoms (see chapter 6). Full length γ 2 and γ 2-3B share an N-terminal domain with unknown function that could localize the AMPK complex to specific compartments or signaling pathways (Pinter et al., 2012).. AMPK levels may also be determined by ubiquitin-dependent protein degradation (Qi et al., 2008; Moreno et al., 2010).

Table 1: Tissue expression of AMPK subunit isoforms

<i>Compound</i>	<i>Heart</i>	<i>Skeletal muscle</i>	<i>Brain</i>	<i>Liver</i>	<i>Lung</i>
Alpha 1	++	++	++	++	++
Alpha 2	+ ¹⁾	+		+	
Beta 1	++	+	++	++	+
Beta 2	++	++	++		+
Gamma 1	++	+	++	+	+
Gamma 2	+ ²⁾	+	+		
Gamma 3		+			

¹⁾ not present in cardiomyocytes ; ²⁾ specific splice variant (Pinter et al., 2012). Data from (Mahlpuu et al., 2004; Quentin et al., 2011; Stapleton et al., 1996; Thornton et al., 1998).

Subcellular distribution. The subcellular distribution and recruitment of AMPK isoforms to specific cellular sites is increasingly recognized as an important factor for their signaling function. AMPK is generally observed as a soluble complex with diffuse cytosolic localization. However, at least $\alpha 2$ -containing complexes in their activated form, e.g. after exercise in skeletal muscle, also translocate into the nucleus to phosphorylate nuclear substrates such as transcription factors, histones, and histone deacetylases (McGee et al., 2003; Suzuki et al., 2007; McGee et al., 2008). Minor portions of AMPK may associate with cellular structures like specific membranes, where processes are regulated by AMPK (e.g. ion channel activity, cell polarity, or cell junction formation) (Forcet and Billaud, 2007; Andersen and Rasmussen, 2012; Nakano and Takashima, 2012; Ramírez Ríos et al. 2014). Myristoylation of the AMPK β -subunit can localize the kinase complex to membranes and increases its activability, thus possibly favoring activation of membrane-bound complexes (Suzuki et al., 2007; Oakhill et al., 2010).

Multiprotein complexes. AMPK can also be recruited into specific complexes via interaction with its upstream kinases, downstream substrates, or more general with scaffolding proteins. However, the AMPK interactome is only partially known so far from some targeted and non-biased interaction studies conducted by us and others (e.g. (Behrends et al., 2010; Klaus et al., 2012)), and more research is needed on this issue. AMPK interaction with LKB1 could recruit AMPK to places of LKB1 localization, including the mitochondrial surface or E-cadherin in adherens junctions (Sebbagh et al., 2009). Close co-localization of both, AMPK and LKB1, can also be mediated by membrane interaction of both, farnesylated LKB1 and myristoylated AMPK (Houde et al., 2014).

Scaffolding proteins can in principle provide high specificity in cell signaling by isolating activated kinases from bulk signaling and directing the information flow into specific pathways. For example, mitochondrial VDAC may represent yet an anchoring protein that recruits AMPK to this organelle (Strogolova et al., 2012). Most interestingly, the scaffold protein axin together with the Ragulator complex at the lysosomal surface have been proposed as important regulators of AMPK activation (Zhang et al., 2014, 2013). These data support a model where axin bound to LKB1 recruits AMPK in the AMP-bound state, leading to AMPK phosphorylation and activation. Further, in particular under nutrient-poor conditions, the axin-LKB1-AMPK complex seems to interact with the Ragulator complex

which is tethered via its LAMTOR1 component to the lysosomal surface. The Ragulator complex, apparently by its interaction with the lysosomal v-type ATPase, seems to be an independent sensor of cellular nutrient conditions. It is known to recruit the nutrient-signaling TORC1 complex (see chapter 5) to lysosomes under nutrient-rich conditions (Bar-Peled and Sabatini, 2014), thus suggesting reciprocal recruitment and activation of axin-LKB1-AMPK or mTORC1, depending on the cellular nutrient state (Hardie, 2014a). It is currently unknown whether such regulation exists in all tissues.

There is also some evidence that AMPK subunit isoforms determine specific protein/protein interactions. The β -subunit may in some cases confer substrate specificity, as has been shown in yeast (Vincent and Carlson, 1999) and plants orthologs (Polge et al., 2008), but with mammalian AMPK (IntAct database (Kerrien et al., 2012)). We recently found the β 2-isoform interacting with Mu- and Pi-type glutathione transferases (GSTs) to favor glutathionylation of the α -subunit (Klaus et al., 2013). However, in case of fumarate hydratase (FH), we identified a specific interaction with α 2-containing AMPK complexes to facilitate FH phosphorylation (Klaus et al., 2012).

4. Activation

AMPK integrates various intra- and extracellular signals and maintains crosstalk with other signaling pathways. This makes the kinase a central signaling hub in sensing and regulating cellular energetics and ATP-dependent functions. Indeed, most recent research revealed that AMPK activation is much more complex than initially anticipated and that it depends on multiple covalent modifications and allosteric effectors (Figure 1). Such AMPK regulation evolved from a more simple state as e.g. in the yeast AMPK homologs that lack allosteric activation by AMP, to the more complex regulation present in vertebrates.

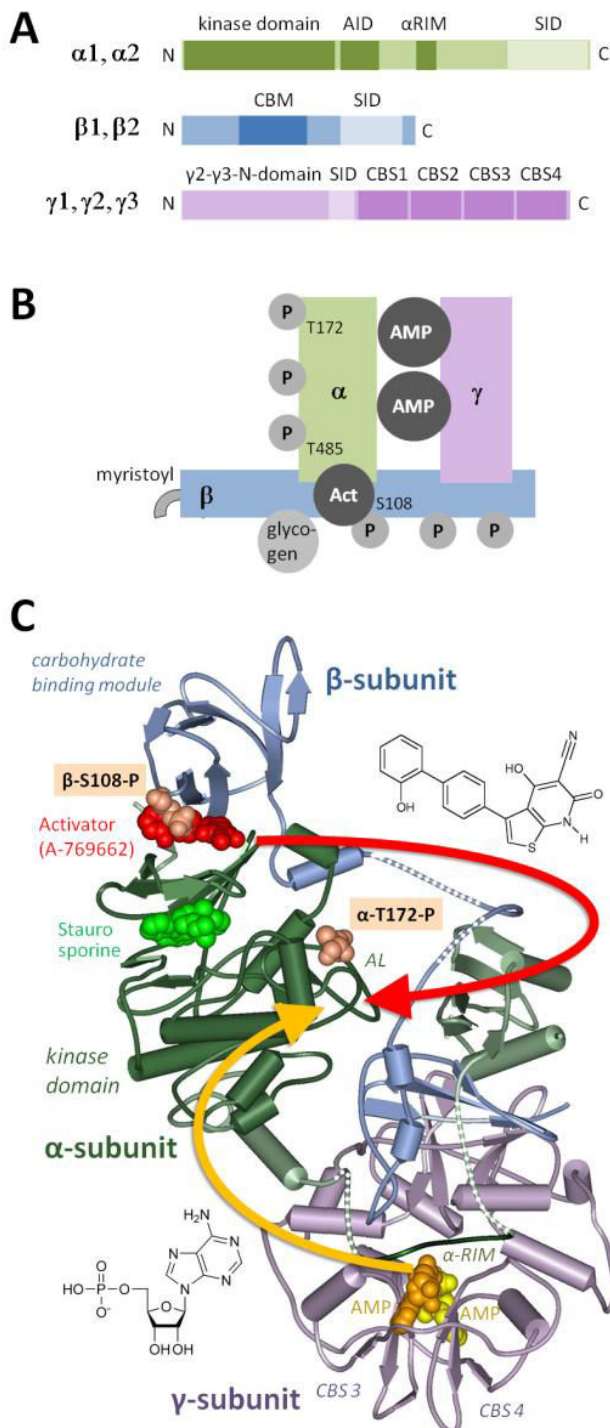


Figure 1: AMPK structure.

(A) AMPK domain structure of the three AMPK subunits (SID, subunit interaction domains; AID, autoinhibitory domain; CBM, carbohydrate binding module; CBS, cystathionine- β synthase). **(B)** AMPK complex topology. Subunit interactions, secondary modifications (phosphorylations; myristoylation), and allosteric interactors (AMP; Act, putative activator at α/β interface). **(C)** Molecular structure and activation of the full-length AMPK heterotrimer (PDB 1CFF; Xiao et al., 2013). Binding of activating AMPK ligands AMP (γ -subunit) and A-769662 (β -subunit) has to be transduced to the α -subunit kinase domain for activation (see arrows), involving conformational changes. AMPK subunits α (green), β (blue) and γ (magenta) with α -subunit kinase domain, activation loop (AL), and regulatory interacting motif (α RIM ; Chen et al., 2013) indicated (dark green) and β -subunit carbohydrate binding module (CBM) labeled; sequences missing in the structure (dashed) include the α -auto-inhibitory domain (AID). Activation-relevant phosphosites (α -T172 in the activation loop, and β -S108 in the CBM; red-brown), activating ligands (A-769662 (red) and AMP (orange/yellow)) and kinase inhibitor Staurosporine in the active site (green) are shown in spacefill representation. For further details see text. (Figure modified from (Viollet et al., 2014)).

Covalent regulation by phosphorylation. The phosphorylation state of the conserved threonine within the kinase domain activation loop (conventionally referred as Thr172) determines the primary activation of AMPK. As compared to an inactive state, this phosphorylation can increase kinase activity by more than 100-fold (Suter et al., 2006). The AMPK phosphorylation state depends on the balance between the activity of different upstream kinases and phosphatases. The two well-established upstream kinases are tumor suppressor kinase complex LKB1-STRAD-MO25 (Woods et al., 2003; Shaw et al., 2004; Hawley et al., 2003) and Ca^{2+} -calmodulin-dependent protein kinase kinases (CamKK), in particular CamKK β (Hawley et al., 2005; Woods et al., 2005; Hurley et al., 2005). LKB1 is the major AMPK kinase in most cells. However, this kinase seems to mostly exhibit constitutive activity and may thus not be the limiting step in AMPK activation. More recent studies suggest that close co-localization of LKB1 with AMPK involving the scaffold protein axin and the lysosomal surface may be necessary for efficient AMPK activation via the LKB pathway (see chapter 3; (Zhang et al., 2014, 2013)). In some cell types, in particular in brain, but much less in heart, AMPK is activated predominantly in a Ca^{2+} -dependent manner by CamKK β . Such CamKK β -mediated AMPK activation might anticipate an increasing energy turnover that accompanies a rise in cytosolic Ca^{2+} during muscle contraction, but its role is not well-understood. Transforming growth factor- β (TGF- β)-activated kinase 1 (TAK1) has been suggested as another AMPK kinase (Herrero-Martín et al., 2009), and also as an AMPK substrate (Kim et al., 2012c). However, TAK-1 is not activated during ischemia, and it is unclear whether it acts via direct AMPK phosphorylation (Xie et al., 2006a).

Protein phosphatases are possibly the more critical parameter governing the α -Thr172 phosphorylation state, and this may be the case for every $\alpha\beta\gamma$ complex isoforms, in every tissues. AMPK covalent activation is modulated by protein phosphatase 1 (PP1) (Garcia-Haro et al., 2010), protein phosphatase 2C (PP2C α) (Sanders et al., 2007a) and the calcium-mediated protein phosphatase 2A (PP2A) (Park et al., 2013). It was also proposed that α -SNAP may exhibit phosphatase activity on AMPK Thr172 according to *in vitro* dephosphorylation assay (Wang and Brautigan, 2013). However, in tissues including heart and endothelial cells, especially expression levels PP2C and 2A, respectively, correlate well with AMPK activation (Wang and Unger, 2005; Wu et al., 2007). There seems to be crosstalk of AMPK with many other cellular signaling pathways. Mainly the α -Thr172 phosphorylation

state is negatively controlled by hierarchical phosphorylation at other sites in the AMPK heterotrimer, in particular in the α -Ser/Thr-rich loop. Protein kinase B (PKB/Akt) that is activated under glucose-rich conditions by insulin signaling, is inhibiting AMPK by phosphorylation at rat α 1-Ser485 (much less so at the equivalent α 2-Ser491) which reduces phosphorylation at the activating α -Thr172 (Hawley et al., 2014; Horman et al., 2006). Thus, hyperactivation of PKB/Akt as occurring in many tumor cells, but also in heart under doxorubicin treatment, can strongly downregulate AMPK activation, with negative effects on proliferation control and cell energetics, respectively. Similar inhibitory phosphorylations of AMPK were reported for protein kinase GSK3 β (Suzuki et al., 2013) and protein kinase A (PKA) (Hurley et al., 2006; Djouder et al., 2010). In the latter case, not the Ser/Thr-loop phosphorylations (including Ser485/Ser491) seem to be inhibitory, but rather another one at α -Ser173 (Djouder et al., 2010). The physiological rationale underlying AMPK inhibition by GSK3 β and PKA is, however, less obvious. AMPK is further negatively controlled by the Ras-Raf-MEK-ERK pathway in a more complex manner, involving negative feedback loops. While active AMPK can reduce MEK/ERK signaling via phosphorylation of upstream B-Raf (Shen et al., 2013), active ERK can reduce AMPK signaling by inhibitory phosphorylation of the AMPK upstream kinase LKB1 (Zheng et al., 2009). Further phosphorylation sites were identified in both AMPK α - and β -subunits, many of them targeted by autophosphorylation, but their functional role remains uncertain. (Auto)phosphorylation of β -Ser108 close to the glycogen binding domain seems to be important at a recently discovered second allosteric regulatory site (see below).

Endocrine signals. Information about the cellular environment and whole body energy and nutrient state is linked to AMPK signaling via endocrine, paracrine, and autocrine mechanisms. These include a diverse array of hormones and cytokines (Table 2). They regulate AMPK mainly by triggering AMPK phosphorylation via upstream kinases, and this regulation often occurs in a tissue-specific manner. Best studied are probably the orexigenic/anorexigenic hormones ghrelin and leptin. In peripheral tissues, leptin activates AMPK to regulate of fatty acid oxidation and glucose uptake. In hypothalamus, leptin inhibits and ghrelin activates AMPK to decrease or increases appetite, respectively, in order to regulate food intake (Steinberg and Kemp, 2009; Steinberg, 2013). Other endocrine factors

that affect AMPK activity are sex hormones, that act via LKB1 (McInnes et al., 2012) and angiotensin 2 (Nagata et al., 2004; Steinberg, 2013).

Table 2: Hormones and cytokines affecting AMPK activity

<i>Compound</i>	<i>Effect</i>	<i>Mechanism</i>	<i>Tissue</i>	<i>Ref.</i>
Leptin	+	AMP increase	Muscle	(Minokoshi et al., 2002)
Leptin	-	melanocortin receptor signaling?	Hypothalamus	(Minokoshi et al., 2004)
Interleukin-6	+	?	Muscle	(Carey et al., 2006)
Tumor necrosis factor α	-	increased PP2C expression	Muscle	(Steinberg et al., 2006)
Resistin	-	?	Liver, muscle, adipose	(Banerjee et al., 2004)
Ghrelin	+	G protein coupled receptor signaling	Hypothalamus, heart	(Kola et al., 2005; Nakazato et al., 2001)
Ghrelin	-	CamKK activation	Liver	(Barazzoni et al., 2005)
Adiponectin	+	adiponectin receptor 1 signaling?	Muscle, adipose, hypothalamus	(Kubota et al., 2007)
Estrogen	+	?	Muscle	(D'Eon et al., 2005)
Testosterone	-	decrease in LKB1 mRNA	Adipocytes	(McInnes et al., 2012)
Dihydrotestosterone				
17 β -estradiol	+	increase in LKB1 mRNA	Adipocytes	(McInnes et al., 2012)
Angiotensin 2	+	AT1R-NADPH oxidase axis	Vascular smooth muscle cells	(Nagata et al., 2004)

Calcium signals. As described above, cellular calcium can regulate the Thr172 phosphorylation state of AMPK via calcium-homeostasis-related kinases in phosphatases, in particular CamKK β (Hawley et al., 2005) and PP2A (Park et al., 2013), respectively. This can also be demonstrated with calcium ionophores (e.g. A23187) in LKB1 deficient cells. Ca²⁺- and AMP-dependent AMPK activation occurs independently and can be synergistic, since AMP-binding (see below) protects the Ca²⁺-induced phosphorylation (Fogarty et al., 2010).

Non-covalent regulation. The second major mechanism of AMPK activation relies on non-covalent, allosteric regulation. It mainly occurs by AMP and ADP, competing with MgATP for binding to the γ -subunit CBS domains. At a low cellular energy state, increases of AMP and, as discovered more recently also of ADP, can be sensed by AMPK as altered AMP/ATP and ADP/ATP concentration ratios (Oakhill et al., 2011; Xiao et al., 2011). In many cell types and in particular in heart and skeletal muscle, breakdown of ATP to ADP at the onset of high workload or cellular stress has only minor immediate effects on ATP levels. Due to the energy buffer and transfer function of the CK/PCr system, global and local ATP pools are rapidly replenished (Schlattner et al., 2006; Wallimann et al., 2011). Thus, ATP is not a very suitable signal for indicating developing energy deficits. However, minor decreases in ATP levels lead to more pronounced relative increases in free ADP and even more in AMP due to the adenylate kinase (AK) reaction. Under these conditions, AK uses two ADP to regenerate ATP and AMP, thus increasing AMP concentrations from the sub-micromolar range under resting conditions to the lower micromolar range (Hardie et al., 2011). To lesser extent, AMP levels also depend on pyrophosphates (cleaving the β -phosphate bond of ATP) and the activity of AMP degradation pathways (AMP-deaminase and 5'-nucleotidase, whose inhibition may be a useful to activate AMPK (Kulkarni et al., 2011)). As a consequence, a decrease in ATP levels by only 10% translates into a 10- to 100-fold increase in AMP, making AMP an ideal second messenger of energy stress. Regulation of AMPK activation by the balance between ATP, ADP and AMP concentrations resembles to what was put forward by Atkinson 50 years ago as “energy charge” regulation (Atkinson, 1968; Hardie and Hawley, 2001; Xiao et al., 2011; Oakhill et al., 2011).

The molecular basis of AMPK activation by AMP and ADP is not yet fully understood, but involves binding to CBS sites on the γ -subunit that trigger multiple interconnected mechanisms. Binding of AMP leads to an up to a ~10-fold allosteric activation of AMPK

(Gowans et al., 2013). Earlier *in vitro* studies suggested that the α 2-subunit has a higher sensitivity to this allosteric activation (Salt et al., 1998a). In addition, AMP and ADP binding increase the phosphorylation status of α -Thr172 through protection of the α -subunit activation loop from dephosphorylation by phosphatases (Davies et al., 1995; Xiao et al., 2011). In addition, AMP (but not ADP) promotes α -Thr172 phosphorylation by LKB1, but not by CamKK β (Gowans et al., 2013). The γ -subunit CBS sites involved in these allosteric effects are sites 1, 3 and 4. However, there is some debate on the role of these sites, in particular which sites mediate direct allosteric activation and which ones the protection of dephosphorylation. There is consensus that changes of AMP and ADP concentrations in the physiological range are mainly sensed at sites 1 and 3, called exchangeable binding sites. Here, free AMP and ADP probably compete mainly with free ATP, since the most abundant Mg²⁺-complexed ATP has 10-fold lower affinity for the CBS sites (Xiao et al., 2011). Sites 1 and 3 differ about 30-fold in their affinity for adenylates, and initial evidence suggested site 1 as high-affinity site, sensing low micromolar concentrations of AMP for allosteric activation, and site 3 as low affinity site, involved in protection of dephosphorylation at higher AMP and ADP concentrations (Xiao et al., 2011). However, the role of CBS sites may not be defined as clearly. A more recent study suggests that site 3 is the most important for allosteric activation (Chen et al., 2012). Indeed, mutation of site 3 residues abrogate allosteric AMPK activation (Chen et al., 2012; Scott et al., 2004), and this site is also in contact with the α -subunit (see below). In addition, site 4 may play a role in allosteric activation. This is a tight AMP-binding site, generally reported as non-exchangeable site since purified protein or protein crystals always retain AMP in this site, even when treated with ATP. However, Chen et al. (Chen et al., 2012) observed ATP at site 4 when co-crystallizing AMPK core complex in presence of 2 mM free ATP, a very high concentration that may not be physiologically relevant. However, ATP binding to site 4 forces site 3 to remain empty and this affects allosteric AMPK activation, consistent with the model of CBS site 3 being the major site of allosteric regulation. A complicating fact is that some nucleotide-binding CBS residues can interact with nucleotides at different sites, thus precluding a clear-cut functional assignment of CBS sites (Hardie, 2014a).

All known direct AMPK activators act via allosteric effects (see chapter 7). They either act like AMP at the CBS sites (e.g. 5-aminoimidazole-4-carboxamide riboside, AICAR; Giri et al.,

2004), or they exert their effects by binding to an entirely different site, discovered only recently (e.g. A-769662; Scott et al., 2008). This site is situated in a cleft between the α -kinase domain and the β -CBM domain, and stabilized by autophosphorylation of the β -Ser108. Occupation of this α/β site confers protection of dephosphorylation. It can be speculated that there exists an endogenous activating metabolite binding at the α/β site, and/or an endogenous activating kinase, able to phosphorylate Ser108 (Hardie, 2014a).

All these allosteric mechanisms, whether they involve binding events at the CBS sites or at the novel α/β site, require close communication between the sensing subunit (γ or β), and the catalytic subunit (α). We and our collaborators have proposed that subunit communication and activation occurs via a conformational switch within the AMPK full-length complex (Riek et al., 2008; Chen et al., 2012). Indeed, AMP-induced conformational changes have been evidenced through structural studies by SAXS (Riek et al., 2008), electron microscopy (Zhu et al., 2011) and X-ray crystallography (Chen et al., 2012) within different parts of the AMPK heterotrimer. Recent structures of the holo-AMPK complex in its active state, as well as low resolution structures in Thr172 phosphorylated and unphosphorylated states, suggest that conformational changes and intramolecular movements involve α -RIM, α -AID, the two lobes of the α -kinase domain, as well as the entire γ -subunit (Chen et al., 2013; Xiao et al., 2011; Calabrese et al., 2014; Li et al., 2014). High resolution apo-AMPK structures of holo-AMPK complex will be necessary to answer the remaining questions, in particular how a different occupation of CBS sites communicates via α -RIM and α -AID with the kinase domain. Collectively, these non-covalent AMPK activation mechanisms add an important layer to the regulation of AMPK activity, since they allow a direct response to intracellular metabolites.

Actual molecular model of allosteric activation. As previously written, allosteric activation of AMPK requires crosstalk between subunits. From numerous studies about AMPK activation mechanism, flexible domains were identified as being involved in the allosteric activation, in that variation of their relative position and orientation in the heterotrimer trigger modulation of the kinase activity.

The first identified element, through crystallographic study (Xiao et al., 2011), is a loop of the α -subunit which directly bind AMP at the level of CBS site 3: the α -hook (recently reassigned

and renamed α -RIM (regulatory subunit interacting motif) (Chen et al., 2013)). Immediately, it was thought that such a loop functions as adenine nucleotide sensor (Chen et al., 2013; Xiao et al., 2011). Moreover, the N-terminus of the loop folds back and is connected to the AID which was identified as being involved in negative regulation of AMPK activity (Crute et al., 1998). In both structures of KD-AID from an inactive fission yeast (Chen et al., 2009) and human (Li et al., 2014), the AID bound to the hinge of the KD (between N- and C-lobes) to lock the KD in an inactive, open conformation. Mutational studies combined to structures suggest that AMP directly activates AMPK by inducing α RIM to bind AMP-occupied CBS3. That in turn is believed to stabilize the interaction of the AID- α RIM with the γ -subunit, consequently pulling the AID away from the inhibitory interaction with the KD. Indeed, in AMP-bound AMPK structures the AID is dissociated from the kinase domain instead binds the CBS site 2, location at which AID may seat when AMPK is allosterically activated. Li et al. reported a structure of AMP-bound AMPK in which the AID packs against the γ -subunit and the KD adopts a closed conformation.

Another highly labile element of the AMPK structure is the CBM. It has been reported that under AMPK activated form, the CBM caps the KD and that this interaction is mediated by phosphorylation of the CBM at Ser108. Indeed, in structure of non-phosphorylated AMPK, the CBM could not be modeled and no density is present at the KD interface whereas the C-terminus of the CBM linker is resolved and points away from the KD. CBM-KD interaction can also be stabilized by synthetic ligands and synthetic compounds reported to activate AMPK in a different manner than nucleotides (A-769662, 991 compound) were visualized in crystal structures at the level of the α/β cleft (Xiao et al., 2013). They activate AMPK by stabilizing interaction between KD and CBM yielding to an activated form of the kinase carrying a close conformation of the KD.

In brief, the N- and C-lobes of the KD can move relatively from each other and are stabilized under opened and inactive conformation when the AID is bound to the KD. When AMP binds CBS site 3, the AID is pulled away from the KD through structural rearrangement of the α RIM, triggering reorganization of N- and C-lobes in an active conformation. AMP-induced increase of activity relies on movements of the AID- α RIM module. On the other side, the KD can also adopt a more active conformation when the CBM caps it, this interaction can be stabilized by phosphorylation of Ser108 or by synthetic ligands (A-769662 or 991).

AMPK activity can also be enhanced through the protection against dephosphorylation of its activation loop (Thr172). It has been reported that AMP and ADP binding on γ is leading to protection against phosphatases. Mutational studies showed that AMP/CBS3 sensing by α RIM is required for this process even if it appears as not be regulated by AID interactions (Li et al., 2014). By contrast this protective effect of adenylates seems to be mediated by domain of β , most probably the CBM and its linker (Xiao et al., 2013). This underlined that AMPK regulation mechanisms are far from being totally elucidated. Indeed, protection against dephosphorylation by AMP (and ADP) relies on conformational changes involving CBS sites, α RIM, but not the AID, and the CBM linker.

A recent study (Li et al., 2014), involving crystallography among other techniques, proposed a consensus model in which all labile regulatory elements of AMPK subunits play a consistent role regarding its physiological activation. AMPK is a molecular machine containing 4 moveable parts: the CBM, the AID, the α RIM and the KD N- and C-lobes. Under conditions involving a healthy adenylates ratio AMPK, is in an ATP-bound state. In the presence of ATP, the interaction between the AID- α RIM and core AMPK is weakened (① - Figure 2), shifting the equilibrium toward AID release from γ to engage the inhibitory interaction with the KD (②). The interaction between AID and KD in turn locks the KD in an open conformation (③) yielding to low catalytic activity. In addition, release of the α RIM/CBS3 interaction promotes a less compact structure of AMPK and the phosphorylated activation loop (red phosphorylation on Figure 2) is more accessible for dephosphorylation. In the presence of AMP (Figure 2 - middle), the AID- α RIM interaction with AMPK core becomes stabilized (④), shifting the equilibrium toward AID- α RIM binding to γ subunit (⑤) (respectively AID with CBS2 and α RIM with CBS3) (Li et al., 2014) which is concomitant to release from the KD (⑥). Relieve from autoinhibition allows relative movements of N- and C-lobes of the KD to adopt a closed, active conformation (⑦). Through incompletely understood conformational changes (⑧), AMP (and ADP to a lesser extent (Gowans et al., 2013)) binding to CBS3 also causes to make AMPK more compact and thereby the activation loop is less accessible to phosphatases (⑧ represents conformational changes occurring at the level of β C-Ter and CBM linker). While adenylates allosterically regulate AMPK activity by varying the overall shape of the KD through modulation of the interaction of the AID with the hinge region of the KD, CBM phosphorylation (blue phosphorylation on Figure 2) and pharmacological

activators modulate the interaction of the CBM with the N-lobes of the KD (Figure 2 - right). Phosphorylation at Ser108 and binding of synthetic ligands (and their hypothesized physiological counterparts) shift the binding equilibrium toward a more stable CBM-KD interaction yielding to a higher activated state of AMPK (9). It has been proposed that CBM with unbound carbohydrates is more potent for shifting this equilibrium toward stable CBM-KD interaction (McBride et al., 2009), rendering the model even more complicated as carbohydrate-CBM interaction goes down in the history.

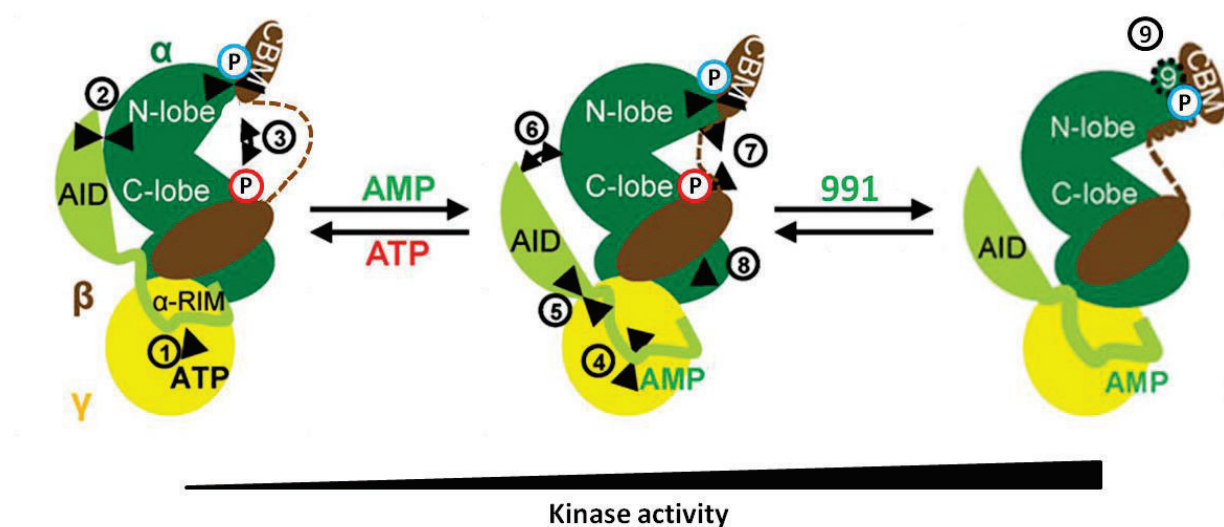


Figure 2: Cartoon model of allosteric AMPK regulation by adenine nucleotides and pharmacological compounds.

Left: AMPK covalently activated; middle: AMPK allosterically activated by adenylates; right: AMPK allosterically activated by both adenylates and synthetic activators. AMPK kinase activity increases from the left to the right. The α -subunit of AMPK is shown in green, with the AID- α RIM module in light green, the β -subunit in brown, and the γ -subunit in yellow. Arrows indicate the directions of allosteric modulator-induced movements within the AMPK complex, as referred to in the text by the numbers in circles next to the arrows. Red P and blue P respectively stand for activation loop and CBM phosphorylations; 9, synthetic compound (e.g. 991). See text for details. Adapted from Li et al., 2014.

Exercise and hypoxia. Given the sensitivity of AMPK for adenine nucleotides, any physiological or pathological situation that changes adenylate ratios will affect AMPK signaling. AMPK is activated by a plethora stimuli such as metabolic stresses, drugs and xenobiotics that either (i) inhibit ATP production, such as starvation for glucose (Salt et al., 1998b) and oxygen (Marsin et al., 2002), or metabolic poisons, or (ii) increase ATP

consumption, such as muscle contraction (Lantier et al., 2014). Muscle contraction and exercise in general trigger rapid activation of AMPK (Chen et al., 2003), and this may be one of the fastest mechanisms that mediate metabolic adaptation to exercise. When AMPK is knocked-out in skeletal muscle of $\beta 1\beta 2$ transgenic mice, they lose exercise tolerance and glucose uptake during contractions, become physically inactive and present a significantly impaired capacity for running linked to reductions in skeletal muscle mitochondrial content (O'Neill et al., 2011). During hypoxia, from the early stage on, a drastic drop in the ATP/AMP level occurs, resulting in AMPK activation.

Other covalent and non-covalent regulations. In addition to the above described conventional regulation of AMPK, there is increasing evidence for additional activation and inactivation mechanisms. Here, different secondary protein modifications play an important role. Myristoylation at Gly2 in the β -subunit increases the sensitivity of AMPK for allosteric activation and promotes Thr172 phosphorylation (Oakhill et al., 2010). The $\beta 2$ subunit, but not $\beta 1$, is sumoylated by the E3-small ubiquitin-like modifier (SUMO) ligase protein inhibitor of activated STAT (PIASy), which attaches SUMO2 but not SUMO1 moieties. This seems to enhance AMPK activity and competes with ubiquitination that results in inactivation of AMPK complex (Rubio et al., 2013). Ubiquitination of AMPK occurs via complexes of laforin (a dual-specificity protein phosphatase) and malin (an E3-ubiquitin ligase), mainly at the β -subunit, and leads to K63-linked ubiquitin chains that are involved in functions different from proteasome degradation (Moreno et al., 2010). Glutathionylation at Cys299 and Cys304 in the α -subunit activates the kinase under oxidative conditions in cellular models and is favored by binding to certain GST isoforms (Klaus et al., 2013). This latter mechanism may be part of a more general redox-regulation of the kinase (Han et al., 2010; Jeon et al., 2012). ROS and RNS activate AMPK, but it is unclear whether this happens via increases in ADP and AMP concentrations, or whether non-canonical mechanisms at the level of AMPK (like glutathionylation) or upstream kinases play a role. *Vice versa*, AMPK regulates NADPH homeostasis and an entire battery of ROS-detoxifying enzymes. Another non-covalent allosteric regulator is glycogen as well as other synthetic branched oligosaccharides that inhibit AMPK activity by binding to the β -CBM domain (McBride et al., 2009) (see above).

5. Regulation

Metabolism. AMPK regulates cellular metabolism at many levels, reducing anabolism (ATP-demanding processes) and up-regulating catabolism (ATP-generating processes) to restore a “healthy” energy status at a cellular and whole body level. To do so, AMPK directly acts on metabolic key enzymes and signaling proteins (acute effects), or on transcription factors (chronic effects, see Figure 3) (Hardie et al., 2012c). Interestingly, drugs of the two main classes of antidiabetic drugs, biguanides (e.g. metformin) and thiazolidinediones (e.g. rosiglitazone), both act at least in part through activation of AMPK (Morrison et al., 2011; Musi et al., 2002). In some organs, (e.g. heart), AMPK is part of the signaling network that allows a predominant use of fatty acid oxidation for ATP generation, but also provides the metabolic flexibility to respond to changes in substrate availability, thus continuously matching ATP generation and demand. Failing of AMPK to provide this flexibility under certain pathological conditions can contribute to pathogenesis (e.g. heart failure (Kim and Dyck, 2014)).

Lipid metabolism. Activated AMPK induces transfer of fatty acid transporter (FAT/CD36) to the plasma membrane to increase fatty acid uptake (Luiken et al., 2003). AMPK further inhibits ATP-consuming lipid synthesis, notably in the liver and in the adipose tissue, but stimulates lipid catabolism for ATP generation. Phosphorylation of acetylCoA carboxylase (ACC) decreases ACC-catalyzed formation of malonyCoA, a precursor in the fatty acid synthesis pathway. At the same time, reducing malonylCoA levels will relieve their inhibition of carnitine palmitoyltransferase 1 (CPT-1), which triggers fatty acid import into mitochondria and subsequent β -oxidation. AMPK also phosphorylates and inhibits other anabolic enzymes: 3-hydroxy-3-methylglutaryl-CoA reductase (HMGCR), a key enzyme in cholesterol synthesis that converts 3-hydroxy-3-methylglutaryl-CoA into mevalonic acid, and glycerol phosphate acyltransferase, involved in triglyceride and phospholipid synthesis (Liao et al., 2014). Since AMPK acts by stimulating lipolysis and inhibiting lipogenesis, its pharmacological activation seems to be useful to treat obesity, diabetes type 2, and more generally the metabolic syndrome (Hardie, 2008b); O’Neill et al., 2013).

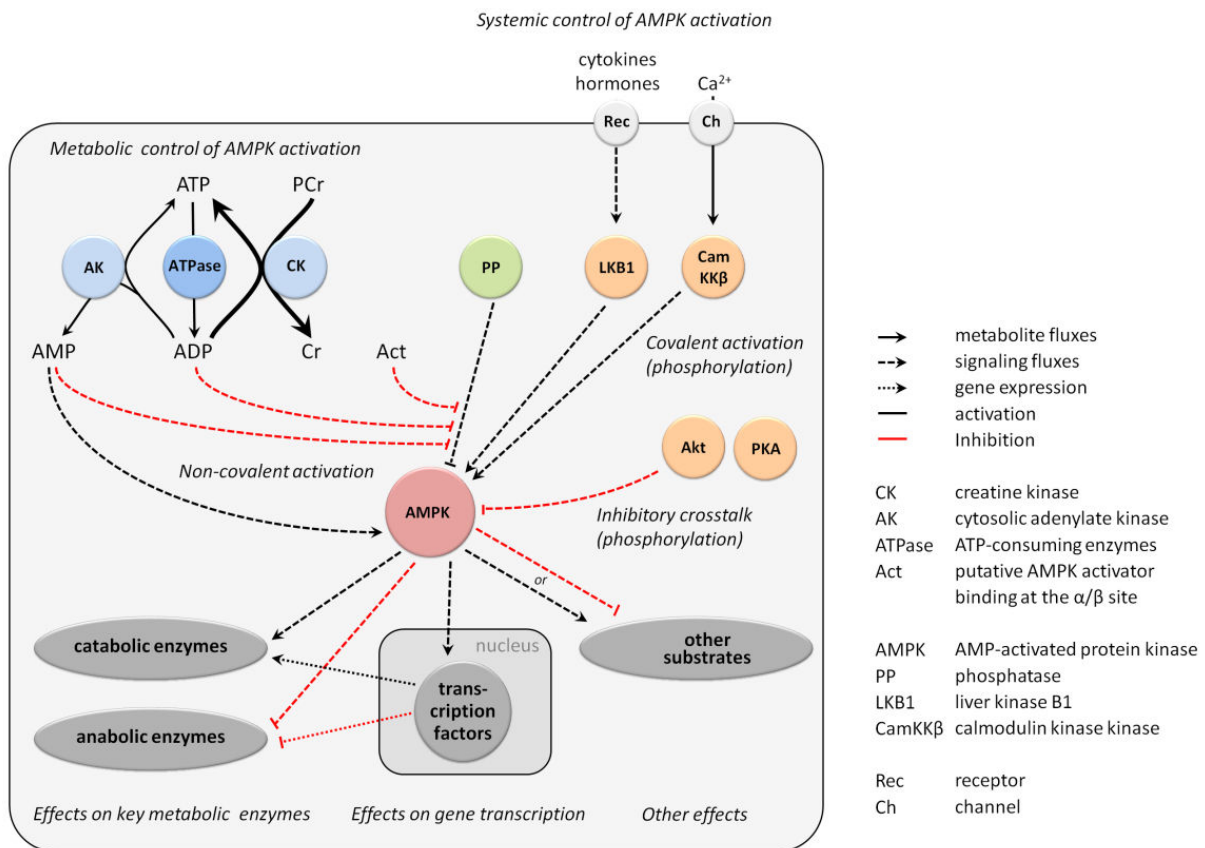


Figure 3: AMPK signaling.

AMPK is activated by intra- and extracellular metabolic and endocrine signals and affects various downstream processes. Activation of AMPK is triggered by upstream kinases (covalent activation by LKB1, CamKK β , inhibition by Akt and PKA) and phosphatases. They mediate mainly extracellular signals carrying e.g. information on the energy and nutrient state of the cellular environment and the entire organism (endocrine signals; systemic control of AMPK). Covalent activation also depends on some intracellular parameters (Ca²⁺, possibly also ROS/RNS), as well as the allosteric ligands. The second layer of regulation is represented by AMPK activation via AMP and ADP (allosteric regulation), both acting as second messengers of cellular energy stress (metabolic control of AMPK). This signaling is linked to conversion of nucleotides via the adenylate kinase (AK) and creatine kinase (CK) reactions. Activated AMPK compensates for ATP loss by accelerating catabolism, inhibiting anabolism, and further effects on cell motility, growth, proliferation, and others, via regulation of key enzymes and transcription factors. For further details see text.

Carbohydrate metabolism. AMPK also interferes with carbohydrate metabolism at different levels, including carbohydrate uptake, glycolysis, and glycogen synthesis. Activated AMPK promotes cellular glucose uptake via glucose transporters GLUT1 (expressed in most cells except muscle, liver and adipose tissue) and GLUT4 (expressed mainly in adipose tissue and striated muscle). AMPK activation promotes GLUT4 translocation to the plasma membrane (Kurth-Kraczek et al., 1999), and stimulates GLUT4 transcription by phosphorylation of the transcription repressor histone deacetylase 5 (HDAC5) which reduces its affinity for the GLUT4 promoter (McGee et al., 2008). GLUT1-dependent glucose uptake is activated via an unclear mechanism that involves GLUT1 already located at the plasma membrane (Barnes et al., 2002). Notably in case of energy deprivation, AMPK phosphorylates and activates the 6-phosphofructo-2-kinase/fructose-2,6-bisphosphatase (PFKFB) to increase the steady-state concentration of fructose-2,6-bisphosphate (Marsin et al., 2000). This metabolite then acts as an allosteric activator of glycolysis by stimulating the glycolytic enzyme 6-phosphofructo-1-kinase (PFK1), a rate-limiting glycolytic enzyme. Once activated, AMPK also represses anabolic glucose storage into glycogen by directly phosphorylating and inactivating glycogen synthase (Bultot et al., 2012). Finally, AMPK affects carbohydrate metabolism indirectly by phosphorylation of the mTor-raptor complex, which was proposed to modulate insulin sensitivity by regulating protein levels of IRS-1 (Haruta et al., 2000; Kahn et al., 2005).

Transcription. AMPK phosphorylates and regulates various transcription factors and coregulators, including forkhead box O (FoxO) proteins FoxO1 and FoxO3 (Kubli and Gustafsson, 2014) and peroxisome proliferator-activated receptor (PPAR) γ coactivator-1 α (PGC-1 α) (Patten and Arany, 2012), both having important roles in the regulation of energy homeostasis and beyond. PGC-1 α is a central transcriptional coactivator that orchestrates mitochondrial biogenesis and dynamics, fuel transport and/or consumption, angiogenesis, and antioxidative effects. PGC-1 α phosphorylation by AMPK results in improved metabolism of fatty acids and more-efficient energy utilization (Schilling and Kelly, 2011). FoxO transcription factors regulate expression of genes involved in the antioxidative stress response and in the balance between apoptosis, autophagy, and energy metabolism.. FoxO-regulated genes also encode proteins that contribute to improved energy metabolism, including FAT/CD36 and GLUT4 indirect metabolic effects.

Growth and proliferation. Many effects of AMPK on cell growth, cell cycle and autophagy are mediated by another evolutionary conserved serine/threonine protein kinase further downstream, the mammalian target of rapamycin (mTor). mTor occurs as two functional multiprotein complexes, mTORC1 and mTORC2 (Loewith et al., 2002). mTORC1 comprises mTOR, Raptor, mLST8 and PRAS40, and is regulated by cellular energy and nutrient state, whereas mTORC2 is not. Raptor also plays a significant role in intracellular localization of mTORC1 in response to amino acid availability, which is an essential cellular signal for mTORC1 activation (Sancak et al., 2008). Activation of mTORC1 occurs at the lysosomal surface as a part of complex, multi-protein assemblies (Bar-Peled and Sabatini, 2014). Active mTORC1 stimulates several ATP demanding cellular processes such as translation, transcription (protein synthesis), ribosome biogenesis, mitochondrial metabolism, proliferation and autophagy. Unlike mTORC2, mTORC1 is sensitive to Rapamycin, a molecule used as immunorepressor due to its capacity to downregulate protein synthesis, notably of antibodies.

Two important substrates of mTORC1 in its response to nutrients and cellular energy status are S6 kinase (S6K) and eIF4E binding proteins (4EBPs). Raptor, a component of mTORC1, functions as a scaffolding protein to recruit such substrates for phosphorylation (Nojima et al., 2003). S6K is a ribosomal kinase regulating translation initiation, mRNA processing and cell growth and notably enhances protein synthesis once phosphorylated. 4EBPs are translational repressors that are inactivated upon phosphorylation by mTORC1. To precisely regulate these mTORC1-dependent, energy-demanding processes, AMPK inhibits mTORC1 signaling through two distinct mechanisms (Inoki et al., 2012). First, it directly phosphorylates Raptor at the conserved Ser722 and Ser792, leading to recruitment of 14-3-3 protein and an inactive mTORC1 complex (Gwinn et al., 2008). Second, it phosphorylates tuberous sclerosis protein 2 (TSC2), a GTPase activating protein (GAP), thus stimulating the downstream GTPase Ras homolog enriched in brain protein (Rheb). This transforms Rheb from its GTP bound form that activates mTORC1, into its inactive, GDP-bound form (Inoki et al., 2003). This latter pathway of mTORC1 regulation by AMPK may depend on cell type and tissue (Wolff et al., 2011). Collectively, the AMPK and mTORC1 pathways serve as a signaling nexus to regulate cellular metabolism, energy homeostasis and cell growth. Disorder of each

pathway may strongly contribute to the development of pathologies such as type II diabetes or cancer.

Autophagy and apoptosis. While AMPK activation by upstream kinases is well studied, much less is known about regulation of AMPK stability and activity by components of the ubiquitin-proteasome system, responsible for cellular recognition and degradation of proteins. Growing evidence suggests that AMPK regulates overall proteasome activity and individual components of the ubiquitin-proteasome system (Ronnebaum et al., 2014). Autophagy is important for maintaining homeostasis when nutrient supply becomes limiting. It is important for the cellular turnover of proteins and organelles, and is rapidly upregulated during stress. In metabolic disorders including obesity and diabetes, autophagy is reduced, leading to accumulation of protein aggregates and dysfunctional organelles which can contribute to pathogenesis.

6. Pharmacological activation

AMPK controls metabolic pathways and cellular processes that are critical to the etiology of various, otherwise unrelated pathologies. For many of them, including type 2 diabetes, obesity and even cardiovascular disease, activation of AMPK has been recognized as a potential treatment, mimicking for example the positive effects of exercise on many of these pathologies. However, one has to keep in mind that systemic, constitutive AMPK activation by drugs also carries risks. These include, as already described above, the highly pleiotropic target spectrum of AMPK, and in particular its central effects as e.g. in hypothalamic appetite control.

A large panel of natural or synthetic agents were reported to activate AMPK (Yun and Ha, 2011). However, the caveat with most of these molecules is that, where analyzed, they do not directly activate AMPK and have numerous cellular effects (Hardie, 2014c). They often include mild inhibition of mitochondrial ATP generation by interfering with either the respiratory chain or mitochondrial ATPase (El-Mir et al., 2000; Gledhill et al., 2007), thus leading to a small but chronic increase in cellular AMP/ATP and ADP/ATP ratios. This group of compounds includes antidiabetic drugs like metformin, and many plant polyphenols like

resveratrol contained in grapes, green tea, peppers, garlic or traditional products of Chinese medicine (Gu et al., 2010; Huang and Lin, 2012; Kim et al., 2012a; Wang et al., 2009; Yang et al., 2012).

Also some direct activators act via the allosteric mechanisms known for AMP. The long known 5-aminoimidazole-4-carboxamide riboside (AICAR; Giri et al., 2004) is metabolized within the cell to ZMP, an AMP analogue that binds to CBS domains and acts like AMP. However, such AMP analogues may affect any AMP-sensitive processes, a condition potentially avoided by the novel AMP analog, 5-(5-hydroxyl-isoxazol-3-yl)-furan-2-phosphonic acid or C2. This compound was reported to be 1000-fold more potent than ZMP *in vitro* (Gómez-Galeno et al., 2010). All these allosteric mechanisms involve the γ -subunit CBS sites, and activation is lost in cells expressing mutant AMPK insensitive to AMP (Hawley et al., 2010).

A third group of AMPK activators exerts its effects by binding to an entirely different site, situated at the interface of α -kinase domain and β -CBM domain. Its occupation confers protection of dephosphorylation and allosteric activation. Activators binding at this site include A-769662 (Scott et al., 2008), the 991 compound (Xiao et al., 2013) and its derivatives, as well as salicylate (Hawley et al., 2012).

As a result of almost 15 years of research, a total of 26 patents has been disclosed, describing 10 classes of direct AMPK activators (Giordanetto and Karis, 2012). However, no direct AMPK activator has succeeded so far in clinical studies, although promising trials are ongoing (Ballantyne et al., 2013). Abbott Laboratories were the first in 2005 to identify thienopyridones as direct AMPK activators¹. High throughput screening first identified A-592107 that was then optimized to yield the more potent A-769662 (EC₅₀: 0.8 μ M) which did not show immediate signs of cytotoxicity or activity at secondary biological targets (Cool et al., 2006). Discovery of A-769662 represented a shift in AMPK-targeted pharmaceutical research, since it demonstrated that the kinase can be directly activated by non-nucleotide ligands. Since then, A-769662 has been used as a standard AMPK activator in basic research,

¹ Abbott Laboratories. Preparation of substituted thieno[2,3-b]pyridones as activators for AMP-activated kinase for the treatment of diabetes and obesity. 2005; US20050038068

and much has been learned about its action mechanism and pharmacology. A-769662 activates AMPK both allosterically and by inhibition of Thr172 dephosphorylation mediated by PP2C, similar to AMP (Goransson et al., 2007; Sanders et al., 2007b). However, it does not bind to the γ -subunit CBS sites, but identified a novel allosteric regulatory site at the interface between the α -kinase and the β -CBM domain (Calabrese et al., 2014; Xiao et al., 2013). Importantly, A-769662 has a much stronger inhibitory effect on β 1-containing complexes as compared to those containing β 2. This showed for the first time that isoform-specific small molecule activators can be developed that would allow a more tissue-specific pharmacological modulation of AMPK activity.

Most recently, it was shown that AMP and A-769662 have a synergistic effect on AMPK activation (Scott et al., 2014; Ducommun et al., 2014), that even allows to bypass phosphorylation of Thr172, a step thought to be essential for AMPK activity (Scott et al., 2014; Viollet et al., 2014). This observation has put a note of caution onto the widespread use of Thr172 phosphorylation as a reliable read-out for AMPK activity (Scott et al., 2014; Viollet et al., 2014). Although in the meantime also some off-target effects of A-769662 have been observed (Benziane et al., 2009; Treebak et al., 2009), the compound remains a very useful tool to explore AMPK-mediated cellular processes.

Most other direct AMPK activators that have been described bear structural similarities to A-769662, such as the 991 compound (Xiao et al., 2013). Only more recently, compounds that do not resemble to such thienopyridones have been described. For most patented direct AMPK activators, there is limited documentation available concerning their selectivity profile across the various AMPK isoform combinations (Giordanetto and Karis, 2012; Yun and Ha, 2011) apart from A-769662 (Scott et al., 2008; Goransson et al., 2007; Sanders et al., 2007b) and the 991 compound (Xiao et al., 2013). Given the plethora of processes controlled by AMPK, heterotrimer-specific AMPK activation would allow to preferentially target a specific tissue and thus has the strongest potential for pharmacological applications.

Taken together, very few structurally different AMPK activators are known so far (Giordanetto and Karis, 2012; Yun and Ha, 2011). Although this could represent a true limitation of potentially AMPK activating compounds, it may also be related to the applied screening procedures. A critical point in screening chemical libraries may be the read-out

system used to identify AMPK activation. AMPK activators bind at allosteric sites, but the read-out generally relies on the activity of the AMPK kinase domain. This implies the use of MgATP and accumulation of ADP and even traces of AMP during the assay. The presence of these nucleotides may obscure effects of activating compounds, at least of those acting at the CBS domains. Tools that report AMPK activation without the need of kinase assays would therefore have a clear advantage.

Concluding remarks. Defects in energy metabolism contribute to the pathogenesis of many diseases. AMPK is now recognized as the central sensor and regulator of cellular energetics, and AMPK activation has been proposed as a suitable strategy for the treatment of insulin resistance/type 2 diabetes, cancer, and some other pathologies (Steinberg and Kemp, 2009). However, the potential for pharmacological activation of AMPK has not yet been analyzed in much detail. For its application in pathologies, more work is still necessary to evaluate efficacy and safety in short-term and long-term activation protocols. There is continued interest of pharmaceutical industry in developing AMPK agonists. Indeed, the search for clinically applicable, specific AMPK activators remains an urgent need to evaluate and fully exploit the pharmacological potential of AMPK. Therefore, new emerging tools facilitating the screening and the identification of promising potent compounds regarding AMPK activation would highly be appreciated. One of such tools could be a kinase activity independent, but conformation sensitive assay for AMPK, since activation of AMPK is accompanied by significant conformational changes.

7. References

- Allard, M.F., Parsons, H.L., Saeedi, R., Wambolt, R.B., and Brownsey, R. (2007). AMPK and metabolic adaptation by the heart to pressure overload. *Am J Physiol Heart Circ Physiol* 292, H140–H148.
- Amodeo, G.A., Rudolph, M.J., and Tong, L. (2007). Crystal structure of the heterotrimer core of *Saccharomyces cerevisiae* AMPK homologue SNF1. *Nature* 449, 492–495.
- Andersen, M.N., and Rasmussen, H.B. (2012). AMPK: A regulator of ion channels. *Commun. Integr. Biol.* 5, 480–484.
- Arad, M., Seidman, C.E., and Seidman, J.G. (2007). AMP-activated protein kinase in the heart: role during health and disease. *Circ Res* 100, 474–488.
- Atkinson, D.E. (1968). The energy charge of the adenylate pool as a regulatory parameter. Interaction with feedback modifiers. *Biochemistry (Mosc.)* 7, 4030–4034.
- Ballantyne, C.M., Davidson, M.H., Macdougall, D.E., Bays, H.E., Dicarlo, L.A., Rosenberg, N.L., Margulies, J., and Newton, R.S. (2013). Efficacy and safety of a novel dual modulator of adenosine triphosphate-citrate lyase and adenosine monophosphate-activated protein kinase in patients with hypercholesterolemia: results of a multicenter, randomized, double-blind, placebo-controlled, parallel-group trial. *J Am Coll Cardiol* 62, 1154–1162.
- Banerjee, R.R., Rangwala, S.M., Shapiro, J.S., Rich, A.S., Rhoades, B., Qi, Y., Wang, J., Rajala, M.W., Pocai, A., Scherer, P.E., et al. (2004). Regulation of fasted blood glucose by resistin. *Science* 303, 1195–1198.
- Barazzoni, R., Bosutti, A., Stebel, M., Cattin, M.R., Roder, E., Visintin, L., Cattin, L., Biolo, G., Zanetti, M., and Guarnieri, G. (2005). Ghrelin regulates mitochondrial-lipid metabolism gene expression and tissue fat distribution in liver and skeletal muscle. *Am. J. Physiol. Endocrinol. Metab.* 288, E228–E235.
- Barnes, K., Ingram, J.C., Porras, O.H., Barros, L.F., Hudson, E.R., Fryer, L.G.D., Fougelle, F., Carling, D., Hardie, D.G., and Baldwin, S.A. (2002). Activation of GLUT1 by metabolic and osmotic stress: potential involvement of AMP-activated protein kinase (AMPK). *J. Cell Sci.* 115, 2433–2442.
- Baskin, K.K., and Taegtmeyer, H. (2011). An expanded role for AMP-activated protein kinase: regulator of myocardial protein degradation. *Trends Cardiovasc Med* 21, 124–127.
- Bateman, A. (1997). The structure of a domain common to archaeobacteria and the homocystinuria disease protein. *Trends Biochem Sci* 22, 12–13.
- Beg, Z.H., Stonik, J.A., and Brewer, H.B. (1980). In vitro and in vivo phosphorylation of rat liver 3-hydroxy-3-methylglutaryl coenzyme A reductase and its modulation by glucagon. *J. Biol. Chem.* 255, 8541–8545.
- Behrends, C., Sowa, M.E., Gygi, S.P., and Harper, J.W. (2010). Network organization of the human autophagy system. *Nature* 466, 68–76.
- Benziane, B., Björnholm, M., Lantier, L., Viollet, B., Zierath, J.R., and Chibalin, A.V. (2009). AMP-activated protein kinase activator A-769662 is an inhibitor of the Na(+)-K(+)-ATPase. *Am. J. Physiol. Cell Physiol.* 297, C1554–C1566.
- Bouhidel, O., Pons, S., Souktani, R., Zini, R., Berdeaux, A., and Ghaleh, B. (2008). Myocardial ischemic postconditioning against ischemia-reperfusion is impaired in ob/ob mice. *Am J Physiol Heart Circ Physiol* 295, H1580–H1586.
- Bultot, L., Guigas, B., Von Wilamowitz-Moellendorff, A., Maisin, L., Vertommen, D., Hussain, N., Beullens, M., Guinovart, J.J., Foretz, M., Viollet, B., et al. (2012). AMP-activated protein kinase phosphorylates and inactivates liver glycogen synthase. *Biochem. J.* 443, 193–203.
- Burwinkel, B., Scott, J.W., Bühner, C., van Landeghem, F.K.H., Cox, G.F., Wilson, C.J., Grahame Hardie, D., and Kilimann, M.W. (2005). Fatal congenital heart glycogenesis caused by a recurrent activating R531Q mutation in the gamma 2-subunit of AMP-activated protein kinase (PRKAG2), not by phosphorylase kinase deficiency. *Am. J. Hum. Genet.* 76, 1034–1049.

- Cai, X.J., Chen, L., Li, L., Feng, M., Li, X., Zhang, K., Rong, Y.Y., Hu, X.B., Zhang, M.X., Zhang, Y., et al. (2010). Adiponectin inhibits lipopolysaccharide-induced adventitial fibroblast migration and transition to myofibroblasts via AdipoR1-AMPK-iNOS pathway. *Mol Endocrinol* 24, 218–228.
- Calabrese, M.F., Rajamohan, F., Harris, M.S., Caspers, N.L., Magyar, R., Withka, J.M., Wang, H., Borzilleri, K.A., Sahasrabudhe, P.V., Hoth, L.R., et al. (2014). Structural basis for AMPK activation: natural and synthetic ligands regulate kinase activity from opposite poles by different molecular mechanisms. *Structure* 22, 1161–1172.
- Calvert, J.W., Gundewar, S., Jha, S., Greer, J.J., Bestermann, W.H., Tian, R., and Lefer, D.J. (2008). Acute metformin therapy confers cardioprotection against myocardial infarction via AMPK-eNOS-mediated signaling. *Diabetes* 57, 696–705.
- Carey, A.L., Steinberg, G.R., Macaulay, S.L., Thomas, W.G., Holmes, A.G., Ramm, G., Prelovsek, O., Hohnen-Behrens, C., Watt, M.J., James, D.E., et al. (2006). Interleukin-6 increases insulin-stimulated glucose disposal in humans and glucose uptake and fatty acid oxidation in vitro via AMP-activated protein kinase. *Diabetes* 55, 2688–2697.
- Carling, D. (2004). The AMP-activated protein kinase cascade—a unifying system for energy control. *Trends Biochem. Sci.* 29, 18–24.
- Chen, L., Jiao, Z.-H., Zheng, L.-S., Zhang, Y.-Y., Xie, S.-T., Wang, Z.-X., and Wu, J.-W. (2009). Structural insight into the autoinhibition mechanism of AMP-activated protein kinase. *Nature* 459, 1146–1149.
- Chen, L., Wang, J., Zhang, Y.-Y., Yan, S.F., Neumann, D., Schlattner, U., Wang, Z.-X., and Wu, J.-W. (2012). AMP-activated protein kinase undergoes nucleotide-dependent conformational changes. *Nat. Struct. Mol. Biol.* 19, 716–718.
- Chen, L., Xin, F.-J., Wang, J., Hu, J., Zhang, Y.-Y., Wan, S., Cao, L.-S., Lu, C., Li, P., Yan, S.F., et al. (2013). Conserved regulatory elements in AMPK. *Nature* 498, E8–E10.
- Chen, Z.-P., Stephens, T.J., Murthy, S., Canny, B.J., Hargreaves, M., Witters, L.A., Kemp, B.E., and McConell, G.K. (2003). Effect of Exercise Intensity on Skeletal Muscle AMPK Signaling in Humans. *Diabetes* 52, 2205–2212.
- Clark, H., Carling, D., and Saggerson, D. (2004). Covalent activation of heart AMP-activated protein kinase in response to physiological concentrations of long-chain fatty acids. *Eur J Biochem* 271, 2215–2224.
- Cool, B., Zinker, B., Chiou, W., Kifle, L., Cao, N., Perham, M., Dickinson, R., Adler, A., Gagne, G., Iyengar, R., et al. (2006). Identification and characterization of a small molecule AMPK activator that treats key components of type 2 diabetes and the metabolic syndrome. *Cell Metab.* 3, 403–416.
- Coven, D.L., Hu, X., Cong, L., Bergeron, R., Shulman, G.I., Hardie, D.G., and Young, L.H. (2003). Physiological role of AMP-activated protein kinase in the heart: graded activation during exercise. *Am J Physiol Endocrinol Metab* 285, E629–E636.
- Crute, B.E., Seefeld, K., Gamble, J., Kemp, B.E., and Witters, L.A. (1998). Functional domains of the alpha1 catalytic subunit of the AMP-activated protein kinase. *J. Biol. Chem.* 273, 35347–35354.
- Curigliano, G., Cardinale, D., Suter, T., Plataniotis, G., de Azambuja, E., Sandri, M.T., Criscitiello, C., Goldhirsch, A., Cipolla, C., Roila, F., et al. (2012). Cardiovascular toxicity induced by chemotherapy, targeted agents and radiotherapy: ESMO Clinical Practice Guidelines. *Ann. Oncol. Off. J. Eur. Soc. Med. Oncol.* ESMO 23 Suppl 7, vii155–vii166.
- Davies, J.K., Wells, D.J., Liu, K., Whitrow, H.R., Daniel, T.D., Grignani, R., Lygate, C.A., Schneider, J.E., Noel, G., Watkins, H., et al. (2006). Characterization of the role of gamma2 R531G mutation in AMP-activated protein kinase in cardiac hypertrophy and Wolff-Parkinson-White syndrome. *Am J Physiol Heart Circ Physiol* 290, H1942–H1951.
- Davies, S.P., Helps, N.R., Cohen, P.T., and Hardie, D.G. (1995). 5'-AMP inhibits dephosphorylation, as well as promoting phosphorylation, of the AMP-activated protein kinase. Studies using bacterially expressed human protein phosphatase-2C alpha and native bovine protein phosphatase-2AC. *FEBS Lett* 377, 421–425.
- D'Eon, T.M., Souza, S.C., Aronovitz, M., Obin, M.S., Fried, S.K., and Greenberg, A.S. (2005). Estrogen regulation of adiposity and fuel partitioning. Evidence of genomic and non-genomic regulation of lipogenic and oxidative pathways. *J. Biol. Chem.* 280, 35983–35991.

- Djouder, N., Tuerk, R.D., Suter, M., Salvioni, P., Thali, R.F., Scholz, R., Vaahtomeri, K., Auchli, Y., Rechsteiner, H., Brunisholz, R.A., et al. (2010). PKA phosphorylates and inactivates AMPK α to promote efficient lipolysis. *EMBO J.* 29, 469–481.
- Dolinsky, V.W., Chan, A.Y., Robillard Frayne, I., Light, P.E., Des Rosiers, C., and Dyck, J.R. (2009). Resveratrol prevents the prohypertrophic effects of oxidative stress on LKB1. *Circulation* 119, 1643–1652.
- Du, J., Guan, T., Zhang, H., Xia, Y., Liu, F., and Zhang, Y. (2008). Inhibitory crosstalk between ERK and AMPK in the growth and proliferation of cardiac fibroblasts. *Biochem Biophys Res Commun* 368, 402–407.
- Ducommun, S., Ford, R.J., Bultot, L., Deak, M., Bertrand, L., Kemp, B.E., Steinberg, G.R., and Sakamoto, K. (2014). Enhanced activation of cellular AMPK by dual-small molecule treatment: AICAR and A769662. *Am. J. Physiol. - Endocrinol. Metab.* 306, E688–E696.
- Dyck, J.R., and Lopaschuk, G.D. (2006). AMPK alterations in cardiac physiology and pathology: enemy or ally? *J Physiol* 574, 95–112.
- El-Mir, M.Y., Nogueira, V., Fontaine, E., Avéret, N., Rigoulet, M., and Leverve, X. (2000). Dimethylbiguanide inhibits cell respiration via an indirect effect targeted on the respiratory chain complex I. *J. Biol. Chem.* 275, 223–228.
- Eschenhagen, T., Force, T., Ewer, M.S., de Keulenaer, G.W., Suter, T.M., Anker, S.D., Avkiran, M., de Azambuja, E., Balligand, J.-L., Brutsaert, D.L., et al. (2011). Cardiovascular side effects of cancer therapies: a position statement from the Heart Failure Association of the European Society of Cardiology. *Eur. J. Heart Fail.* 13, 1–10.
- Esteve-Puig, R., Canals, F., Colome, N., Merlino, G., and Recio, J.A. (2009). Uncoupling of the LKB1-AMPK α energy sensor pathway by growth factors and oncogenic BRAF. *PLoS One* 4, e4771.
- Ewer, M.S., and Ewer, S.M. (2010). Cardiotoxicity of anticancer treatments: what the cardiologist needs to know. *Nat. Rev. Cardiol.* 7, 564–575.
- Ferrer, A., Caelles, C., Massot, N., and Hegardt, F.G. (1985). Activation of rat liver cytosolic 3-hydroxy-3-methylglutaryl Coenzyme A reductase kinase by adenosine 5'-monophosphate. *Biochem. Biophys. Res. Commun.* 132, 497–504.
- Fogarty, S., Hawley, S.A., Green, K.A., Saner, N., Mustard, K.J., and Hardie, D.G. (2010). Calmodulin-dependent protein kinase kinase-beta activates AMPK without forming a stable complex: synergistic effects of Ca²⁺ and AMP. *Biochem J* 426, 109–118.
- Forcet, C., and Billaud, M. (2007). Dialogue between LKB1 and AMPK: a hot topic at the cellular pole. *Sci. STKE Signal Transduct. Knowl. Environ.* 2007, pe51.
- Frederich, M., Zhang, L., and Balschi, J.A. (2005). Hypoxia and AMP independently regulate AMP-activated protein kinase activity in heart. *Am J Physiol Heart Circ Physiol* 288, H2412–H2421.
- Gabrielson, K., Bedja, D., Pin, S., Tsao, A., Gama, L., Yuan, B., and Muratore, N. (2007). Heat shock protein 90 and ErbB2 in the cardiac response to doxorubicin injury. *Cancer Res.* 67, 1436–1441.
- Garcia-Haro, L., Garcia-Gimeno, M.A., Neumann, D., Beullens, M., Bollen, M., and Sanz, P. (2010). The PP1-R6 protein phosphatase holoenzyme is involved in the glucose-induced dephosphorylation and inactivation of AMP-activated protein kinase, a key regulator of insulin secretion, in MIN6 beta cells. *FASEB J. Off. Publ. Fed. Am. Soc. Exp. Biol.* 24, 5080–5091.
- Gianni, L., Herman, E.H., Lipshultz, S.E., Minotti, G., Sarvazyan, N., and Sawyer, D.B. (2008). Anthracycline cardiotoxicity: from bench to bedside. *J. Clin. Oncol. Off. J. Am. Soc. Clin. Oncol.* 26, 3777–3784.
- Giordanetto, F., and Karis, D. (2012). Direct AMP-activated protein kinase activators: a review of evidence from the patent literature. *Expert Opin. Ther. Pat.* 22, 1467–1477.
- Giri, S., Nath, N., Smith, B., Viollet, B., Singh, A.K., and Singh, I. (2004). 5-aminoimidazole-4-carboxamide-1-beta-4-ribofuranoside inhibits proinflammatory response in glial cells: a possible role of AMP-activated protein kinase. *J. Neurosci. Off. J. Soc. Neurosci.* 24, 479–487.
- Gledhill, J.R., Montgomery, M.G., Leslie, A.G.W., and Walker, J.E. (2007). Mechanism of inhibition of bovine F1-ATPase by resveratrol and related polyphenols. *Proc. Natl. Acad. Sci. U. S. A.* 104, 13632–13637.

- Gómez-Galeno, J.E., Dang, Q., Nguyen, T.H., Boyer, S.H., Grote, M.P., Sun, Z., Chen, M., Craigo, W.A., van Poelje, P.D., MacKenna, D.A., et al. (2010). A Potent and Selective AMPK Activator That Inhibits de Novo Lipogenesis. *ACS Med. Chem. Lett.* *1*, 478–482.
- Goransson, O., McBride, A., Hawley, S.A., Ross, F.A., Shpiro, N., Foretz, M., Viollet, B., Hardie, D.G., and Sakamoto, K. (2007). Mechanism of action of A-769662, a valuable tool for activation of AMP-activated protein kinase. *J Biol Chem* *282*, 32549–32560.
- Gowans, G.J., Hawley, S.A., Ross, F.A., and Hardie, D.G. (2013). AMP Is a True Physiological Regulator of AMP-Activated Protein Kinase by Both Allosteric Activation and Enhancing Net Phosphorylation. *Cell Metab.* *18*, 556–566.
- Gratia, S., Kay, L., Potenza, L., Seffouh, A., Novel-Chate, V., Schnebelen, C., Sestili, P., Schlattner, U., and Tokarska-Schlattner, M. (2012). Inhibition of AMPK signalling by doxorubicin: at the crossroads of the cardiac responses to energetic, oxidative, and genotoxic stress. *Cardiovasc Res* *95*, 290–299.
- Gu, Y., Zhang, Y., Shi, X., Li, X., Hong, J., Chen, J., Gu, W., Lu, X., Xu, G., and Ning, G. (2010). Effect of traditional Chinese medicine berberine on type 2 diabetes based on comprehensive metabonomics. *Talanta* *81*, 766–772.
- Gwinn, D.M., Shackelford, D.B., Egan, D.F., Mihaylova, M.M., Mery, A., Vasquez, D.S., Turk, B.E., and Shaw, R.J. (2008). AMPK phosphorylation of raptor mediates a metabolic checkpoint. *Mol. Cell* *30*, 214–226.
- Hahn-Windgassen, A., Nogueira, V., Chen, C.C., Skeen, J.E., Sonenberg, N., and Hay, N. (2005). Akt activates the mammalian target of rapamycin by regulating cellular ATP level and AMPK activity. *J Biol Chem* *280*, 32081–32089.
- Han, Y., Wang, Q., Song, P., Zhu, Y., and Zou, M.-H. (2010). Redox regulation of the AMP-activated protein kinase. *PLoS One* *5*, e15420.
- Hanks, S.K., Quinn, A.M., and Hunter, T. (1988). The protein kinase family: conserved features and deduced phylogeny of the catalytic domains. *Science* *241*, 42–52.
- Hardie, D.G. (2007). AMP-activated/SNF1 protein kinases: conserved guardians of cellular energy. *Nat Rev Mol Cell Biol* *8*, 774–785.
- Hardie, D.G. (2008a). Role of AMP-activated protein kinase in the metabolic syndrome and in heart disease. *FEBS Lett.* *582*, 81–89.
- Hardie, D.G. (2008b). AMPK: a key regulator of energy balance in the single cell and the whole organism. *Int. J. Obes.* *32*, S7–S12.
- Hardie, D.G. (2011). AMP-activated protein kinase: an energy sensor that regulates all aspects of cell function. *Genes Dev* *25*, 1895–1908.
- Hardie, D.G. (2014a). AMPK—Sensing Energy while Talking to Other Signaling Pathways. *Cell Metab.* *20*, 939–952.
- Hardie, D.G. (2014b). AMPK: positive and negative regulation, and its role in whole-body energy homeostasis. *Curr. Opin. Cell Biol.* *33C*, 1–7.
- Hardie, D.G. (2014c). AMP-activated protein kinase: maintaining energy homeostasis at the cellular and whole-body levels. *Annu. Rev. Nutr.* *34*, 31–55.
- Hardie, D.G., and Ashford, M.L.J. (2014). AMPK: Regulating Energy Balance at the Cellular and Whole Body Levels. *Physiology* *29*, 99–107.
- Hardie, D.G., and Carling, D. (1997). The AMP-Activated Protein Kinase—fuel gauge of the mammalian cell? *Eur. J. Biochem.* *246*, 259–273.
- Hardie, D.G., and Hawley, S.A. (2001). AMP-activated protein kinase: the energy charge hypothesis revisited. *BioEssays News Rev. Mol. Cell. Dev. Biol.* *23*, 1112–1119.
- Hardie, D.G., and Sakamoto, K. (2006). AMPK: a key sensor of fuel and energy status in skeletal muscle. *Physiol. Bethesda* *21*, 48–60.
- Hardie, D.G., Salt, I.P., Hawley, S.A., and Davies, S.P. (1999). AMP-activated protein kinase: an ultrasensitive system for monitoring cellular energy charge. *Biochem. J.* *338 (Pt 3)*, 717–722.

- Hardie, D.G., Scott, J.W., Pan, D.A., and Hudson, E.R. (2003). Management of cellular energy by the AMP-activated protein kinase system. *FEBS Lett.* *546*, 113–120.
- Hardie, D.G., Carling, D., and Gamblin, S.J. (2011). AMP-activated protein kinase: also regulated by ADP? *Trends Biochem. Sci.* *36*, 470–477.
- Hardie, D.G., Ross, F.A., and Hawley, S.A. (2012a). AMPK: a nutrient and energy sensor that maintains energy homeostasis. *Nat Rev Mol Cell Biol* *13*, 251–262.
- Hardie, D.G., Ross, F.A., and Hawley, S.A. (2012b). AMPK: a nutrient and energy sensor that maintains energy homeostasis. *Nat. Rev. Mol. Cell Biol.* *13*, 251–262.
- Hardie, D.G., Ross, F.A., and Hawley, S.A. (2012c). AMP-Activated Protein Kinase: A Target for Drugs both Ancient and Modern. *Chem. Biol.* *19*, 1222–1236.
- Haruta, T., Uno, T., Kawahara, J., Takano, A., Egawa, K., Sharma, P.M., Olefsky, J.M., and Kobayashi, M. (2000). A rapamycin-sensitive pathway down-regulates insulin signaling via phosphorylation and proteasomal degradation of insulin receptor substrate-1. *Mol. Endocrinol. Baltim. Md* *14*, 783–794.
- Hawley, S.A., Davison, M., Woods, A., Davies, S.P., Beri, R.K., Carling, D., and Hardie, D.G. (1996). Characterization of the AMP-activated protein kinase kinase from rat liver and identification of threonine 172 as the major site at which it phosphorylates AMP-activated protein kinase. *J. Biol. Chem.* *271*, 27879–27887.
- Hawley, S.A., Boudeau, J., Reid, J.L., Mustard, K.J., Udd, L., Makela, T.P., Alessi, D.R., and Hardie, D.G. (2003). Complexes between the LKB1 tumor suppressor, STRAD alpha/beta and MO25 alpha/beta are upstream kinases in the AMP-activated protein kinase cascade. *J Biol* *2*, 28.
- Hawley, S.A., Pan, D.A., Mustard, K.J., Ross, L., Bain, J., Edelman, A.M., Frenguelli, B.G., and Hardie, D.G. (2005). Calmodulin-dependent protein kinase kinase-beta is an alternative upstream kinase for AMP-activated protein kinase. *Cell Metab.* *2*, 9–19.
- Hawley, S.A., Ross, F.A., Chevtzoff, C., Green, K.A., Evans, A., Fogarty, S., Towler, M.C., Brown, L.J., Ogunbayo, O.A., Evans, A.M., et al. (2010). Use of cells expressing gamma subunit variants to identify diverse mechanisms of AMPK activation. *Cell Metab.* *11*, 554–565.
- Hawley, S.A., Fullerton, M.D., Ross, F.A., Schertzer, J.D., Chevtzoff, C., Walker, K.J., Peggie, M.W., Zibrova, D., Green, K.A., Mustard, K.J., et al. (2012). The ancient drug salicylate directly activates AMP-activated protein kinase. *Science* *336*, 918–922.
- Hawley, S.A., Ross, F.A., Gowans, G.J., Tibarewal, P., Leslie, N.R., and Hardie, D.G. (2014). Phosphorylation by Akt within the ST loop of AMPK-alpha1 down-regulates its activation in tumour cells. *Biochem J* *459*, 275–287.
- Herrero-Martín, G., Høyer-Hansen, M., García-García, C., Fumarola, C., Farkas, T., López-Rivas, A., and Jäättelä, M. (2009). TAK1 activates AMPK-dependent cytoprotective autophagy in TRAIL-treated epithelial cells. *EMBO J.* *28*, 677–685.
- Horie, T., Ono, K., Nishi, H., Nagao, K., Kinoshita, M., Watanabe, S., Kuwabara, Y., Nakashima, Y., Takanabe-Mori, R., Nishi, E., et al. (2010). Acute doxorubicin cardiotoxicity is associated with miR-146a-induced inhibition of the neuregulin-ErbB pathway. *Cardiovasc. Res.* *87*, 656–664.
- Horman, S., Vertommen, D., Heath, R., Neumann, D., Mouton, V., Woods, A., Schlattner, U., Wallimann, T., Carling, D., Hue, L., et al. (2006). Insulin antagonizes ischemia-induced Thr172 phosphorylation of AMP-activated protein kinase alpha-subunits in heart via hierarchical phosphorylation of Ser485/491. *J. Biol. Chem.* *281*, 5335–5340.
- Houde, V.P., Ritorto, M.S., Gourlay, R., Varghese, J., Davies, P., Shpiro, N., Sakamoto, K., and Alessi, D.R. (2014). Investigation of LKB1 Ser431 phosphorylation and Cys433 farnesylation using mouse knockin analysis reveals an unexpected role of prenylation in regulating AMPK activity. *Biochem J* *458*, 41–56.
- Hu, X., Xu, X., Lu, Z., Zhang, P., Fassett, J., Zhang, Y., Xin, Y., Hall, J.L., Viollet, B., Bache, R.J., et al. (2011). AMP activated protein kinase-alpha2 regulates expression of estrogen-related receptor-alpha, a metabolic transcription factor related to heart failure development. *Hypertension* *58*, 696–703.
- Huang, H.C., and Lin, J.K. (2012). Pu-erh tea, green tea, and black tea suppresses hyperlipidemia, hyperleptinemia and fatty acid synthase through activating AMPK in rats fed a high-fructose diet. *Food Funct* *3*, 170–177.

- Hurley, R.L., Anderson, K.A., Franzone, J.M., Kemp, B.E., Means, A.R., and Witters, L.A. (2005). The Ca²⁺/calmodulin-dependent protein kinase kinases are AMP-activated protein kinase kinases. *J Biol Chem* **280**, 29060–29066.
- Hurley, R.L., Barré, L.K., Wood, S.D., Anderson, K.A., Kemp, B.E., Means, A.R., and Witters, L.A. (2006). Regulation of AMP-activated protein kinase by multisite phosphorylation in response to agents that elevate cellular cAMP. *J. Biol. Chem.* **281**, 36662–36672.
- Ignoul, S., and Eggermont, J. (2005). CBS domains: structure, function, and pathology in human proteins. *Am. J. Physiol. - Cell Physiol.* **289**, C1369–C1378.
- Ikeda, Y., Sato, K., Pimentel, D.R., Sam, F., Shaw, R.J., Dyck, J.R., and Walsh, K. (2009). Cardiac-specific deletion of LKB1 leads to hypertrophy and dysfunction. *J Biol Chem* **284**, 35839–35849.
- Inoki, K., Li, Y., Xu, T., and Guan, K.-L. (2003). Rheb GTPase is a direct target of TSC2 GAP activity and regulates mTOR signaling. *Genes Dev.* **17**, 1829–1834.
- Inoki, K., Kim, J., and Guan, K.-L. (2012). AMPK and mTOR in Cellular Energy Homeostasis and Drug Targets. *Annu. Rev. Pharmacol. Toxicol.* **52**, 381–400.
- Jeon, S.-M., Chandel, N.S., and Hay, N. (2012). AMPK regulates NADPH homeostasis to promote tumour cell survival during energy stress. *Nature* **485**, 661–665.
- Kahn, B.B., Alquier, T., Carling, D., and Hardie, D.G. (2005). AMP-activated protein kinase: ancient energy gauge provides clues to modern understanding of metabolism. *Cell Metab* **1**, 15–25.
- Kang, S., Chemaly, E.R., Hajjar, R.J., and Lebeche, D. (2011). Resistin promotes cardiac hypertrophy via the AMP-activated protein kinase/mammalian target of rapamycin (AMPK/mTOR) and c-Jun N-terminal kinase/insulin receptor substrate 1 (JNK/IRS1) pathways. *J Biol Chem* **286**, 18465–18473.
- Kawaguchi, T., Takemura, G., Kanamori, H., Takeyama, T., Watanabe, T., Morishita, K., Ogino, A., Tsujimoto, A., Goto, K., Maruyama, R., et al. (2012). Prior starvation mitigates acute doxorubicin cardiotoxicity through restoration of autophagy in affected cardiomyocytes. *Cardiovasc Res* **96**, 456–465.
- Kazgan, N., Williams, T., Forsberg, L.J., and Brenman, J.E. (2010). Identification of a nuclear export signal in the catalytic subunit of AMP-activated protein kinase. *Mol Biol Cell* **21**, 3433–3442.
- Kehat, I., and Molkentin, J.D. (2010). Extracellular signal-regulated kinase 1/2 (ERK1/2) signaling in cardiac hypertrophy. *Ann. N. Y. Acad. Sci.* **1188**, 96–102.
- Kelly, M., Keller, C., Avilucea, P.R., Keller, P., Luo, Z., Xiang, X., Giralt, M., Hidalgo, J., Saha, A.K., Pedersen, B.K., et al. (2004). AMPK activity is diminished in tissues of IL-6 knockout mice: the effect of exercise. *Biochem Biophys Res Commun* **320**, 449–454.
- Kemp, B.E. (2004). Bateman domains and adenosine derivatives form a binding contract. *J. Clin. Invest.* **113**, 182–184.
- Kerrien, S., Aranda, B., Breuza, L., Bridge, A., Broackes-Carter, F., Chen, C., Duesbury, M., Dumousseau, M., Feuermann, M., Hinz, U., et al. (2012). The IntAct molecular interaction database in 2012. *Nucleic Acids Res.* **40**, D841–D846.
- Khalil, H., Peltzer, N., Walicki, J., Yang, J.-Y., Dubuis, G., Gardiol, N., Held, W., Bigliardi, P., Marsland, B., Liaudet, L., et al. (2012). Caspase-3 protects stressed organs against cell death. *Mol. Cell. Biol.* **32**, 4523–4533.
- Kim, T.T., and Dyck, J.R.B. (2014). Is AMPK the savior of the failing heart? *Trends Endocrinol. Metab.* **TEM**.
- Kim, A.S., Miller, E.J., and Young, L.H. (2009a). AMP-activated protein kinase: a core signalling pathway in the heart. *Acta Physiol.* **196**, 37–53.
- Kim, A.S., Miller, E.J., and Young, L.H. (2009b). AMP-activated protein kinase: a core signalling pathway in the heart. *Acta Physiol.* **196**, 37–53.
- Kim, A.S., Miller, E.J., Wright, T.M., Li, J., Qi, D., Atsina, K., Zaha, V., Sakamoto, K., and Young, L.H. (2011). A small molecule AMPK activator protects the heart against ischemia-reperfusion injury. *J Mol Cell Cardiol* **51**, 24–32.

- Kim, E.J., Lee, D.H., Kim, H.J., Lee, S.J., Ban, J.O., Cho, M.C., Jeong, H.S., Yang, Y., Hong, J.T., and Yoon do, Y. (2012a). Thiacremonone, a sulfur compound isolated from garlic, attenuates lipid accumulation partially mediated via AMPK activation in 3T3-L1 adipocytes. *J Nutr Biochem* 23, 1552–1558.
- Kim, M., Shen, M., Ngoy, S., Karamanlidis, G., Liao, R., and Tian, R. (2012b). AMPK isoform expression in the normal and failing hearts. *J. Mol. Cell. Cardiol.* 52, 1066–1073.
- Kim, M.-J., Jeon, D.S., Shin, D.I., and Lee, M.Y. (2010). ROLE OF AMP-ACTIVATED PROTEIN KINASE IN CARDIOPROTECTION IN DOXORUBICIN-INDUCED CARDIOMYOPATHY OF MICE. *J. Am. Coll. Cardiol.* 55, A31.E294–A31.E294.
- Kim, S.Y., Jeong, S., Jung, E., Baik, K.-H., Chang, M.H., Kim, S.A., Shim, J.-H., Chun, E., and Lee, K.-Y. (2012c). AMP-activated protein kinase- α 1 as an activating kinase of TGF- β -activated kinase 1 has a key role in inflammatory signals. *Cell Death Dis.* 3, e357.
- Klaus, A., Polge, C., Zorman, S., Auchli, Y., Brunisholz, R., and Schlattner, U. (2012). A two-dimensional screen for AMPK substrates identifies tumor suppressor fumarate hydratase as a preferential AMPK α 2 substrate. *J. Proteomics* 75, 3304–3313.
- Klaus, A., Zorman, S., Berthier, A., Polge, C., Ramirez, S., Michelland, S., Sève, M., Vertommen, D., Rider, M., Lentze, N., et al. (2013). Glutathione S-transferases interact with AMP-activated protein kinase: evidence for S-glutathionylation and activation in vitro. *PLoS One* 8, e62497.
- Ko, H.J., Zhang, Z., Jung, D.Y., Jun, J.Y., Ma, Z., Jones, K.E., Chan, S.Y., and Kim, J.K. (2009). Nutrient stress activates inflammation and reduces glucose metabolism by suppressing AMP-activated protein kinase in the heart. *Diabetes* 58, 2536–2546.
- Kobayashi, S., Volden, P., Timm, D., Mao, K., Xu, X., and Liang, Q. (2010). Transcription factor GATA4 inhibits doxorubicin-induced autophagy and cardiomyocyte death. *J. Biol. Chem.* 285, 793–804.
- Kola, B., Hubina, E., Tucci, S.A., Kirkham, T.C., Garcia, E.A., Mitchell, S.E., Williams, L.M., Hawley, S.A., Hardie, D.G., Grossman, A.B., et al. (2005). Cannabinoids and ghrelin have both central and peripheral metabolic and cardiac effects via AMP-activated protein kinase. *J. Biol. Chem.* 280, 25196–25201.
- Konishi, M., Haraguchi, G., Ohigashi, H., Ishihara, T., Saito, K., Nakano, Y., and Isobe, M. (2011). Adiponectin protects against doxorubicin-induced cardiomyopathy by anti-apoptotic effects through AMPK up-regulation. *Cardiovasc Res* 89, 309–319.
- Kovacic, S., Soltys, C.L., Barr, A.J., Shiojima, I., Walsh, K., and Dyck, J.R. (2003). Akt activity negatively regulates phosphorylation of AMP-activated protein kinase in the heart. *J Biol Chem* 278, 39422–39427.
- Kubli, D.A., and Gustafsson, A.B. (2014). Cardiomyocyte health: adapting to metabolic changes through autophagy. *Trends Endocrinol Metab* 25, 156–164.
- Kubota, N., Yano, W., Kubota, T., Yamauchi, T., Itoh, S., Kumagai, H., Kozono, H., Takamoto, I., Okamoto, S., Shiuchi, T., et al. (2007). Adiponectin stimulates AMP-activated protein kinase in the hypothalamus and increases food intake. *Cell Metab.* 6, 55–68.
- Kudo, N., Barr, A.J., Barr, R.L., Desai, S., and Lopaschuk, G.D. (1995). High rates of fatty acid oxidation during reperfusion of ischemic hearts are associated with a decrease in malonyl-CoA levels due to an increase in 5'-AMP-activated protein kinase inhibition of acetyl-CoA carboxylase. *J Biol Chem* 270, 17513–17520.
- Kudo, N., Gillespie, J.G., Kung, L., Witters, L.A., Schulz, R., Clanachan, A.S., and Lopaschuk, G.D. (1996). Characterization of 5'AMP-activated protein kinase activity in the heart and its role in inhibiting acetyl-CoA carboxylase during reperfusion following ischemia. *Biochim Biophys Acta* 1301, 67–75.
- Kulkarni, S.S., Karlsson, H.K.R., Szekeres, F., Chibalin, A.V., Krook, A., and Zierath, J.R. (2011). Suppression of 5'-nucleotidase enzymes promotes AMP-activated protein kinase (AMPK) phosphorylation and metabolism in human and mouse skeletal muscle. *J. Biol. Chem.* 286, 34567–34574.
- Kurth-Kraczek, E.J., Hirshman, M.F., Goodyear, L.J., and Winder, W.W. (1999). 5' AMP-activated protein kinase activation causes GLUT4 translocation in skeletal muscle. *Diabetes* 48, 1667–1671.
- Lantier, L., Fentz, J., Mounier, R., Leclerc, J., Treebak, J.T., Pehmøller, C., Sanz, N., Sakakibara, I., Saint-Amand, E., Rimbaud, S., et al. (2014). AMPK controls exercise endurance, mitochondrial oxidative capacity, and skeletal muscle integrity. *FASEB J. Off. Publ. Fed. Am. Soc. Exp. Biol.*

- Lee, E.-R., Kim, J.-Y., Kang, Y.-J., Ahn, J.-Y., Kim, J.-H., Kim, B.-W., Choi, H.-Y., Jeong, M.-Y., and Cho, S.-G. (2006). Interplay between PI3K/Akt and MAPK signaling pathways in DNA-damaging drug-induced apoptosis. *Biochim. Biophys. Acta* 1763, 958–968.
- Li, H.L., Yin, R., Chen, D., Liu, D., Wang, D., Yang, Q., and Dong, Y.G. (2007). Long-term activation of adenosine monophosphate-activated protein kinase attenuates pressure-overload-induced cardiac hypertrophy. *J Cell Biochem* 100, 1086–1099.
- Li, J., Miller, E.J., Ninomiya-Tsuji, J., Russell, R.R., and Young, L.H. (2005). AMP-activated protein kinase activates p38 mitogen-activated protein kinase by increasing recruitment of p38 MAPK to TAB1 in the ischemic heart. *Circ. Res.* 97, 872–879.
- Li, X., Wang, L., Zhou, X.E., Ke, J., de Waal, P.W., Gu, X., Tan, M.H.E., Wang, D., Wu, D., Xu, H.E., et al. (2014). Structural basis of AMPK regulation by adenine nucleotides and glycogen. *Cell Res.*
- Liao, C.-C., Ou, T.-T., Huang, H.-P., and Wang, C.-J. (2014). The inhibition of oleic acid induced hepatic lipogenesis and the promotion of lipolysis by caffeic acid via up-regulation of AMP-activated kinase. *J. Sci. Food Agric.* 94, 1154–1162.
- Loewith, R., Jacinto, E., Wullschleger, S., Lorberg, A., Crespo, J.L., Bonenfant, D., Oppliger, W., Jenoe, P., and Hall, M.N. (2002). Two TOR complexes, only one of which is rapamycin sensitive, have distinct roles in cell growth control. *Mol. Cell* 10, 457–468.
- Lou, H., Danelisen, I., and Singal, P.K. (2005). Involvement of mitogen-activated protein kinases in adriamycin-induced cardiomyopathy. *Am. J. Physiol. Heart Circ. Physiol.* 288, H1925–H1930.
- Luiken, J.J., Coort, S.L., Willems, J., Coumans, W.A., Bonen, A., van der Vusse, G.J., and Glatz, J.F. (2003). Contraction-induced fatty acid translocase/CD36 translocation in rat cardiac myocytes is mediated through AMP-activated protein kinase signaling. *Diabetes* 52, 1627–1634.
- Ma, H., Wang, J., Thomas, D.P., Tong, C., Leng, L., Wang, W., Merk, M., Zierow, S., Bernhagen, J., Ren, J., et al. (2010). Impaired macrophage migration inhibitory factor-AMP-activated protein kinase activation and ischemic recovery in the senescent heart. *Circulation* 122, 282–292.
- Mahlapuu, M., Johansson, C., Lindgren, K., Hjalm, G., Barnes, B.R., Krook, A., Zierath, J.R., Andersson, L., and Marklund, S. (2004). Expression profiling of the gamma-subunit isoforms of AMP-activated protein kinase suggests a major role for gamma3 in white skeletal muscle. *Am J Physiol Endocrinol Metab* 286, E194–E200.
- Makinde, A.O., Gamble, J., and Lopaschuk, G.D. (1997). Upregulation of 5'-AMP-activated protein kinase is responsible for the increase in myocardial fatty acid oxidation rates following birth in the newborn rabbit. *Circ. Res.* 80, 482–489.
- Marsin, A.-S., Bertrand, L., Rider, M.H., Deprez, J., Beauloye, C., Vincent, M.F., Van der Berghe, G., Carling, D., and Hue, L. (2000). Phosphorylation and activation of heart PFK-2 by AMPK has a role in the stimulation of glycolysis during ischaemia. *Curr. Biol.* 10, 1247–1255.
- Marsin, A.-S., Bouzin, C., Bertrand, L., and Hue, L. (2002). The Stimulation of Glycolysis by Hypoxia in Activated Monocytes Is Mediated by AMP-activated Protein Kinase and Inducible 6-Phosphofructo-2-kinase. *J. Biol. Chem.* 277, 30778–30783.
- McBride, A., Ghilagaber, S., Nikolaev, A., and Hardie, D.G. (2009). The glycogen-binding domain on the AMPK beta subunit allows the kinase to act as a glycogen sensor. *Cell Metab.* 9, 23–34.
- McGaffin, K.R., Moravec, C.S., and McTiernan, C.F. (2009). Leptin signaling in the failing and mechanically unloaded human heart. *Circ Heart Fail* 2, 676–683.
- McGee, S.L., Howlett, K.F., Starkie, R.L., Cameron-Smith, D., Kemp, B.E., and Hargreaves, M. (2003). Exercise Increases Nuclear AMPK α 2 in Human Skeletal Muscle. *Diabetes* 52, 926–928.
- McGee, S.L., Denderen, B.J.W. van, Howlett, K.F., Mollica, J., Schertzer, J.D., Kemp, B.E., and Hargreaves, M. (2008). AMP-Activated Protein Kinase Regulates GLUT4 Transcription by Phosphorylating Histone Deacetylase 5. *Diabetes* 57, 860–867.
- McInnes, K.J., Brown, K.A., Hunger, N.I., and Simpson, E.R. (2012). Regulation of LKB1 expression by sex hormones in adipocytes. *Int. J. Obes.* 2005 36, 982–985.

- Menna, P., Salvatorelli, E., Gianni, L., and Minotti, G. (2008). Anthracycline cardiotoxicity. *Top. Curr. Chem.* **283**, 21–44.
- Mihaylova, M.M., and Shaw, R.J. (2011). The AMPK signalling pathway coordinates cell growth, autophagy and metabolism. *Nat Cell Biol* **13**, 1016–1023.
- Miller, E.J., Li, J., Leng, L., McDonald, C., Atsumi, T., Bucala, R., and Young, L.H. (2008). Macrophage migration inhibitory factor stimulates AMP-activated protein kinase in the ischaemic heart. *Nature* **451**, 578–582.
- Minokoshi, Y., Kim, Y.-B., Peroni, O.D., Fryer, L.G.D., Müller, C., Carling, D., and Kahn, B.B. (2002). Leptin stimulates fatty-acid oxidation by activating AMP-activated protein kinase. *Nature* **415**, 339–343.
- Minokoshi, Y., Alquier, T., Furukawa, N., Kim, Y.-B., Lee, A., Xue, B., Mu, J., Fougère, F., Ferré, P., Birnbaum, M.J., et al. (2004). AMP-kinase regulates food intake by responding to hormonal and nutrient signals in the hypothalamus. *Nature* **428**, 569–574.
- Minotti, G., Menna, P., Salvatorelli, E., Cairo, G., and Gianni, L. (2004). Anthracyclines: molecular advances and pharmacologic developments in antitumor activity and cardiotoxicity. *Pharmacol. Rev.* **56**, 185–229.
- Minotti, G., Salvatorelli, E., and Menna, P. (2010). Pharmacological foundations of cardio-oncology. *J. Pharmacol. Exp. Ther.* **334**, 2–8.
- Moreno, D., Towler, M.C., Hardie, D.G., Knecht, E., and Sanz, P. (2010). The laforin-malin complex, involved in Lafora disease, promotes the incorporation of K63-linked ubiquitin chains into AMP-activated protein kinase beta subunits. *Mol. Biol. Cell* **21**, 2578–2588.
- Morrison, A., Yan, X., Tong, C., and Li, J. (2011). Acute rosiglitazone treatment is cardioprotective against ischemia-reperfusion injury by modulating AMPK, Akt, and JNK signaling in nondiabetic mice. *Am J Physiol Heart Circ Physiol* **301**, H895–H902.
- Mungai, P.T., Waypa, G.B., Jairaman, A., Prakriya, M., Dokic, D., Ball, M.K., and Schumacker, P.T. (2011). Hypoxia triggers AMPK activation through reactive oxygen species-mediated activation of calcium release-activated calcium channels. *Mol Cell Biol* **31**, 3531–3545.
- Musi, N., Hirshman, M.F., Nygren, J., Svanfeldt, M., Bavenholm, P., Rooyackers, O., Zhou, G., Williamson, J.M., Ljunqvist, O., Efendic, S., et al. (2002). Metformin increases AMP-activated protein kinase activity in skeletal muscle of subjects with type 2 diabetes. *Diabetes* **51**, 2074–2081.
- Musi, N., Hirshman, M.F., Arad, M., Xing, Y., Fujii, N., Pomerleau, J., Ahmad, F., Berul, C.I., Seidman, J.G., Tian, R., et al. (2005). Functional role of AMP-activated protein kinase in the heart during exercise. *FEBS Lett* **579**, 2045–2050.
- Nagata, D., Takeda, R., Sata, M., Satonaka, H., Suzuki, E., Nagano, T., and Hirata, Y. (2004). AMP-activated protein kinase inhibits angiotensin II-stimulated vascular smooth muscle cell proliferation. *Circulation* **110**, 444–451.
- Nakano, A., and Takashima, S. (2012). LKB1 and AMP-activated protein kinase: regulators of cell polarity. *Genes Cells Devoted Mol. Cell. Mech.* **17**, 737–747.
- Nakazato, M., Murakami, N., Date, Y., Kojima, M., Matsuo, H., Kangawa, K., and Matsukura, S. (2001). A role for ghrelin in the central regulation of feeding. *Nature* **409**, 194–198.
- Neumann, D., Suter, M., Tuerk, R., Riek, U., and Wallimann, T. (2007). Co-expression of LKB1, MO25alpha and STRADalpha in bacteria yield the functional and active heterotrimeric complex. *Mol Biotechnol* **36**, 220–231.
- Nojima, H., Tokunaga, C., Eguchi, S., Oshiro, N., Hidayat, S., Yoshino, K., Hara, K., Tanaka, N., Avruch, J., and Yonezawa, K. (2003). The mammalian target of rapamycin (mTOR) partner, raptor, binds the mTOR substrates p70 S6 kinase and 4E-BP1 through their TOR signaling (TOS) motif. *J. Biol. Chem.* **278**, 15461–15464.
- Oakhill, J.S., Chen, Z.-P., Scott, J.W., Steel, R., Castelli, L.A., Ling, N., Macaulay, S.L., and Kemp, B.E. (2010). β -Subunit myristoylation is the gatekeeper for initiating metabolic stress sensing by AMP-activated protein kinase (AMPK). *Proc. Natl. Acad. Sci. U. S. A.* **107**, 19237–19241.
- Oakhill, J.S., Steel, R., Chen, Z.-P., Scott, J.W., Ling, N., Tam, S., and Kemp, B.E. (2011). AMPK is a direct adenylate charge-regulated protein kinase. *Science* **332**, 1433–1435.

- Oliveira, S.M., Zhang, Y.H., Solis, R.S., Isackson, H., Bellahcene, M., Yavari, A., Pinter, K., Davies, J.K., Ge, Y., Ashrafian, H., et al. (2012). AMP-activated protein kinase phosphorylates cardiac troponin I and alters contractility of murine ventricular myocytes. *Circ Res* 110, 1192–1201.
- O'Neill, H.M., Maarbjerg, S.J., Crane, J.D., Jeppesen, J., Jørgensen, S.B., Schertzer, J.D., Shyroka, O., Kiens, B., van Denderen, B.J., Tarnopolsky, M.A., et al. (2011). AMP-activated protein kinase (AMPK) beta1beta2 muscle null mice reveal an essential role for AMPK in maintaining mitochondrial content and glucose uptake during exercise. *Proc. Natl. Acad. Sci. U. S. A.* 108, 16092–16097.
- O'Neill, H.M., Holloway, G.P., and Steinberg, G.R. (2013). AMPK regulation of fatty acid metabolism and mitochondrial biogenesis: Implications for obesity. *Mol. Cell. Endocrinol.* 366, 135–151.
- Paiva, M.A., Rutter-Locher, Z., Goncalves, L.M., Providencia, L.A., Davidson, S.M., Yellon, D.M., and Mocanu, M.M. (2011). Enhancing AMPK activation during ischemia protects the diabetic heart against reperfusion injury. *Am J Physiol Heart Circ Physiol* 300, H2123–H2134.
- Pang, T., Xiong, B., Li, J.-Y., Qiu, B.-Y., Jin, G.-Z., Shen, J.-K., and Li, J. (2007). Conserved α -Helix Acts as Autoinhibitory Sequence in AMP-activated Protein Kinase α Subunits. *J. Biol. Chem.* 282, 495–506.
- Pankuweit, S., Ruppert, V., and Maisch, B. (2004). Inflammation in dilated cardiomyopathy. *Herz* 29, 788–793.
- Park, S., Scheffler, T.L., Rossie, S.S., and Gerrard, D.E. (2013). AMPK activity is regulated by calcium-mediated protein phosphatase 2A activity. *Cell Calcium* 53, 217–223.
- Patten, I.S., and Arany, Z. (2012). PGC-1 coactivators in the cardiovascular system. *Trends Endocrinol. Metab.* TEM 23, 90–97.
- Bar-Peled, L., and Sabatini, D.M. (2014). Regulation of mTORC1 by amino acids. *Trends Cell Biol.* 24, 400–406.
- Pinter, K., Grignani, R.T., Czibik, G., Farza, H., Watkins, H., and Redwood, C. (2012). Embryonic expression of AMPK γ subunits and the identification of a novel γ 2 transcript variant in adult heart. *J. Mol. Cell. Cardiol.* 53, 342–349.
- Polekhina, G., Gupta, A., van Denderen, B.J.W., Feil, S.C., Kemp, B.E., Stapleton, D., and Parker, M.W. (2005). Structural basis for glycogen recognition by AMP-activated protein kinase. *Struct. Lond. Engl.* 1993 13, 1453–1462.
- Polge, C., Jossier, M., Crozet, P., Gissot, L., and Thomas, M. (2008). Beta-subunits of the SnRK1 complexes share a common ancestral function together with expression and function specificities; physical interaction with nitrate reductase specifically occurs via AKINbeta1-subunit. *Plant Physiol.* 148, 1570–1582.
- Qi, J., Gong, J., Zhao, T., Zhao, J., Lam, P., Ye, J., Li, J.Z., Wu, J., Zhou, H.-M., and Li, P. (2008). Downregulation of AMP-activated protein kinase by Cidea-mediated ubiquitination and degradation in brown adipose tissue. *EMBO J.* 27, 1537–1548.
- Quentin, T., Kitz, J., Steinmetz, M., Poppe, A., Bar, K., and Kratzner, R. (2011). Different expression of the catalytic alpha subunits of the AMP activated protein kinase—an immunohistochemical study in human tissue. *Histol Histopathol* 26, 589–596.
- Rana, S., Blowers, E.C., and Natarajan, A. (2014). Small Molecule Adenosine 5'-Monophosphate Activated Protein Kinase (AMPK) Modulators and Human Diseases. *J. Med. Chem.*
- Riek, U., Scholz, R., Konarev, P., Rufer, A., Suter, M., Nazabal, A., Ringler, P., Chami, M., Muller, S.A., Neumann, D., et al. (2008). Structural Properties of AMP-activated Protein Kinase: DIMERIZATION, MOLECULAR SHAPE, AND CHANGES UPON LIGAND BINDING. *J. Biol. Chem.* 283, 18331–18343.
- Ronnebaum, S.M., and Patterson, C. (2010). The FoxO family in cardiac function and dysfunction. *Annu. Rev. Physiol.* 72, 81–94.
- Ronnebaum, S.M., Patterson, C., and Schisler, J.C. (2014). Hey U(PS): Metabolic and Proteolytic Homeostasis Linked via AMPK and the Ubiquitin Proteasome System. *Mol Endocrinol* me20141180.
- Rubio, T., Vernia, S., and Sanz, P. (2013). Sumoylation of AMPKbeta2 subunit enhances AMP-activated protein kinase activity. *Mol Biol Cell* 24, 1801–1811, S1–S4.
- Russell, R., 3rd (2003). The Role of AMP-activated protein kinase in fuel selection by the stressed heart. *Curr Hypertens Rep* 5, 459–465.

- Russell, R.R., 3rd, Li, J., Coven, D.L., Pypaert, M., Zechner, C., Palmeri, M., Giordano, F.J., Mu, J., Birnbaum, M.J., and Young, L.H. (2004). AMP-activated protein kinase mediates ischemic glucose uptake and prevents postischemic cardiac dysfunction, apoptosis, and injury. *J Clin Invest* *114*, 495–503.
- Saks, V., Favier, R., Guzun, R., Schlattner, U., and Wallimann, T. (2006). Molecular system bioenergetics: regulation of substrate supply in response to heart energy demands. *J Physiol* *577*, 769–777.
- Salminen, A., Hyttinen, J.M., and Kaarniranta, K. (2011). AMP-activated protein kinase inhibits NF-kappaB signaling and inflammation: impact on healthspan and lifespan. *J Mol Med Berl* *89*, 667–676.
- Salt, I.P., and Palmer, T.M. (2012). Exploiting the anti-inflammatory effects of AMP-activated protein kinase activation. *Expert Opin Investig Drugs* *21*, 1155–1167.
- Salt, I., Celler, J.W., Hawley, S.A., Prescott, A., Woods, A., Carling, D., and Hardie, D.G. (1998a). AMP-activated protein kinase: greater AMP dependence, and preferential nuclear localization, of complexes containing the alpha2 isoform. *Biochem. J.* *334 (Pt 1)*, 177–187.
- Salt, I.P., Johnson, G., Ashcroft, S.J., and Hardie, D.G. (1998b). AMP-activated protein kinase is activated by low glucose in cell lines derived from pancreatic beta cells, and may regulate insulin release. *Biochem. J.* *335 (Pt 3)*, 533–539.
- Sancak, Y., Peterson, T.R., Shaul, Y.D., Lindquist, R.A., Thoreen, C.C., Bar-Peled, L., and Sabatini, D.M. (2008). The Rag GTPases bind raptor and mediate amino acid signaling to mTORC1. *Science* *320*, 1496–1501.
- Sanders, M.J., Grondin, P.O., Hegarty, B.D., Snowden, M.A., and Carling, D. (2007a). Investigating the mechanism for AMP activation of the AMP-activated protein kinase cascade. *Biochem. J.* *403*, 139–148.
- Sanders, M.J., Ali, Z.S., Hegarty, B.D., Heath, R., Snowden, M.A., and Carling, D. (2007b). Defining the mechanism of activation of AMP-activated protein kinase by the small molecule A-769662, a member of the thienopyridone family. *J Biol Chem* *282*, 32539–32548.
- Sartoretto, J.L., Kalwa, H., Pluth, M.D., Lippard, S.J., and Michel, T. (2011). Hydrogen peroxide differentially modulates cardiac myocyte nitric oxide synthesis. *Proc Natl Acad Sci U S A* *108*, 15792–15797.
- Sasaki, H., Asanuma, H., Fujita, M., Takahama, H., Wakeno, M., Ito, S., Ogai, A., Asakura, M., Kim, J., Minamino, T., et al. (2009). Metformin prevents progression of heart failure in dogs: role of AMP-activated protein kinase. *Circulation* *119*, 2568–2577.
- Schilling, J., and Kelly, D.P. (2011). The PGC-1 cascade as a therapeutic target for heart failure. *J. Mol. Cell. Cardiol.* *51*, 578–583.
- Schlattner, U., Tokarska-Schlattner, M., and Wallimann, T. (2006). Mitochondrial creatine kinase in human health and disease. *Biochim Biophys Acta* *1762*, 164–180.
- Scott, J.W., Hawley, S.A., Green, K.A., Anis, M., Stewart, G., Scullion, G.A., Norman, D.G., and Hardie, D.G. (2004). CBS domains form energy-sensing modules whose binding of adenosine ligands is disrupted by disease mutations. *J. Clin. Invest.* *113*, 274–284.
- Scott, J.W., van Denderen, B.J.W., Jorgensen, S.B., Honeyman, J.E., Steinberg, G.R., Oakhill, J.S., Iseli, T.J., Koay, A., Gooley, P.R., Stapleton, D., et al. (2008). Thienopyridone drugs are selective activators of AMP-activated protein kinase beta1-containing complexes. *Chem. Biol.* *15*, 1220–1230.
- Scott, J.W., Ling, N., Issa, S.M.A., Dite, T.A., O'Brien, M.T., Chen, Z.-P., Galic, S., Langendorf, C.G., Steinberg, G.R., Kemp, B.E., et al. (2014). Small Molecule Drug A-769662 and AMP Synergistically Activate Naive AMPK Independent of Upstream Kinase Signaling. *Chem. Biol.*
- Sebbagh, M., Santoni, M.-J., Hall, B., Borg, J.-P., and Schwartz, M.A. (2009). Regulation of LKB1/STRAD localization and function by E-cadherin. *Curr. Biol. CB* *19*, 37–42.
- Shaw, R.J. (2009). LKB1 and AMP-activated protein kinase control of mTOR signalling and growth. *Acta Physiol.* *196*, 65–80.
- Shaw, R.J., Kosmatka, M., Bardeesy, N., Hurley, R.L., Witters, L.A., DePinho, R.A., and Cantley, L.C. (2004). The tumor suppressor LKB1 kinase directly activates AMP-activated kinase and regulates apoptosis in response to energy stress. *Proc. Natl. Acad. Sci. U. S. A.* *101*, 3329–3335.

- Shen, C.H., Yuan, P., Perez-Lorenzo, R., Zhang, Y., Lee, S.X., Ou, Y., Asara, J.M., Cantley, L.C., and Zheng, B. (2013). Phosphorylation of BRAF by AMPK impairs BRAF-KSR1 association and cell proliferation. *Mol Cell* 52, 161–172.
- Shibata, R., Ouchi, N., Kihara, S., Sato, K., Funahashi, T., and Walsh, K. (2004). Adiponectin stimulates angiogenesis in response to tissue ischemia through stimulation of amp-activated protein kinase signaling. *J Biol Chem* 279, 28670–28674.
- Shibata, R., Sato, K., Pimentel, D.R., Takemura, Y., Kihara, S., Ohashi, K., Funahashi, T., Ouchi, N., and Walsh, K. (2005). Adiponectin protects against myocardial ischemia-reperfusion injury through AMPK- and COX-2-dependent mechanisms. *Nat Med* 11, 1096–1103.
- Shinmura, K., Tamaki, K., Saito, K., Nakano, Y., Tobe, T., and Bolli, R. (2007). Cardioprotective effects of short-term caloric restriction are mediated by adiponectin via activation of AMP-activated protein kinase. *Circulation* 116, 2809–2817.
- Soltys, C.L., Kovacic, S., and Dyck, J.R. (2006). Activation of cardiac AMP-activated protein kinase by LKB1 expression or chemical hypoxia is blunted by increased Akt activity. *Am J Physiol Heart Circ Physiol* 290, H2472–H2479.
- Srivastava, R.A.K., Pinkosky, S.L., Filippov, S., Hanselman, J.C., Cramer, C.T., and Newton, R.S. (2012). AMP-activated protein kinase: an emerging drug target to regulate imbalances in lipid and carbohydrate metabolism to treat cardio-metabolic diseases Thematic Review Series: New Lipid and Lipoprotein Targets for the Treatment of Cardiometabolic Diseases. *J. Lipid Res.* 53, 2490–2514.
- Stapleton, D., Mitchelhill, K.I., Gao, G., Widmer, J., Michell, B.J., Teh, T., House, C.M., Fernandez, C.S., Cox, T., Witters, L.A., et al. (1996). Mammalian AMP-activated protein kinase subfamily. *J. Biol. Chem.* 271, 611–614.
- Steinberg, G.R. (2013). AMPK and the endocrine control of energy metabolism. *Mol. Cell. Endocrinol.* 366, 125–126.
- Steinberg, G.R., and Kemp, B.E. (2009). AMPK in Health and Disease. *Physiol. Rev.* 89, 1025–1078.
- Steinberg, G.R., Michell, B.J., van Denderen, B.J.W., Watt, M.J., Carey, A.L., Fam, B.C., Andrikopoulos, S., Proietto, J., Görgün, C.Z., Carling, D., et al. (2006). Tumor necrosis factor alpha-induced skeletal muscle insulin resistance involves suppression of AMP-kinase signaling. *Cell Metab.* 4, 465–474.
- Strogolova, V., Orlova, M., Shevade, A., and Kuchin, S. (2012). Mitochondrial porin Por1 and its homolog Por2 contribute to the positive control of Snf1 protein kinase in *Saccharomyces cerevisiae*. *Eukaryot. Cell* 11, 1568–1572.
- Sukhodub, A., Jovanovic, S., Du, Q., Budas, G., Clelland, A.K., Shen, M., Sakamoto, K., Tian, R., and Jovanovic, A. (2007). AMP-activated protein kinase mediates preconditioning in cardiomyocytes by regulating activity and trafficking of sarcolemmal ATP-sensitive K(+) channels. *J Cell Physiol* 210, 224–236.
- Sussman, M.A., Völkers, M., Fischer, K., Bailey, B., Cottage, C.T., Din, S., Gude, N., Avitabile, D., Alvarez, R., Sundararaman, B., et al. (2011). Myocardial AKT: the omnipresent nexus. *Physiol. Rev.* 91, 1023–1070.
- Suter, M., Riek, U., Tuerk, R., Schlattner, U., Wallimann, T., and Neumann, D. (2006). Dissecting the Role of 5'-AMP for Allosteric Stimulation, Activation, and Deactivation of AMP-activated Protein Kinase. *J. Biol. Chem.* 281, 32207–32216.
- Suzuki, A., Okamoto, S., Lee, S., Saito, K., Shiuchi, T., and Minokoshi, Y. (2007). Leptin stimulates fatty acid oxidation and peroxisome proliferator-activated receptor alpha gene expression in mouse C2C12 myoblasts by changing the subcellular localization of the alpha2 form of AMP-activated protein kinase. *Mol. Cell. Biol.* 27, 4317–4327.
- Suzuki, T., Bridges, D., Nakada, D., Skiniotis, G., Morrison, S.J., Lin, J.D., Saltiel, A.R., and Inoki, K. (2013). Inhibition of AMPK catabolic action by GSK3. *Mol Cell* 50, 407–419.
- Terai, K., Hiramoto, Y., Masaki, M., Sugiyama, S., Kuroda, T., Hori, M., Kawase, I., and Hirota, H. (2005). AMP-activated protein kinase protects cardiomyocytes against hypoxic injury through attenuation of endoplasmic reticulum stress. *Mol Cell Biol* 25, 9554–9575.
- Thornton, C., Snowden, M.A., and Carling, D. (1998). Identification of a novel AMP-activated protein kinase beta subunit isoform that is highly expressed in skeletal muscle. *J. Biol. Chem.* 273, 12443–12450.

- Tian, R., Musi, N., D'Agostino, J., Hirshman, M.F., and Goodyear, L.J. (2001). Increased adenosine monophosphate-activated protein kinase activity in rat hearts with pressure-overload hypertrophy. *Circulation* 104, 1664–1669.
- Tokarska-Schlattner, M., Zaugg, M., da Silva, R., Lucchinetti, E., Schaub, M.C., Wallimann, T., and Schlattner, U. (2005). Acute toxicity of doxorubicin on isolated perfused heart: response of kinases regulating energy supply. *Am J Physiol Heart Circ Physiol* 289, H37–H47.
- Tokarska-Schlattner, M., Lucchinetti, E., Zaugg, M., Kay, L., Gratia, S., Guzun, R., Saks, V., and Schlattner, U. (2010). Early effects of doxorubicin in perfused heart: transcriptional profiling reveals inhibition of cellular stress response genes. *Am J Physiol Regul Integr Comp Physiol* 298, R1075–R1088.
- Townley, R., and Shapiro, L. (2007). Crystal structures of the adenylate sensor from fission yeast AMP-activated protein kinase. *Science* 315, 1726–1729.
- Treebak, J.T., Birk, J.B., Hansen, B.F., Olsen, G.S., and Wojtaszewski, J.F.P. (2009). A-769662 activates AMPK beta1-containing complexes but induces glucose uptake through a PI3-kinase-dependent pathway in mouse skeletal muscle. *Am. J. Physiol. Cell Physiol.* 297, C1041–C1052.
- Vincent, O., and Carlson, M. (1999). Gal83 mediates the interaction of the Snf1 kinase complex with the transcription activator Sip4. *EMBO J.* 18, 6672–6681.
- Viollet, B., Athea, Y., Mounier, R., Guigas, B., Zarrinpashneh, E., Horman, S., Lantier, L., Hebrard, S., Devin-Leclerc, J., Beauloye, C., et al. (2009). AMPK: Lessons from transgenic and knockout animals. *Front. Biosci. Landmark Ed.* 14, 19.
- Viollet, B., Foretz, M., and Schlattner, U. (2014). Bypassing AMPK phosphorylation. *Chem. Biol.* 21, 567–569.
- Wallimann, T., Tokarska-Schlattner, M., and Schlattner, U. (2011). The creatine kinase system and pleiotropic effects of creatine. *Amino Acids* 40, 1271–1296.
- Wang, L., and Brautigan, D.L. (2013). α -SNAP inhibits AMPK signaling to reduce mitochondrial biogenesis and dephosphorylates Thr172 in AMPK α in vitro. *Nat. Commun.* 4, 1559.
- Wang, M., and Unger, R.H. (2005). Role of PP2C in cardiac lipid accumulation in obese rodents and its prevention by troglitazone. *Am. J. Physiol. Endocrinol. Metab.* 288, E216–E221.
- Wang, J., Ma, H., Zhang, X., He, L., Wu, J., Gao, X., Ren, J., and Li, J. (2009). A novel AMPK activator from Chinese herb medicine and ischemia phosphorylate the cardiac transcription factor FOXO3. *Int J Physiol Pathophysiol Pharmacol* 1, 116–126.
- Wang, S., Song, P., and Zou, M.H. (2012a). AMP-activated protein kinase, stress responses and cardiovascular diseases. *Clin. Sci.* 122, 555–573.
- Wang, S., Song, P., and Zou, M.H. (2012b). Inhibition of AMP-activated protein kinase alpha (AMPKalpha) by doxorubicin accentuates genotoxic stress and cell death in mouse embryonic fibroblasts and cardiomyocytes: role of p53 and SIRT1. *J Biol Chem* 287, 8001–8012.
- Watt, M.J., Dzamko, N., Thomas, W.G., Rose-John, S., Ernst, M., Carling, D., Kemp, B.E., Febbraio, M.A., and Steinberg, G.R. (2006). CNTF reverses obesity-induced insulin resistance by activating skeletal muscle AMPK. *Nat Med* 12, 541–548.
- Winder, W.W., and Hardie, D.G. (1996). Inactivation of acetyl-CoA carboxylase and activation of AMP-activated protein kinase in muscle during exercise. *Am. J. Physiol. - Endocrinol. Metab.* 270, E299–E304.
- Winder, W.W., and Hardie, D.G. (1999). AMP-activated protein kinase, a metabolic master switch: possible roles in type 2 diabetes. *Am. J. Physiol.* 277, E1–E10.
- Wolff, N.C., Vega-Rubin-de-Celis, S., Xie, X.-J., Castrillon, D.H., Kabbani, W., and Brugarolas, J. (2011). Cell-type-dependent regulation of mTORC1 by REDD1 and the tumor suppressors TSC1/TSC2 and LKB1 in response to hypoxia. *Mol. Cell. Biol.* 31, 1870–1884.
- Woods, A., Johnstone, S.R., Dickerson, K., Leiper, F.C., Fryer, L.G.D., Neumann, D., Schlattner, U., Wallimann, T., Carlson, M., and Carling, D. (2003). LKB1 is the upstream kinase in the AMP-activated protein kinase cascade. *Curr. Biol. CB* 13, 2004–2008.

- Woods, A., Dickerson, K., Heath, R., Hong, S.-P., Momcilovic, M., Johnstone, S.R., Carlson, M., and Carling, D. (2005). Ca²⁺/calmodulin-dependent protein kinase kinase- β acts upstream of AMP-activated protein kinase in mammalian cells. *Cell Metab.* 2, 21–33.
- Wu, Y., Song, P., Xu, J., Zhang, M., and Zou, M.-H. (2007). Activation of protein phosphatase 2A by palmitate inhibits AMP-activated protein kinase. *J. Biol. Chem.* 282, 9777–9788.
- Xiao, B., Heath, R., Saiu, P., Leiper, F.C., Leone, P., Jing, C., Walker, P.A., Haire, L., Eccleston, J.F., Davis, C.T., et al. (2007). Structural basis for AMP binding to mammalian AMP-activated protein kinase. *Nature* 449, 496–500.
- Xiao, B., Sanders, M.J., Underwood, E., Heath, R., Mayer, F.V., Carmena, D., Jing, C., Walker, P.A., Eccleston, J.F., Haire, L.F., et al. (2011). Structure of mammalian AMPK and its regulation by ADP. *Nature* 472, 230–233.
- Xiao, B., Sanders, M.J., Carmena, D., Bright, N.J., Haire, L.F., Underwood, E., Patel, B.R., Heath, R.B., Walker, P.A., Hallen, S., et al. (2013a). Structural basis of AMPK regulation by small molecule activators. *Nat. Commun.* 4, 3017.
- Xiao, B., Sanders, M.J., Carmena, D., Bright, N.J., Haire, L.F., Underwood, E., Patel, B.R., Heath, R.B., Walker, P.A., Hallen, S., et al. (2013b). Structural basis of AMPK regulation by small molecule activators. *Nat Commun* 4, 3017.
- Xie, M., Zhang, D., Dyck, J.R., Li, Y., Zhang, H., Morishima, M., Mann, D.L., Taffet, G.E., Baldini, A., Khoury, D.S., et al. (2006a). A pivotal role for endogenous TGF- β -activated kinase-1 in the LKB1/AMP-activated protein kinase energy-sensor pathway. *Proc Natl Acad Sci U S A* 103, 17378–17383.
- Xie, Z., Dong, Y., Zhang, M., Cui, M.Z., Cohen, R.A., Riek, U., Neumann, D., Schlattner, U., and Zou, M.H. (2006b). Activation of protein kinase C zeta by peroxynitrite regulates LKB1-dependent AMP-activated protein kinase in cultured endothelial cells. *J Biol Chem* 281, 6366–6375.
- Yang, H.J., Jang, D.-J., and Hwang, J.-T. (2012). Anti-diabetic effects of Korean red pepper via AMPK and PPAR- γ activation in C2C12 myotubes. *J. Funct. Foods* 4, 552–558.
- Young, L.H. (2008). AMP-activated protein kinase conducts the ischemic stress response orchestra. *Circulation* 117, 832–840.
- Yun, H., and Ha, J. (2011). AMP-activated protein kinase modulators: a patent review (2006 – 2010). *Expert Opin. Ther. Pat.* 21, 983–1005.
- Zaha, V.G., and Young, L.H. (2012a). AMP-activated protein kinase regulation and biological actions in the heart. *Circ Res* 111, 800–814.
- Zaha, V.G., and Young, L.H. (2012b). AMP-activated protein kinase regulation and biological actions in the heart. *Circ Res* 111, 800–814.
- Zhang, B.B., Zhou, G., and Li, C. (2009). AMPK: An Emerging Drug Target for Diabetes and the Metabolic Syndrome. *Cell Metab.* 9, 407–416.
- Zhang, C.S., Jiang, B., Li, M., Zhu, M., Peng, Y., Zhang, Y.L., Wu, Y.Q., Li, T.Y., Liang, Y., Lu, Z., et al. (2014). The Lysosomal v-ATPase-Ragulator Complex Is a Common Activator for AMPK and mTORC1, Acting as a Switch between Catabolism and Anabolism. *Cell Metab* 20, 526–540.
- Zhang, P., Hu, X., Xu, X., Fassett, J., Zhu, G., Viollet, B., Xu, W., Wiczer, B., Bernlohr, D.A., Bache, R.J., et al. (2008). AMP activated protein kinase- α 2 deficiency exacerbates pressure-overload-induced left ventricular hypertrophy and dysfunction in mice. *Hypertension* 52, 918–924.
- Zhang, Y.L., Guo, H., Zhang, C.S., Lin, S.Y., Yin, Z., Peng, Y., Luo, H., Shi, Y., Lian, G., Zhang, C., et al. (2013). AMP as a low-energy charge signal autonomously initiates assembly of AXIN-AMPK-LKB1 complex for AMPK activation. *Cell Metab* 18, 546–555.
- Zheng, B., Jeong, J.H., Asara, J.M., Yuan, Y.Y., Granter, S.R., Chin, L., and Cantley, L.C. (2009). Oncogenic B-RAF negatively regulates the tumor suppressor LKB1 to promote melanoma cell proliferation. *Mol Cell* 33, 237–247.
- Zhu, L., Chen, L., Zhou, X.-M., Zhang, Y.-Y., Zhang, Y.-J., Zhao, J., Ji, S.-R., Wu, J.-W., and Wu, Y. (2011). Structural Insights into the Architecture and Allostery of Full-Length AMP-Activated Protein Kinase. *Structure* 19, 515–522.

Zmijewski, J.W., Banerjee, S., Bae, H., Friggeri, A., Lazarowski, E.R., and Abraham, E. (2010). Exposure to hydrogen peroxide induces oxidation and activation of AMP-activated protein kinase. *J Biol Chem* 285, 33154–33164.

Zou, M.H., Hou, X.Y., Shi, C.M., Nagata, D., Walsh, K., and Cohen, R.A. (2002). Modulation by peroxynitrite of Akt- and AMP-activated kinase-dependent Ser1179 phosphorylation of endothelial nitric oxide synthase. *J Biol Chem* 277, 32552–32557.

Zou, M.H., Kirkpatrick, S.S., Davis, B.J., Nelson, J.S., Wiles, W.G. th, Schlattner, U., Neumann, D., Brownlee, M., Freeman, M.B., and Goldman, M.H. (2004). Activation of the AMP-activated protein kinase by the anti-diabetic drug metformin in vivo. Role of mitochondrial reactive nitrogen species. *J Biol Chem* 279, 43940–43951.

Abbott Laboratories. Preparation of substituted thieno[2,3-b]pyridones as activators for AMP-activated kinase for the treatment of diabetes and obesity. 2005; US20050038068.

Introduction 2

Genetically encoded fluorescent biosensors to explore energy metabolism in single cells in space and time

1. Introduction	51
2. Genetically encoded fluorescent biosensors	52
3. Conventional techniques to study cell energetics	63
4. Designing genetically encoded fluorescent biosensors to study cell energetics	65
5. Calcium	68
6. PKA activity reporter and derived biosensor	70
7. Adenine nucleotides	71
8. NADH	78
9. Other metabolites.....	81
10. AMPK	81
11. Summary	83
12. References.....	85

Abstract. To ensure their functions while living on, cells have to maintain their energy homeostasis, notably by balancing energy-requiring processes with energy-producing ones, i.e. their energy metabolism. A key-feature of pathological cells consists in the loss of their ability to preserve this homeostasis. Thus monitoring the cellular energy metabolism in order to better understand its intricate regulation will provide crucial insights for the treatment of many diseases. Within the toolkit for exploring cellular energy metabolism, genetically encoded fluorescent biosensors are of prime importance. They represent a non-invasive *in vivo* method and are designed to follow, in time and space, a parameter of interest. At the beginning chapter, the working principles of these probes for the energy metabolism are presented and the limitations of conventionally used techniques are discussed. Then, available genetically encoded fluorescent biosensors dedicated to the monitoring of key parameters of the energy metabolism are described and discussed.

Résumé. Pour assurer leurs fonctions tout en perdurant, les cellules doivent maintenir leur homéostasie énergétique, notamment en équilibrant catabolisme (production d'énergie) et anabolisme (consommation d'énergie), i.e. leur métabolisme énergétique. Une signature caractéristique des cellules en état pathologique consiste en la perte de leur capacité à préserver cette homéostasie. Donc, suivre en temps réel et dans l'espace le métabolisme énergétique cellulaire afin d'en comprendre les mécanismes apparait crucial pour la recherche de traitements contre de nombreuses pathologies. Les biosenseurs fluorescents et codés génétiquement représentent des méthodes de choix pour l'exploration du métabolisme énergétique car ils sont non-invasifs et dédiés au suivi particulier d'un paramètre d'intérêt. Les principes de fonctionnement de ces sondes pour l'étude du métabolisme énergétique ainsi que les limitations des techniques conventionnelles seront présentés au début de ce chapitre. Seront ensuite présentés et discutés les biosenseurs existants et dédiés au monitoring de paramètres clés du métabolisme énergétique.

1. Introduction

A basic requirement of life is the constant input of energy. At the cellular level, ATP-consuming anabolic processes have to be constantly balanced with ATP-producing catabolic processes to maintain energy homeostasis. An inability to maintain this homeostasis is a hallmark of many otherwise unrelated pathologies. Thus, closely monitoring cellular energetics can inform about pathological processes and their modulation by drugs or other treatments.

Given the complexity of the cellular metabolic network, macro-parameters like cellular adenylates levels (ATP, ADP, AMP) are the most appropriate to describe cellular energetics. Classically, adenylates are quantified by biochemical methods in cellular extracts via HPLC separation or, in case of ATP, by luminescence assays (Tseng and Kung, 2015). However, this approach has a poor spatial and temporal resolution. Using non-invasive nuclear magnetic resonance (NMR) in tissue or cell samples increases temporal resolution, but is still unable to detect sub-cellular events unless working on isolated purified organelles (Gout et al., 2014). This becomes a considerable limitation when studying metabolism and its regulation at a systems level within a cell or tissue. It is widely accepted now that cells are not only heterogeneous in their physical structure, including highly complex membrane systems and multi-protein complexes, but that also cell metabolism and signaling are far from being homogeneously distributed within the cell (Tsou et al., 2011). A true understanding of cell metabolism thus requires non-invasive *in vivo* methods that allow tracing of metabolic changes at a micrometer scale and in real time. This type of approach also yields the quantitative information needed for the development of predictive mathematical models. Describing cell function by such models is a prime goal of systems biology, and obtaining the appropriate, high quality, time- and space-resolved quantitative data still represents a bottleneck for systems approaches (Huang, 2011).

A convenient way to monitor cellular parameters is the use of environment-sensitive fluorescent dyes. Ratiometric fluorescent probes have proven their versatility in cell biology since decades, whether they monitor concentration changes like e.g. of calcium (Miyawaki et al., 1999), or biophysical parameters like membrane potential (Kuznetsov et al., 2005). During recent years, genetically encoded fluorescent biosensors are emerging as another

tool of choice. Such protein sensors allow application of classical protein engineering to generate the required sensitivities and specificities, and mostly exploit Fluorescence (or Förster) Energy Transfer (FRET) between two appropriate fluorophores. However, also biosensors based on a single fluorophore are possible. This review summarizes available sensors and their advantages as compared to conventional techniques, and describes their increasing application for monitoring cell energetics and related parameters.

2. Genetically encoded fluorescent biosensors

Biosensors are devices based on a biological element such as macromolecules or even cells, which detect a specific analyte. When the biosensor interacts with the compound for which it has been designed, a measurable signal is produced. Because sensing elements, notably for energy metabolism, are already present in nature, it is obvious that development of biosensor should be bio-inspired. As generally understood, a genetically encoded biosensor is a molecular system which uses a macromolecular domain expressed by the cellular machinery (protein or RNA) as a biological recognition element for detection of the metabolic/biological event. Fluorescent genetically encoded biosensors are based on protein containing the recognition element together with at least one fluorescent protein tag. They are capable to convert the analyte detection into a fluorescence signal.

Genetically encoded biosensors represent a convenient, non-invasive way for monitoring signals within living cells, and an increasing number of such sensors for detecting different kinds of molecular events has been developed and applied during recent years (Palmer et al., 2011). Since they are produced by the cellular protein synthesis machinery, they can be used for sensing applications in cell culture, tissues or even animals (Kamioka et al., 2013). They offer numerous advantages, such as the possibility to engineer and optimize specificity and affinity for the given biomolecule, and to target them to specific subcellular compartments, protein complexes or membranes. In principle, they can offer high spatial resolution and versatility.

In addition, genetically encoded biosensors, by principle, can be transfected avoiding the stress generation and metabolism alteration that may be triggered by the direct loading of non-encoded biosensors onto cells.

The biosensor field has been driven by the successful introduction of a large variety of Green Fluorescent Proteins (GFP) in combination with FRET. FRET-based biosensors contain a recognition element fused to a couple of fluorescent proteins presenting overlapping excitation and emission spectra and thus capable of showing FRET. The sensing mechanism may then consist in binding or dissociation of a biomolecule or a covalent modification of the sensor, but in any case has to trigger changes in conformation, intramolecular domain interactions or oligomeric structure of the sensor that alters the distance between the two fluorophores and thus translates the primary signal into a change in FRET.

Two-fluorophore biosensors: fluorescence resonance energy transfer. The theory of resonance energy transfer was originally developed by Theodor Förster. It takes place between two different fluorophores, donor and acceptor, where the emission spectrum of the donor overlaps with the excitation spectrum of the acceptor. FRET occurs through non-radiative dipole–dipole coupling and leads to quenching of donor fluorescence and reduction of its fluorescence lifetime, accompanied by an increase in acceptor fluorescence emission. All these parameters can be exploited for detection. FRET efficiency is inversely proportional to the sixth power of the distance between donor and acceptor. This makes FRET extremely sensitive to small changes in a distance range between 2 and 8 nm (Figure 1), a distance range relevant to intramolecular conformational changes. It can thus be used as a sort of molecular ruler, as shown e.g. by using precision spectroscopic approaches in structural biology (Mekler et al., 2002). However, for most applications in cell biology, the given signal-to-noise ratios limit FRET experiments to a more binary readout, distinguishing high-FRET and low-FRET situations. Experimentally, FRET is here usually quantified by the ratio between acceptor and donor emission peaks, but fluorescence lifetime is increasingly exploited as a more reliable readout.

In addition to distance, there are other parameters affecting FRET that can be used to optimize a FRET biosensor. These include the region of overlap between donor and acceptor spectra, as well as the quantum yield of the donor and the extinction coefficient of the

acceptor. Thus, FRET can be maximized by choosing a fluorophore couple having significant overlap in their spectral profiles, including a donor of highest quantum yield and an acceptor with highest absorbance. Further, FRET coupling depends on the angle between the two fluorophores, i.e. donor emission moment dipole and acceptor absorption dipole moment, similar as the position of a radio antenna can affect its reception. If the donor and acceptor are aligned parallel to each other, FRET efficiency will be higher than if they are oriented perpendicular. It is generally difficult to optimize this parameter experimentally, although fluorophores rigidly fused to the protein of interest may have dramatic effects (Piljić et al., 2011). Thus, unlike radiative mechanisms, FRET can yield structural information about the donor and acceptor pair. The surrounding solvent does not alter FRET but can have major impact on spectral properties of donor and acceptor fluorophores and thus indirectly affect FRET. This is a major issue to be verified for a given FRET measurement, as shown e.g. for pH-effects on YFP (yellow fluorescence protein) fluorescence by Willemse et al. (Willemse et al., 2007).

Fluorescence lifetime imaging. Every fluorescent molecules show an exponential decay in their fluorescence and the rate of this exponential decay is sensitive to changes in the environment which quench the fluorescence. The fluorescence lifetime defines the average amount of time that a molecule spends in the excited state upon absorption of exciting photon. Thus, the basic concept of FLIM is related to that of acceptor photobleaching. The donor fluorescence is quenched by FRET, and the amount of quenching can be determined by measuring the shortening of the fluorescence decay time of the donor in the presence of FRET. In this manner, FLIM gives an unambiguous value of the FRET efficiency. Thus, in FLIM this is the lifetime of the fluorophore signal rather than its intensity that it monitored. The advantage of measuring the fluorescence lifetime of chromophores is that this parameter is directly dependent upon excited-state reactions but independent of chromophore concentration and light-path length, parameters that are difficult to control inside a cell. Fluorescence lifetime image acquisition is also rapid enough to make measurements in live cells feasible. By means of measurements of excited-state reactions using FLIM parameters such as pH (Sanders et al., 1995), Ca^{2+} (Lakowicz et al., 1994) concentration and proteolytic processing (Bastiaens and Jovin, 1996) have been studied. This microscopic technique has

been described for both the time- and frequency-domain for confocal microscopy (Bastiaens and Squire, 1999).

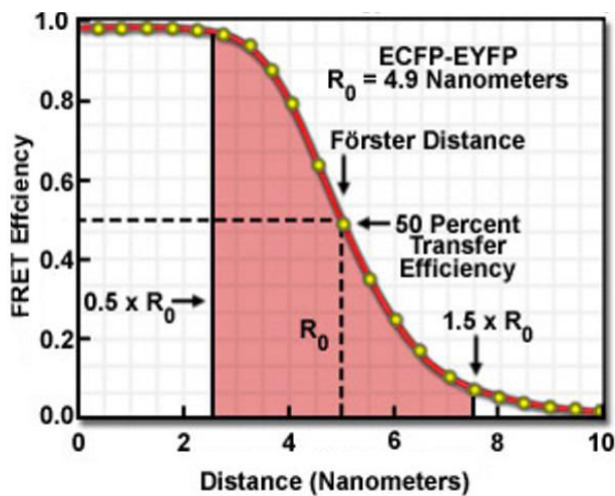


Figure 1: Distance dependence of FRET efficiency.

FRET efficiency E of the fluorophore couple enhanced cyan fluorescent proteins (ECFP) and yellow fluorescent proteins (EYFP). The Förster theory shows that E varies as the inverse sixth power of the distance between the two molecules (denoted by r). For any pair of fluorescent molecules, the Förster distance $R(0)$ (also termed Förster radius) can be calculated as the value where E is at 50% of its maximum. The useful range for measuring FRET is within 0.5 and $1.5 \times R(0)$, indicated by the red shaded region (adapted from <http://www.microscopyu.com/articles/fluorescence/fret/fretintro.html>).

One-fluorophore biosensors. By taking profit of the fluorescent protein sensitivity to environment, genetically encoded biosensors containing single fluorophores have been developed to monitor parameters such as pH or redox potential. Although wild-type GFP fluorescence is not particularly sensitive to pH changes in the physiological range, variants were generated showing pKa of 7.2 and making them suitable for measurement of cytosolic, mitochondrial and Golgi pH in living cells (pHluorin) (Llopis et al., 1998). Because H^+ transfer within the fluorophore is likely involved in the generation of fluorescence, mutations of the protonated amino acid residues (or in a close structural proximity that form hydrogen bonds with them) can result in GFP variants with altered sensitivity to changes in pH. The dependence of fluorescence on pH can be described by a one- H^+ -binding equilibrium, in which the H^+ -bound state is non-fluorescent (Kneen et al., 1998). Depending on their pKa, FP variants would be suitable to measure pH in different cellular compartments: EGFP with a

pKa \sim 6.0 can be used in acidic compartment such as the Golgi apparatus, whereas YFP that has a pKa \sim 7.1 work better in the more basic cytoplasm (Llopis et al., 1998). Through the same mutational approaches, FP variants sensitive to reduction-oxidation were generated: reduction-oxidation-sensitive green fluorescent proteins (roGFPs). Since chromophore fluorescence is also dependent upon the extent of disulfide bond formation of the disulfide bond, roGFPs were engineered to have a fluorescence altered by redox changes (Hanson et al., 2004). Such biosensors based on single fluorescent protein were used as biosensor for cellular redox changes in cells (Liu et al., 2014).

Circularly permuted fluorescent proteins. Linking the natural N- and C-termini, while creating novel N- and C-termini by cleavage at another position in the sequence, creates so-called circularly permuted fluorescent proteins (cpFP) (Baird et al., 1999), a type of mutation that also occurs as evolutionary event. It has been observed that cpFPs can yield high sensitivity of their fluorescence to the surrounding environment. This can be exploited to generate alternative fluorescent biosensors carrying a single fluorescent protein which reports a change in its close surrounding without the need for FRET (Baird et al., 1999; Hung et al., 2011; Zhao et al., 2011). In this case, the recognition element of the biosensor is inserted within the amino acid sequence of the cpFP. Molecular events at the recognition element can then be monitored through variations in the absorption or emission spectrum of the cpFP. As in case of FRET, such events can comprise, conformational changes, association/dissociation of protein complexes or binding of metabolites.

Green fluorescent proteins. Many different fluorescent proteins were derived from GFP and optimized for FRET applications by molecular engineering, in particular by altering spectral properties and increasing quantum yield. For these applications, GFPs were mutated mainly within their linear sequence. More recently, also circular permutation was applied to GFP engineering to improve and fine-tune FRET efficiency (Nagai et al., 2004) and generate single fluorophore cpFP-based sensors. The increasing number of engineered GFP-derived proteins now offers a large panel of optimized FRET couples with different spectral properties. In particular, the sensitivity of absorption and emission spectra to environmental variations e.g. in pH (Griesbeck et al., 2001; Nagai et al., 2002) and their tendency to oligomerize have been reduced, while brightness and photostability have been improved (Rizzo et al., 2004; Shaner et al., 2004). For example, as compared to YFP, citrine has been developed for increased

resistance to pH changes and reduced photobleaching. These issues will not be further discussed here, since a large number of specialized reviews is available (Palmer et al., 2011; Shaner et al., 2005).

Advantages and disadvantages of fluorescent biosensors in biological research. FRET- and cpFP-based genetically encoded biosensors are used in biological research to monitor events occurring with other macromolecules or small ligands such as association and dissociation, or conformational changes within proteins or protein complexes. The coding sequence of biosensors and their regulatory elements can be tailored to fine-tune the biosensor's biological and spectral properties, its subcellular targeting or its expression level.

Monitoring fluorescent FRET and cpFP signals is non-detrimental and non-destructive, and suitable to observe spatial and temporal events such as fluctuations of ions, metabolites or enzyme activities in living cells. Another important advantage of FRET over other types of fluorescence signals is its inherent ratiometric property, as it is determined by the ratio between acceptor and donor emission peaks. This has a clear advantage as compared to measuring mere intensity changes that are affected by unequal sensor expression and/or cellular distribution, as well as inhomogeneous cell morphology that all may affect quality and quantity of emitted light. Ratiometric FRET measurements allow normalization and reliable quantification of the signal, correcting for most of the cellular disturbances.

Genetically encoded biosensors can be multiplexed, since in principle a set of biosensors with sufficiently different spectral properties can be used together to monitor different parameters in parallel at the same time under a given condition. Such advanced applications will be necessary to generate massive, quantitative data for systems biology and model generation. Due to the large panel of available fluorescent biosensors, it is already now possible to follow fluctuations of a plethora of metabolic parameters. In the following, this review will present available, genetically encoded fluorescent biosensors that can be harnessed to explore directly or indirectly energy metabolism within a cell.

As mentioned, an intrinsic property of biosensors expressed in a cell as compared to analysis of cell extracts is temporal and spatial information. It should be kept in mind that in case of concentration measurements, the sensor will generally “see” the local concentration of a

given metabolite or ion, and thus report the accessible pools, not the inaccessible or otherwise structurally bound or compartmentalized molecules.

Finally, the spectral properties of FPs, but also the sensing mechanism (association/dissociation events, conformational changes), can be affected by cellular parameters like pH, ion concentrations, membrane potentials etc. Thus, efforts have to be made for each fluorescent biosensor, in particular for cellular *in vivo* application, to ensure that the readout truly depends only on the parameter of interest.

Which are the prime indicators to follow when analyzing cellular energy metabolism? Important macro-indicators are certainly the concentrations of adenine nucleotides (ATP, ADP, and AMP) and nicotinamide adenine dinucleotides (NAD, NADP). These determine *adenylate energy charge* (Atkinson, 1968; Hardie and Hawley, 2001) and *redox state* (Williamson et al., 1967), respectively, two global parameters that control many metabolic reactions. More indirectly, information about the cellular energy state can also be obtained from cellular fluctuations of small signaling molecules like Ca^{2+} or cAMP, and enzymes related to the cited processes like AMP-activated protein kinase (AMPK) or protein kinase A (PKA), and which are therefore included in this review.

ATP, ADP, AMP, CR and PCr. The concentrations of ATP (in the following indicated in brackets, e.g. [ATP]) are often used as the only measure of cellular energy state. However, [ADP] should not be omitted because it is the [ATP]/[ADP] ratio that determines the thermodynamic efficiency of energy-dependent reactions in a biological system. In addition, ADP is still an “energy-rich” compound and the adenylate kinase (AK) reaction can use two ADP to regenerate one ATP and one AMP. Since cellular [AMP] is in the sub-micromolar range under normal conditions, the AK reaction also translates small decreases in [ATP] via the ADP intermediate into large relative changes in [AMP] and thus makes AMP a sort of second messenger of energy stress (Figure 2). Consequently, all three adenylates are needed to describe the cellular energy state, as already proposed Atkinson and Walton with the *energy charge* (EC) concept: $EC = ([ATP] + \frac{1}{2}[ADP]) / ([ATP] + [ADP] + [AMP])$ (Atkinson and Walton, 1967). Another important parameter in cells and tissues with highly fluctuating energy requirements is phosphocreatine (PCr). PCr is the high-energy product of the enzyme creatine kinase (CK) that confers to creatine (Cr) its pleiotropic effects. The CK/PCr systems

functions as an immediately available spatial and temporal energy buffer. The CK/PCr energy shuttle, an intracellular energy transport system, connects sites of ATP production (glycolysis and mitochondrial oxidative phosphorylation) with subcellular sites of ATP utilization (ATPases) (Wallimann et al., 2011). The PCr/Cr shuttling therefore overcome diffusion limitations of ADP and ATP and is of prime importance in cells and tissues with high and intermittent energy fluctuations (Dorsten et al., 1997). CK isoenzymes catalyze the reversible phosphate transfer from ATP to Cr yielding PCr and ADP: $ATP + Cr \leftrightarrow ADP + PCr$. The PCr/CK shuttle constitutes the first safeguard to prevent sudden drops of ATP concentration. However, once the PCr pool is exhausted, the [ATP] also declines accompanied with a rise in ADP. Through the action of AK, ADP will be used to regenerate some ATP, triggering at the same time a sharp increase in [AMP]. This constitutes the signal for activation of AMPK that will restore cellular energy charge through its acute but also in depth action, by limiting energy demanding anabolism and stimulating energy generating catabolism.

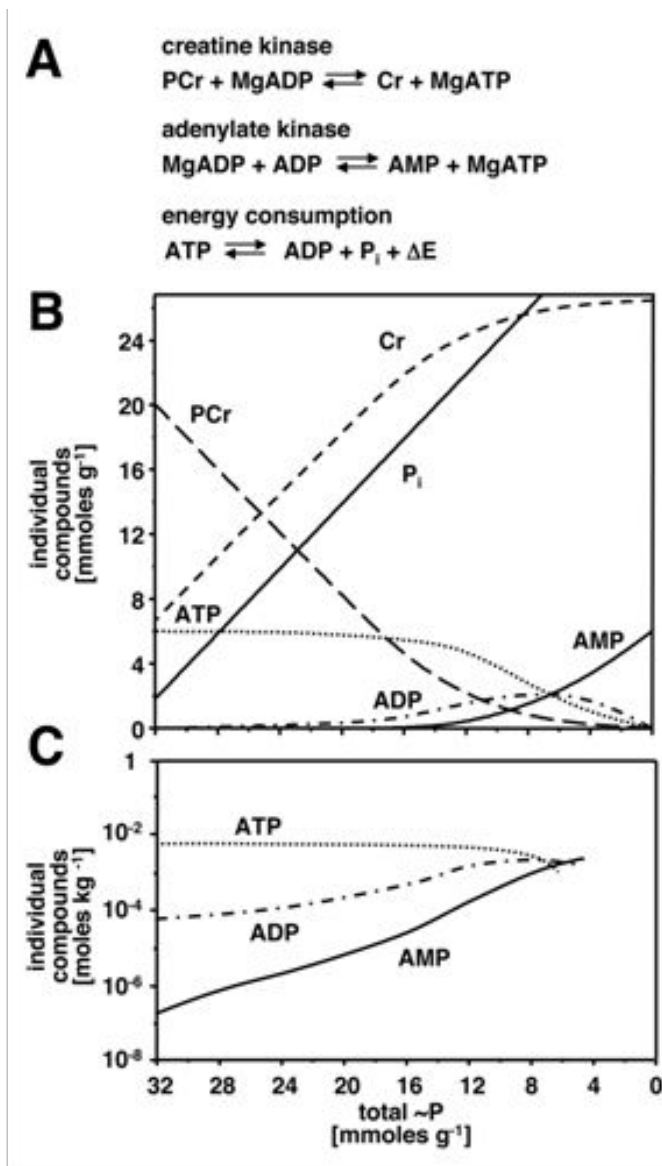


Figure 2: Simulation of pool sizes of energy-related metabolites occurring during cell stimulation until exhaustion.

(A) Enzymatic reactions (CK, AK and a generalized ATPase) considered in the model. Note: This is a simplified model assuming CK and AdK reactions at equilibrium and the enzymes homogeneously distributed in the cell, different from true *in vivo* situations. (B) Simulated cellular concentration changes of PCr, adenine nucleotides, inorganic phosphate [Pi] and Cr at decreasing “high energy” phosphates, corresponding to a transition from rest to high work-load and exhaustion (modified from McGilvery and Murray, 1974). Note: At rest, [PCr] and [ATP] are high, while [ADP] is very low and [AMP] is virtually non-measurable. With “high energy” phosphate consumption, [ATP] remains constant until more than 80% of the PCr pool is consumed, and only then [ADP] and [AMP] start to rise dramatically. (C) Changes of the same metabolite concentrations shown on a logarithmic scale. Note: [AMP] shows the largest changes, increasing from the beginning rather exponentially over several orders of magnitude, as reflected by the approximately linear curve on the logarithmic scale. This transmits into large relative changes in the AMP/ATP (and ADP/ATP) ratios that are the signals sensed by AMPK.

NAD(H) and NADP(H). Anabolic and catabolic metabolism rely on redox reactions and thus the cellular *redox state* which usually defined as $[\text{NAD}^+]/[\text{NADH}]$ and $[\text{NADP}]/[\text{NADPH}]$ ratios. *Vice versa*, these ratios are allosteric regulators of many of these reactions, e.g. in glycolysis, and are thus a readout of metabolic activity of the cell and, indirectly, also of its energy state. Large parts of these nicotinamide adenine dinucleotides are structurally bound and thus metabolically not accessible, as it is also the case for ADP. Biosensors may distinguish between free and bound pools, while biochemical methods always yield the entire pool size.

Calcium. Calcium signaling can be seen under two angles: Ca^{2+} acts (i) in signal transduction and activates ion channel or (ii) as a second messenger. Variations in Ca^{2+} gradient concentration through ion channels at the cellular membrane participate in changes in the membrane potential. Calcium is notably involved in the maintenance of the depolarization in heart or in the neuronal synaptic transmission. Calcium also has an important physiological role as a secondary messenger. Its release from intra- and extracellular stores increases cytosolic $[\text{Ca}^{2+}]$ which generally triggers increased ATP turnover, e.g. by stimulating both ATP-dependent motor proteins as during muscle contraction, as well as mitochondrial ATP generation (Astrup, 2008; Chouhan et al., 2012). Cytosolic Ca^{2+} resting concentration is maintained in the nanomolar range through its active pumping to extracellular space, endoplasmic reticulum and mitochondria. Specific signals mediated by G-protein coupled receptors or receptor tyrosine kinase trigger the opening of ion channel and Ca^{2+} release occurs. Ca^{2+} mediated events on metabolism are then mediated through its binding to protein, especially calmodulin that may activate calcium-calmodulin-dependent protein kinase or act on other cellular effector (Clapham, 2007). When calcium binds to calmodulin large conformational changes occurs and this switch was adapted to a fluorescence resonance energy transfer based Ca^{2+} sensors which enable a better understanding of Ca^{2+} signaling (Palmer and Tsien, 2006). Work with Ca^{2+} -sensitive fluorescent dyes has shown that Ca^{2+} variations are highly dynamic in space and time (Mank et al., 2006), thus accurate spatiotemporal measurements are required to monitor Ca^{2+} fluctuations.

AMP-activated protein kinase. In principle, the activity of any enzyme that depends for its reaction on the above mentioned metabolites or signaling molecules can serve as a readout. However, there are certain signaling proteins that evolved to precisely detect physiological changes within these parameters. The probably best example is AMP-activated protein kinase (AMPK) that detects changes in the equilibrium of adenylates, since it is allosterically activated by AMP and (to less degree) by ADP, and inhibited by ATP (Hardie et al., 2012). Thus, AMPK activity has been proposed as an appropriate reporter of the *adenylate energy charge* (Oakhill et al., 2012). However, AMPK is primarily activated by a covalent activation step that involves phosphorylation by upstream kinases like LBK1 or CamKK β . Only allosteric AMPK activation, not the covalent activation, is a good readout for cellular energy state. The current standards to detect AMPK activity, e.g. monitoring phosphorylation of an AMPK substrate like acetyl CoA carboxylase (ACC) *in vivo* or of synthetic SAMS peptide *in vitro*, do not distinguish between both activation mechanisms. However, AMPK is activated at a basal state by systemic signaling (e.g. hormones for appetite regulation) via its upstream kinases. A reporter dedicated to the monitoring of AMPK allosteric activation by adenylates would represent a great advantage when studying energy metabolism: it would permit to specifically consider AMPK activation due to cellular energy state variation. Such sensor was aimed to be generated during the present work.

Protein kinase A. Activation of PKA is less directly linked to cellular energy state, although it stimulates glucose and glycogen utilization and regulates mitochondrial function (Leadsham and Gourlay, 2010). More importantly, PKA became the prototype of a genetically encoded fluorescent biosensor, pioneered by the by Tsien group in 2001 (Zhang et al., 2001). This opened the novel and exciting opportunity to follow PKA enzyme activation and cAMP metabolite concentration in real time and space (for recent reviews see: (Almahariq et al., 2014; Carlucci et al., 2008; Wong and Scott, 2004).

3. Conventional techniques to study cell energetics

Conventionally, parameters of cellular energy state are measured in cell extracts in an end-point assay format.

Chromatographic techniques. Routinely, metabolites like different nucleotides are quantified by end-point assays in protein-free extracts using chromatographic methods (e.g: ion exchange chromatography, HPLC possibly coupled to MS or even thin layer chromatography). Among the different methods used to assay high-energy phosphates in biological samples, HPLC has the advantages of high sensitivity and efficiency. Another advantage of chromatographic techniques, especially HPLC, is the possibility of performing the separation and simultaneous rapid determination of not only nucleotides but also nucleosides, nitrogen bases, Cr, and PCr (Teerlink et al., 1993), (Harmsen et al., 1982). However, these techniques provide results that do not exactly reflect the real situation. In addition, and transient events cannot be followed. As with any invasive procedure, this method is prone to errors due to the complex and drastic extraction procedure (cell lysis and protein precipitation), or *in vitro* transformation of the metabolites (e.g. spontaneous ATP hydrolysis). Also, because of the high rate of conversion of ATP to ADP and AMP under ATPases activity in fresh samples, protocols should include inactivation of ATPase enzymes when collecting tissue or cell samples for ATP measurement (Manfredi et al., 2002).

Immunoblotting and AMPK activity. Monitoring AMPK activity not only provides information about this signaling pathway, which constitutes a major hub for sensing and regulating cellular energy metabolism. It is also often considered as a suitable surrogate for directly measuring changes in energy state, *i.e.* reflecting changes in the adenylate pools. However, the conventional techniques applied in fact do not allow drawing such conclusions. Common immunodetection of the phosphorylated, active form of AMPK, or *in vitro* phosphorylation assays of immunoprecipitated protein, report only the covalent activation step that mainly depends on the activity of upstream kinases and phosphatases. Immunodetection of phosphorylated AMPK substrates reports both types of activation, covalent and allosteric, but does not distinguish between them, and may report activity with time lag and for extended time periods, even when AMPK activity is down again. Preparation of cells extracts also introduces a number of biases, linked e.g. to the action of phosphatases.

In any case, these kinds of detection *in vitro* will not detect transient and localized AMPK activation within a cell. Some classical approaches allow non-invasive monitoring of energy-related parameters in cells or tissues, thus avoiding problems related to the handling of cell extracts.

NMR. Non-invasive ^{31}P -nuclear magnetic resonance (NMR) spectroscopy has been long the method of choice for determining adenylates and phosphocreatine. The rate of ATP synthesis can be measured by observing ^{31}P magnetization transfer between inorganic phosphate and the γ phosphate resonance of ATP (Lebon et al., 2001) or the phosphate in PCr. If adenylate kinase (AK) or creatine kinase (CK) equilibria are taken into account, AMP, ADP and creatine kinase concentrations can be extrapolated as well (Kemp et al., 2015). Although ^{31}P -NMR spectroscopy offers good temporal resolution, spatial resolution is much too low for single cell imaging. Importantly, ATP synthesis by oxidative phosphorylation and glycolysis cannot be distinguished. Although NMR has been routinely used to investigate mitochondrial ATP synthesis and by deduction mitochondrial energy coupling, this was only applied to muscle and situations with highly active oxidative metabolism, and not e.g. to resting skeletal muscle with predominant glycolytic ATP generation (Kemp and Brindle, 2012). Also, only ATP available for the transfer reactions is monitored, there has been a long dispute on “NMR-invisible”, bound or compartmentalized pools of ATP and PCr (Takami et al., 1988, Bak and Ingwall, 1992).

Luminescence. Another non-invasive technique widely used to evaluate cellular energy state status consists in measuring the ATP concentration through luciferase-based assays. Luciferase is a protein that uses Mg-ATP to convert luciferin into luciferyl adenylate. The latter releases AMP when reacting with molecular oxygen and this step is followed by a spontaneous decarboxylation which triggers the formation of excited oxyluciferin. Light is finally emitted when oxyluciferin returns from the excited state to the ground state and the emission intensity is proportional to [ATP]. A great number of bioluminescence procedures were developed and the detection limit of ATP was at the femtomol level for the most sensitive (Lyman and DeVincenzo, 1967). However, despite its high sensitivity these methods present limitations. Determination of intracellular [ATP] can be impeded by interference with extracellular ATP.

Another disadvantage of this method is that detection itself changes adenylate concentrations by using ATP and oxygen and generating AMP. When working on cells expressing firefly luciferase (Kennedy et al., 1999), chemiluminescence by luciferase depends not only on the intracellular ATP level but also on the luciferase concentration, as well as oxygen, and luciferin. Moreover, pH also affects luciferase activity. The ATP consumption inherent to luciferase-based methods may secondarily trigger cellular responses, especially via the AMPK pathway. In addition, the dim luminescence of luciferase requires longer exposure time for image acquisition, making real-time observation difficult. Most often ATP bioluminescence is measured on cell extracts meaning that before the measurement of bioluminescence, cellular ATP must first be extracted. Extraction procedures can interfere with the luciferin–luciferase system (Yang et al., 2002) and the use of extraction substances, neutralization of extractants, and other steps performed on extracted components also affect the cellular ATP content (Lee et al., 2012). This type of sensors based on luciferase is mainly used *in vitro* (Yang et al., 2002) after cell lysis, but has been also applied in cells, and even for analysis of subcellular ATP heterogeneities by targeting luciferase to different cellular locations (Gajewski et al., 2003).

Intrinsic fluorescence. Only very few energy-related metabolites can be monitored directly *in situ* due to their intrinsic fluorescence, like NADH or NADPH when using a costly UV-laser equipped confocal microscope. Real time monitoring of NAD(P)H, a metabolite mainly present in the mitochondria, permitted to follow the mitochondrial permeability transition pore (PTP). A transient opening of the PTP induces NAD(P)H diffusion out of the mitochondria that can be visualized as an increase in the area and fluorescence intensity of NAD(P)H (Dumas et al., 2009) linking PTP opening to inhibition of mitochondrial respiration.

4. Designing genetically encoded fluorescent biosensors to study cell energetics

As compared to the above non-invasive methods, the use of genetically encoded biosensors has several conceptual advantages: (i) they allow to obtain spatial resolution in a cell or a tissue, and they can be even addressed to a specific cellular sub-compartment, (ii) they do

not chemically modify the bound metabolite, (iii) in principle, any metabolite can be measured for which a recognition elements with affinities in the physiological range exists and that can be linked to conformational changes or protein-protein interactions for a FRET signal. FRET is indeed extremely sensitive to small changes in a distance range relevant for small conformational changes.

Various FRET biosensors have been developed to study energy metabolism and most of them are utilizing as recognition elements proteins and, less often, RNA (Paige et al., 2012). Protein-based biosensors can be easily engineered by modifying their DNA coding sequence, transfected and will then be constitutively processed by the cellular machinery. Fluorescent biosensors in living cells can be detected using a great variety of common instruments, including fluorescence microplate readers, flow cytometers, wide-field fluorescence microscope and single photon confocal microscope.

During biosensors design, the main point of the strategy depends on an association/dissociation event or on the induction of conformational changes in the biosensor structure upon molecular recognition, which can be inherent to the recognition element itself or engineered. Either the recognition element directly undergoes some conformational changes when the biological phenomenon occurs (like binding of a metabolite, or a modification in form of a phosphorylation); or the conformational change is indirectly induced by the occupied (or modified) recognition element but rather induced to its interaction with a second binding domain. All FRET-based biosensors contain conformationally responsive receptors coupled to fluorophores. This allows to follow the fluctuations of a studied parameter based on variations of the fluorescence signal. From these parameter-induced conformational changes or association/dissociation event, depends the successful development of fluorescence-based biosensors. Thus, success relies on the selection of the recognition element. Because the sensing of elements, notably for energy metabolism, is already present in nature, development of biosensor should be bio-inspired. Another key concern, when creating and using a genetically encoded probe, consists in knowing whether it will perturb the biological systems by either catalysis or buffering. Once the recognition element selected, further optimizations can be achieved to modify affinity/sensitivity and selectivity notably through molecular engineering and mutagenesis. It is difficult to predict conformational changes and their amplitude as a result

of ligand binding, so, until date, most examples of biosensors are using proteins that are already known to undergo conformational changes upon binding of their ligand (Berg et al., 2009; Imamura et al., 2009; Zhao et al., 2011).

Genetically encoded fluorescent biosensors represent a new emerging toolbox which enables new questions to be addressed concerning the dynamics of metabolites (e.g. adenylates) in cellular energy metabolism. As compared to non-direct biochemical techniques, fluorescent biosensors provide capacity of measurement with higher spatial and temporal resolutions. In addition, they allow direct measurement in single living cell of parameters that could vary considerably from a cell from to another (e.g. total ATP amount). Before fluorescent biosensor development, these effects were averaged, minimized and sometimes returned as non-visible due undesired- but method-dependent- normalization and bias. As many events of the metabolism are transient, the development of such method will provide new insights in energy metabolism.

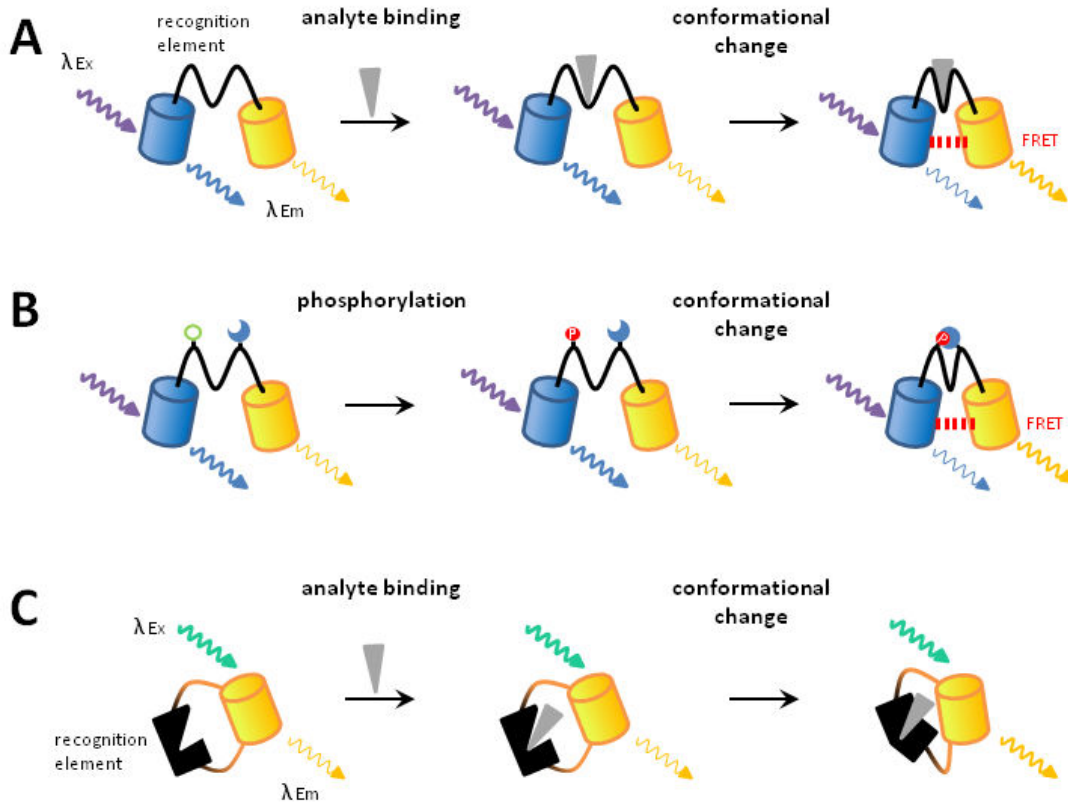


Figure 3: Genetically encoded fluorescent biosensors principle and design.

A- The recognition element, flanked with two fluorescent proteins, undergoes conformational changes when bound to the analyte. **B-** The recognition element, flanked with two fluorescent proteins, is a target of specific posttranslational modification that undergoes conformational changes once enzymatically modified. **C-** Once the analyte attached to the recognition element, leading to conformational changes, the single fluorescent protein, inserted within the amino acid sequence of the recognition element, has its fluorescent properties altered. Analyte depicted as a grey triangle (**A** and **C**), posttranslational modification is shown, for example, as a phosphorylation (**B**). Excitation light is representing as a wavy arrow directed to the schematized biosensor and emitted lights as wavy arrows issued from the biosensors. Blue and yellows cylinders represent a pair of fluorescent proteins (e.g. here CFP and YFP).

5. Calcium

The FRET-based biosensors field for energy metabolism emerged in 1997 with a sensor for Ca^{2+} (Miyawaki et al., 1997). Because calcium fluxes are among the most dynamic intracellular signals, following calcium variations required a great resolution and specific localization. Miyawaki et al. created a set of GECIs, named Cameleons, which can specifically be targeted to intracellular localization (cytosol, nucleus or endoplasmic reticulum). Using

these biosensors, they revealed transient waves and sparks of Ca^{2+} in real time and with a cellular high resolution. Authors immediately figured out that their approach can be expanded to other metabolites and suggested that fluorescent indicators for analytes other than Ca^{2+} might be engineered by sandwiching other conformationally responsive receptors between GFP donors and acceptors. This work paved the way, not only for a whole series of GECIs but also, for FRET-based biosensors targeting other ions or metabolites. GECI, in its strictest sense, also includes sensors that use chemiluminescence (Baubet et al., 2000). This type of probes will not be further discussed but reviews can be consulted (Chiesa et al., 2001; Créton et al., 1999; Kendall and Badminton, 1998). GECIs permitted to reconsider Ca^{2+} cellular repartition and showed that Ca^{2+} is a cellular messenger with non-uniform distribution inside the cells and that its signaling occurs locally as wave and sparks. Ca^{2+} metabolism is strongly interconnected to energy metabolism, especially in muscle, notably because AMPK, a key regulator of energy metabolism, is activated by $\text{CaMKK}\beta$. Thus, GECIs can be used to investigate, in time and space, cellular energy metabolism.

Cameleons (Miyawaki et al., 1997; Nagai et al., 2004), TN-XL (Mank et al., 2006) or GCaMP (Tian et al., 2009) are examples of GECIs. Cameleons recognition elements consist in calmodulin (Cam) and its binding peptide M13 from myosin light chain kinase sandwiched together between BFP and GFP (or CFP and YFP). Upon binding, $\text{Cam}/\text{Ca}^{2+}$ enclose the M13 peptide generating a conformational change which leads to FRET signal increase. M13 peptide was inserted to magnify the amplitude of the conformational changes of the sensor, but its insertion was also thought to reduce the ability the sensor could have to activate calmodulin-dependent target proteins. GCaMP and Pericams (Nagai et al., 2001) recognition module contains the same modules than Cameleons biosensors. The difference resides in the presence of cpFP which were inserted in the sequence of the probes, between the M13 peptide and Cam. Other GECIs, such as TN-XL are employing Troponin C (TnC) as the recognition element. TnC by contrast to Cam prevent any interaction that may occur between the sensor and numerous Cam-binding proteins. In addition to be different in their Ca^{2+} binding module, TnC based sensors lack secondary binding peptides as M13 (Heim and Griesbeck, 2004). A large number of variants of these two models of GECIs have been created, varying in their FRET pairs, sensitivity, localization targeting signal... Reviews well describing this topic are available (Kotlikoff, 2007; Mank and Griesbeck, 2008).

6. PKA activity reporter and derived biosensor

Activity reporters dedicated to the monitoring of activity of important family of kinases are also available. The one that pioneered this field targets PKA activity: a kinase activity reporter, AKAR (Zhang et al., 2001). This sensor consists in a FRET pair (eCFP and Citrine variants) flanking a phosphoamino acid binding domain (14–3–3 τ) bound to a PKA-specific phosphorylatable peptide sequence. 14–3–3 τ mediates signal transduction through binding to the PKA-phosphorylated peptide and flexible amino acid linkers were inserted between the biosensor components. Improvements (e.g. linker engineering, exchange of phosphopeptide-recognition-domain and FPs) were implemented in AKAR, finally yielding AKAR3 (Allen and Zhang, 2006). It contains cpVenus instead of Citrine, the forkhead-associated domain (FHA) as phosphoamino acid binding domain and shows twice the dynamic range of its predecessor (30-40%). Through different subcellular targeting sequences, it also can be targeted to the plasma membrane, mitochondria, the endoplasmic reticulum or Golgi to specifically study cAMP signaling. Indeed, the use of AKAR3 provides new insights about PKA activation dynamics depending on its localization. Although PKA does not have an as important role in regulating whole cellular energy metabolism as compared to AMPK, data concerning the cross-correlation between GPCRs signaling, cAMP metabolism and the whole cellular metabolism are crucial to understand energy metabolism through a systemic vision. The second messenger cAMP and the associated kinases regulate several biochemical processes, including the glycogen, sugar, and lipid metabolisms. Fluorescent biosensor to follow cAMP dynamics used in parallel with biosensors monitoring other parameters of the energy metabolism, provide insight concerning the role of cAMP in the energy metabolism (Di Benedetto et al., 2013; Castro et al., 2014).

Numbers of genetically encoded fluorescent biosensors for cAMP already exists and they are largely described in reviews (Binkowski et al., 2011a). Some of them rely on fluorescent proteins either flanked on the regulatory- and catalytic- subunits of the main cAMP effector, PKA (Zaccolo et al., 2000) or on the Exchange Protein directly Activated by cAMP (Epac) (Klarenbeek and Jalink, 2014). Analogously to AKAR (i.e. a FRET pair flanking a substrate motif peptide fused subsequently to its recognition domain) a sensor for the monitoring of PKD activity, DKAR, was also developed and its use notably showed that PKD is regulated by elevation of intracellular Ca²⁺ under addition to diacylglycerol (Kunkel et al., 2007).

7. Adenine nucleotides

A milestone in the development of biosensor for energy metabolism relied in the generation of genetically encoded biosensors for ATP, overcoming problems linked to [ATP] measurements using conventional techniques (see above). Two major sensors have been generated by the Noji group (Imamura et al., 2009; Nakano et al., 2011) and the Yellen group (Berg et al., 2009; Tantama et al., 2013). The first biosensor contains 2 FPs whereas the second is based on single cpFP.

So called ATeam sensors, developed by Imamura et al., allow the dynamic monitoring of [ATP] fluctuations (Imamura et al., 2009). These sensors display, as recognition element for ATP, the ATP binding domain from the ϵ subunit of bacterial F_0F_1 -ATP synthase from *Bacillus subtilis* that is fused to either CFP/YFP or GFP/OFD variant pair. The ϵ subunit regulates the ATP synthase activity depending on ATP availability, thus its ATP binding domain was used as recognition element due to its native ability to sense ATP. More importantly, the ϵ subunit undergoes large conformational changes upon ATP binding, passing from an elongated shape when bound to Mg^{2+} -ADP to a contracted hairpin-like structure when bound to ATP (Feniouk et al., 2006). These two points make the ATP-binding domain of ϵ subunit suitable for the elaboration of FRET sensors for ATP. The initial FRET dynamic range was not considerably large thus authors replaced the fluorescent acceptor mVenus by cpVenus, based on the Cameleon biosensor study (Nagai et al., 2004). In addition, different versions of the ATeam sensor were created depending on the FRET pair used (mseCFP/cp173-mVenus or cp173-mEGFP/mKO), which allows to monitor the [ATP] variations in combination with other fluorescent biosensors targeted to other parameters of choice, avoiding excitation and emission fluorescence overlap. Weak dimerization may occur between of FPs yielding artificial FRET, thus involved residues were identified and mutated to generate monomeric FP. Ala 206, a residue present in FPs of ATeam was previously identified to be involved in weak dimerization of FPs but also to play a role in the FRET amplitude exhibited by biosensors (Kotera et al., 2010). This work showed that the weak dimerization property of FP yielded high-performance biosensors with the greatest dynamic range.

AT1.03 shows a K_d of 3.3 mM for ATP at 37°C and can be used to measure ATP levels in the millimolar range, whereas AT3.10, which use the ϵ subunit of *Bacillus* sp. PS3, has a higher

affinity with a K_d of 7.4 μM at 37°C. By comparing the two different ϵ subunit isoform sequences, the affinity for ATP was further tuned by swapping amino acids positioned nearby the ATP binding pocket. This yielded AT1.03^{YEMK} and AT3.10^{MGK} which have affinities for ATP of 1.2 mM and 14 μM respectively. This supports that ATeam sensor affinity for ATP can be adjusted to conduct individual experiments. During ATeam characterization, authors raised an important issue concerning saturation of the FRET signal and the sensor response has to be calibrated to avoid situations of FRET signal saturation leading to non-interpretable data. ATeam selectivity for nucleotides was examined *in vitro*: addition of 10 mM GTP or ADP has little effect on AT1.03 signal, but AT3.10 has K_d for GTP and ADP of 2.6 mM and 230 μM respectively. The fluorescence signal was characterized as being stable during pH fluctuations from 7.1 to 8.5 and supporting that small variation in the physiological range should not affect significantly measurement done with ATeam. However, cytoplasmic pH is near 7.3 (Llopis et al., 1998) and effect of pH lower than 7.1 on the fluorescent signal may have been examined since local acidic cellular event can happen in some cellular subcompartments (Llopis et al., 1998). According to its association and dissociation constants, AT1.03 can follow ATP dynamics changes with rates up to 0.1s^{-1} . During AT1.03 characterization Imamura et al. observed that the K_d for ATP increases dramatically with the temperature (five-fold over a 10°C variation). By targeting ATeam1.03 variants to different subcellular compartments, it was shown that ATP concentration was significantly lower in mitochondria than in the cytosol or the nucleus.

As a second proof of concept Ateam was used in cells to follow ATP fluctuations under inhibition of glycolysis (10 mM 2-deoxyglucose - 2DG) or OXPHOS (1 mM potassium cyanide - KCN). Addition of 10 mM 2DG reduces ATP concentration from 7 mM to 3-4 mM whereas KCN alone had no effect. Interestingly a synergistic effect between 2DG and KCN was reported with a dramatic drop of the ATP concentration to ~ 1 mM. However, such a situation represents an extreme stress which may trigger the modification of cellular parameters, such as pH changes, that may alter the FRET signal. In addition, the effect of magnesium was not studied despite a free-ATP concentration monitored *in vivo* as being ~ 7 mM, which suggests that the binding of ATP to ATeam induces the removal of Mg^{2+} previously bound. Despite few limitations, the use of ATeam sensors is becoming more and

more important and this is illustrated by the large number of studies, listed below, involving ATeam sensors.

Ateam sensor was used in single cell to monitor ATP while Ca^{2+} concentrations fluctuations were monitored at the same time (Nakano et al., 2011). This study showed that histamine stimulation in HeLa cells increases ATP and Ca^{2+} level. Also, Forkink et al. (Forkink et al., 2014) followed the fluctuations of ATP in HEK293 cells by targeting ATeam1.03 and its “dead variant” to cytosol and mitochondria. This was combined to other techniques (notably pH monitoring using SypHer sensor (Poburko et al., 2011)) and results confirmed that ATP concentration in mitochondria was lower than in the cytosol and, more interestingly, deciphered how complexes (I-IV) of mitochondrial OXPHOS system react under complex I inhibition, and explain the resulting $\Delta\Psi$ dephosphorylation. ATeam biosensors were used to follow ATP concentration in HuH7 cells during Hepatitis C virus replication (Ando et al., 2012). This showed, through the reduction of ATP level in the cytoplasm, that cells implicated in viral replication actively consumed ATP. Interestingly, formation of ATP-enriched dot-like structure that co-localize with non-structural viral protein was visualized: ATP concentrations were estimated to be 5 mM at replication site and 1 mM at peripheral sites not involved in HCV replication. The uniform ATP concentration (2 mM) in non-replicating cells supports the local ATP-consumption during the HCV genome replication. These ATP concentrations were below those observed in HeLa cells by Imamura et al. (Imamura et al., 2009) suggesting variability among cell types. Ateam 1.03 was even used in nematode vulva cells of *Caenorhabditis elegans*, in which differences between ATP concentration in cytosol and mitochondria were showed even if no changes in their level were seen (Kishikawa et al., 2012). The stability of the ATP concentrations during tested conditions was attributed to variations of the K_d ATP with the temperature.

As previously mentioned, genetically encoded biosensor can, in principle, be tuned and optimized. Thus, Ateam1.03NL was generated with optimized affinity at lower temperature (Tsuyama et al., 2013). At 25°C, this new version detects ATP fluctuations in a more sensitive manner than the initial ATeam1.03, making it more suitable for single cell imaging of ATP dynamics in *Drosophila melanogaster* and *C. elegans*, two organisms considered as model for bioenergetics and metabolic studies (Baker and Thummel, 2007; Harrison and Haddad, 2011).

ATeam sensor was also used in hippocampal neurons where it was shown that ATP is mostly synthesized to maintain Na^+/K^+ transmembrane ion gradients to ensure neuronal activities (Toloe et al., 2014). Such an approach may help to better understand mechanisms governing the activity of neuronal networks, especially under pathological conditions.

During another study Ca^{2+} -coupled endoplasmic reticulum dynamics was examined (Vishnu et al., 2014). This study shows specific regulation of ER ATP homeostasis depending on the cell-type. It also presents that intracellular Ca^{2+} -release is coupled to an ATP increase within the ER, itself under the control of energy stress sensor AMPK. Through a movie, Vevea et al. present how to use mitoGO-ATeam (ATeam variant for mitochondria carrying a Green/Orange FRET pair) coupled to a genetically encoded mitochondrial redox state sensor (roGFP) at subcellular resolution in living yeast (Vevea et al., 2013).

To summarise, despite ATeam sensor limitations, notably because it covers a concentration range larger than physiological [ATP] fluctuation - meaning that its whole range of fluorescent variations cannot be totally exploited in cells - its use allows monitoring of ATP dynamics with a resolution in time and space that has never been achieved before.

Another genetically encoded fluorescent biosensor for spatiotemporal analysis of the ATP/ADP ratio was also developed to investigate energy metabolism (Berg et al., 2009). A cpFP variant (cpmVenus) was inserted within the T loop of the ATP binding protein GlnK1 from *Methanococcus jannaschii*, resulting in an initial sensor named QV5. Initially designed to monitor ATP fluctuations, this version rather behaves as a reporter of ADP/ATP levels than ATP concentration. Indeed, its affinity for Mg^{2+} -ATP is approximately 40 nM and ADP can compete with ATP to bind the same site with an affinity of $\sim 0.2 \mu\text{M}$ making the sensor, *in fine*, almost insensitive to physiological ATP or ADP concentrations variations. The extremely high affinity for ATP combined to the defective selectivity over ADP would seem to reject the sensor for ATP sensing. However, it reports relative affinity of the receptor for ATP and ADP and therefore the steady-state that depends on the ATP/ADP ratio. ATP and ADP compete to bind the nucleotide binding site but only ATP triggers closure of the T loop and maximal change in the fluorescence. Thus competition by ADP will lower the affinity of the sensor toward ATP. To support this Berg et al. determined that the K_d for ATP became $\sim 1 \mu\text{M}$ in presence of $5 \mu\text{M}$ ADP, as compared to $0.04 \mu\text{M}$ when ADP is absent. They also showed that

magnesium concentration influenced the fluorescence signal as shown by modulating free-ATP/Mg²⁺ATP ratio supporting that the sensor is binding Mg²⁺ATP.

Extensive engineering, via mutagenesis, yielded the Perceval sensor which exhibits faster kinetics as compared to a previous time constant of about one minute. In addition, Perceval presents a lower sensitivity for 2-ketoglutarate as compared to initial QV5 sensor which showed a reduced response to ATP in presence of 2-KG and an apparent K_d for 2-KG of ~ 0.3 mM. In addition, mutations yield an improvement of the K_r from ~ 0.2 to ~ 0.5 , which is defined as corresponding to the ATP/ADP ratio which yields to the “half-maximal response”. However the ATP/ADP ratio is in the range of 3 to 10 in a cell “fully charged”. Thus, the whole amplitude of response of Perceval cannot be fully exploited *in vivo*. It has even been suggested that ATP/ADP ratio varies to over a greater range under healthy condition (~ 3 in mouse pancreatic beta cells (Nilsson et al., 1996); ~ 8 in rat brain tissue (Erecińska and Silver, 1994). Indeed, most estimates of ATP/ADP ratio are measurements of total nucleotide content, making the ATP/ADP free ratio suspected to be higher (2- to 20 fold) because ADP sequestration may be greater than for ATP (Koretsky et al., 1990; Mörikofer-Zwez and Walter, 1989). Perceval can sense variations in the ATP/ADP ratio from 1 to ~ 5 , which correspond to drastic metabolic inhibition, Berg et al. recognize that their sensor is dedicated to studies of high energy deficits as expected in ischemia, anoxia or important energy consumption states.

Rise of ATP triggers a decrease of the absorption at 405nm and an increase of the absorption peak at 490nm (via measurement of emission at 530nm). Thus, although Perceval contains one (circularly permuted) fluorescent protein a ratiometric measurement can be extracted out its fluorescence signal and normalization can be achieved during *in vivo* studies. As a proof of concept use of Perceval showed that 2-deoxyglucose treatment on HEK293 cells triggers a decrease in the ATP/ADP ratio. Such a sensor that follows metabolite relative amount should to be a more reliable indicator of metabolism from cell to cell due to the variation of absolute amount of ATP, ADP or AMP from cell-to-cell. Perceval fluorescence is influenced by pH fluctuations, thus authors concurrently measured intracellular pH using the pH indicator dye SNARF-5F to be able to correct fluorescence changes owing to pH.

Optimization by structure-guided engineering of initial Perceval yield PercevalHR (Tantama et al., 2013). Its sensitivity was increase through high range and PercevalHR senses ATP/ADP ratio from ~ 0.4 to 40 which correspond respectively to 10 and 92% sensor saturation. This optimized amplitude matched with the ATP/ADP ratio range expected in mammalian cells and the sensor conserves kinetics for ATP and ADP unloading in the second range. Tantama et al. transfected astrocyte and investigate how acute fluctuations in glucose supply affect cellular energy balance. One limitation authors presented concerning Perceval HR relies in its sensitivity to pH. The pH influences the fluorescent dynamic range ($\Delta F_{\max}/F_{\text{initial}}$) from ~ 5 to 2, in addition to diminish the K_r approximately 5-fold (from 10 to 2) over a variation of pH from ~ 6.7 to ~ 7.8 . According to this restriction, authors suggested to co-express the pH biosensor pHRed, in view to its spectral properties, for cell-by-cell correction of pH bias. For ATP-dependent reactions the ATP/ADP ratio influences the reaction reversibility and the driving force, whereas total ATP is a determinant of reaction rate and total turnover. Thus, they also suggested, as a very promising method to follow energy changes, to use PercevalHR in parallel to ATeam biosensor to dissect the distinct metabolic consequences of changes in the ATP/ADP ratio and in the total ATP level.

Only few studies involving Perceval sensor have been published. In one of them was examined the compartmentalized changes in Ca^{2+} and ATP/ADP ratio in single primary mouse β -cells, by combining patch-clamp electrophysiology with simultaneous real-time imaging (Tarasov et al., 2012). They used recombinant targeted Pericam (Nagai et al., 2001) and Perceval, as well as Fura-Red, a fluorescent Ca^{2+} indicator. As a control, authors investigated the effect of pH on Perceval signal and concluded that fluctuation of pH had minimal effects. Measured $\text{ATP/ADP}_{\text{cyt}}$ ratio varied from 0.9 to 1.35 over a pH range from 6.6 to 7.8. They showed that mitochondrial Ca^{2+} uniporter (MCU) and $\text{Na}^+/\text{Ca}^{2+}$ exchanger (NCLX) are mediating the Ca^{2+} uptake in the excitable β -cell. Authors also reported that changes in Ca^{2+} located in the mitochondrial matrix are critical concerning increases in cytosolic ATP/ADP ratio. As they could be required for glucose insulin secretion (Wiederkehr et al., 2011), authors suggested that modulation of MCU activity may provide strategies to improve imperfect insulin secretion in some forms of diabetes. In another study, involving similar settings, it was shown that during electrical stimulation mitochondria are deciphering cytosolic Ca^{2+} oscillation frequency as stable increases in $\text{Ca}^{2+}_{\text{mit}}$ and $\text{ATP/ADP}_{\text{cyt}}$ (Tarasov et

al., 2013). These results support an integration of cytosolic pulses by mitochondria to modulate $\text{Ca}^{2+}_{\text{mit}}$ changes and ATP synthesis. Their conclusion concerned type 2 diabetes and suggested that a disturbance in the generation of $\text{Ca}^{2+}_{\text{cyt}}$ oscillations may consist in an upstream event which contributes to alter the downstream ATP production and finally the insulin secretion. The experimental procedure followed by Tarasov et al. involving several biosensor at the meantime is described in details (Tarasov and Rutter, 2014).

Perceval was also used to examine Ca^{2+} variation in cross-correlation to ATP concentration variation in β -cells (Li et al., 2013). In their hands, Li et al. determined that Perceval fluorescence signal increases in a dose-dependent and reversible manner with a half-maximal effect occurring at 2.2 mmol/L ATP. Surprisingly, authors of this study proposed that Perceval expressed in insulin-secreting cells detects physiologically relevant ATP concentration rather than ATP/ADP ratio. Indeed, they observed that variation of the ATP/ADP ratio from 1 to 10 by decreasing ADP from 1 to 0.1 mmol/L had no influence on Perceval fluorescence. In contrast, when they add ADP alone at 1 mmol/L it induced a prompt fluorescence increase which is markedly reduced when they added ApA5, an inhibitor of AK. For them, the ADP-dependent fluorescence increase reflected the conversion of ADP into ATP by AK. Authors also, confirmed the pH-sensitivity of the probe but assured that observed fluorescence changes are induced by glucose and could not be related to cytoplasmic pH variations. Li et al. showed from their analysis of the dynamic relationship between Ca^{2+} and ATP at the sub-plasma membrane, that glucose induces oscillations of ATP_{pm} and $\text{Ca}^{2+}_{\text{pm}}$, with each Ca^{2+} increase corresponding to reduction of ATP. This bidirectional connection between Ca^{2+} and ATP, which is central to the generation of metabolic and ionic oscillations, shows pulsatile insulin secretion.

As elucidated, listed sensors for adenylates pool variations are offering important advantages face to indirect or invasive measurement methods. The dynamic monitoring of adenylate pool variation offers access to a precise analysis of adenylate variation. In addition to their advantage during live cell imaging, such tools allow to distinguish regional variations of ATP and ADP at submicron scale. The Webb lab also generates biosensors for ADP (Kunzelmann and Webb, 2009, 2010) and GDP (Kunzelmann and Webb, 2011) but these do not involve fluorescent protein to transduce signal but rather a diethylaminocoumarin fluorophore coupled to a bacterial actin homologue, ParM, as protein framework. These

sensors are not fully genetically encoded and thus, require different experimental procedure. However, ATP hydrolysis is one of the most fundamental reactions in biological systems, thus following ADP fluctuations represents a direct way of monitoring enzymatic-driven ATP conversion. ADP, and even more AMP variations are considered as the real reporter of metabolic stress in the cell due to greater range of amplitude fluctuation as compared to ATP (Hardie et al., 2011), thus sensors targeted to AMP or ADP are promising tools to study energy metabolism.

8. NADH

NADH is a coenzyme present in all living systems. It exists under a reduced and an oxidized form, NADH and NAD^+ respectively, thus allowing the electron transport from one reaction to another. The NADH/NAD^+ couple is therefore strongly connected to a wide range of reactions involved in redox- and energy- metabolisms.

The ratio between the reduced and oxidized forms, NADH/NAD^+ , is admitted to be a key parameter in glycolysis regulation and is more generally defined as the readout of the whole cellular redox state. Conventional NADH measurement is based on chemical determination or UV-autofluorescence imaging. Both methods are presenting limitations which may be linked to pH changes, uncontrolled contamination from the mitochondrial fraction, cell injury resulting from UV irradiation and to the unspecific assessment of NADH (face to NADPH). Generally, studies involving NADH measurement focus on mitochondrial NADH levels (Mayevsky, 2009). The NAD^+/NADH ratio in mitochondria is reported as varying from 2 to 16 (Kasimova et al., 2006; Williamson et al., 1967). To overcome disadvantages of usual techniques, two groups simultaneously presented two genetically encoded biosensors for NADH and NADH/NAD^+ intracellular detection: Peredox (Hung et al., 2011) and Frex (Zhao et al., 2011).

These two bio-inspired sensors are based the conformational changes triggered upon the binding of NADH to the DNA binding domain of the Rex protein. Once NADH attached, it adopts a more closed conformation. In addition, Rex does not possess any catalytic activity supporting that Rex-based biosensors are not modifying the level of cellular NADH neither by

consumption nor by diminishing its cytosolic-free fraction: its buffering effect would be negligible like cytosolic NADH is buffered by the endogenous protein-bound pool in a larger extent. Both of the sensors combined a cpFP (T-Sapphire or cpYFP) to the bacterial protein Rex. Concerning their design, the Rex dimer is connected through the cpFP as a single amino acid chain, making the conformational changes propagated within the β -barrel of the cpFP and triggering modifications of its emission fluorescence.

The two sensors allow to monitor NADH/NAD⁺ redox state and its subcellular analysis when specifically tagged with organelle-specific signal peptides. In addition to present advantages of genetically encoded biosensors such as sensitivity and dynamic direct spatiotemporal measurement, they avoid interferences linked to NADH relative availability, due to its coenzyme nature, which can affect indirect measurements.

Extensive directed-mutagenesis of both recognition element and fluorescent proteins yielded versions of these sensors suitable for experiments in cells and which give interpretable results in presence of pH variation or NADH concentrations varying by orders of magnitude.

Although the first version of Peredox was reporting $[NADH]x[H^+]/[NAD^+]$ authors engineered by random mutagenesis their biosensor to reduce its pH sensitivity. Peredox present almost same sensitivity for NADH/NAD⁺ (NAD⁺/NADH ratio from 480 to 40) on a pH range going from 6.7 to 7.7. However, presented sensitivities do not allow the use of Peredox in mitochondria as NADH/NAD⁺ ratio has been estimated to be 100- to 1000-fold higher than in the cytosol. Use of Peredox was validated through observations of NADH/NAD⁺ redox states in various cells, such as primary mouse astrocytes and neurons. Imaging methods, technical considerations related to Peredox and explanation on how to measure cytosolic NADH/NAD⁺ ratios in individual living cells are presented in Hung and Yellen, 2014.

By contrast, Frex is presented as being sensitive to pH. However, Frex and cpYFP respond in a very similar way to pH changes, thus the effect of pH on NADH measurement can be corrected through normalization of the Frex signal by cpYFP fluorescence measured in parallel. Authors, generated variants of Frex, by site directed mutagenesis of the NADH binding site. These variants show different affinities for NADH and thus, can be used in subcellular compartments containing various NADH concentration. FrexH has an affinity of ~

40 nM as compared to Frex which has an initial affinity of $\sim 3.7 \mu\text{M}$ at pH 7.4, increasing to $\sim 11 \mu\text{M}$ at pH 8.0. In addition, the sensitivity of the sensor for NADH analogs, such as NADPH, was also abolished. Using Frex, NADH fluctuations under metabolic challenges (NADH addition in the medium; 3-NP; rotenone) were followed in different subcellular compartments including mitochondria (Zhao et al., 2011).

Frex and FrexH are based on the Rex isoform from *B. subtilis* whereas Peredox relies on the isoform of *Thermus aquaticus*. Also, Frex does not contain its DNA binding domain anymore. Frex and Peredox exhibited respectively a 900% and a 150% increase in fluorescence upon NADH binding. This makes the Frex sensor more resolving when studying subtle differences in NADH levels. The high sensitivity of Peredox does not permit investigation at the level of the mitochondria and renders the sensor saturated under normal physiological conditions (3 to 5 mM glucose in the medium). This means that the probe should be calibrated with pyruvate and lactate (Hung et al., 2011). However, Frex is sensitive to pH and fluorescence correction using cpYFP measurement in parallel has to be done. By contrast, Peredox is relatively resistant to pH, making it more suitable for conditions with fluctuating intracellular pH levels. As peredox is too sensitive to measure NADH levels in mitochondria it is advisable to evaluate NADH_{mit} via common autofluorescence techniques as most intracellular NADH is located there. The Frex sensor is specific for NADH and by extension cannot measure the critical NADH/NAD^+ ratio. However, although NAD^+ competes with NADH during sensor binding, Peredox is not perfect a perfect reflector of NADH/NAD^+ ratio because its fluorescence varies significantly under different NAD^+ concentrations, even when the NADH/NAD^+ ratio remains relatively constant. A short comparison of both sensors Frex and Peredox discussing their benefits and limitations is available (Zhao and Yang, 2012).

Frex and Peredox sensors represent promising tool to monitor NADH/NAD^+ fluctuation in real time and space in living cell. However, by contrast to the ATeam sensor, we are regretting that studies using these sensors were only achieved by the groups who created them.

9. Other metabolites

Genetically encoded fluorescent biosensors to follow fluctuations of intermediate species of different pathways of the metabolism had also been developed (glucose (Behjousiar et al., 2012; Deuschle et al., 2006), 2-oxoglutarate (Zhang and Ye, 2014), glutamate (Hires et al., 2008), lactate (San Martín et al., 2013), citrate (Ewald et al., 2011), and others C4 carboxylates (Bourdès et al., 2012). These sensors are useful for the evaluation of metabolic manipulations at the level of specific step of given metabolic pathways. Such biosensors provide details essential for the understanding of the cellular energy metabolism through a systemic point of view.

10.AMPK

Examination of the impact of metabolic challenges (disease, treatment etc...) at the level of the energy metabolism can also be achieved through the analysis of key regulating enzymes of the cellular energy homeostasis.

AMP-activated protein kinase (AMPK) is considered as the master regulator of energy homeostasis in eukaryotic cell. Increase of AMP/ATP ratio due to energy stress triggers AMPK activation. AMPK activity modulates the whole metabolism and aims to recover energy homeostasis by inhibiting anabolic pathways and stimulating catabolic pathways. Tsou et al. developed a genetically encoded fluorescent biosensor for AMPK activity monitoring: AMPK Activity Reporter (AMPKAR) (Tsou et al., 2011). Similarly to PKA and PKD activity reporters, the designed sensor consists of the FRET pair eCFP and cpVenus which flanked an AMPK substrate motif peptide fused to the phospho-threonine-binding domain FHA1. When activated AMPK phosphorylates the substrate motif driving its subsequent binding to the FHA1 module and resulting in the juxtaposition of donor and acceptor fluorophores, yielding FRET. Live monitoring of AMPK activity may provide crucial information concerning effects of treatment, diseases, and stresses regarding cellular energy homeostasis and metabolism. Aware of the cautionary note Willemse et al. reported (Willemse et al., 2007), authors validated that the FRET signal variation is not linked to ATP hydrolysis and only to AMPK activity. Due to similarities among the optimal substrate motifs

of PKA, PKC, PKD and AMPK, they also examined whether activation of these kinases would produce any changes in the AMPKAR signal. Like other genetically encoded biosensor, such a reporter allows the spatiotemporal analysis of transient events in the context of living cells. As already mentioned, this represents an advantage when studying enzyme activities by contrast to their analysis by immunoblotting techniques. As AMPKAR can also be dephosphorylated, it allows the monitoring of events that are reversible with a real-time readout. However, AMPKAR is most probably dephosphorylated under kinetics varying from dephosphorylation kinetics of the AMPK targets. In addition, the allosteric activation due to AMP increase and the modulation of AMPK phosphorylation status by AMP and ADP may be hardly monitored due to the phosphorylation dependent readout. AMPK remains active when phosphorylated and bound to ATP. Hence, despite considerations of AMP and ADP as reporter of energetic stress (Hardie et al., 2011), AMPKAR appears to not be totally suitable to follow subtle changes in AMPK activity due to transient variations in the adenylates pool.

Validation of the AMPKAR sensor was assessed through comparison of results obtained using the sensor with other obtained by immunoblotting analysis. It was shown that AMPKAR generates data consistent with other biochemical approaches and which show a greater spatiotemporal resolution. Using AMPKAR, it was shown that the AMPK magnitude-response is related to the level of the applied stimuli. Also, the mechanism by which cells produce a global phenotypic gradual AMPK-response was reported: the more moderate is the stress, the more variable is the AMPK response from cell to cell. This means that a light response, linked to a moderate energetic stress would in fact be the average of a wide variety of response intensities, while a strong response to a severe metabolic stress would correspond to a uniform response of great amplitude.

Because the heterogeneity among individual cells is a common feature of dynamic cellular processes, genetically encoded fluorescent sensors should be considered as tools of choice to investigate cellular response to stress. Biosensors allow the better understanding of how a various cell-to-cell response contributes to the overall tissue level phenotype. Indeed, which properties are varying and which are robust from cells to cells could be investigated. Recently, a first study using AMPKAR was published (Miyamoto et al., 2015) and it reported an improved version of AMPKAR. The fluorescent proteins have been replaced and organelle-targeting sequences have been appended to study the compartmentalization of

the AMPK signaling. Interestingly, it was observed that the brain-specific kinases (BRSK 1/2) could also phosphorylate the AMPK activity reporter, thus AMPKAR was renamed into ABKAR for AMPK/BRSK activity reporter. Thus, such a sensor should only be used in non-neuronal cells, lacking the expression of BRSK 1/2, to focus on AMPK signaling.

AMPK is activated through systemic pathways by phosphorylation on the activation loop but also in a metabolic manner by adenylates fluctuations. As previously mentioned, a sensor specifically addressed to the allosteric activation of AMPK would allow the monitoring of AMPK activation due to energy balance disturbance during metabolic stress. Such sensor that exclusively reports allosteric activation of AMPK was aimed to be created during the presented work. With a larger scope than studying energy metabolism, such sensors can be considered as promising tools for the identification, by screening procedures based on allosterically reporting AMPK, of new drugs for the treatments of metabolic diseases.

11. Summary

As FRET signal is easily imaged, non-destructive, and proved to be one of the most versatile fluorescent readout, numerous FRET-based genetically encoded biosensors were designed and created during the last decade. In addition, despite their non ratiometric readout, cpFP-based fluorescent biosensors emerged offering greater range in fluorescence fluctuation. Many genetically encoded fluorescent biosensors have been developed to monitor metabolites fluctuations within their metabolic pathways. Glucose (Behjousiar et al., 2012; Deuschle et al., 2006), tryptophan (Kaper et al., 2007), arginine (Bogner and Ludewig, 2007), glutamine (Gruenwald et al., 2012), glutamate (Hires et al., 2008), leucine and histidine (Okada et al., 2009), lactate (San Martín et al., 2013), citrate (Ewald et al., 2011) and others C4 carboxylates (Bourdès et al., 2012) can be monitored using such biosensors. Cellular parameters which globally regulate these pathways can also be followed using biosensors, such as ATP (Imamura et al., 2009), NADH (Hung et al., 2011; Zhao et al., 2011), or AMPK activity (Tsou et al., 2011). In addition, several fluorescent biosensors have been developed for cAMP (Binkowski et al., 2011b). Unlike conventional methods, which indirectly generate punctual and isolated data, genetically encoded fluorescent biosensors can be used for spatiotemporal analysis of the energy metabolism. Thus, they allow to study transient

events, such as the dynamics of energy metabolites (ATP, NADH, Ca^{2+}), occurring in living cells under metabolic challenges. In addition, such probes generate information from the sub cellular compartment, where they can be targeted, to the whole cell population and thus provide insight of biological response from various level. Studies involving genetically encoded biosensors can be conducted at different level and can easily be achieved simultaneously due to the large number of fluorescent proteins available. Such approach has been proved to be suitable for analyzing metabolic phenomena *in situ* with an integrated vision.

12. References

- Allen, M.D., and Zhang, J. (2006). Subcellular dynamics of protein kinase A activity visualized by FRET-based reporters. *Biochem. Biophys. Res. Commun.* *348*, 716–721.
- Almahariq, M., Mei, F.C., and Cheng, X. (2014). Cyclic AMP sensor EPAC proteins and energy homeostasis. *Trends Endocrinol. Metab.* *25*, 60–71.
- Ando, T., Imamura, H., Suzuki, R., Aizaki, H., Watanabe, T., Wakita, T., and Suzuki, T. (2012). Visualization and measurement of ATP levels in living cells replicating hepatitis C virus genome RNA. *PLoS Pathog.* *8*, e1002561.
- Astrup, A. (2008). The role of calcium in energy balance and obesity: the search for mechanisms. *Am. J. Clin. Nutr.* *88*, 873–874.
- Atkinson, D.E. (1968). The energy charge of the adenylate pool as a regulatory parameter. Interaction with feedback modifiers. *Biochemistry (Mosc.)* *7*, 4030–4034.
- Atkinson, D.E., and Walton, G.M. (1967). Adenosine triphosphate conservation in metabolic regulation. Rat liver citrate cleavage enzyme. *J. Biol. Chem.* *242*, 3239–3241.
- Baird, G.S., Zacharias, D.A., and Tsien, R.Y. (1999). Circular permutation and receptor insertion within green fluorescent proteins. *Proc. Natl. Acad. Sci. U. S. A.* *96*, 11241–11246.
- Bak, M.I., and Ingwall, J.S. (1992). NMR-invisible ATP in heart: fact or fiction? *Am. J. Physiol. - Endocrinol. Metab.* *262*, E943–E947.
- Baker, K.D., and Thummel, C.S. (2007). Diabetic larvae and obese flies—emerging studies of metabolism in *Drosophila*. *Cell Metab.* *6*, 257–266.
- Bastiaens, P.I.H., and Squire, A. (1999). Fluorescence lifetime imaging microscopy: spatial resolution of biochemical processes in the cell. *Trends Cell Biol.* *9*, 48–52.
- Bastiaens, P.I., and Jovin, T.M. (1996). Microspectroscopic imaging tracks the intracellular processing of a signal transduction protein: fluorescent-labeled protein kinase C beta I. *Proc. Natl. Acad. Sci. U. S. A.* *93*, 8407–8412.
- Baubet, V., Le Mouellic, H., Campbell, A.K., Lucas-Meunier, E., Fossier, P., and Brûlet, P. (2000). Chimeric green fluorescent protein-aequorin as bioluminescent Ca²⁺ reporters at the single-cell level. *Proc. Natl. Acad. Sci. U. S. A.* *97*, 7260–7265.
- Behjousiar, A., Kontoravdi, C., and Polizzi, K.M. (2012). In situ monitoring of intracellular glucose and glutamine in CHO cell culture. *PLoS One* *7*, e34512.
- Di Benedetto, G., Scalzotto, E., Mongillo, M., and Pozzan, T. (2013). Mitochondrial Ca²⁺ uptake induces cyclic AMP generation in the matrix and modulates organelle ATP levels. *Cell Metab.* *17*, 965–975.
- Berg, J., Hung, Y.P., and Yellen, G. (2009). A genetically encoded fluorescent reporter of ATP/ADP ratio. *Nat. Methods* *6*, 161–166.
- Binkowski, B.F., Fan, F., and Wood, K.V. (2011a). Luminescent biosensors for real-time monitoring of intracellular cAMP. *Methods Mol. Biol. Clifton NJ* *756*, 263–271.
- Binkowski, B.F., Butler, B.L., Stecha, P.F., Eggers, C.T., Otto, P., Zimmerman, K., Vidugiris, G., Wood, M.G., Encell, L.P., Fan, F., et al. (2011b). A luminescent biosensor with increased dynamic range for intracellular cAMP. *ACS Chem. Biol.* *6*, 1193–1197.
- Bogner, M., and Ludewig, U. (2007). Visualization of arginine influx into plant cells using a specific FRET-sensor. *J. Fluoresc.* *17*, 350–360.
- Bourdès, A., Rudder, S., East, A.K., and Poole, P.S. (2012). Mining the *Sinorhizobium meliloti* transportome to develop FRET biosensors for sugars, dicarboxylates and cyclic polyols. *PLoS One* *7*, e43578.
- Carlucci, A., Lignitto, L., and Feliciello, A. (2008). Control of mitochondria dynamics and oxidative metabolism by cAMP, AKAPs and the proteasome. *Trends Cell Biol.* *18*, 604–613.
- Castro, L.R.V., Guiot, E., Polito, M., Paupardin-Tritsch, D., and Vincent, P. (2014). Decoding spatial and temporal features of neuronal cAMP/PKA signaling with FRET biosensors. *Biotechnol. J.* *9*, 192–202.

- Chiesa, A., Rapizzi, E., Tosello, V., Pinton, P., de Virgilio, M., Fogarty, K.E., and Rizzuto, R. (2001). Recombinant aequorin and green fluorescent protein as valuable tools in the study of cell signalling. *Biochem. J.* 355, 1–12.
- Chouhan, A.K., Ivannikov, M.V., Lu, Z., Sugimori, M., Llinas, R.R., and Macleod, G.T. (2012). Cytosolic calcium coordinates mitochondrial energy metabolism with presynaptic activity. *J. Neurosci. Off. J. Soc. Neurosci.* 32, 1233–1243.
- Clapham, D.E. (2007). Calcium Signaling. *Cell* 131, 1047–1058.
- Créton, R., Kreiling, J.A., and Jaffe, L.F. (1999). Calcium imaging with chemiluminescence. *Microsc. Res. Tech.* 46, 390–397.
- Deuschle, K., Chaudhuri, B., Okumoto, S., Lager, I., Lalonde, S., and Frommer, W.B. (2006). Rapid metabolism of glucose detected with FRET glucose nanosensors in epidermal cells and intact roots of Arabidopsis RNA-silencing mutants. *Plant Cell* 18, 2314–2325.
- Dorsten, F.A., Wyss, M., Wallimann, T., and Nicolay, K. (1997). Activation of sea-urchin sperm motility is accompanied by an increase in the creatine kinase exchange flux. *Biochem. J.* 325, 411–416.
- Dumas, J.F., Argaud, L., Cottet-Rousselle, C., Vial, G., Gonzalez, C., Detaille, D., Lerverve, X., and Fontaine, E. (2009). Effect of transient and permanent permeability transition pore opening on NAD(P)H localization in intact cells. *J. Biol. Chem.* 284, 15117–15125.
- Erecińska, M., and Silver, I.A. (1994). Ions and energy in mammalian brain. *Prog. Neurobiol.* 43, 37–71.
- Ewald, J.C., Reich, S., Baumann, S., Frommer, W.B., and Zamboni, N. (2011). Engineering genetically encoded nanosensors for real-time in vivo measurements of citrate concentrations. *PloS One* 6, e28245.
- Feniouk, B.A., Suzuki, T., and Yoshida, M. (2006). The role of subunit epsilon in the catalysis and regulation of FOF1-ATP synthase. *Biochim. Biophys. Acta* 1757, 326–338.
- Forkink, M., Manjeri, G.R., Liemburg-Apers, D.C., Nibbeling, E., Blanchard, M., Wojtala, A., Smeitink, J.A.M., Wieckowski, M.R., Willems, P.H.G.M., and Koopman, W.J.H. (2014). Mitochondrial hyperpolarization during chronic complex I inhibition is sustained by low activity of complex II, III, IV and V. *Biochim. Biophys. Acta* 1837, 1247–1256.
- Gajewski, C.D., Yang, L., Schon, E.A., and Manfredi, G. (2003). New Insights into the Bioenergetics of Mitochondrial Disorders Using Intracellular ATP Reporters. *Mol. Biol. Cell* 14, 3628–3635.
- Gout, E., Rébeillé, F., Douce, R., and Bligny, R. (2014). Interplay of Mg²⁺, ADP, and ATP in the cytosol and mitochondria: Unravelling the role of Mg²⁺ in cell respiration. *Proc. Natl. Acad. Sci.* 111, E4560–E4567.
- Griesbeck, O., Baird, G.S., Campbell, R.E., Zacharias, D.A., and Tsien, R.Y. (2001). Reducing the environmental sensitivity of yellow fluorescent protein. Mechanism and applications. *J. Biol. Chem.* 276, 29188–29194.
- Gruenwald, K., Holland, J.T., Stromberg, V., Ahmad, A., Watcharakichkorn, D., and Okumoto, S. (2012). Visualization of glutamine transporter activities in living cells using genetically encoded glutamine sensors. *PloS One* 7, e38591.
- Hanson, G.T., Aggeler, R., Oglesbee, D., Cannon, M., Capaldi, R.A., Tsien, R.Y., and Remington, S.J. (2004). Investigating Mitochondrial Redox Potential with Redox-sensitive Green Fluorescent Protein Indicators. *J. Biol. Chem.* 279, 13044–13053.
- Hardie, D.G., and Hawley, S.A. (2001). AMP-activated protein kinase: the energy charge hypothesis revisited. *Bioessays* 23, 1112–1119.
- Hardie, D.G., Carling, D., and Gamblin, S.J. (2011). AMP-activated protein kinase: also regulated by ADP? *Trends Biochem Sci* 36, 470–477.
- Hardie, D.G., Ross, F.A., and Hawley, S.A. (2012). AMPK: a nutrient and energy sensor that maintains energy homeostasis. *Nat Rev Mol Cell Biol* 13, 251–262.
- Harmsen, E., De Tombe, P.P., and De Jong, J.W. (1982). Simultaneous determination of myocardial adenine nucleotides and creatine phosphate by high-performance liquid chromatography. *J. Chromatogr. B. Biomed. Sci. App.* 230, 131–136.

- Harrison, J.F., and Haddad, G.G. (2011). Effects of oxygen on growth and size: synthesis of molecular, organismal, and evolutionary studies with *Drosophila melanogaster*. *Annu. Rev. Physiol.* *73*, 95–113.
- Heim, N., and Griesbeck, O. (2004). Genetically encoded indicators of cellular calcium dynamics based on troponin C and green fluorescent protein. *J. Biol. Chem.* *279*, 14280–14286.
- Hires, S.A., Zhu, Y., and Tsien, R.Y. (2008). Optical measurement of synaptic glutamate spillover and reuptake by linker optimized glutamate-sensitive fluorescent reporters. *Proc. Natl. Acad. Sci. U. S. A.* *105*, 4411–4416.
- Huang, S. (2011). Systems biology of stem cells: three useful perspectives to help overcome the paradigm of linear pathways. *Philos. Trans. R. Soc. B Biol. Sci.* *366*, 2247–2259.
- Hung, Y.P., and Yellen, G. (2014). Live-cell imaging of cytosolic NADH-NAD⁺ redox state using a genetically encoded fluorescent biosensor. *Methods Mol. Biol. Clifton NJ* *1071*, 83–95.
- Hung, Y.P., Albeck, J.G., Tantama, M., and Yellen, G. (2011). Imaging cytosolic NADH-NAD(+) redox state with a genetically encoded fluorescent biosensor. *Cell Metab.* *14*, 545–554.
- Imamura, H., Nhat, K.P.H., Togawa, H., Saito, K., Iino, R., Kato-Yamada, Y., Nagai, T., and Noji, H. (2009). Visualization of ATP levels inside single living cells with fluorescence resonance energy transfer-based genetically encoded indicators. *Proc. Natl. Acad. Sci. U. S. A.* *106*, 15651–15656.
- Kamioka, Y., Sumiyama, K., Mizuno, R., and Matsuda, M. (2013). Live imaging of transgenic mice expressing FRET biosensors. *Conf. Proc. Annu. Int. Conf. IEEE Eng. Med. Biol. Soc. IEEE Eng. Med. Biol. Soc. Annu. Conf. 2013*, 125–128.
- Kaper, T., Looger, L.L., Takana, H., Platten, M., Steinman, L., and Frommer, W.B. (2007). Nanosensor detection of an immunoregulatory tryptophan influx/kynurenine efflux cycle. *PLoS Biol.* *5*, e257.
- Kasimova, M.R., Grigienė, J., Krab, K., Hagedorn, P.H., Flyvbjerg, H., Andersen, P.E., and Møller, I.M. (2006). The free NADH concentration is kept constant in plant mitochondria under different metabolic conditions. *Plant Cell* *18*, 688–698.
- Kemp, G.J., and Brindle, K.M. (2012). What do magnetic resonance-based measurements of Pi→ATP flux tell us about skeletal muscle metabolism? *Diabetes* *61*, 1927–1934.
- Kemp, G.J., Ahmad, R.E., Nicolay, K., and Prompers, J.J. (2015). Quantification of skeletal muscle mitochondrial function by ³¹P magnetic resonance spectroscopy techniques: a quantitative review. *Acta Physiol. Oxf. Engl.* *213*, 107–144.
- Kendall, J.M., and Badminton, M.N. (1998). *Aequorea victoria* bioluminescence moves into an exciting new era. *Trends Biotechnol.* *16*, 216–224.
- Kennedy, H.J., Pouli, A.E., Ainscow, E.K., Jouaville, L.S., Rizzuto, R., and Rutter, G.A. (1999). Glucose generates sub-plasma membrane ATP microdomains in single islet beta-cells. Potential role for strategically located mitochondria. *J. Biol. Chem.* *274*, 13281–13291.
- Kishikawa, J., Fujikawa, M., Imamura, H., Yasuda, K., Noji, H., Ishii, N., Mitani, S., and Yokoyama, K. (2012). MRT letter: Expression of ATP sensor protein in *Caenorhabditis elegans*. *Microsc. Res. Tech.* *75*, 15–19.
- Klarenbeek, J., and Jalink, K. (2014). Detecting cAMP with an EPAC-based FRET sensor in single living cells. *Methods Mol. Biol. Clifton NJ* *1071*, 49–58.
- Kneen, M., Farinas, J., Li, Y., and Verkman, A.S. (1998). Green fluorescent protein as a noninvasive intracellular pH indicator. *Biophys. J.* *74*, 1591–1599.
- Koretsky, A.P., Brosnan, M.J., Chen, L.H., Chen, J.D., and Van Dyke, T. (1990). NMR detection of creatine kinase expressed in liver of transgenic mice: determination of free ADP levels. *Proc. Natl. Acad. Sci. U. S. A.* *87*, 3112–3116.
- Kotera, I., Iwasaki, T., Imamura, H., Noji, H., and Nagai, T. (2010). Reversible dimerization of *Aequorea victoria* fluorescent proteins increases the dynamic range of FRET-based indicators. *ACS Chem. Biol.* *5*, 215–222.
- Kotlikoff, M.I. (2007). Genetically encoded Ca²⁺ indicators: using genetics and molecular design to understand complex physiology. *J. Physiol.* *578*, 55–67.

- Kunkel, M.T., Toker, A., Tsien, R.Y., and Newton, A.C. (2007). Calcium-dependent regulation of protein kinase D revealed by a genetically encoded kinase activity reporter. *J. Biol. Chem.* *282*, 6733–6742.
- Kunzelmann, S., and Webb, M.R. (2009). A biosensor for fluorescent determination of ADP with high time resolution. *J. Biol. Chem.* *284*, 33130–33138.
- Kunzelmann, S., and Webb, M.R. (2010). A fluorescent, reagentless biosensor for ADP based on tetramethylrhodamine-labeled ParM. *ACS Chem. Biol.* *5*, 415–425.
- Kunzelmann, S., and Webb, M.R. (2011). Fluorescence detection of GDP in real time with the reagentless biosensor rhodamine-ParM. *Biochem. J.* *440*, 43–49.
- Kuznetsov, A., Bindokas, V.P., Marks, J.D., and Philipson, L.H. (2005). FRET-based voltage probes for confocal imaging: membrane potential oscillations throughout pancreatic islets. *Am. J. Physiol. Cell Physiol.* *289*, C224–C229.
- Lakowicz, J.R., Szmacinski, H., Nowaczyk, K., Lederer, W.J., Kirby, M.S., and Johnson, M.L. (1994). Fluorescence lifetime imaging of intracellular calcium in COS cells using Quin-2. *Cell Calcium* *15*, 7–27.
- Leadsham, J.E., and Gourlay, C.W. (2010). cAMP/PKA signaling balances respiratory activity with mitochondria dependent apoptosis via transcriptional regulation. *BMC Cell Biol.* *11*, 92.
- Lebon, V., Dufour, S., Petersen, K.F., Ren, J., Jucker, B.M., Slezak, L.A., Cline, G.W., Rothman, D.L., and Shulman, G.I. (2001). Effect of triiodothyronine on mitochondrial energy coupling in human skeletal muscle. *J. Clin. Invest.* *108*, 733–737.
- Lee, M.-S., Park, W.-S., Kim, Y.H., Ahn, W.G., Kwon, S.-H., and Her, S. (2012). Intracellular ATP assay of live cells using PTD-conjugated luciferase. *Sensors* *12*, 15628–15637.
- Li, J., Shuai, H.Y., Gylfe, E., and Tengholm, A. (2013). Oscillations of sub-membrane ATP in glucose-stimulated beta cells depend on negative feedback from Ca²⁺. *Diabetologia* *56*, 1577–1586.
- Liu, X., Wu, J., Liu, H., Zong, N., and Zhao, J. (2014). RoGFP1 is a quantitative biosensor in maize cells for cellular redox changes caused by environmental and endogenous stimuli. *Biochem. Biophys. Res. Commun.* *452*, 503–508.
- Llopis, J., McCaffery, J.M., Miyawaki, A., Farquhar, M.G., and Tsien, R.Y. (1998). Measurement of cytosolic, mitochondrial, and Golgi pH in single living cells with green fluorescent proteins. *Proc. Natl. Acad. Sci. U. S. A.* *95*, 6803–6808.
- Lyman, G.E., and DeVincenzo, J.P. (1967). Determination of picogram amounts of ATP using the luciferin-luciferase enzyme system. *Anal. Biochem.* *21*, 435–443.
- Manfredi, G., Yang, L., Gajewski, C.D., and Mattiazzi, M. (2002). Measurements of ATP in mammalian cells. *Methods* *26*, 317–326.
- Mank, M., and Griesbeck, O. (2008). Genetically encoded calcium indicators. *Chem. Rev.* *108*, 1550–1564.
- Mank, M., Reiff, D.F., Heim, N., Friedrich, M.W., Borst, A., and Griesbeck, O. (2006). A FRET-based calcium biosensor with fast signal kinetics and high fluorescence change. *Biophys. J.* *90*, 1790–1796.
- Mayevsky, A. (2009). Mitochondrial function and energy metabolism in cancer cells: past overview and future perspectives. *Mitochondrion* *9*, 165–179.
- McGilver, R.W., and Murray, T.W. (1974). Calculated equilibria of phosphocreatine and adenosine phosphates during utilization of high energy phosphate by muscle. *J. Biol. Chem.* *249*, 5845–5850.
- Mekler, V., Kortkhonjia, E., Mukhopadhyay, J., Knight, J., Revyakin, A., Kapanidis, A.N., Niu, W., Ebricht, Y.W., Levy, R., and Ebricht, R.H. (2002). Structural Organization of Bacterial RNA Polymerase Holoenzyme and the RNA Polymerase-Promoter Open Complex. *Cell* *108*, 599–614.
- Miyamoto, T., Rho, E., Sample, V., Akano, H., Magari, M., Ueno, T., Gorshkov, K., Chen, M., Tokumitsu, H., Zhang, J., et al. (2015). Compartmentalized AMPK Signaling Illuminated by Genetically Encoded Molecular Sensors and Actuators. *Cell Rep.*
- Miyawaki, A., Llopis, J., Heim, R., McCaffery, J.M., Adams, J.A., Ikura, M., and Tsien, R.Y. (1997). Fluorescent indicators for Ca²⁺ based on green fluorescent proteins and calmodulin. *Nature* *388*, 882–887.

- Miyawaki, A., Griesbeck, O., Heim, R., and Tsien, R.Y. (1999). Dynamic and quantitative Ca²⁺ measurements using improved cameleons. *Proc. Natl. Acad. Sci.* *96*, 2135–2140.
- Mörköfer-Zwez, S., and Walter, P. (1989). Binding of ADP to rat liver cytosolic proteins and its influence on the ratio of free ATP/free ADP. *Biochem. J.* *259*, 117–124.
- Nagai, T., Sawano, A., Park, E.S., and Miyawaki, A. (2001). Circularly permuted green fluorescent proteins engineered to sense Ca²⁺. *Proc. Natl. Acad. Sci. U. S. A.* *98*, 3197–3202.
- Nagai, T., Ibata, K., Park, E.S., Kubota, M., Mikoshiba, K., and Miyawaki, A. (2002). A variant of yellow fluorescent protein with fast and efficient maturation for cell-biological applications. *Nat. Biotechnol.* *20*, 87–90.
- Nagai, T., Yamada, S., Tominaga, T., Ichikawa, M., and Miyawaki, A. (2004). Expanded dynamic range of fluorescent indicators for Ca²⁺ by circularly permuted yellow fluorescent proteins. *Proc. Natl. Acad. Sci. U. S. A.* *101*, 10554–10559.
- Nakano, M., Imamura, H., Nagai, T., and Noji, H. (2011). Ca²⁺ regulation of mitochondrial ATP synthesis visualized at the single cell level. *ACS Chem. Biol.* *6*, 709–715.
- Nilsson, T., Schultz, V., Berggren, P.O., Corkey, B.E., and Tornheim, K. (1996). Temporal patterns of changes in ATP/ADP ratio, glucose 6-phosphate and cytoplasmic free Ca²⁺ in glucose-stimulated pancreatic beta-cells. *Biochem. J.* *314 (Pt 1)*, 91–94.
- Oakhill, J.S., Scott, J.W., and Kemp, B.E. (2012). AMPK functions as an adenylate charge-regulated protein kinase. *Trends Endocrinol Metab* *23*, 125–132.
- Okada, S., Ota, K., and Ito, T. (2009). Circular permutation of ligand-binding module improves dynamic range of genetically encoded FRET-based nanosensor. *Protein Sci. Publ. Protein Soc.* *18*, 2518–2527.
- Paige, J.S., Nguyen-Duc, T., Song, W., and Jaffrey, S.R. (2012). Fluorescence Imaging of Cellular Metabolites with RNA. *Science* *335*, 1194–1194.
- Palmer, A.E., and Tsien, R.Y. (2006). Measuring calcium signaling using genetically targetable fluorescent indicators. *Nat. Protoc.* *1*, 1057–1065.
- Palmer, A.E., Qin, Y., Park, J.G., and McCombs, J.E. (2011). Design and application of genetically encoded biosensors. *Trends Biotechnol.* *29*, 144–152.
- Piljić, A., de Diego, I., Wilmanns, M., and Schultz, C. (2011). Rapid development of genetically encoded FRET reporters. *ACS Chem. Biol.* *6*, 685–691.
- Poburko, D., Santo-Domingo, J., and Demarex, N. (2011). Dynamic regulation of the mitochondrial proton gradient during cytosolic calcium elevations. *J. Biol. Chem.* *286*, 11672–11684.
- Rizzo, M.A., Springer, G.H., Granada, B., and Piston, D.W. (2004). An improved cyan fluorescent protein variant useful for FRET. *Nat. Biotechnol.* *22*, 445–449.
- Sanders, R., Draaijer, A., Gerritsen, H.C., Houpt, P.M., and Levine, Y.K. (1995). Quantitative pH imaging in cells using confocal fluorescence lifetime imaging microscopy. *Anal. Biochem.* *227*, 302–308.
- San Martín, A., Ceballo, S., Ruminot, I., Lerchundi, R., Frommer, W.B., and Barros, L.F. (2013). A genetically encoded FRET lactate sensor and its use to detect the Warburg effect in single cancer cells. *PLoS One* *8*, e57712.
- Shaner, N.C., Campbell, R.E., Steinbach, P.A., Giepmans, B.N.G., Palmer, A.E., and Tsien, R.Y. (2004). Improved monomeric red, orange and yellow fluorescent proteins derived from *Discosoma* sp. red fluorescent protein. *Nat. Biotechnol.* *22*, 1567–1572.
- Shaner, N.C., Steinbach, P.A., and Tsien, R.Y. (2005). A guide to choosing fluorescent proteins. *Nat. Methods* *2*, 905–909.
- Takami, H., Furuya, E., Tagawa, K., Seo, Y., Murakami, M., Watari, H., Matsuda, H., Hirose, H., and Kawashima, Y. (1988). NMR-invisible ATP in rat heart and its change in ischemia. *J. Biochem. (Tokyo)* *104*, 35–39.
- Tantama, M., Martínez-François, J.R., Mongeon, R., and Yellen, G. (2013). Imaging energy status in live cells with a fluorescent biosensor of the intracellular ATP-to-ADP ratio. *Nat. Commun.* *4*, 2550.

- Tarasov, A.I., and Rutter, G.A. (2014). Use of genetically encoded sensors to monitor cytosolic ATP/ADP ratio in living cells. *Methods Enzymol.* 542, 289–311.
- Tarasov, A.I., Semplici, F., Ravier, M.A., Bellomo, E.A., Pullen, T.J., Gilon, P., Sekler, I., Rizzuto, R., and Rutter, G.A. (2012). The mitochondrial Ca²⁺ uniporter MCU is essential for glucose-induced ATP increases in pancreatic β -cells. *PLoS One* 7, e39722.
- Tarasov, A.I., Semplici, F., Li, D., Rizzuto, R., Ravier, M.A., Gilon, P., and Rutter, G.A. (2013). Frequency-dependent mitochondrial Ca(2+) accumulation regulates ATP synthesis in pancreatic β cells. *Pflüg. Arch. Eur. J. Physiol.* 465, 543–554.
- Teerlink, T., Hennekes, M., Bussemaker, J., and Groeneveld, J. (1993). Simultaneous determination of creatine compounds and adenine nucleotides in myocardial tissue by high-performance liquid chromatography. *Anal. Biochem.* 214, 278–283.
- Tian, L., Hires, S.A., Mao, T., Huber, D., Chiappe, M.E., Chalasani, S.H., Petreanu, L., Akerboom, J., McKinney, S.A., Schreier, E.R., et al. (2009). Imaging neural activity in worms, flies and mice with improved GCaMP calcium indicators. *Nat. Methods* 6, 875–881.
- Toloe, J., Mollajew, R., Kügler, S., and Mironov, S.L. (2014). Metabolic differences in hippocampal “Rett” neurons revealed by ATP imaging. *Mol. Cell. Neurosci.* 59, 47–56.
- Tseng, J.-C., and Kung, A.L. (2015). Quantitative bioluminescence imaging of mouse tumor models. *Cold Spring Harb. Protoc.* 2015, pdb.prot078261.
- Tsou, P., Zheng, B., Hsu, C.H., Sasaki, A.T., and Cantley, L.C. (2011). A fluorescent reporter of AMPK activity and cellular energy stress. *Cell Metab* 13, 476–486.
- Tsuyama, T., Kishikawa, J., Han, Y.-W., Harada, Y., Tsubouchi, A., Noji, H., Kakizuka, A., Yokoyama, K., Uemura, T., and Imamura, H. (2013). In vivo fluorescent adenosine 5'-triphosphate (ATP) imaging of *Drosophila melanogaster* and *Caenorhabditis elegans* by using a genetically encoded fluorescent ATP biosensor optimized for low temperatures. *Anal. Chem.* 85, 7889–7896.
- Vevea, J.D., Wolken, D.M.A., Swayne, T.C., White, A.B., and Pon, L.A. (2013). Ratiometric biosensors that measure mitochondrial redox state and ATP in living yeast cells. *J. Vis. Exp. JoVE.*
- Vishnu, N., Jadoon Khan, M., Karsten, F., Groschner, L.N., Waldeck-Weiermair, M., Rost, R., Hallstrom, S., Imamura, H., Graier, W.F., and Malli, R. (2014). ATP increases within the lumen of the endoplasmic reticulum upon intracellular Ca²⁺ release. *Mol Biol Cell* 25, 368–379.
- Wallimann, T., Tokarska-Schlattner, M., and Schlattner, U. (2011). The creatine kinase system and pleiotropic effects of creatine. *Amino Acids* 40, 1271–1296.
- Wiederkehr, A., Szanda, G., Akhmedov, D., Matak, C., Heizmann, C.W., Schoonjans, K., Pozzan, T., Spät, A., and Wollheim, C.B. (2011). Mitochondrial matrix calcium is an activating signal for hormone secretion. *Cell Metab.* 13, 601–611.
- Willemse, M., Janssen, E., de Lange, F., Wieringa, B., and Fransen, J. (2007). ATP and FRET—a cautionary note. *Nat. Biotechnol.* 25, 170–172.
- Williamson, D.H., Lund, P., and Krebs, H.A. (1967). The redox state of free nicotinamide-adenine dinucleotide in the cytoplasm and mitochondria of rat liver. *Biochem. J.* 103, 514–527.
- Wong, W., and Scott, J.D. (2004). AKAP signalling complexes: focal points in space and time. *Nat. Rev. Mol. Cell Biol.* 5, 959–970.
- Yang, N.-C., Ho, W.-M., Chen, Y.-H., and Hu, M.-L. (2002). A Convenient One-Step Extraction of Cellular ATP Using Boiling Water for the Luciferin–Luciferase Assay of ATP. *Anal. Biochem.* 306, 323–327.
- Zaccolo, M., De Giorgi, F., Cho, C.Y., Feng, L., Knapp, T., Negulescu, P.A., Taylor, S.S., Tsien, R.Y., and Pozzan, T. (2000). A genetically encoded, fluorescent indicator for cyclic AMP in living cells. *Nat. Cell Biol.* 2, 25–29.
- Zhang, C., and Ye, B.-C. (2014). A single fluorescent protein-based sensor for in vivo 2-oxoglutarate detection in cell. *Biosens. Bioelectron.* 54, 15–19.
- Zhang, J., Ma, Y., Taylor, S.S., and Tsien, R.Y. (2001). Genetically encoded reporters of protein kinase A activity reveal impact of substrate tethering. *Proc. Natl. Acad. Sci. U. S. A.* 98, 14997–15002.

Zhao, Y., and Yang, Y. (2012). Frex and FrexH: Indicators of metabolic states in living cells. *Bioeng. Bugs* 3, 181–188.

Zhao, Y., Jin, J., Hu, Q., Zhou, H.-M., Yi, J., Yu, Z., Xu, L., Wang, X., Yang, Y., and Loscalzo, J. (2011). Genetically encoded fluorescent sensors for intracellular NADH detection. *Cell Metab.* 14, 555–566.

Materials and Methods

1.	FRET principles.....	97
1.1.	FRET definition	97
1.2.	FRET signal	98
1.3.	FRET ratio.....	98
1.4.	Rationales for generation of a FRET sensor based on AMPK.....	99
2.	Molecular cloning	100
2.1.	Materials, buffers and solutions.....	100
2.2.	Genes of interest	100
2.3.	Bacterial strains.....	100
2.4.	Cell culture.....	101
2.4.1.	Cultivation of Escherichia coli (E.coli).....	101
2.4.2.	Transformation competent cells.....	101
2.5.	Nucleic acids biochemistry.....	102
2.5.1.	Concentration determination of nucleic acids	102
2.5.2.	Agarose gel electrophoresis	102
2.5.3.	DNA extraction from agarose gels	102
2.5.4.	Polymerase chain reaction (PCR)	102
2.5.5.	Restriction digestion of DNA	103
2.5.6.	DNA ligation	103
2.5.7.	Sequence and ligation independent cloning (SLIC)	103
2.5.8.	Self-SLIC.....	104
2.5.9.	Preparation of plasmid DNA.....	106
2.5.10.	Cre-loxP recombination of acceptor and donor plasmids.....	106
2.6.	ACEMBL	106
2.7.	AMPfret general construction by molecular cloning	107
2.7.1.	pACE-derived vectors.....	107
2.7.2.	pDC-derived vectors.....	109
2.7.3.	pDS-derived vectors.....	109
2.7.4.	pACEMBL vectors.....	110

2.8.	Site directed mutagenesis using self-SLIC	111
2.9.	FRET pair replacement.....	113
2.10.	AMPfret 2 nd generation	115
2.11.	Cloning in the MutliMam expression system	116
3.	Protein Biochemistry.....	117
3.1.	Materials for protein purification, buffers and other equipment.....	117
3.2.	Denaturing polyacrylamide gel electrophoresis (SDS-PAGE).....	117
3.3.	Concentration determination of proteins	118
3.4.	Expression and purification.....	118
4.	Characterization of AMPfret sensor in vitro	120
4.1.	HPLC analysis	120
4.2.	Enzymatic assay	120
4.3.	Enzymatic kinetic of CBS site mutants and effect of AMP.....	120
4.4.	ADP dependent protection from dephosphorylation	121
4.5.	FRET assay.....	121
4.6.	Ratio between free ATP and Mg ²⁺ -ATP estimation	123
4.7.	ATP analogues.....	123
5.	Characterization of AMPFret sensor in cellulo:	124
5.1.	Cell culture, transfection.....	124
5.2.	Confocal microscopy.....	124
5.3.	AICAR.....	124
5.4.	Ischemia reperfusion	125
5.5.	Western Blotting:	125
5.5.1.	Protein Extraction	125
5.5.2.	SDS-PAGE and Immunoblot	126

Parts of these methods have been published in:

Structural Proteomics: High Throughput Methods, Methods in Molecular Biology Volume 1261, 2015, pp 63-89. doi: 10.1007/978-1-4939-2230-7_4

Characterization and Production of Protein Complexes by Co-expression in *Escherichia coli*.
Matthias Haffke, Martin Marek, Martin Pelosse, Marie-Laure Diebold, Uwe Schlattner, Imre Berger, Christophe Romier.

1. FRET principles

1.1. FRET definition

Förster Resonance Energy Transfer (FRET), or Fluorescence Resonance Energy Transfer describes a distance-dependent physical process by which energy is transferred non-radiatively from an excited molecular fluorophore (the donor) to another fluorophore (the acceptor) by means of intermolecular long-range dipole–dipole coupling. Indeed, in FRET, a donor fluorophore is excited by incident light, and if an acceptor is in close proximity, the excited state energy from the donor can be transferred. This leads to a reduction in the donor's fluorescence intensity and excited state lifetime, and an increase in the acceptor's emission intensity. Förster (Förster, 1959) showed that the efficiency (E) of this process depends on 1) the inverse sixth power of intermolecular distance between donor and acceptor: $E=1/(1+(R/R_0)^6)$ where R_0 is the distance at which half of the energy is transferred, 2) the relative orientation of the dyes and also on 3) their spectral characteristics.

The fact that FRET depends on the inverse sixth-distance between donor and acceptor makes it a sensitive technique for investigating a variety of biological phenomena that produce changes in molecular proximity. FRET can be an accurate measurement of molecular proximity at angstrom distances (10–100 Å) and particularly highly efficient if the donor and acceptor are positioned within the distance at which half the excitation energy of the donor is transferred to the acceptor, typically 2–7 nm (the Förster radius R_0). It was shown that FRET can be used as a spectroscopic ruler (Stryer and Haugland, 1967) and that, by measuring E and knowing or calculating R_0 , distance could be inferred - typically in the order of R_0 . However, FRET is in general better suited for detecting changes in distance (conformation or association) rather than absolute distances. Indeed, E depends on the relative orientation of the dyes which can most of the time be poorly measured, especially because probe size and attachment methods cause uncertainty in probe final position with respect to the biomolecular backbone. FRET is one of the few tools available for measuring nanometer scale distances and especially changes in distances, both *in vitro* and *in vivo*. Actually, technological advances in light microscopy imaging and spectroscopy, combined with the increasing number of genetically encoded fluorescent proteins available, provide the tools necessary to obtain suitable spatiotemporal resolution when studying molecular

dynamics inside living cells, such as conformational changes in proteins or associations. Indeed, the widely used donor and acceptor fluorophores, which form a FRET pair, derived from a class of autofluorescent proteins that are all based on green fluorescent protein (GFP).

Inherent to FRET principles, GFPs are considered as workable FRET pairs when their spectroscopic properties include 1) separation in excitation spectra for selective stimulation of the donor GFP, 2) an overlap (>30%) between the emission spectrum of the donor and the excitation spectrum of the acceptor to obtain efficient energy transfer, 3) and reasonable separation in emission spectra between donor and acceptor to allow independent measurement of their respective fluorescence.

1.2. FRET signal

Typical FRET measurement consists in the excitation of the donor at a given wavelength (λ_{exc}), which relies on donor specific spectroscopic properties, followed by the monitoring of emitted fluorescence. The later can be done through the recording of the wavelengths spectrum covering both donor and acceptor emission spectra. Fluorescence spectrum emitted by a FRET pair would consist in a combination (overlap) of both donor and acceptor emission spectra. This recorded spectrum is specific to a unique given FRET pair and presents prints of donor and acceptor emission spectra which would both relatively vary depending on the distance separating the fluorophores. Thus, a FRET pair emission spectrum presents two peaks corresponding to the maximum emission values of the donor and the acceptor, with the donor at lower λ value. The ratio between the acceptor and the donor maximum emission peak intensities is defined as the FRET signal. The FRET signal directly reflects the FRET efficiency and thus the relative distance and/or orientation of the fluorophores under fixed conditions.

1.3. FRET ratio

In the present work, the FRET ratio refers to a variation in the FRET ratio exhibited by a FRET construct when tested under fixed recording parameters and various experimental

conditions. In other words, if the application of an experimental parameter triggers a variation in the FRET signal of the fluorescently tagged construct, a FRET ratio would be observed, reporting distance- and/or orientation-changes between donor and acceptor. The FRET ratio will change as the efficiency of FRET increases or decreases.

1.4. Rationales for generation of a FRET sensor based on AMPK

At the beginning of the present work no information concerning the molecular mechanism of AMPK allosteric activation was available in literature. The only known fact was that conformational changes in the whole AMPK heterotrimer were coupled to AMP induced allosteric activation of the kinase as visualized by small angle X-ray scattering (SAXS) (Riek et al., 2008). This was later confirmed by studies based on electron microscopy (Zhu et al., 2011) and co-crystallization (Chen et al., 2012) studies. Hence, according to the actual knowledge concerning the nature of the conformational changes induced by AMP at that time, it was decided to cover all the eventual movements that may happen between the termini of AMPK subunits. In order to achieve this, a matrix approach was established: all combinations of whole AMPK heterotrimer tagged on two of its three subunits with either a CFP variant (CFP or mseCFP_{Δ11}) or a YFP variant (YFP or cpVenus) at the N- or C-terminus were created. In order to map conformational changes occurring in the whole AMPK heterotrimer the $\alpha 2$ subunit was tagged with CFP (or variant) at either N- or C-terminus, $\beta 2$ subunit was tagged with YFP (or variant) at either N- or C-terminus and $\gamma 1$ -subunit was tagged at its N-terminus or C-terminus with both CFP and YFP. AMPK construct harboring γ -subunit tagged with YFP will provide information about movement between $\alpha 2$ and $\gamma 1$, as $\alpha 2$ is fused to CFP. AMPK constructs containing γ -subunit tagged with CFP will give insights relative to conformational changes that may happen between $\beta 2$ and $\gamma 1$, as $\beta 2$ is tagged using YFP.

2. Molecular cloning

2.1. Materials, buffers and solutions

Restriction enzymes, T4 DNA polymerase, T4 DNA ligase and PCR kits (Phusion polymerase) were purchased from New England Biolabs. Buffers for restriction enzymes and DNA polymerases were obtained as 10x or 5x stock solutions from New England Biolabs. Miniprep plasmid, gel extraction and PCR Cleaning kits from Qiagen. Commercial kits used are listed below:

Name	Purpose	Source
QIAprep Spin Miniprep Kit	Plasmid extraction and purification	Qiagen
QIAquick PCR Purification Kit	PCR product purification	Qiagen
QIAquick Gel Extraction Kit	DNA extraction from agarose gels	Qiagen

2.2. Genes of interest

Coding sequences for AMPK subunits used in this work are AMPK α 2 catalytic subunit from *Rattus Norvegicus* (Prkaa2; Gene ID: 78975), AMPK β 2 subunit from *Homo Sapiens* (PRKAB2; Gene ID: 5565) and γ 1 subunit isoform from *Rattus Norvegicus* (Prkag1; Gene ID: 25520). Fluorescent proteins forming FRET pairs used in the presented work are derived from GFP from *Aequorea Victoria*. FRET pair can be formed by ECFP (Heim and Tsien, 1996; Heim et al., 1995) / eYFP (Berger et al., 2004) or mseCFP Δ 11 (Matsuda et al., 2008) / cp173Venus (Imamura et al., 2009). The later derives from Venus (Nagai et al., 2002) which carries the F46L mutation which accelerates the chromophore maturation at 27°C and also the F64L/M153T/V163A/S175G mutations that confer a relative tolerance to acidosis and Cl⁻ exposure.

2.3. Bacterial strains

All bacterial strains are listed below with their corresponding genotype. Top10 cells were used for amplification of Acceptor plasmids or Acceptor-Donor fusions. BW23473 cells were used for amplification of Donor plasmids.

Strain	Genotype	Source
Top10	F- mcrA Δ (mrr-hsdRMS-mcrBC) ϕ 80lacZ Δ M15 Δ lacX74 nupG recA1 araD139 Δ (ara-leu)7697 galE15 galK16 rpsL(StrR) endA1 λ -	Invitrogen
BW23473	F-, Δ (argF-lac)169, Δ uidA3::pir+, recA1, rpoS396(Am)?, endA9(del-ins)::FRT, rph-1, hsdR514, rob-1, creC510	Berger group
BL21 <i>Star</i> (DE3)	F-ompT hsdSB (rB-, mB-) gal dcm rne131 (DE3)	Invitrogen

2.4. Cell culture

2.4.1. Cultivation of *Escherichia coli* (E.coli)

E. coli cells were cultivated in LB medium or on LB agar plates supplemented with appropriate antibiotics. Optical densities (ODs) of cultures were measured in plastic cuvettes with 1 cm path-length in a Biowave 3000 CO8000 Cell Density Meter at 600 nm wavelength using LB medium as a reference.

2.4.2. Transformation competent cells

Chemically competent *E. coli* cells were mixed with 5-10 μ L of ligation, 5-10 μ L Cre-LoxP recombination reaction or 100 ng of plasmid and incubated on ice for 30 min. Bacteria were heat shocked at 42 °C for 45 sec and subsequently kept on ice for 1 min. 600 μ L of LB medium were added, the cells were incubated at 37 °C in a shaker for 1 hour or over-night and plated on LB agar plates supplemented with appropriate antibiotics to select positive transformants. Antibiotic concentrations used were 30 μ g/ml for Chloramphenicol, 100 μ g/ml for Ampicillin and 50 μ g/mL for Spectinomycin.

Larger nucleic acids constructs (pACEMBL vectors carrying AMPfret constructs) were sometimes transformed in electrocompetent cells. Plasmids solution were desalted on Millipore membrane against pure water, mixed with electrocompetent cells in electroporation cuvette (BioRad) and transformation was realized with a MicroPulser Electroporator (BioRad). Immediately after, sterile 600 μ L of LB medium were added, the cells were incubated at 37 °C in a shaker for 1 hour or over-night and plated on LB agar plates supplemented with appropriate antibiotics to select positive transformants.

2.5. Nucleic acids biochemistry

2.5.1. Concentration determination of nucleic acids

The concentration of nucleic acids in aqueous solutions was determined by measuring the absorbance at 260 nm against a reference solution according to the following equation:

$$1 \text{ OD}_{260} = 50 \text{ } \mu\text{g/ml doubled stranded DNA}$$

2.5.2. Agarose gel electrophoresis

DNA molecules were analyzed by agarose gel electrophoresis. Agarose gels contained 0.5-2 % agarose in 1x TBE (178 mM Tris, 178 mM Boric acid, 4 mM EDTA, pH 8.0) depending on size of the DNA molecules to be analyzed. Ethidium bromide was added to a final concentration of 0.05 $\mu\text{L/mL}$ to the gel for subsequent visualization of the DNA bands by UV light. For loading on agarose gels, DNA samples were mixed in a 1:6 (v/v) ratio with loading dye (6x BX-DNA loading dye: 30 % (v/v) glycerol, 0.125 % (w/v) bromophenol blue, 0.125 % (w/v) xylene cyanol FF or 6x OG-DNA loading dye: 30 % (v/v) glycerol, 0.125 % (w/v) Orange G) and separated at 80 to 120 V for 30 min to 2 h depending on percentage of agarose in the gel and size of DNA molecules.

2.5.3. DNA extraction from agarose gels

DNA bands were excised from agarose gels using sterile scalpel blades on an UV table at 365 nm wavelength. The DNA was extracted from the excised agarose gel slices using a QIAquick Gel Extraction Kit following the manufacturer's instructions.

2.5.4. Polymerase chain reaction (PCR)

PCR was used to amplify genes of interest or to introduce mutations in these genes following a self-SLIC procedure. In general, 10-50 ng of template DNA were mixed with 10 μL 5x HF or 10 μL 5x GC-Phusion Buffer, up to 3 μL DMSO, 1 μL of forward primer and 1 μL reverse primer at 100 mM concentration, 1 μL of a 10 mM dNTP Mix, 1 U of Phusion® High-Fidelity DNA Polymerase and filled up to 50 μL total volume with H_2O .

Typically, the template was initially denatured at 98 °C for 60 s, following a cycling through a denaturing step at 98 °C for 30 s, an annealing step at a temperature 5 °C lower than the

melting temperature of the primers used in the reaction for 20 s and an elongation step at 72 °C for 30 s per kb of gene to be amplified. The cycle of denaturing, annealing and elongation was repeated 30x, followed by a final elongation step at 72 °C for 5 min. The PCR was stored at 4 °C (short-term) or -20 °C (long-term) until further use.

2.5.5. Restriction digestion of DNA

Restriction digestion was used to generate compatible sticky ends in vectors and PCR products for subsequent ligation or to validate recombinant plasmids by restriction mapping. Restriction digestions were carried out according to the enzyme manufacturer's manuals. In general, 1 µg of plasmid DNA were digested with 1 U of enzyme for 1 h at the recommended incubation temperature.

2.5.6. DNA ligation

Vector and insert with compatible sticky ends were ligated using T4 DNA Ligase. Vector (150 ng) and insert were mixed in a 1:3 molar ratio in a 10 µL reaction, supplemented with 1 µL 10x T4 DNA Ligase Buffer and 1 µL T4 DNA Ligase and incubated at room temperature for 1 h. The complete ligation reaction was used for transformation of chemically competent cells.

2.5.7. Sequence and ligation independent cloning (SLIC)

SLIC was essentially performed as described previously (Li and Elledge, 2007). In brief, 1 µg of linear insert and 1 µg of linearized vector (by restriction digestion or PCR amplification) were treated separately with 0.5 U T4 DNA Polymerase in 20 µL reaction volume containing 2 µL NEBuffer2.1 at RT for 30 min. The reaction was stopped by adding 2 µL of 10 mM dCTP and kept on ice. Subsequently, 150 ng of T4 DNA Polymerase treated vector were mixed with T4 DNA Polymerase treated insert in a 1:1 molar ratio in a 10 µL reaction volume containing 1 µL of 10x T4 DNA Ligase buffer and incubated at 37 °C for 30 min. The complete reaction mix was used for transformation of chemically competent cells.

2.5.8. Self-SLIC

Self-SLIC was used to introduce mutations such as deletions, insertions or point mutations into coding sequences (Figure 8). Self-SLIC is an insert free SLIC reaction, resulting in self-ligation of the amplified vector with the modified sequence. In brief, the vector was amplified by standard PCR reactions using the mutagenic primers. PCR template was digested by adding 20 U of *DpnI* directly to the PCR reaction and incubating at 37 °C for 4 h. The PCR product was purified by agarose gel electrophoresis and subsequent gel extraction. 1 µg of the vector was treated with 0.5 U T4 DNA Polymerase in a 20 µL reaction containing 2 µL NEBuffer2.1 at RT for 30 min. The reaction was stopped by adding 2 µL 10 mM dCTP and kept on ice. Subsequently, 300 ng of T4 DNA Polymerase treated vector were denatured at 98 °C for 5 min in a 10 µL reaction volume containing 1 µL of 10x T4 DNA Ligase Buffer. The reaction was slowly cooled down to room temperature and directly used for transformation of chemically competent cells.

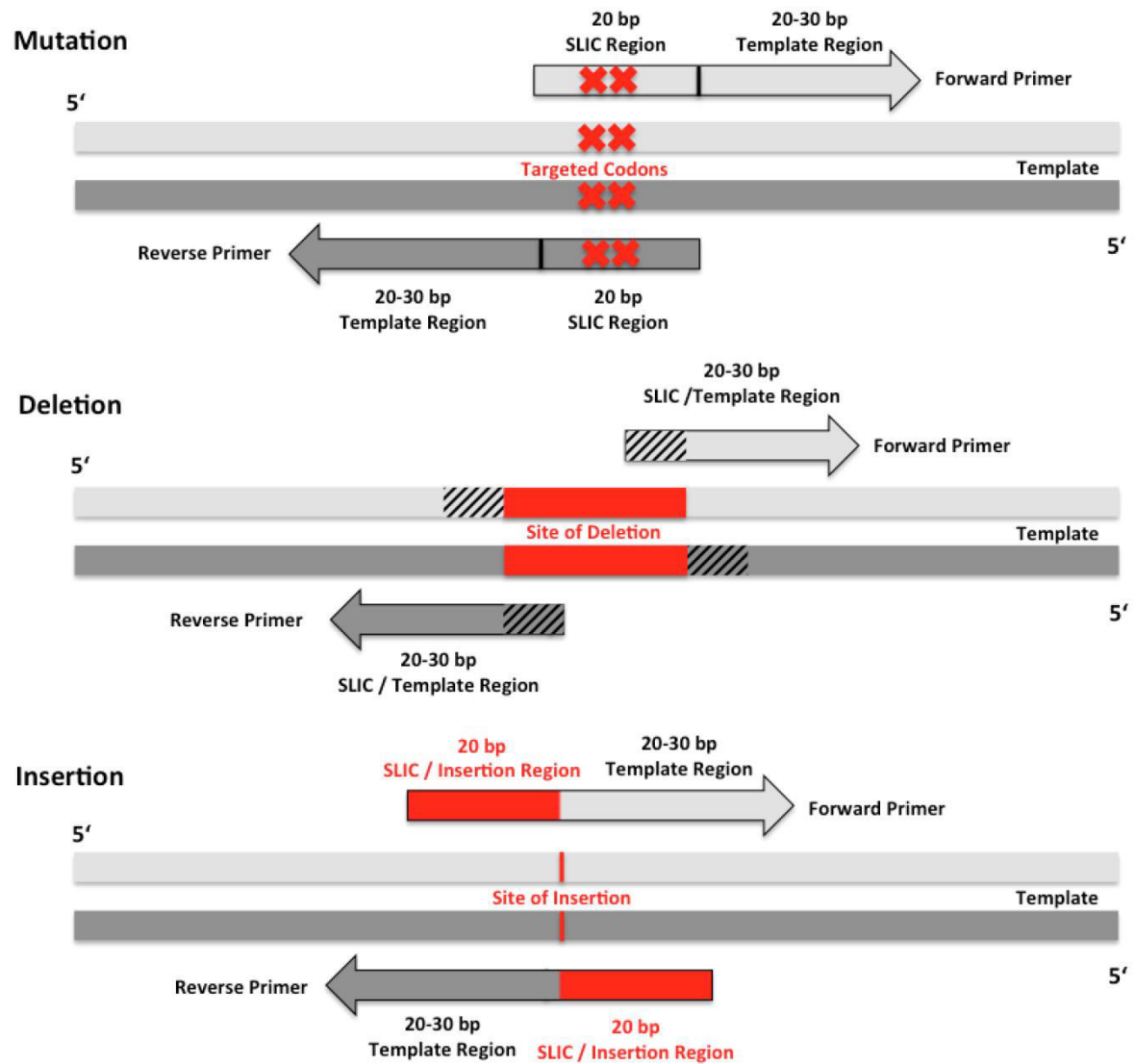


Figure 1: Modification of coding sequences by self-SLIC.

Self-SLIC principle and primer design for gene modification in ACEMBL vectors. Schematic representation of the self-SLIC procedures and the design of the corresponding primers to introduce point mutations (top), deletions (middle) or insertions (bottom) into coding sequences. Sites of modifications are indicated in red. **Top:** Primer design for site directed mutagenesis to exchange codons within a 20 bp sequence of choice. The targeted codons are indicated with red crosses. The complete 20 bp SLIC Region can be used for mutations. Care should be taken that the Template Region is longer and has a higher melting temperature than the 20 bp SLIC Region to avoid unspecific side products in the PCR reaction. **Middle:** Primer design to introduce deletions. The deleted region within the template is indicated in red. Note that the primers carry a combined SLIC Region, utilizing 10 bp at the 5' site and 10 bp at the 3' site of the deleted sequence, resulting in a 20 bp overall SLIC Region. **Bottom:** Primer design for inserting additional sequences up to 20 bp at a targeted site. The site of insertion is indicated with a red line on the template double strand. Care should be taken that the Template Region is longer and has a higher melting temperature than the 20 bp SLIC / Insertion Region to avoid primer dimer formation or unspecific PCR products. From Haffke et al. Characterization and production of protein complexes by co-expression in *Escherichia coli*. *Methods in Molecular Biology*. (Haffke et al., 2015).

2.5.9. Preparation of plasmid DNA

Plasmid DNA was isolated from 5-20 mL bacterial cultures using the QIAprep Spin Miniprep Kit following the manufacturer's manual. For culture volumes >10 mL, the volumes of the buffers P1, P2 and N3 were doubled.

2.5.10. Cre-loxP recombination of acceptor and donor plasmids

For Cre-LoxP recombination of Acceptor and Donor plasmids, 1 µg of Acceptor was mixed with a 1:1 molar ratio of Donor(s) in a 10 µL reaction volume containing 1 µL 10x Cre Buffer (500 mM Tris/HCl pH 7.5, 330 mM NaCl, 100 mM MgCl₂) and 1 µL Cre-Recombinase and incubated at 37 °C for 1 h. The complete reaction mix was used for transformation of chemically competent cells.

2.6. ACEMBL

ACEMBL is a 3rd generation expression system created at EMBL Grenoble outstation, which applies tandem recombination steps for rapidly assembling many genes into multigene expression cassettes. Of course, ACEMBL also offers the option to employ conventional approaches involving restriction enzymes and ligases. Different expression systems are available with vector versions carrying different promoters and terminators depending on the chosen expression host organism (prokaryotic, mammalian or insect cell). In our case, the *MultiColi* expression system was used for bacterial expression, in *E.coli*, of our AMPK-FP constructs that we termed AMPfret. A single gene (here: AMPK subunit) or a multigene assembly (here: AMPK subunit tagged with FP), were inserted in vectors at the level of their multiple integration element (MIE) using sequence ligation independent cloning (Li and Elledge, 2007) (SLIC) or conventional methods involving restriction enzymes and ligases. At the core of the ACEMBL technology are five small de novo designed vectors, classified as acceptors or donors depending on their replication origin. Acceptors (pACE1, pACE2), carrying origins of replication derived from ColE1 and named oriBR322, can be amplified in all common *E. coli* strains. They also contain ampicillin or tetracyclin resistance markers. By opposition, donors (pDC, pDS, pDK) are containing conditional origins of replication derived from phage R6Ky, which make their propagation dependent on hosts expressing the *pir*

gene. Each donor vector contains its own resistance marker which can be kanamycin, chloramphenicol, or spectinomycin. All vectors of the ACEMBL expression system contain a loxP imperfect inverted repeat which is used to fuse them together via Cre recombination (Fig. 2). Up to three donor vectors can be used in conjunction with one acceptor vector.

Cloning of AMPK subunits (α_2 , β_2 and γ_1), FRET pair fluorescent proteins and directed mutagenesis were achieved using i) conventional restriction enzyme and ligase or ii) sequence and ligation-independent cloning (SLIC) (Li and Elledge, 2007), an advanced cloning method previously described and which allows the assembly of multiple DNA fragments in a single reaction using *in vitro* homologous recombination and single-strand annealing.

2.7. AMPfret general construction by molecular cloning

Cloning of AMPfret variants was achieved using the *MultiColi* (Bieniossek et al., 2009) expression system from the ACEMBL suite. One acceptor, pACE1, and two donors, pDC and pDS, were chosen among the vectors of the *MultiColi* expression system. pACE1 was selected to clone all the α_2 -derived constructs, and pDC and pDS were chosen to clone β_2 - and γ_1 -based constructs respectively. Indeed, the α_2 , β_2 and γ_1 AMPK subunits tagged or not at N- or C-terminus with fluorescent protein (cyan fluorescent protein (CFP) and yellow fluorescent protein (YFP) or corresponding variants), were cloned in the pACE, pDC and pDS vectors respectively, of the ACEMBL expression system (Bieniossek et al., 2009) using SLIC (Li and Elledge, 2007) and conventional cloning (see annex Vector Map). These vectors, containing a single subunit, fluorescently tagged or not, were fused via their Lox-P site using the CRE-recombinase (EMBL Heidelberg): this yielded a single expression vector coding for a chimeric AMPK that contains two of its three subunits fused to either a CFP variant or a YFP variant: every AMPfret construct includes the FRET pair CFP/YFP or the optimized derivative mseCFP $_{\Delta 111}$ /cpVenus.

2.7.1. pACE-derived vectors

Available pACE1 vector containing α_2 tagged (pACE α_2 _{old}) presented mutations and truncations at the level of α_2 N-Terminus (results from sequencing). In addition, the

previously followed cloning strategy resulted in the presence of an ATG codon in between the T7 promoter and the Met codon of the α_2 subunit. As a consequence, an undesirable open reading frame was also present in the pACE α_2 _{old} located upstream the encoded AMPK catalytic subunit. The presence of this extra coding sequence would have finally lower the expression of α_2 subunit and of the whole heterotrimer by extension. To fix this quickly, a DNA piece, covering the α_2 N-Ter and the pACE promoter region and coding for a deca-Histidine tag at α_2 N-Ter cleavable by the Tobacco etch virus (TEV) protease was ordered to Genscript. This piece was received cloned in the pUC vector. The repairing piece was extracted using EcoRI and BglII restriction enzymes and then cloned using T4 DNA ligase in the pACE α_2 _{old} previously opened with EcoRI and BglII. The pACE10HisTEV α_2 (pACE α_2) was obtained; its nucleotide sequence was verified by restriction enzyme digestion and sequencing. As mentioned above, the newly created vector also encodes a decaHis-tag, cleavable by the TEV protease, at the N-terminus of the α_2 subunit in order to facilitate the purification of recombinantly expressed protein complex derived from whole AMPK heterotrimer.

DNA fragment coding for eCFP and intended for cloning in pACE α_2 in order to generate pACE α_2 -eCFP was amplified by PCR using 5HindIIIeCFP and 3eCFPXhoI primers (see primers list). Amplified eCFP fragment, as well as pACE α_2 , were separately digested using HindIII and XhoI, gel extract and finally ligated. pACE α_2 -eCFP was obtained and its DNA sequence was verified by enzyme restriction digestions and sequencing (up- and down-stream elements and coding sequence).

Concerning pACEeCFP- α_2 generation, eCFP coding sequence was amplified using 5His10TEVNde1eCFP and 3eCFP2Gly α_2 primers while pACE α_2 was opened by digestion with NdeI. After T4 DNA polymerase treatment of PCR amplified fragment and linearized backbone, eCFP produced fragment was cloned in pACE α_2 by SLIC and pACEeCFP- α_2 was obtained. Note that, in the meantime, nucleotides coding for two glycins were inserted in between eCFP and α_2 as linker sequence. pACEeCFP- α_2 DNA sequence was verified by enzyme restriction digestions and sequencing (up- and down-stream elements and coding sequence).

2.7.2. pDC-derived vectors

Available vectors constituted of pDC and containing $\beta 2$ subunits were all presenting truncation covering $\beta 2$ C-Ter and the T7 terminator region (e.g. pDC $\beta 2_{old}$): codons for fourteen $\beta 2$ amino acids (YKKKYVTLLYKPI) were missing in addition to the stop codon and the T7 terminator. To fix this simply and quickly, a DNA piece coding for missing $\beta 2$ C-Ter and a part of pDC was ordered (Genscript). It was received included in the pUC vector and extracted using HindIII and NsiI. The repairing nucleotide sequence was then cloned in the pDC $\beta 2_{old}$ previously digested with both HindIII and NsiI. Resulting plasmid, pDC $\beta 2$, was verified by restriction digest and sequencing.

Once the pDC $\beta 2$ vector fixed, I generated coding plasmids for $\beta 2$ -subunit tagged with a FP at its termini. Hence, the YFP gene contained in the pUCSMBP3TAF1His-YFP (kind gift from Yan Nie) was amplified by PCR using primers 5ApallYFP and 3YFPSphI. Next, the produced YFP fragment and pDC $\beta 2$ were both digested with ApalI and SphI and ligated to generate pDC $\beta 2$ -YFP. pDC $\beta 2$ -YFP nucleotides sequence was verified by restriction digest and sequencing.

The YFP gene was also amplified by PCR using the 5NdeIYFP, 3YFPStuI primers pair. Resulting fragment and pDC $\beta 2$ were both digested with NdeI and StuI and then ligated together to get pDCYFP- $\beta 2$. pDCYFP- $\beta 2$ nucleotides sequence was verified by restriction digest and sequencing.

2.7.3. pDS-derived vectors

$\gamma 1$ -subunit gene was first amplified by PCR using primers 5pDSNdeI $\gamma 1$ and 3 $\gamma 1$ SpeIpDS. Beside, pDS vector was opened by digestion with NdeI and SpeI. Resulting linearized plasmid and $\gamma 1$ gene previously amplified were treated with T4 DNA polymerase and fused together via SLIC to yield to pDS $\gamma 1$. Obtained vector sequence was verified by restriction digest and sequencing.

To facilitate cloning of $\gamma 1$ subunit gene flanked with CFP or YFP either at 3' end either at 5' end primers were designed in a way that both genes ($\gamma 1$ and FP) can be cloned simultaneously by SLIC in pDS digested with NdeI and SpeI restriction enzymes. Therefore linearized pDS with NdeI and SpeI can be used for cloning of pDS $\gamma 1$ -eCFP, pDS $\gamma 1$ -YFP, pDS $\gamma 1$ -CFP and pDS $\gamma 1$ -YFP.

To create pDS γ 1-eCFP γ 1-subunit and eCFP genes were respectively amplified by PCR using 5pDSNdeI γ 1/3g1NheIeCFP and 5NheIeCFP/3eCFPSpeI pDS primers pairs. Both amplified DNA fragments were ligated simultaneously by SLIC, after having been digested by T4 DNA polymerase, into the pDS vector previously opened with NdeI and SpeI and treated with T4 DNA polymerase. Resulting vector sequence, coding for γ 1-eCFP, was verified by restriction digest and sequencing.

For the generation of pDS γ eCFP- γ 1, the γ 1-subunit was amplified by PCR and eCFP genes using 5eCFPNheI γ 1/3g1SpeI pDS and 5NdeIeCFP/3eCFPNheI primers pairs respectively. Both amplified DNA fragments were ligated simultaneously by SLIC, after having been digested by T4 DNA polymerase, into the pDS vector previously opened with NdeI and SpeI and treated with T4 DNA polymerase. Resulting vector sequence, coding for eCFP- γ 1, was verified by restriction digest and sequencing.

To get pDS γ 1YFP, γ 1- subunit and YFP genes were respectively amplified by PCR using the 5pDSNdeI γ 1/3g1NheIYFP and 5NheIYFP/3YFPSpeI pDS primers pairs. Both amplified DNA fragments were ligated simultaneously by SLIC, after having been digested by T4 DNA polymerase, into the pDS vector previously opened with NdeI and SpeI and treated with T4 DNA polymerase. Resulting vector sequence, coding for γ 1-YFP, was verified by restriction digest and sequencing.

DSYFP γ 1 was obtained as following: γ 1- subunit and YFP genes were respectively amplified by PCR using the 5YFPNheI γ 1/3g1SpeI pDS and 5pSDNdeIYFP/3YFPNheI primers pair. Then, both amplified DNA fragments were ligated simultaneously by SLIC, after having been digested by T4 DNA polymerase, into the pDS vector previously opened with NdeI and SpeI and treated with T4 DNA polymerase. Resulting vector sequence, coding for YFP- γ 1, was verified by restriction digest and sequencing.

2.7.4. pACEMBL vectors

Once all vectors coding for single subunit tagged or not with fluorescent protein created, all combinations of vectors coding for the AMPK heterotrimer tagged with CFP and YFP at different termini were generated (Table 1). They were obtained through the recombination of one copy of one of the pACE-derived vectors with one pDC-derived vector and one pDS-

derived vector (respectively coding for α -, β - and γ -subunits, fluorescently tagged or not). All backbones of vectors of the ACEMBL suite are carrying a Lox-P site which allows their fusion by recombination using Cre recombinase (EMBL Heidelberg). The only limit of this assembling step relies in the fact that it can result in fusion vectors containing more than one copy of initial plasmids. Indeed, the recombination can also occur between several copy of donor and acceptor as long as the resulting plasmid contains at least one non-conditional replication origin and the three different antibiotic resistance genes to be spread in bacteria. Also, a scrupulous inspection by restriction enzyme digestion was realized after recombination to ensure that pACEMBL vectors coding for AMPfret variants are carrying only one copy of each desired acceptor or donors. Such verification is helpful to further get stoichiometric expression of AMPfret subunits.

For example, pACEMBL AMPfretA was obtained through the assembly of pACE α 2-CFP with pDC β 2-YFP and pDSy1 by Cre recombination through their loxP sites. Fusion product was selected after transformation into bacterial strains that do not carry the *pir* gene (Top10 or Omnimax strains) and sprawl on LB-Agar plates containing ampicillin, chloramphenicol and spectinomycin. The fusion vector maps were created using the CreACEMBLER software and fusion vector composition was verified by restriction digest of miniprep vectors. A special attention was given to the selection of fusion plasmid that contained only one copy of each plasmid. Indeed, plasmids resulting of recombination contain at least one copy of acceptors or donors, but also plasmids containing more copies will grow. However, the latter plasmids are bigger than the expected size (larger vectors are more difficult to transform) and would yield to non-stoichiometric expression of the different protein subunits.

2.8. Site directed mutagenesis using self-SLIC

To realize mutation of the AMPK coding sequences present in the ACEMBL vectors, an original strategy based on self-SLIC was designed (Haffke et al., 2015) (Fig. 8). As described above, it consisted in amplifying the whole backbone of a coding vector using primers that contain the desired mutation plus an overlapping region which will allow their self-annealing after T4 DNA polymerase treatment. The latter uses the exonuclease activity exhibited by the T4 DNA polymerase in absence of nucleotides. As determined by Li et al. T4 DNA

polymerase chops ~20 nucleotides off in 30 minutes (Li and Elledge, 2007). Such advanced method for site directed mutagenesis presents the great advantage of allowing the generation of mutated vectors through a single step PCR - which generates the entire modified coding vector - only followed by a DpnI digestion to remove the template and a quick T4 DNA polymerase treatment of the PCR product that allows the self-recircularization of the newly created plasmid. This method emerged from the increasingly reliable polymerases available nowadays for PCR, but sequencing of the generated vectors is still highly advised and was done for every constructs generated in the present work.

To identify clones carrying the mutated vector, silent mutations are included in the mutagenic primers that introduce new restriction sites without changing amino acid sequence, resulting in an altered restriction pattern. This approach takes profit of the redundancy of the genetic code. Identification of such silent mutations creating novel restriction sites by single nucleotide replacement was done with SiteFind (Evans and Liu, 2005). This strategy resulted in the insertion of PstI, XhoI, EcoRV, NheI and PvuII restriction sites in plasmids coding for pDSy1CBS1, pDSy1CBS3, pDSy1CBS4, pACE α 2T172A and pACE α 2T172D respectively (each tagged or not with fluorescent protein).

To generate the CBS mutants, a single PCR using 5L128D+V129D and 3L128D+V129D primers (see annex: 3.4) was done on pDSy1 and pDSy1YFP to generate the linearized pDSy1CBS1 and pDSy1YFPCBS1 vectors. This was followed by a DpnI digestion step to remove the PCR template. Finally, digestion of the PCR products by the T4 DNA polymerase created single strand ends and lead to the recircularization by self-annealing of the pDSy1CBS1 and pDSy1YFPCBS1 plasmids.

Following the same strategy, pDSy1CBS3 and pDSy1YFPCBS3 were obtained using 5V275GL276G and 3V275GL276G primers. pDSy1CBS4 and pDSy1YFPCBS4 were created using 5S315P and 3S315P primers, pACE α 2T172A and pACE α 2T172ACFP with the 5T172A / 3T172A primers pairs and finally pACE α 2T172D and pACE α 2T172DCFP with 5T172D and 3T172D as primers.

After having identified the correct clones carrying the desired mutations by restriction digest, nucleotide sequences of pDSy1CBS1, pDSy1CBS1YFP, pDSy1CBS3, pDSy1CBS3YFP,

pDS γ 1CBS4, pDS γ 1CBS4YFP, pACE α 2T172A, pACE α 2T172ACFP, pACE α 2T172D and pACE α 2T172DCFP were controlled by sequencing.

2.9. FRET pair replacement

Having available the pcDNA3.1ATeam1.03 coding for the ATP sensor ATeam1.03 (Imamura et al., 2009) (kind gift from Hiromi Imamura), which contained an updated CFP/YFP derived FRET pair, it was decided to replace the existing FRET pair present in AMPfret constructs (A-L) by mseCFP Δ ₁₁/cp173-mVenus. All AMPfret constructs (A-L) were updated with the mseCFP Δ ₁₁/cp173-mVenus FRET pair but only updated version of AMPfretC (AMPfret 1.1) was expressed and purified.

The nucleotide sequence coding for ATeam1.03 sensor was thus used as a PCR template and mseCFP Δ ₁₁ as well as cp173-mVenus were amplified in order to clone them in existing AMPK subunits coding vectors issued from the *MultiColi* expression system. First, each pACE1, pDC and pDS vectors which contained respectively α 2-, β 2- and γ 1-subunit tagged with FPs at their termini were enzymatically opened in order to remove the contained sequence coding for CFP or YFP.

Then, the mseCFP Δ ₁₁ coding sequence was amplified by PCR using 5HindIII CFPtrunc and 3XhoI CFPtrunc primers (see annex - Primer list) and cloned into pACE α 2 using HindIII and XhoI restriction sites. This yielded to pACE α 2-mseCFP Δ ₁₁. Also, mseCFP Δ ₁₁ nucleotide sequence was PCR amplified using 5SLICCFPtruncNde1 and 3SLICCFPtrunc2gly primers and cloned into pACE α 2 pre-opened with Nde1 using the SLIC method. This yielded to pACEmseCFP Δ ₁₁ α 2.

When cloning mseCFP Δ ₁₁ in pACE α 2 vector at α 2 N- or C-terminus, PCR mixtures containing amplified sequences of FP were diligently treated with the DpnI restriction enzyme in order to cut into pieces the pcDNA3.1ATeam1.03 used as template. Profit was taken concerning DpnI restriction enzyme properties: it chops the methylated DNA issued from bacteria (miniprep) and used as template for PCR reaction but does not have any activity against unmethylated DNA (PCR amplified). Indeed pcDNA3.1, like pACE1, carries ampicillin

resistance; hence such step reduced considerably the possible background related to the transformation of bacteria with the template.

mseCFP_{Δ11} gene was amplified by PCR using 5NheICFPtrunc and 3PmeICFPtrunc primers and cloned into pDSy1 using NheI and PmeI restriction sites. This yielded to pDSy1mseCFP_{Δ11}. Again mseCFP_{Δ11} coding sequence was amplified by PCR using 5NdeICFPtrunc and 3NheICFPtrunc primers and cloned into pDSy1 using NdeI and NheI restriction sites. This yielded to pDSmseCFP_{Δ11}γ1.

Cp173-mVenus gene was amplified by PCR using 5ApallcpVenus and 3cpVenusSphI primers and cloned into pDCβ2 using Apall and SphI restriction sites. This yielded to pDCβ2cp173-mVenus. cp173-mVenus coding sequence was amplified by PCR using 5NdeIcpVenus and 3cpVenusStuI primers and cloned into pDCβ2 using NdeI and StuI restriction sites (instead of StuI, EcoR147 - Fermentas - was used). This yielded to pDCcp173-mVenusβ2.

cp173-mVenus gene was amplified by PCR using 5NheIcpVenus and 3PmeIcpVenus primers and cloned into pDSy1 using NheI and PmeI restriction sites. This yielded to pDSy1cp173-mVenus. cp173-mVenus coding sequence was also amplified using 5NdeIcpVenus and 3NheIcpVenus primers and cloned into pDSy1 using NdeI and NheI restriction sites. This yielded to pDScp173-mVenusγ1.

As done for the AMPfret 1.0 derived mutants (CBS sites and T172) silent mutations were introduced and positive clones carrying newly generated vectors, including updated fluorescent proteins genes, were selected through their modified restriction pattern. Their sequences were finally all validated by sequencing.

Once sequenced, newly generated vectors carrying sequence coding for single AMPK subunit tagged with updated fluorescent protein were then assembled by Cre recombination through their loxP sites in order to get all pACEMBL vectors coding for AMPfret variants (A-L) containing the updated FRET pair (mseCFP_{Δ11} an cp173-mVenus). New versions of AMPfretA and AMPfretC (AMPfret1.1) containing updated FRET pair were expressed and purified following the protocol previously used for AMPfret A-L constructs.

2.10. AMPfret 2nd generation

In order to magnify the AMP-induced FRET ratio of AMPfret, positive constructs (AMPfretA and AMPfretC) were molecularly engineered. Two different strategies were applied in parallel: the first consisted in the removal of non-folded residues located at the termini of AMPK subunits and fluorescent proteins. Residues were identified through the examination of X-ray structure available at that time (PDB ID: 2Y94 (Xiao et al., 2011)) and secondary structure prediction (nps@consensus, ClustalW2 and psipred servers). Deletion of residues forming linkers between AMPK subunits and fluorescent proteins would have for results to render AMPfret structure more compact and it was expected that AMP-induced conformational changes would be better translate by FRET. Two residues (AR) were removed at $\alpha 2$ C-terminus making the amino acids sequence ending in an α -helix motif. At $\beta 2$ C-terminus the residues KPI were deleted making it ending through a β -strand motif. At $\gamma 1$ C-terminus, residues LTGGEEKP were deleted making the truncated subunit ending on an α -helix motif. Structure predictions realized by combining results issued from nps@consensus and PSIPRED servers are presented in the annex (annex - chapter) and deleted residues are boxed in red.

Primers were designed to remove Ala551 and Arg552 at the C-Ter of the $\alpha 2$ -subunit as well as the HindIII restriction site previously present between $\alpha 2$ C-Ter and CFP which was coding for 2 additional residues (LysLeu). pACE $\alpha 2$ -CFP was amplified by PCR using 5a2-_{AR}CFP and 3a2-_{AR}CFP primers. Resulting linearized vector was treated 30 min with T4 DNA polymerase. This created single strand DNA extremities that could self-anneal due to sequence homology, leading to the self recircularization of the mutated vector. pACE $\alpha 2$ -_{AR}-CFP was generated.

Using the same approach, Lys268, Pro269 and Ile270 had been removed from the $\beta 2$ -subunit C-Ter additionally to the ApalI restriction site previously present between $\beta 2$ C-Ter and YFP and which was coding for ValHis. In this case 5b2-_{KPI}YFP and 3b2-_{KPI}YFP primers were used and pDC $\beta 2$ -_{KPI}-YFP was obtained.

Finally, Leu323, Thr324, Gly325, Gly326, Glu327, Lys328, Lys329 and Pro330 had been removed from the $\gamma 1$ C-Ter, just as the NheI restriction site present between the $\gamma 1$ C-Ter and YFP and which was coding Ala Ser. To mutate pDS $\gamma 1$ -YFP coding vector into pDS $\gamma 1$ -LTGGEEKP-YFP, I used 5g1-LTGGEEKP-YFP and 3g1-LTGGEEKP-YFP primers.

As restriction sites previously located between AMPK subunits and fluorescent proteins had been removed, right clones containing desired mutations were easily selected. Sequences of pACE α 2-_{AR}-CFP, pDC β 2-_{KPI}-YFP and pDS γ 1-_{LTGGEEKP}-YFP were verified by sequencing. Plasmids were then fused by Cre recombination in a way that optimized versions of AMPfret A and AMPfret C with shorter linkers were obtained after expression and purification, respectively named AMPfret A_{deletion} and AMPfret C_{deletion}.

The second strategy relied on the observation made by Sivaramakrishnan et al. that ER/K amino acids repeat forms a rigid α -helix motif, and consisted in positioning such motif between the α -subunit and CFP (Sivaramakrishnan and Spudich, 2011; Sivaramakrishnan et al., 2008). In addition of the small assumed α -helix insertion, deletions of unfolded amino acids located at α 2 C-terminus and CFP N-terminus were also applied. It was decided to insert only one α -helix as linker between α -subunit and CFP to fix one fluorophore relatively to the other all the while avoiding to pull them away from each other. These optimizations were realized using the “self SLIC” method already used to generate AMPfret CBS mutants.

The modified vector, named pACE α 2-_{helix}-CFP, was obtained using the self-SLIC method already described above and the primers pair 5a2-8AAhelix-CFP / 3a2-8AAhelix-CFP. pACE α 2-_{helix}-CFP was fused to vectors coding for shortened AMPK subunits tagged with FP to give pACEMBL AMPfretA _{α -helix} (pACE α 2-_{helix}-CFP x pDC β 2-_{KPI}-YFP x pDS γ 1) and pACEMBL AMPfretC _{α -helix} (pACE α 2-_{helix}-CFP x pDC β 2 x pDS γ 1-_{LTGGEEKP}-YFP).

2.11. Cloning in the MutliMam expression system

AMPfret 2.1 subunits were cloned in the vectors (pACEMam2, pMDS and pMDK) of the *MultiMam* expression system. These vectors were chosen because they are all carrying the CAG promoter. Created plasmids were fused via their Lox-P site to yield to a single mammalian expression vector coding for the sensor AMPfret 2.1. The mutated version of AMPfret 2.1 that does not respond anymore to AMP (CBS site 3 mutant) was also generated and cloned in the *MultiMam* expression system to be further used as a negative control. Also, during the cloning of these AMPfret constructs, the His tag and the TEV cleavage site located at alpha N-terminus were removed.

3. Protein Biochemistry

3.1. Materials for protein purification, buffers and other equipment

Ni²⁺-NTA resin (Qiagen) was used for immobilized metal affinity chromatography (IMAC) purification of His-tagged proteins in BioRad gravity flow columns. All chromatography columns for protein purification on ÄKTA Basic or Purifier system were obtained from GE Healthcare.

All buffers and solutions were prepared with ultrapure water (Millipore systems) and filtered with a 0.22 µm filter. The pH was adjusted using HCl or NaOH if not otherwise stated.

3.2. Denaturing polyacrylamide gel electrophoresis (SDS-PAGE)

Proteins were analyzed by SDS-polyacrylamide gel electrophoresis (SDS-PAGE) with 7,5-12 % Tris-Glycine, depending on protein size and required resolution range. Gels were casted containing a stacking gel layer with lower acrylamide percentage (5 %) on top of a separating gel layer with higher percentage acrylamide (7,5-12 %).

For Tris-Glycine SDS-PAGE, the stacking layer contained 125 mM Tris/HCl (pH 6.8), 0.1 % (w/v) SDS, 6 % acrylamide/bis-acrylamide (37.5:1) and polymerized with 0.4 % (v/v) APS / 0.05 % (v/v) TEMED. The separating layer was casted with 375 mM Tris/HCl (pH 8.8), 0.1 % SDS, 7,5-12 % acrylamide/bis-acrylamide (37.5:1) and polymerized with 0.4 % (v/v) APS / 0.05 % (v/v) TEMED.

Protein samples were mixed 1:6 with 6x protein loading dye (200 mM Tris/HCl pH 6.8, 8 % (w/v) SDS, 40 % glycerol, 4 % (v/v) β-mercaptoethanol, 50 mM EDTA and 0.08 % (w/v) bromophenol blue) and denatured by heating at 95 °C for 2 min. Tris-Glycine SDS-PAGE was run in 1x SDS-PAGE running buffer (25 mM Tris/HCl pH 8.2, 192 mM glycine, 0.1 % (w/v) SDS). Protein bands were visualized by Coomassie staining with 40 % (v/v) Ethanol, 10 % (v/v) acetic acid and 0.2 % (w/v) Coomassie Brilliant Blue G-250. Background staining was removed by destaining gels in 5 % (v/v) Ethanol and 7.5 % (v/v) acetic acid.

3.3. Concentration determination of proteins

Protein concentrations were determined by measurement of the absorbance at 280 nm against a reference buffer with a Nanodrop 1000 spectrophotometer (Thermo Scientific). Protein concentration was calculated from the absorbance using appropriate extinction coefficients calculated with *ProtParam* (<http://web.expasy.org/protaram>) from the protein sequence.

3.4. Expression and purification

BL21 (DE3) *Star* cells were transformed by electroporation and protein expression was carried out overnight at 18°C in autoinducing medium (Studier, 2005). Such medium allows high densities bacterial culture and were reported as yielding to higher amount of soluble recombinantly expressed protein than common IPTG induction. Cells were collected by centrifugation at 6000 rpm (9000 x g) for 20 min using a Beckman Coulter centrifuge (rotor JLA-8.1000), suspended in PBS and finally pelleted again. This washing step was realized to remove any residual trace of culture medium which may alter further purification steps. Pellets were flash frozen in liquid nitrogen until purification. For purification, bacterial cells were suspended in Lysis buffer (0,5 M sucrose, 30% glycerol, 50 mM Tris pH8, 100 mM NaCl, 2 mM MgCl₂, 2 mM β-mercaptoethanol, lysosyme 1 mg/mL, 20 mM imidazole and protease inhibitors (Complete EDTA-free tablet (Roche), leupeptin (Sigma) and pepstatin (Sigma))). To limit further eventual DNA contamination, 200 U Benzonase were added to the suspension and it was gently stirred for 1 h at 8 °C. All further purification steps were carried out at 8 °C. Cells were then completely lysed by sonication using a Misonix Sonicator 4000 (5 min total at 80% - 20 sec ON / 1 min OFF). Cell-free extract obtained by centrifugation at 4 °C, 25000 rpm (75500 x g) for 80min (rotor JA 25.50) was applied on Ni-NTA Superflow resin (Qiagen) preequilibrated with lysis buffer. Resin was washed using washing buffer (50 mM Tris pH8, 100 mM NaCl, 20 mM Imidazole, 2 mM MgCl₂, 2 mM β-mercaptoethanol) and high salt buffer (wash buffer + 1 M NaCl) to remove eventual nucleic acid bound to the resin. Proteins were eluted by applying elution buffer (wash buffer + 400 mM Imidazole). Imidazole was removed through an overnight dialysis in buffer A (50 mM Tris pH8, 100 mM NaCl, 2 mM MgCl₂, 2 mM β-mercaptoethanol). Eluted proteins were passed over a 5 mL QXL column (GE Healthcare) in order to remove proteins bound to nucleic acids and non-stoichiometric AMPK

complexes. This was done using a HPLC Äkta purifier and injection was achieved using a 50 mL Superloop (GE Healthcare). Flowrate was set up to the column limitation (5 mL/min). Column was washed with 10 column volume Buffer A. Proteins were eluted using a 100 mL gradient of buffer B (50 mM Tris pH8, 1M NaCl, 2mM MgCl₂, 2mM βME) and were collected at a corresponding salt concentration of ~200 mM NaCl. Finally chimeric AMPK heterotrimers were applied to a Superose 6 gel filtration column (GE Healthcare) preequilibrated with SEC buffer (50 mM Tris pH8, 200 mM NaCl, 2 mM MgCl₂, 2 mM β-mercaptoethanol, 5 mM Spermidine (Sigma)). Spermidine diminished concentration dependent AMPK oligomer formation (U. Riek thesis). This step was done with a flowrate of 0,5 mL/min and fluorescently tagged AMPK eluted at a volume corresponding to globular protein of a ~280 kDa molecular weight, suggesting a rather elongated shape (real molecular weight 183 kDa). After adding glycerol to a final concentration of 50 %, the purified AMPK and AMPFRET constructs were placed in -20°C freezer and were stored there for further experiments. As AMPK is known to be unstable to freeze-thaw cycle, protein solutions were kept at -20 °C in glycerol to avoid freezing of the solution.

4. Characterization of AMPfret sensor in vitro

4.1. HPLC analysis

ATP containing buffers were always freshly prepared to limit contaminations by ADP and AMP through spontaneous hydrolysis. Therefore, the true concentrations of adenine nucleotides in ATP and NAD solutions were determined by HPLC (Varian equipped with a Proplus autosampler 410) (stationary phase: Polaris C18 (Agilent) / mobile phase: 60% CH₃CN 40% H₂O). Standard nucleotide mixtures were analyzed to evaluate ATP and ADP spontaneous hydrolysis. Quantification of ATP, ADP and AMP present in analyzed solution were calculated using calibration curves established for each nucleotides. Nucleotides elution was followed at 254 nm.

4.2. Enzymatic assay

AMPK 221WT and AMPfret constructs (3 pmol) were activated by incubation with purified CamKK β (1pmol) for 20min at 30°C in kinase buffer (200 μ M ATP, 40 μ M AMP, 5 mM MgCl₂, 1 mM DTT and 10 mM Hepes pH 7.4). Purified GST-ACC fragment (200 pmol), a reference substrate of AMPK was then incubated for 20 min at 37°C in presence or absence (negative control) of pre-activated AMPK 221WT or AMPFret constructs in kinase buffer containing 200 μ M [γ -³²P]-ATP (specific activity 650 mCi/mmol ATP). Reaction mixtures were then separated on SDS-PAGE gel. Specific AMPfret activities, i.e. ³²P insertion on ACC, were revealed by reading of autoradiograms using a Typhoon, Amersham Biosciences. Activities were evaluated with ImageJ 1.46. AMP-dependent allosteric activation was evaluated under same conditions unlike various concentrations of AMP were used and AMPK kinase activity was revealed by immunoblotting against P-ACC and ACC as unlabeled ATP was used (antibodies from Cell Signaling).

4.3. Enzymatic kinetic of CBS site mutants and effect of AMP

Enzymatic kinetic of AMPfret sensor and CBS site AMPfret mutants was performed as a normal enzymatic assay in presence or absence of AMP in the kinase buffer (\pm 20 μ M). Less

AMPfret sensor was used (200 fmol) in this test to clearly see the increase of activity at low time points. To stop the reaction at different time points protein loading dye (Laemmli buffer) was added to the reaction mixture and it was immediately heated at 90 °C for 5min. Note that equal amount of proteins was introduced (assessed by protein concentration measurement using NanoDrop - Thermo Scientific - and SDS-PAGE bands densitometry), in a considered experiment.

4.4. ADP dependent protection from dephosphorylation

Pre-phosphorylated AMPfret constructs by CamKK β (see 4.2), were repurified over a gel filtration column (Superose 6 10/300) to remove the upstream kinase and the nucleotides. Then, 50 ng of each AMPfret construct were incubated with 200 ng of PP2C α (Sigma) for 2 hours at 37°C in presence of various amounts of ADP (0 - 200 μ M). The reaction was stop by adding Laemmli buffer to the reaction mixture and the sample were heated 3min at 95°C. Phosphorylation status of AMPfret constructs was evaluated by immunoblotting against P-Thr172 and total α -subunit (antibodies from Cell Signaling). Note that the amount of PP2C α to use and other test conditions were determined through preliminary tests, and that the purity of the phosphatase was not high (results not shown).

4.5. FRET assay

Settings and shutters aperture were set in agreement with notice and in order to have a fluorescent signal without notch in the recorded spectrum. Settings values are presented in the legend Figure 14 which represents the light path (in white), the shutters (1 - 4) and the sample position (c) inside the fluorimeter. As presented on Fig. 14, spectrum can be recorded simultaneously through two detectors located right after the shutter 4 (PMT values were set to 1000 for both detectors).

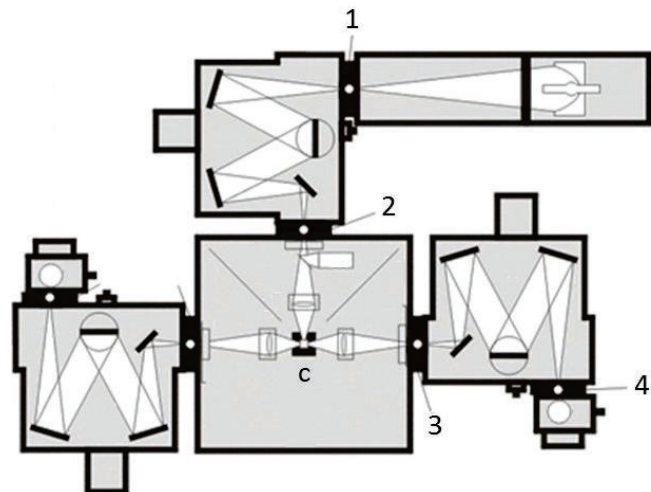


Figure 14: Scheme illustrating the path light in the fluorimeter during *in vitro* experiment involving AMPfret and shutters (1-4).

AMPfret incubated with various concentration of adenylates or others chemicals is placed in the cuvette (c). Adjustment screws for shutters (1-4) were positioned as following: 1- value: 10 (2nd turn); 2- value: 30 (1st turn); 3- value: 5 (3rd turn) and 4- value: 30 (5th turn).

CFP excitation and emission settings were set through the PTI software (Felix) interface. Excitation was set to 430nm, and emission is recorded from 451 to 601 nm with a step size of 1nm, integration time of 0,2 second.

FRET signal variation in presence of different compound (nucleotides, chemicals, ions) was measured using a fluorimeter (Photon Technology International). AMPfret constructs (20 pmol) were incubated in a quartz cuvette (Hellma) in a final volume of 150 μ L (spectro buffer: 50 mM Tris pH8, 200 mM NaCl, 5 mM MgCl₂, 2 mM β -mercaptoethanol). Effects of nucleotides and other compounds (previously prepared in the spectro buffer) on the AMPfret FRET ratio were determined by comparing FRET ratio (ratio of emission maxima of YFP at 527 nm and CFP at 476nm, taking 4 nm window) in their presence or absence. Excitation wavelength was set to 430 nm, and emission spectra were recorded from 450 to 600nm with an integration time of 0,2 sec. Mg²⁺ effect on FRET was investigated in spectro buffer with variable concentrations of Mg²⁺ (0 - 10 mM). Once acquired using the Felix software, spectra were treated under Excel or SigmaPlot.

4.6. Ratio between free ATP and Mg²⁺-ATP estimation

Ratios between Mg²⁺ and free ATP and the derived amount of Mg²⁺-ATP were calculated using maxchelator software at <http://maxchelator.stanford.edu> at the given experimental conditions (pH, salt concentration and temperature).

4.7. ATP analogues

Experiments involving ATP analogs were done using the Non-hydrolysable ATP test kit from Jena Bioscience. ATP analogues were prepared in spectro buffer (50 mM Tris pH8, 200 mM NaCl, 2 mM β-mercaptoethanol, 5mM MgCl₂).

5. Characterization of AMPFret sensor in cellulo:

5.1. Cell culture, transfection

3T3-L1, HepG2, HuH7 and HeLa cells were cultured in glucose containing DMEM (4,5 g/L) (Institut de Biotechnologies Jacques Boy) supplemented with SVF (10 %) (Pan-Biotech, lot P291905), 10 mM Hepes (PAA cell culture company), penicillin and streptomycin (Gibco) as well as non-essential amino acids (Sigma). Once cells reached ~80% confluence, medium was replaced by OptiMEM (Lifetechnologies) and AMPfret A_{helix} coding plasmid was transfected using Lipofectamine2000 (Lifetechnologies). After 5 to 6 hours, OptiMEM was exchanged by complete DMEM and cells grew for > 24 hours until their observations under the confocal microscope.

Cell line	Origin	Morphology	Organism
3T3-L1	Embryo tissue	Fibroblast	<i>Mouse</i>
HepG2	Liver carcinoma	Epithelial	<i>Human</i>
HuH7	Liver carcinoma	Epithelial	<i>Human</i>
HeLa	Cervical cancer	Epithelial	<i>Human</i>

5.2. Confocal microscopy

3T3-L1 and HeLa cells, cultivated and transfected in 8 wells LabTek cover glass plates (Nunc), were observed with a Leica TCS SP2 AOBS confocal microscope. LabTek plates were placed in an incubation chamber in which the temperature and O₂ concentration were maintained at 37 °C and 21%, respectively.

HepG2 cells were grown and transfected in petri dishes containing circular glass slides. Slide were then mounted a specific support that allow medium exchange within the incubation chamber using airtight tubing and syringes.

5.3. AICAR

Without moving the Labtek, 200 µL medium was replaced by the same volume of complete medium containing 2mM AICAR (1mM final). Excitation wavelength was set to 458nm using the Argon laser and emission spectra showing FRET signal were monitored through λ scans

from 463 nm to 600 nm every 15 minutes. Using the Leica Confocal Software (LCS), ROI (region of interest) were drawn in order to cover entire cells. FRET signal variations were calculated from those measured emission spectra.

5.4. Ischemia reperfusion

During 1 hour of ischemia, the O₂ concentration was set to 2% in the chamber and complete medium was replaced by a deprived one that no more contains nutrients (calcium chloride 200 mg/L, iron nitrate 0,1 mg/L, magnesium sulfate 97,7 mg/L, potassium chloride 400 mg/L, sodium chloride 6400 mg/L, sodium dihydrogen phosphate 125 mg/L, phenol red 15 mg/L and sodium hydrogen carbonate 3,7 mg/L). Deprived medium was bubbled using nitrogen for at least 10 min before being added onto the cells. After 1 hour of ischemia, reperfusion was done by replacing the deprived medium by complete medium and restoring O₂ to 21%. Reperfusion was carried on for 1 hour. All along ischemia reperfusion, FRET ratio was monitored every minute by recording simultaneously both mseCFP_{Δ11} and cpVenus emitted signal through windows of 4nm using two independent channels.

5.5. Western Blotting:

5.5.1. Protein Extraction

After the removal of the media, Petri dishes containing adherent HeLa or 3T3-L1 cells were immediately flash-frozen in liquid nitrogen. Then on ice, 200 μL of buffer containing 50 mM Tris pH8, 200 mM NaCl, 2 mM beta-mercaptoethanol were added per petri dish and cells were scratched using a scraper. The 200 μL of buffer containing the cells were transferred in Eppendorf tubes which were frozen in liquid Nitrogen. After thawing, cells were sonicated 5 seconds using a sonicator equipped with a micro tip. Lysates were centrifuged in a cooled table top centrifuge for 10 min and 16000 x g at 4°C and the supernatant was kept.

5.5.2. SDS-PAGE and Immunoblot

Highlighting of AICAR-dependent activation of AMPK in 3T3-L1 cells (correlation with AMPFret ratio increase): Proteins were quantified using the Bradford reagent. Sample volumes with identical protein content were added to protein loading dye (Laemmli buffer), heated at 90 °C for 1 min, and loaded onto 7,5% acrylamide SDS-PAGE gels. Proteins migrated for 1 h at 180 V and were then transferred onto a nitrocellulose membrane using the wet transfer method for 2 h at a constant voltage of 100 V. Membranes were saturated 1 h at room temperature with TBS-Tween 0,1%, milk 5%, incubated overnight at 4 °C with antibodies diluted in TBS-Tween 0,1%, milk 5% (anti-acetyl-CoA carboxylase from rabbit (1:1000, Cell Signaling), anti phospho-Acetyl-Coa carboxylase from rabbit (1:1000, Cell Signaling) and anti β -Tubulin from rabbit (1:1000, Cell Signaling)). After three washing steps of 15 min each using TBS-Tween 0,1%, secondary antibody (donkey anti-rabbit IgG, 1:3000, GE Healthcare) conjugated with horseradish peroxidase and diluted in TBS-Tween 0,1%, milk 5% were applied to the membrane for 1h at room temperature. After three washing steps of 15 min each using TBS-Tween 0,1%, revelation solution was added on top of the membrane and bands were visualized using a digital imager. Phospho-ACC and ACC bands were quantified using ImageJ 1.46.

Aim of the work

The project presented here aims to develop genetically encoded sensors for cellular energy state based on the AMP-activated protein kinase (AMPK). As presented during the introduction, AMPK is a large heterotrimeric complex that is regulated by a number of signals, in particular a decrease in the ATP/AMP ratio. Thus, affinities of the kinase have evolved in the “natural” range of these nucleotides. Creation of such genetically encoded sensors for energy metabolism is also expected to advance the current knowledge about the complex AMPK regulation and its downstream signaling. In addition, they are envisaged to facilitate screening and identification of putative synthetic activators or inhibitors of AMPK.

The AMPK-based sensors presented herein take advantage of the i) partial structural characterization available at the beginning of the work and particularly ii) the discovery of AMP-induced conformational changes occurring in the whole heterotrimer, and which our group previously discovered. In addition, our high-throughput cloning and expression technologies (ACEMBL expression system) have paved the way for an innovative molecular engineering which largely facilitates the creation of these genetically encoded biosensors.

In more details, the project aims at the construction, validation and application of genetic sensors based on fluorescence resonance energy transfer (FRET) and on a systematic permutation of different linkers and fluorescent protein tags at the termini of the three AMPK subunits to finally select AMPK variants with maximal FRET. All constructs, including controls to assure specificity of the signal, will be analyzed *in vitro* (with recombinant protein) and *in vivo* (in cells). The complex activation mechanisms of AMPK will also be analyzed at a molecular level. Such intracellular genetic probes will allow for the first time and without ATP consumption a quantitative, real-time read-out of spatiotemporal dynamics (i) in ATP/AMP ratios (indicative of the cellular energy state) or (ii) in AMPK allosteric activation using live cell imaging. Given the dysfunctional energetics in various pathologies (cancer, metabolic and neuromuscular diseases), such unique and polyvalent tools would have broad applications in fundamental (molecular mechanisms of AMPK activation, cell signaling, systems biology) and applied research (effects of therapeutic drugs). Thus, academic as well as industrial benefits can be expected from this project.

Results

An AMPK-based genetically encoded fluorescent biosensor: AMPfret

1.	Generating AMPK-based biosensors	133
1.1.	Construction principles and cloning.....	133
1.1.1.	<i>MultiColi</i> expression system	133
1.1.2.	Optimizing bacterial expression	138
1.2.	Overview of the FRET optimization strategy	140
2.	First generation of biosensors: AMPfret 1.0	143
2.1.	Site-specific mutant constructs	144
2.2.	Optimization: FRET pair exchange	147
2.3.	Expression and purification	150
2.3.1.	Expression optimization	150
2.3.2.	Increasing the solubility.....	152
2.3.3.	Purification procedure.....	154
3.	Characterization of AMPfret 1.0	159
3.1.	Enzymatic activity.....	159
3.2.	FRET signal variations as a readout of AMP-induced conformational changes.....	160
3.3.	Salt and pH controls.....	166
3.4.	AMPfret responds to AMP and ADP physiological concentrations.	168
3.4.1.	The AMP-response	168
3.4.2.	The ADP-response	171
4.	Exploring molecular mechanisms of AMPK complex regulation by adenylates	174
4.1.	AMPK CBS sites	174
4.2.	AMPK CBS sites and allosteric activation by AMP	175
4.3.	AMPK CBS sites and protection against dephosphorylation by ADP.....	178
4.4.	Thr172 phospho-status does not condition AMP-dependent conformational changes. .	180
4.5.	Free- and Mg-complexed ATP in AMPK allosteric activation.....	182
4.6.	ATP analogues	184

5.	An optimized AMPfret biosensor: AMPfret 2.0	187
5.1.	Optimization: linker engineering	187
5.2.	Reducing flexibility by linker shortening	187
5.3.	Reducing flexibility with a putative rigid α -helix.	191
5.4.	AMPfret 2.0 presents an improved FRET signal variation	194
5.5.	AMPfret 2.0 responds to AMP and ADP physiological concentrations.....	196
5.5.1.	The AMP response.....	196
5.5.2.	The ADP response	197
5.6.	AMPfret 2.0 reports physiological fluctuations of adenylates mixes	199
6.	AMPfret: a tool to screen and identify AMPK direct interactors.....	203
6.1.	In vitro screening of AMPK interactors	203
6.2.	NAD ⁺ putative interaction with AMPK.	206
7.	AMPfret in cellulo	208
7.1.	AMPK activation by AICAR	208
7.2.	Ischemia-reperfusion	211
8.	References.....	215

Abstract. Based on the ability of AMPK to discriminate ATP versus AMP and ADP and our current conformational switch model characterizing AMPK allosteric activation, we conceived the genetically encoded biosensor AMPfret (Figure 1). Such biosensor would allow molecular analysis of complex allosteric activation mechanisms of AMPK, direct screening of AMPK allosteric activators *in vitro* or in cells, and ultimately monitoring of energy metabolism in real time and space *in cellulo*.

Résumé. Tirant profit de la capacité qu'a l'AMPK pour discriminer l'ATP face à l'AMP et l'ADP tout en nous basant sur notre modèle actuel de changement de conformation lors de l'activation allostérique de l'AMPK, nous avons conçu et produit un biosenseur fluorescent codé génétiquement (Figure 1). Ce biosenseur nous a permis d'effectuer une analyse moléculaire des mécanismes complexes de l'activation allostérique de l'AMPK. De plus, ce senseur représente un outil de choix i) pour le criblage direct d'activateurs allostérique *in vitro* ou *in cellulo*, et ultimement ii) pour suivre en temps réel le métabolisme énergétique de cellules.

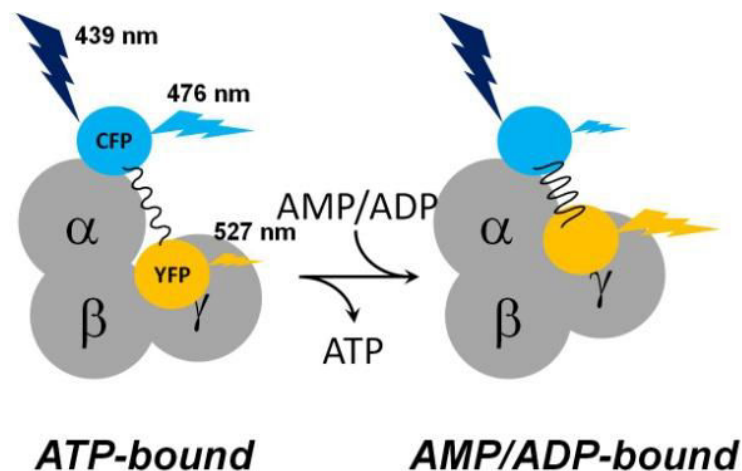


Figure 1: Conformational switch model showing the operating mode of AMPfret sensors.

AMPfret sensors are constructed from an AMPK heterotrimer (consisting of α -, β -, and γ -subunits, grey circles) with two additional GFP-derived fluorescent proteins (CFP, YFP, cyan and yellow circles) fused to different N- and C-termini of AMPK subunits. Assuming that binding of AMP (and ADP) to at least two CBS domains in the AMPK γ -subunit induces a conformational change which reduces distance and / or orientation between the fluorophore couple, this would increase fluorescence resonance energy transfer (FRET) between the two fluorophores. Experimentally, when CFP is excited at 439 nm, FRET would reduce direct CFP fluorescence emission at 476 nm, while energy transferred to YFP would increase YFP fluorescence emission at 527 nm. FRET by long-range dipole interaction is indicated by a wave line.

1. Generating AMPK-based biosensors

1.1. Construction principles and cloning

1.1.1. *MultiColi* expression system

The basic idea of this approach consisted in tagging the heterotrimeric AMPK with two fluorescent proteins (FPs) in a way close enough to permit FRET variations due to conformational changes which go along with allosteric activation (Chen et al., 2012; Riek et al., 2008; Zhu et al., 2011). For the purpose of facilitating the cloning and expression of these constructs, we used the *MultiColi* expression system (Bieniossek et al., 2009) from the ACEMBL suite, a technology especially designed for expression of protein complexes. Indeed, ACEMBL allows the easy handling of genes coding for multiprotein complexes through a set of minimalistic plasmids, followed by simultaneous expression of the entire protein complex, as plasmids can be fused or split on purpose by Cre-recombination. *MultiColi* is dedicated to protein complex expression in bacteria. Using this technology, AMPK α -subunit alone or tagged with CFP at its N-terminus or C-terminus was cloned into the pACE1 vector, β -subunit alone or tagged with YFP at its N-terminus or C-terminus was cloned into the pDC vector and the γ -subunit alone or tagged with CFP or YFP at its N-terminus or C-terminus was cloned into the pDS vector (Figure 2 and Table 1). pACE1 carries a resistance gene for ampicillin, pDC for chloramphenicol and pDS for spectinomycin. Once the cloning was verified by restriction digestions (Figure 2) and sequencing (data not shown), vectors were fused via their lox-P site using Cre recombinase. Due to the presence of the R6K γ conditional origin of replication within the donors backbone (for details see Material & Methods chapter), replication of the final plasmid depends on expression of the *pir* gene product by the host. Thus, in regular expression strains, the plasmids have to rely on fusion with an acceptor plasmid for productive replication. Donors or donor-donor fusions can nonetheless be used even for expression when not fused with an acceptor, by using expression strains carrying a genomic insertion of the *pir* gene. The *pir*⁺ bacterial strains, such as the BW23473 cells were used during the cloning steps involving only donor vectors.

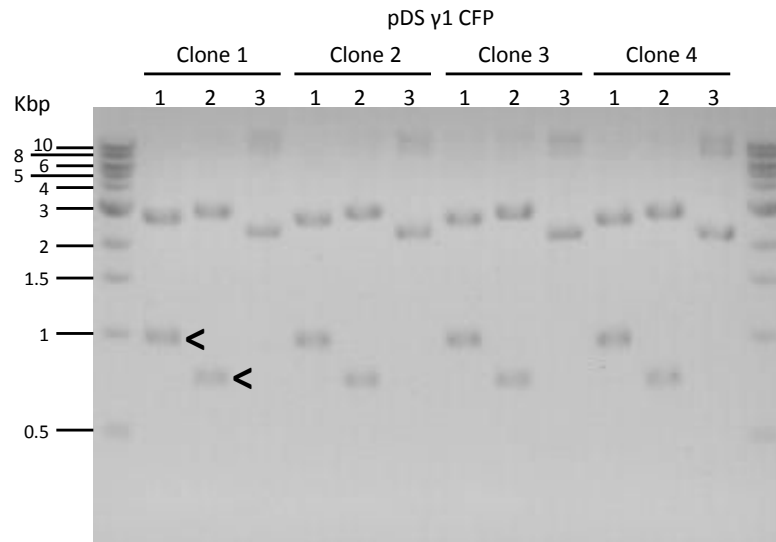


Figure 2: Example of cloning verification by restriction digest (e.g. here pDS γ 1CFP).

Four different pDS γ 1-CFP clones (1 - 4) were digested by restriction enzymes and loaded onto an agarose gel 1%. 350 ng of each clone were digested by Nde1 (10 Units) and Nhe1 (5 Units) to cut out the γ 1 gene (1 - band at 1 kbp). Same amount of plasmid was digested by Nhe1 (5 Units) and Spe1 (5 Units) to cut out the CFP coding sequence (2 - band at 747 bp). Same amount of each clone, undigested, was also loaded onto the gel (3). Lane 1 and 14 show a DNA size ladder. Note that empty pDS vector is about 1.8 kbp and that all clones look correct as they all seem to contain γ 1 and CFP (1 kbp and 747 bp respectively).

Once single subunit coding vectors, fluorescently tagged or not, were obtained, those coding for β and γ subunits were fused with empty pACE1 to perform preliminary expression tests, and the same was done using directly the α -derived constructs. Single subunit expression tests were done for all α -, β -, and γ -based constructs in order to identify at an early stage any failure that could yield non-optimal expression of the AMPfret heterotrimer. Expression of whole heterotrimers was done in *pir*⁻ bacteria transformed with the fusion product of pACE1, pDC and pDS, (yielding a single nucleotide chain coding for the AMPK heterotrimer), which will grow when plated on ampicillin, chloramphenicol and spectinomycin containing LB-agar. Plasmid DNA preparations of grown colonies and restriction analysis then allowed the selection of fusion vectors having integrated stoichiometric amounts of each AMPK subunit-encoding vector. Indeed, Cre recombination could result in larger vectors than expected, containing several copies of a plasmid. Thus, the ACEMBL expression system also allows modulation of subunit stoichiometry when expressing protein complexes.

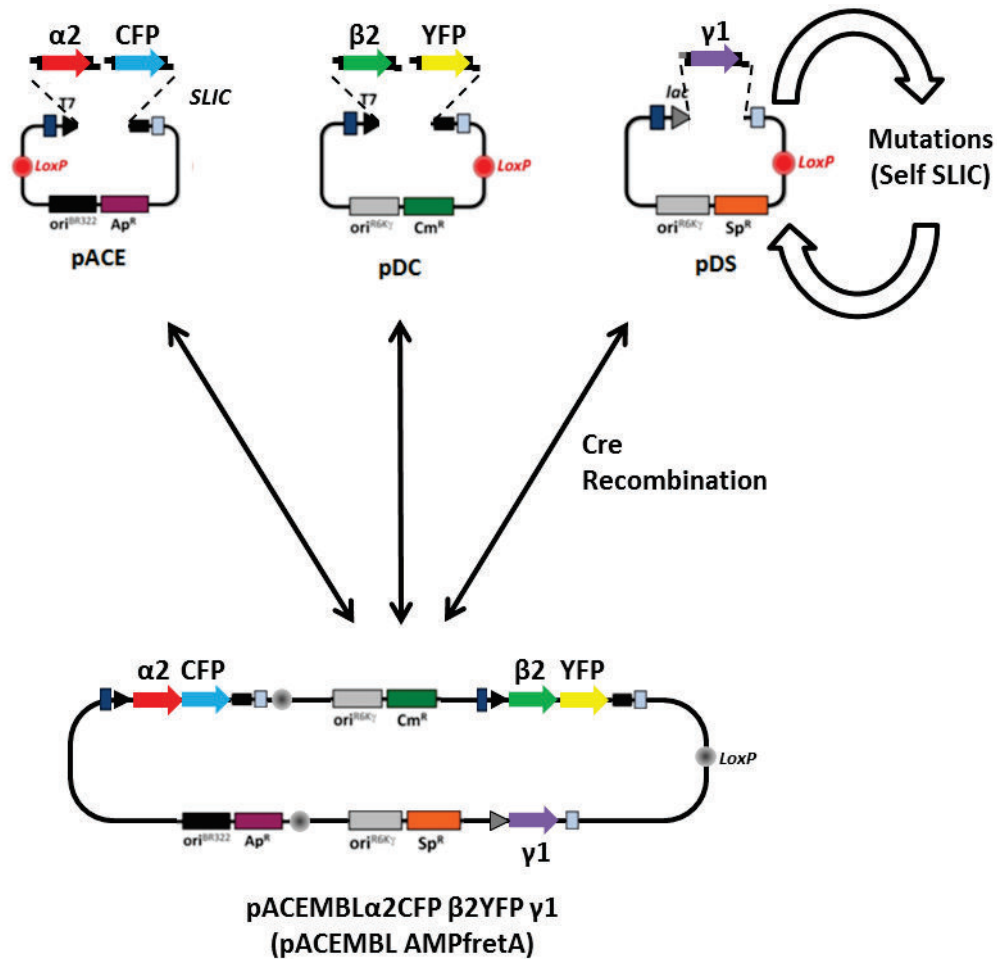


Figure 3: Cloning strategy of AMPfret in ACEMBL MultiColi expression system.

AMPK subunit genes ($\alpha 2$, $\beta 2$ and $\gamma 1$ genes depicted by red, green and purple arrows respectively) flanked or not by a fluorescent protein (CFP and YFP genes are shown as blue and yellow arrow respectively) were cloned into the ACEMBL acceptor and donor vectors using SLIC or conventional cloning methods. Vectors containing genes of interest can be quickly and easily modified via self SLIC (e.g. for site directed mutagenesis). Acceptor and donors are assembled via their LoxP site by Cre recombination to generate a single expression plasmid coding for AMPfret heterotrimeric protein complex. Fused vectors can be disassembled as Cre recombination is reversible to obtain modification of single acceptor or donor vector. The figure presents how the AMPfretA coding vector was created. Vector elements are represented according to the legend of Figure 4.

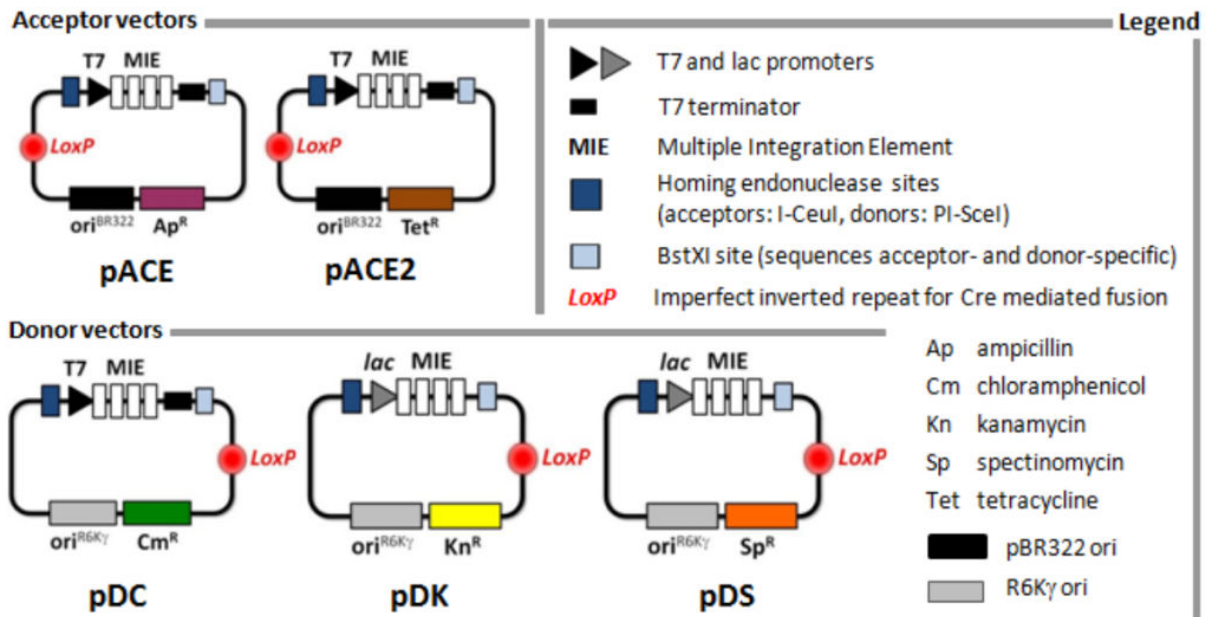


Figure 4: ACEMBL system for multi-protein complex production in *E. coli*.

Vectors are classified as either acceptors or donors depending on their replication origin. Elements present within the nucleotide sequences are listed in the legend (from MultiColi User Manual Vers. 2.0, June 2011).

The complete cloning strategy and vector maps of plasmids, containing single AMPK subunit tagged (or not) with fluorescent protein, are presented in more detail in the annex (2. Molecular cloning), including vectors initially available and all plasmids created during this thesis work.

To ensure that AMPK subunits tagged (or not), were well expressed in *E. coli*, single subunit expression tests were realized (Figure 5). These could provide crucial information before starting large scale expression of AMPK chimeric constructs. As donor vectors contain a conditional replication origin, all pDC- and pDS-derived vectors (β 2 vectors and γ 1 vectors, respectively) were fused by Cre-recombination to empty pACE1. This allowed expressions of β 2 and γ 1 variants in *E. coli* expression strains, to detect potential problems at an early stage, possibly linked to mutation/deletion in up- and down-stream elements of the expression cassettes.

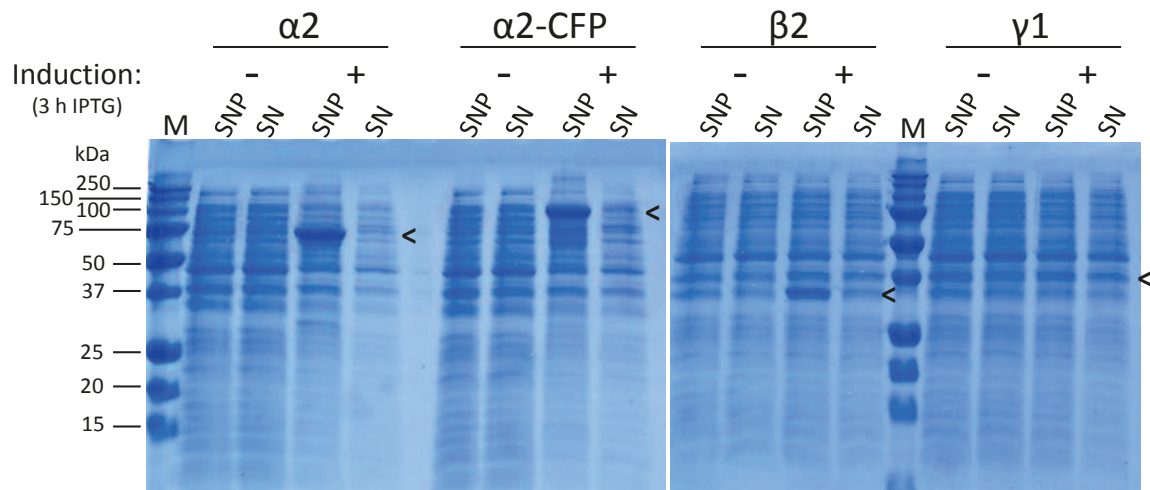


Figure 5: Single subunit expression tests.

Small scale expression test were realized using single subunit coding vector, e.g. here subunits $\alpha 2$, $\alpha 2$ -CFP, $\beta 2$ and $\gamma 1$. Equivalent number of lysed bacteria was used for each SNP/SN condition (ca. 3 millions). Molecular weight marker is shown on both gels (M). Supernatant + pellet (SNP) and supernatant only (SN) fractions were loaded onto 12% SDS-PAGE gel before (-) and after induction (+) by 1 mM IPTG for 3 hours at 37°C. Molecular weight of $\alpha 2$ is 65 kDa, $\alpha 2$ -CFP is 93 kDa, $\beta 2$ is 30 kDa and $\gamma 1$ is 37 kDa. Note that single AMPK subunits are mainly insoluble when expressed under such conditions and that protein expression using the Lac promoter ($\gamma 1$) are weaker than those done with the classical T7 promoter ($\alpha 2$, $\alpha 2$ -CFP and $\beta 2$). $\gamma 1$ is not visible at this resolution.

Every subunit version was expressed at 37°C in *E. coli* BL21 DE3* (Invitrogen) for 3h after IPTG induction. Even if not all were entirely soluble (especially α -subunits), they gave visible bands after expression when protein amount equivalent to 3 million of bacteria (according to bacterial culture OD) lysed by sonication was loaded onto a 12% SDS-PAGE gel and colored by Coomassie staining (Figure 5). Probably, α -subunits need to be associated to other subunits to become soluble. However, $\gamma 1$ subunits tagged (or not) with CFP or YFP were considerably less expressed than $\alpha 2$ and $\beta 2$, and this may be due to the presence of the Lac promoter in the pDS vector. Lac promoter is known to induce weaker expression as compared to the T7 promoter which is present in pACE and pDC vectors (Figure 5 and Figure 7).

1.1.2. Optimizing bacterial expression

The choice of promoters in the ACEMBL vectors can serve for fine tuning expression of a given component within a protein complex relative to others. To obtain a stoichiometric molar ratio of each subunit during expression, we replaced the Lac promoter present in pDS (γ vectors) by the T7 promoter also present in pACE (α vectors) and pDC (β vectors). As a result, all AMPK subunits were expressed under the control of the T7 promoter. As the fragment to clone was very small and given the restriction sites available for cloning into pDS, an original strategy was established (Figure 6). pDS γ 1 (harboring the Lac promoter) and pACE (harboring the T7 promoter) were opened at the level their Nde1 restriction sites that are both located right downstream to their promoters. They were then ligated together and the resulting fusion plasmid was cut with AvrII to separate pACE1 containing the Lac promoter (pACELac) from the pDS vector with the T7 promoter inserted (pDS γ 1T7pro). The fusion vector was simultaneously digested with MfeI to cut pACELac into pieces in order to facilitate gel extraction of pDS γ 1T7pro since empty pACE and pDS γ 1 have similar size.

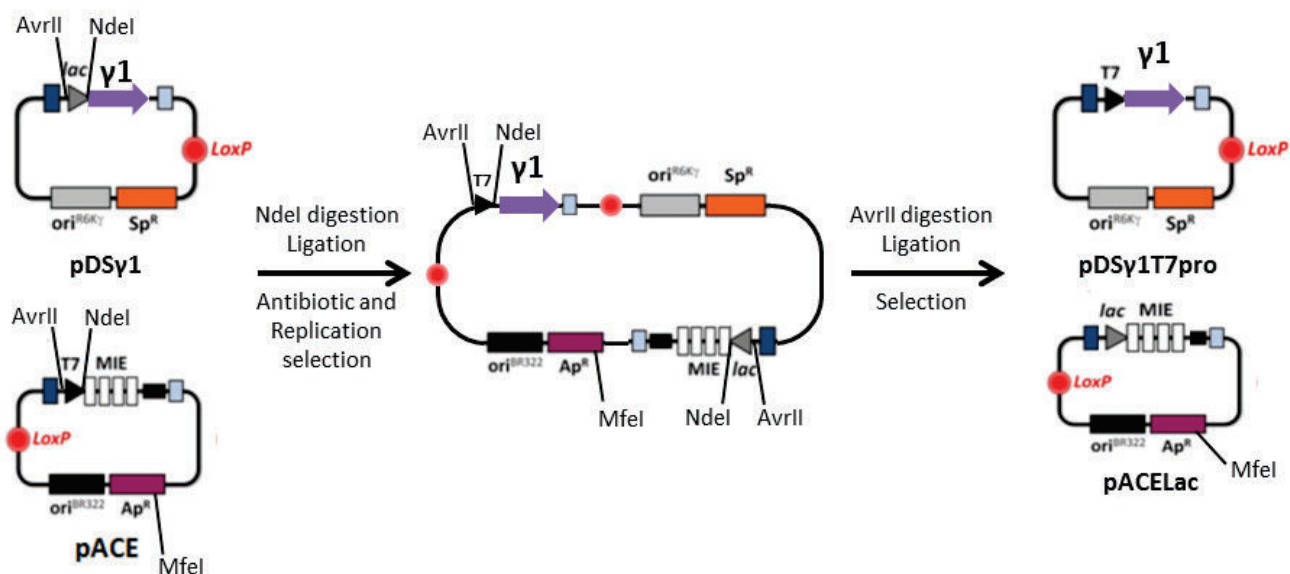


Figure 6: Promoter exchange in pDS γ 1.

pACE and pDS γ 1 were opened at the level of their Nde1 restriction site, both positioned right downstream to their respective promoter. They were ligated together and transformed into Top10 (or Omnimax) cells. Cells were plated on ampicillin and spectinomycin. After a plasmid miniprep, the fusion vector was digested with AvrII into two pieces, corresponding to linearized pDS γ 1 (containing T7 promoter) and pACELac. The band corresponding to the linearized pDS γ 1T7Pro was extracted from the gel and finally self-recircularization led to the creation of pDS γ 1, including T7 promoter.

Cloning was verified by restriction digest using Sph1 and sequencing (Macrogen). AMPK complex is known to be soluble during purification when it contains all three subunits. To evaluate the benefits of having inserted the T7 promoter in pDS (γ vectors), small scale expression and purification was done with AMPK α 2 β 2 γ 1 (for short: AMPK221), corresponding to the heterotrimer coded by pACE1 α 2, pDC β 2, pDS γ 1 fused by Cre recombination.

It has to be noted that a cleavable purification tag consisting of ten histidine residues followed by a TEV protease recognition site, was inserted at the α 2 N-terminus during the cloning strategies (see Material & Methods and Annexes chapters). We then compared the expressed and purified proteins on SDS-PAGE gel when using either T7 or Lac promoter (Figure 7). A single purification step, in form of an AMPK heterotrimer pull down from lysis supernatant, was applied using Ni²⁺-NTA beads. The γ -subunit appeared to be more expressed when cloned in pDS containing the T7 promoter (Figure 7-B) as compared to Lac promoter (Figure 7-A). More importantly, AMPK221 when cloned in vectors that all contained the T7 promoter gives, after purification, much higher yield of soluble heterotrimer, close to a 1:1:1 stoichiometry. However, purification of AMPK221, when expressed 3 hours at 37°C under IPTG induction, yielded too low amounts of pure protein (<0,5 mg/L culture), which required optimization of the purification procedure.

According to the advantages of the pDST7pro, the genes for the γ 1-subunits tagged with fluorescent protein (CFP or YFP) were also cloned into this vector, following the same strategy as above (see Annexes chapter). Thus, all γ 1-constructs in this work are based on the pDST7Pro, which will be shortly named pDS.

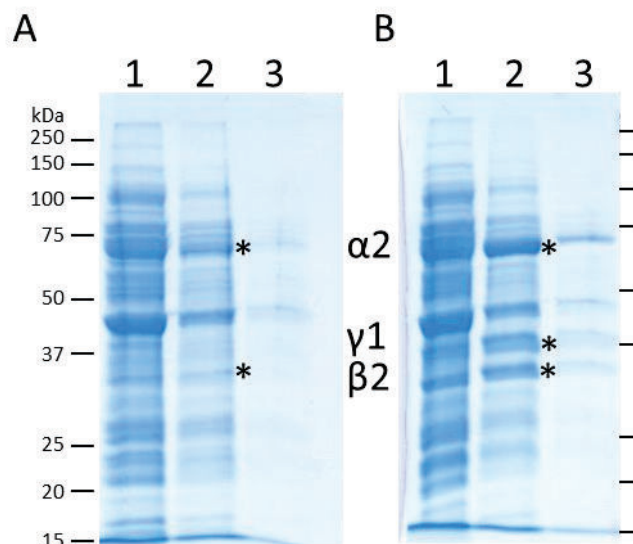


Figure 7: Heterotrimer expression test: γ expression with Lac of T7 promoter

SDS-PAGE gel shows Ni-NTA elution fractions of AMPK221 with γ 1 expression controlled by Lac promoter (A) or T7 promoter (B). α 2- and β 2-subunits are both under the control of the T7 promoter. Molecular weight marker is shown on both sides of the figure. A: Lanes 1-3: IMAC elutions with buffers containing 100 mM, 200 mM or 400 mM imidazole. B: Lanes 1-3: IMAC elution fractions with buffers containing 100 mM, 200 mM or 400 mM imidazole. Note: γ 1-subunit (37 kDa) expression appears weaker when under the control of the Lac promoter as compared to T7 promoter. In addition, the T7 promoter in pDS also improves the stoichiometric molar ratio of solubilized AMPK221 complex.

1.2. Overview of the FRET optimization strategy

The entire AMPfret library evolved over several optimization steps as summarized in Table 1. In addition to the position of the fluorescent tags, both the fluorophores and sequences connecting AMPK subunits to these fluorophores were shortened or engineered (e.g. by adding an artificial α -helix). An overview of this optimization strategy is presented in Figure 8.

Initially, 12 different AMPfret constructs (A-L) were generated (Table 1). They represent all the possible permutations for having two of the AMPK subunits tagged at either N- or C-termini with a fluorescent protein. Out of these variants, 2 constructs (AMPfret A and C) were retained since they showed significant FRET variation depending on the presence AMP. Since AMPfret C construct showed the most important FRET variation, it was used for initial characterization, including CBS site mutants (AMPfret 1.0).

A first step of construct optimization consisted in exchanging the fluorescent proteins eCFP/YFP into more advanced GFP derivatives (mseCFP_{Δ11}/cpVenus). The resulting version of AMPfret C carrying a more recent version of FRET pair was named AMPfret 1.1 and was used for control experiments to estimate AMPfret pH and salt stability.

A second step of optimization was performed with both AMPfret A and C constructs. The linker located between AMPK subunits and the fluorescent proteins was modified (length and nature). First, a short unfolded amino acid sequence, located in between the AMPK subunits and the fluorescent protein, were deleted. Second, a rigid linker was inserted between α C-terminus and CFP. Since only AMPfret A containing a rigid linker showed improved FRET in presence of AMP, this construct was retained as AMPfret 2.0. Most *in vitro* tests, under fixed and controlled conditions, were done using this construct. The eCFP/YFP FRET pair was then also replaced by mseCFP_{Δ11}/cpVenus. This construct, AMPfret 2.1, was mainly used for AMPfret characterization in cells.

Optimization did not change the overall AMPfret response to changes in AMP concentration. However, the additional α -helix increased the measurable change in FRET ratio at a given change in AMP levels, and mseCFP_{Δ11}/cpVenus increased stability of the FRET signal in respect to salt and pH (see 3.3 and 5.1).

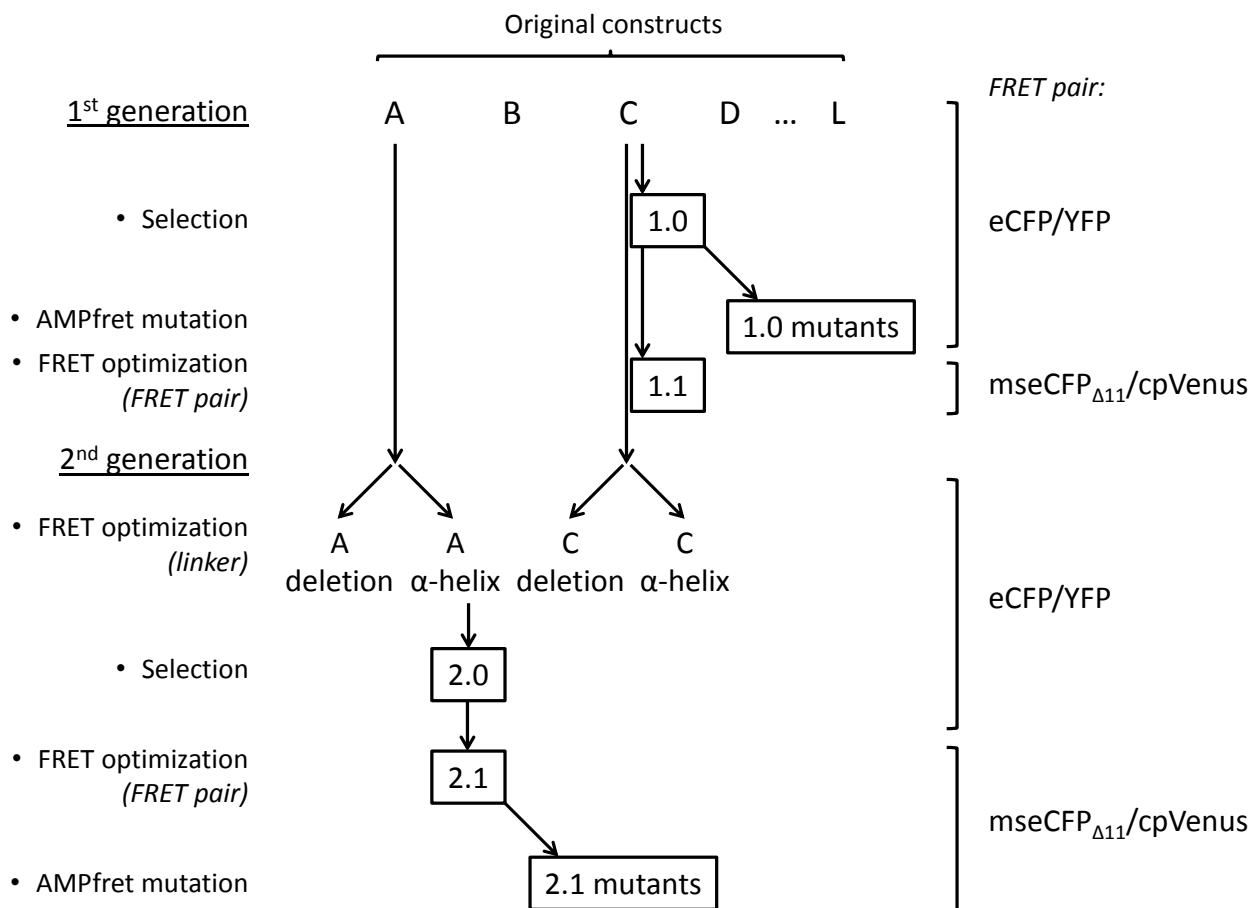


Figure 8: Optimization strategy for AMPfret.

From the 12 initially realized constructs (A-L), 2 were identified as responding positively to AMP through variation in their FRET ratio (A and C). AMPfret 1.0 is based on construct C and used for mutations of CBS sites and Thr172. AMPfret 2.0 is based on A and used for further mutations. FRET pairs present in a given AMPfret construct are mentioned to the right. See text for details.

2. First generation of biosensors: AMPfret 1.0

Once all vectors coding for AMPK single subunits tagged with fluorescent protein were obtained and sequenced, all permutations of AMPK heterotrimer containing a FRET pair were obtained. The strategy consisted in tagging two of the three AMPK subunits at their N- or C-termini with an individual fluorescent protein (FP) of a FRET couple, Cyan Fluorescent Protein (CFP) and Yellow Fluorescent Protein (YFP), thus tagging either α and β , α and γ or β and γ . This approach gave rise to 12 different constructs (Table 1). Since no details on conformational changes in full-length AMPK complex are known, such a non-biased matrix approach was essential. It allowed the screening of all potential terminal fluorophore positions to identify those that are informative.

Once having all constructs expressed and purified, we quantified the AMP-induced changes in FRET ratio. Constructs showing such changes could represent suitable reporters of AMP-related conformational changes and allosteric activation of AMPK. They could also serve to map conformational changes within the AMPK heterotrimer. Further analysis of purified AMPfret constructs showed that all protein complexes were obtained properly folded, monomeric, pure and that they were conserving features of native AMPK (see Results chapter part 3.).

AMPfret construct	Vector name and composition
AMPK 221	pACEMBL $\alpha_2 - \beta_2 - \gamma_1$
AMPfret A	pACEMBL α_2 -CFP - β_2 -YFP - γ_1
AMPfret B	pACEMBL CFP- α_2 - β_2 -YFP - γ_1
AMPfret C	pACEMBL α_2 -CFP - β_2 - γ_1 -YFP
AMPfret D	pACEMBL α_2 -CFP - β_2 - YFP- γ_1
AMPfret E	pACEMBL CFP- α_2 - β_2 - γ_1 -YFP
AMPfret F	pACEMBL CFP- α_2 - β_2 - YFP- γ_1
AMPfret G	pACEMBL α_2 - β_2 -YFP - γ_1 -CFP
AMPfret H	pACEMBL α_2 - YFP- β_2 - γ_1 -CFP
AMPfret I	pACEMBL α_2 - β_2 -YFP - CFP- γ_1
AMPfret J	pACEMBL α_2 - YFP- β_2 - CFP- γ_1
AMPfret K	pACEMBL α_2 -CFP - YFP- β_2 - γ_1
AMPfret L	pACEMBL CFP- α_2 - YFP- β_2 - γ_1

Table 1: AMPfret coding vectors.

Overview of the 12 initial chimeric AMPfret constructs containing two fluorescent protein tags permuted at the N- and C-termini of the three AMPK subunits. pACEMBL, plasmid resulting from the Cre-LoxP fusion of vectors pACE, pDC and pDS, all part of the *MutliColi* expression system; CFP, Cyan Fluorescent Protein; YFP, Yellow Fluorescent Protein; α_2 , β_2 , γ_1 , AMPK subunits.

2.1. Site-specific mutant constructs

To investigate AMPK regulation by adenylates, we mutated critical sites within the γ -CBS sites involved in adenylates binding. These constructs were based on previously generated and characterized γ -mutants, that are deficient in AMP (and other adenylate) binding to specific CBS sites (Chen et al., 2012).

Based on collaborator's work (Chen et al., 2012), the following CBS sites were mutated (Figure 9): (1) residues Leu128 and Val129 were mutated into two Asp to block adenylate

binding at the level of CBS site 1 by disrupting interactions between γ -subunit residues and the adenine ring (Figure 9-B); (2) Val275 and Leu276 were replaced by two Gly to prevent nucleotide binding at CBS site 3, again perturbing interactions between CBS site residues and the adenine ring (Figure 9-C); (3) Ser315 was exchanged to Pro in CBS site 4 which should prevent AMP binding by remodeling the binding pocket for the α -phosphate group; in contrast to a possible mutation at Ile311 which would interfere with the binding of the adenine ring. S315P mutation should strongly affect bending at the peptidic chain in addition to altering the side chain (Figure 9-D). The so called “non-exchangeable” CBS4 site was also mutated, since Chen et al. proposed a model in which this site may participate in allosteric activation of AMPK.

Another residue involved in adenylate binding at AMPK CBS site 3 is Arg298 (labeled in grey on Figure 9-A). The γ 1-Arg298 is the analog of γ 2-Arg531. The R531Q mutation in γ 2 causes a hereditary heart disease (fatal congenital non-lysosomal cardiac glycogenosis) (Burwinkel et al., 2005). Mutation of AMPK at Arg531 impedes allosteric activation by AMP. R531G (Hawley et al., 2010) and R531Q mutations were reported to have a particularly severe effect in that they generate completely AMP-insensitive complexes. Arg298 could have been chosen to create a CBS site 3 mutant. However, it is positioned in-between CBS sites 3 and 4, so its effects may not be clearly assigned to either CBS3 or CBS4. Chen et al. visualized Arg298 as forming ionic bond with the phosphate group of AMP-3 (Figure 9-A) whereas Scott et al. (Scott et al., 2007) claimed that Arg531 is part of the CBS site 4. According to available literature, the amino acids chosen for mutation in our study are involved in nucleotide binding at only one single CBS site.

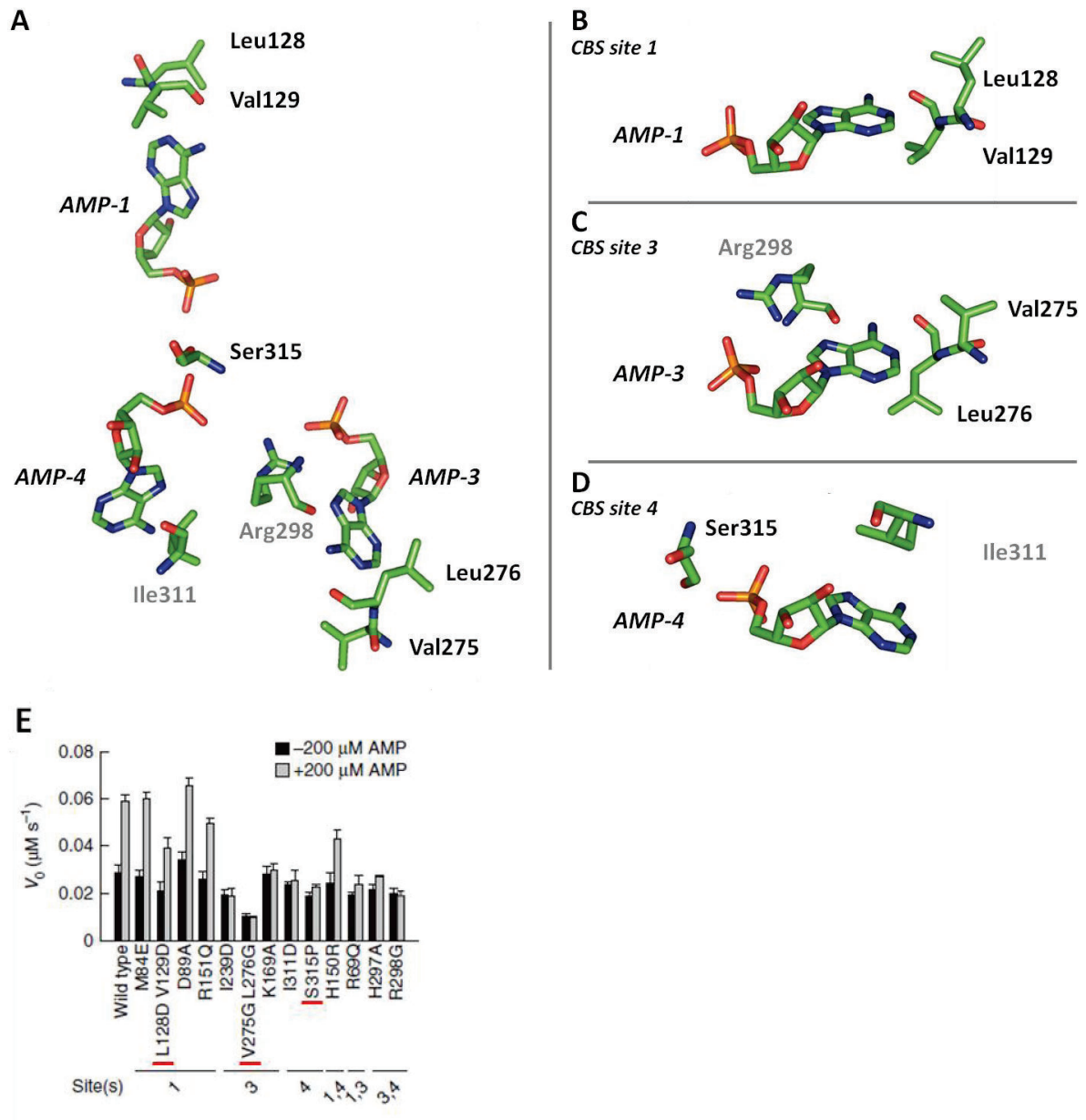


Figure 9: Adenine nucleotide binding at the γ 1 AMPK CBS sites.

A-D: Residues involved in nucleotides binding at γ 1 AMPK CBS sites 1, 3 and 4 (details from PDB ID: 4EAI). AMP moieties are numbered according to the CBS site. Amino acids mutated to selectively inhibit nucleotide binding at the level of specific CBS sites (black) or reported to be involved in nucleotide binding but not mutated (grey). **A-:** overview of AMPs bound to γ 1. **B-D:** Details of AMP binding residues. **E-: Effects of CBS-mutations on the AMP-dependence of AMPK activity** (mean and SEM, $n = 3$). The assay was performed in the presence of 5 nM AMPK, 1 mM ATP and 200 μM SAMS peptide (a synthetic substrate for AMPK), with or without 200 μM AMP. Red bars indicate the residues mutated in this work. Residues were selected according to their apparent implication in AMP-dependent activation of AMPK. From Chen et al. (Chen et al., 2012)

Additional mutations of α 2-Thr 172 were generated to yield kinase dead protein (T172A) or constitutively active kinase (T172D) (Stein et al., 2000) where aspartate mimicks phosphorylation of the activation loop in the kinase domain.

ACEMBL plasmids coding for single, mutated α 2- or γ 1-AMPK subunits, were fused by Cre recombination to create vectors coding for modified heterotrimeric AMPfret protein complexes. As previously, final stoichiometry of the fused vectors was verified by restriction digests (results not shown). All mentioned AMPfret mutants were derived from AMPfret 1.0 (α 2-CFP β 2 γ 1-YFP).

2.2. Optimization: FRET pair exchange

Using the first generation of AMPfret sensor (AMPfret 1.0), difficulties related to YFP pH sensitivity were encountered as reported earlier (Willemse et al., 2007). A pH sensitivity of AMPfret was observed during experiments when using non-buffered ATP solution and pH measurements, due to spontaneous hydrolysis of ATP in aqueous solution (Figure 10).

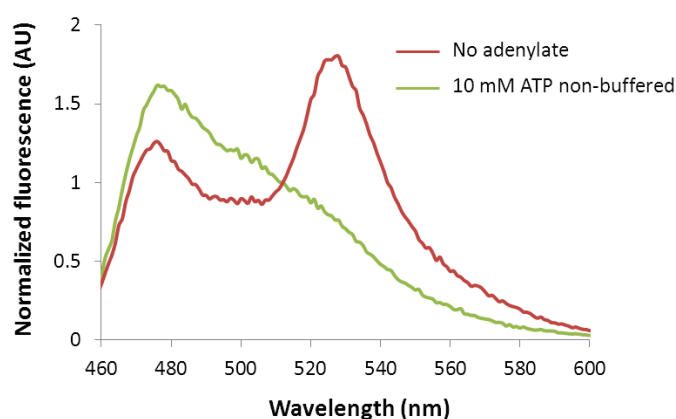


Figure 10: pH sensitivity of YFP due to acidity of non-buffered ATP solution (10 mM).

Emission spectra of AMPfret A before (red line) and after (green line) addition of non-buffered 1 M ATP stock solution (final ATP concentration 10 mM). Note that a non-buffered 1 M ATP solution is acidic and quenches the YFP signal at higher wavelengths.

In addition, when the solution becomes more acidic, this will further favor spontaneous hydrolysis of ATP. Acidification has drastic effects on YFP fluorescence when experiments are carried out in non-buffered solutions (Figure 10). During *in vitro* experiments, such problems

can easily be circumvented by precise pH control in buffered solutions. However, YFP pH sensitivity may interfere when AMPfret is expressed in cells. To reduce such sensitivity, the original eCFP/YFP FRET pair was replaced by monomeric super enhanced CFP and circularly permuted monomeric Venus (mseCFP_{Δ11}/cp173-mVenus) as successfully applied in the ATeam 1.03 sensor (Imamura et al., 2009). mseCFP (Matsuda et al., 2008) is an optimized variant of CFP that has been optimized to avoid oligomerization. Venus (Nagai et al., 2002) is an enhanced variant of YFP with reduced pH sensitivity, also reported to remain monomeric (due to an A206K mutation). Thus, in addition to reduced pH sensitivity, the FRET pair exchange will also limit eventual dimerization of the sensor under non-controlled concentration conditions (e.g. when transfected *in cellulo*).

It has been demonstrated that the dynamic range of a FRET signal can be significantly enhanced by altering the relative orientations between donor and acceptor fluorescent proteins using a circularly permuted fluorescent protein (Nagai et al., 2004). The circularly permuted variant of mVenus used in ATeam constructs has its new N-terminus at the 173rd amino acid (cp173-mVenus), and yields a greater dynamic range than mVenus. Both mseCFP_{Δ11} as well as cp173-mVenus were PCR-amplified from pcDNA3.1ATeams1.3 (kind gift from Hiromi Imamura). Vectors coding for all AMPK subunits tagged either at N- or C-terminus with one of these fluorescent proteins (mseCFP_{Δ11} or cp173-mVenus) were generated using conventional cloning and “self-SLIC” (see Material & Methods chapter). Correct vectors were selected by restriction patterns and verified by sequencing. Newly created vectors were then assembled by non-homologous recombination using their Lox-P sites, thus replacing the FRET pair in all AMPfret constructs (A-L). Only the improved version of AMPfret C, named AMPfret 1.1, was expressed and purified following the protocol previously used for AMPfret 1.0 (see Results chapter 2.3).

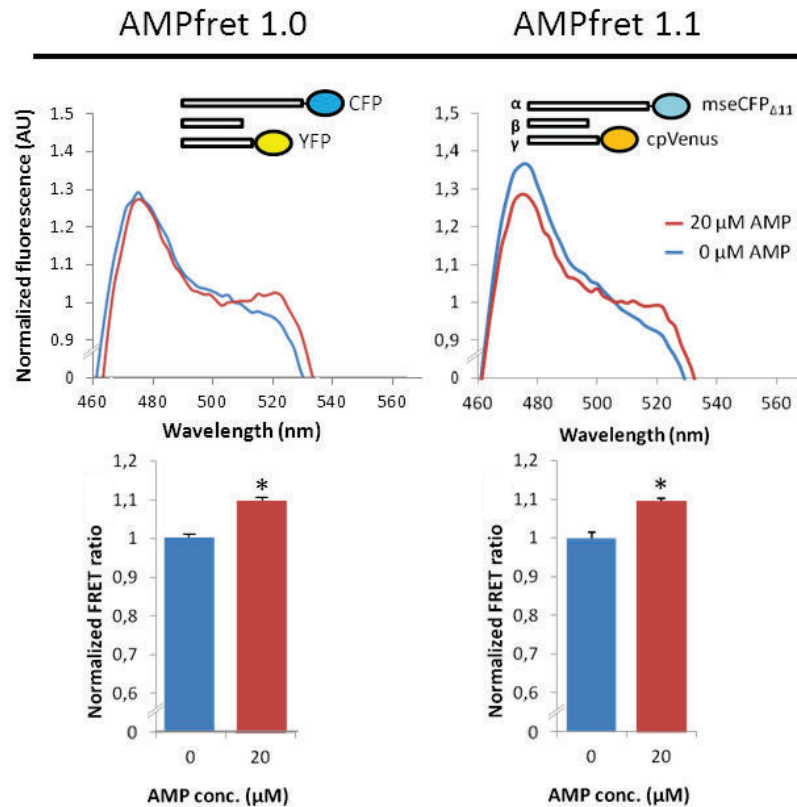


Figure 11: An improved FRET pair in AMPfret 1.1.

Insertion of the mseCFP Δ 11/cpVenus into AMPfret 1.0 yields AMPfret 1.1 construct. Both show slightly different spectra but the same amplitude response for AMP-induced FRET signal variation (lower panel). Spectra in presence of ATP or AMP were normalized using the CFP/YFP isosbestic point at 512 nm. Bars represent mean \pm SEM ($n \geq 5$), significance was assessed through a Students test: * $p < 0,001$.

Pure AMPfret 1.1 was incubated (or not) with AMP (20 μ M) and its FRET ratio compared to AMPfret 1.0. Unfortunately, exchange of the FRET pair did not trigger any obvious improvement in the AMP-dependent FRET signal variation (Figure 11). This suggests that the re-orientation of the fluorescent protein relatively to each other (circular permutation of Venus) has no beneficial effect on FRET signal variation of this construct. However, it remarkably reduced AMPfret sensor pH sensitivity. As described further below (Figure 19), the AMPfret 1.1 FRET signal appears to be stable over a pH range of 6,5 – 8,5.

2.3. Expression and purification

2.3.1. Expression optimization

The strategy consisted in testing all the initial chimeric AMPK constructs in presence or absence of the allosteric AMPK activator AMP to see whether its binding induces conformational changes visible through FRET variations. For such a screening, all twelve AMPfret constructs (Table 1) were produced in *E.coli* and purified according to the same protocol established after intense optimization. Several expression conditions were tested in small-scale cultures (< 100 mL) varying bacterial strains, induction period, temperature and medium. Expression conditions were compared on SDS-PAGE gels, and the one with the highest yield of soluble material was selected. First, we tested standard conditions by the expression of AMPK221 for 3 h after induction with 1 mM IPTG at 37 °C or 20 °C and overnight expression at 20°C after IPTG induction. In parallel, different bacterial strains were tested (BL21 (DE3) *Star*, Rosetta (DE3), C43 (DE3)). Globally, expressions done under these different conditions did not differ in protein yield when normalized to final OD of the bacterial culture. Thus, strain BL21 DE3 *Star* (Invitrogen), a widely used host, was chosen. However, in some cases, proteins appeared to be non-soluble when comparing supernatant (SN) and supernatant + pellet (SNP) fractions loaded on SDS-PAGE gel after sonication of bacteria in PBS (Figure 5 and Figure 12). To reduce this problem and to increase the protein solubility, expressions with a heat shock step (20 min at 47°C) (Oganesyan et al., 2007) or in LB media containing various concentration of salt (Oganesyan et al., 2007) (0.1 - 0.5 M) have also been tested without obvious effects.

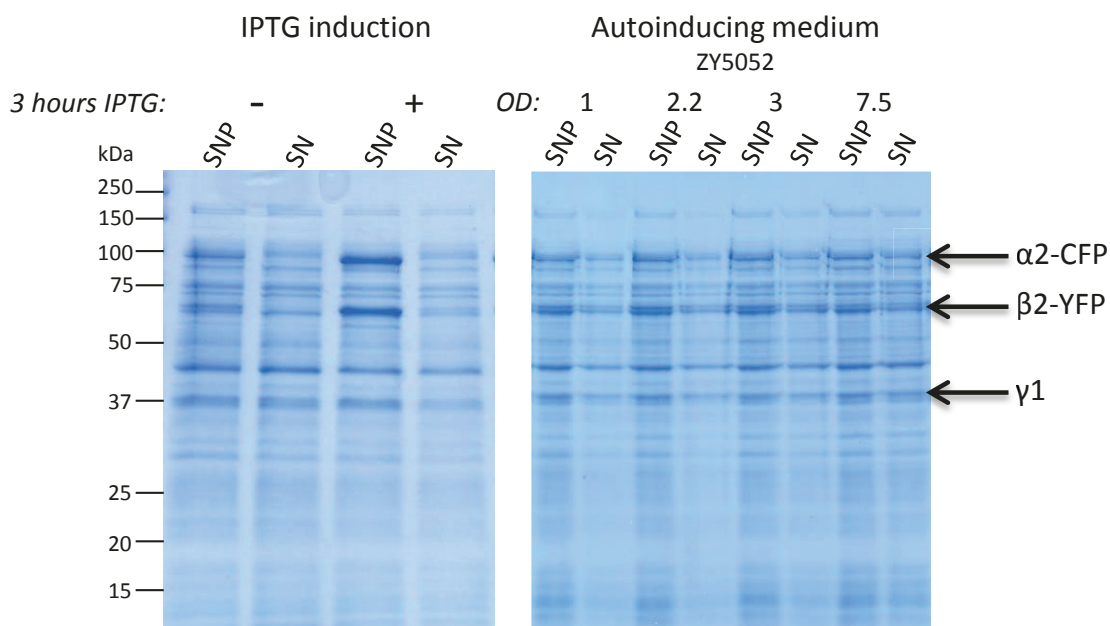


Figure 12: Comparison of expression conditions.

AMPfret A expressed in BL21 (DE3) cells either under IPTG induction for 3 hours at 37°C (before: - and after +) (left) or in autoinducing medium overnight at 18°C (right). The OD of the bacterial culture at which samples were taken is mentioned above the gel (right). An equivalent number of lysed bacteria was used for each SNP/SN condition (ca. 3 millions). Molecular weight marker is shown on the left. Supernatant + pellet (SNP) and supernatant only (SN) fractions were loaded onto 12% SDS-PAGE. Molecular weight of α 2-CFP is 93 kDa, β 2-YFP is 68 kDa and γ 1 is 37 kDa. Note that single AMPfret A solubility is improved when autoinducing medium is used as compared as induction with IPTG.

Increasing the number of cells harvested at the end of the expression could be a solution to obtain a better yield of protein per liter of culture. When expression was done in Terrific Broth (TB) medium at 20 °C overnight, pellets were about three-fold heavier than when culture was done in common LB-Miller growth medium. Final OD of the bacterial culture was about 9 in TB medium as compared to 3 in LB medium. In contrast to the LB medium, TB is a buffered medium (phosphate buffer) that contains five-times more yeast extract. However, the solubility of recombinant AMPK was still low. Thus, it was attempted to “slow-down” the expression rate by using the autoinducing medium ZYP-5052 (Studier, 2005), to increase the proper folding of recombinant proteins and hence their solubility. Induction in autoinducing medium is reported to occur more smoothly by a switch in substrate usage (glucose to lactose). Final OD in TB and ZYP-5052 media were comparable (OD ~ 8,5). The amount of AMPfret construct per cell was lower when expressed in autoinducing medium compared to

expression under IPTG induction (band intensities in SNP fractions, Figure 12). However, it clearly appeared that expressed protein was more soluble when using autoinducing medium (band intensities in SN fractions, Figure 12). Also, related to final bacterial culture OD, the amount of expressed protein in autoinducing medium was higher than with LB and IPTG induction. According to these data (Figure 12), all AMPfret constructs in this project were expressed in ZYP-5052 medium, overnight at 18-20 °C. This yielded suitable amounts of protein even if an important portion of expressed proteins still remained insoluble.

2.3.2. Increasing the solubility

Efforts were also made to increase the solubility of recombinantly produced protein during extraction and purification. Cell debris pelleted after sonication by centrifugation contained fluorescent material, suggesting that AMPfret proteins were lost. Efforts were made to identify a lysis buffer which yields the best solubilization. It was observed earlier that presence in the lysis buffer of 0,5 M sucrose, as well as 30% (w/v) glycerol, greatly increased the soluble fraction of AMPK (Riek, 2006). This lysis buffer was previously used for the purification of AMPK applied to SAXS experiments that revealed AMP-induced conformational changes correlating with allosteric activation (Riek et al., 2008). Different modifications of this lysis buffers have been tested and the amount of soluble protein was assessed through SDS-PAGE (Figure 13). Lysis buffer containing 0,5 M sucrose, 30% (w/v) glycerol, 50 mM Tris pH 8, 100 mM NaCl, 2 mM MgCl₂ and 2 mM β-mercaptoethanol was selected as providing the highest amount of soluble protein after sonication. Riek et al. used buffers containing 0.5 M sucrose and 30% (w/v) glycerol all along the different steps of the purification (Riek et al., 2008). Interestingly, it was found here that the presence of sucrose and glycerol which helps to solubilize the recombinantly expressed protein from *E.coli* is not required during further purification steps, but significantly increases the portion of soluble proteins in initial cell lysates. Final preparations of AMPK 221 and AMPfret constructs were obtained pure without encountering any solubility problems when using buffers that do not contain sucrose or glycerol anymore (Figure 13). Thus, 0,5 M sucrose and 30% (w/v) glycerol were only added in lysis buffer and not in other buffers used for purification. Although few solubilization problems occurred when concentrating AMPfret constructs to very high

concentration (> 10 mg/mL), this problem was not addressed because it is established that AMPK forms oligomers and can even precipitate at high concentration.

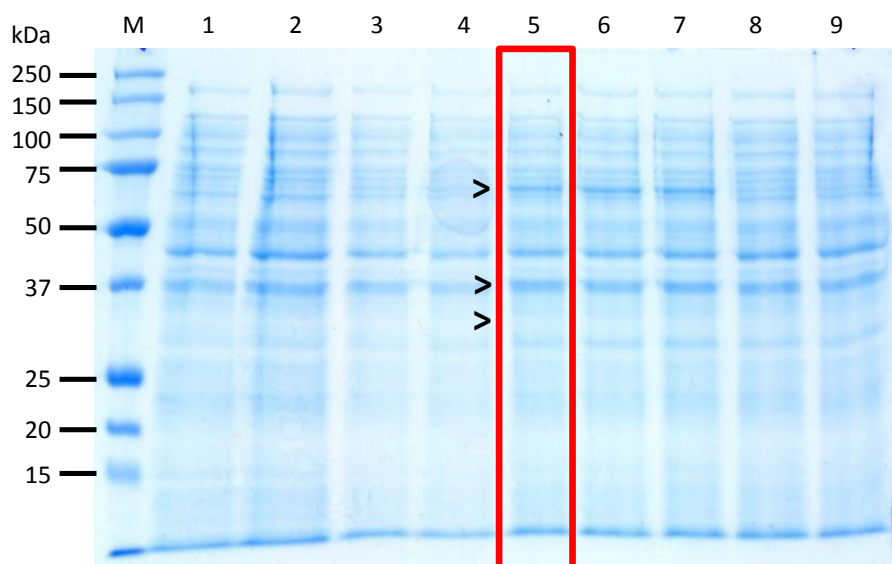


Figure 13: Screening of lysis buffers.

12% SDS PAGE gel showing the supernatant fraction of BL21DE3* cells expressing AMPK $\alpha_2\beta_2\gamma_1$ lysed in different buffers. Arrows indicate the position of AMPK subunits (α_2 : 65 kDa; β_2 : 30 kDa; γ_1 : 37 kDa). Red square corresponds to the selected lysis buffer. Lanes: **M**: Marker; **1**: 50 mM Tris pH 8, 300 mM NaCl, glycerol 10% (v/v); **2**: 50 mM Hepes pH 8, 300 mM NaCl, glycerol 10% (v/v); **3**: 50 mM Tris pH 8, 300 mM NaCl, glycerol 10% (v/v), 0.5 M Sucrose; **4**: 50 mM Hepes pH 8, 300 mM NaCl, glycerol 10% (v/v), 0.5 M Sucrose; **5**: 50 mM Tris pH 8, 300 mM NaCl, glycerol 30% (w/v), 0.5 M Sucrose; **6**: 50 mM Hepes pH 8, 300 mM NaCl, glycerol 30% (w/v), 0.5 M Sucrose; **7**: 50 mM Tris pH 8.5, 300 mM NaCl, glycerol 30% (w/v), 0.5 M Sucrose; **8**: 50 mM Tris pH 8, 300 mM NaCl, glycerol 30% (w/v); **9**: 50 mM Hepes pH 8, 300 mM NaCl, glycerol 30% (w/v).

Another aspect to consider when improving protein solubility is the lysis procedure (e.g. sonication, French press or microfluidizer). Here, incubation of cell pellets resuspended in a lysis buffer containing 1 mg/mL lysozyme for 30 min to 1 hour at 8°C and sonication was selected. It is noticeable that cell pellets harvested after cell culture and their corresponding supernatants after sonication were of a yellow/green color due to the presence of CFP and YFP suggesting a proper folding of the fluorescent proteins. All along the purification, fractions containing AMPfret constructs were having the same yellow/green color. This was convenient to follow protein elution on IMAC, ion exchange and gel filtration columns.

2.3.3. Purification procedure

All purifications of AMPfret constructs were done following the same procedure. They were all obtained in pure form following a classical 3-step approach which included a metal affinity chromatography based on nickel or cobalt ions (as AMPfret constructs have a 10His-tag fused to the $\alpha 2$ N-terminus) followed by an ion exchange chromatography and finally, a size exclusion chromatography. As AMPfret constructs all derive from AMPK, and AMPK heterotrimer tends to be a rather unstable protein with a strong tendency to aggregate and denature *in vitro* (Riek, 2006), all the purification steps were carried out in the cold room (~ 8 °C). In addition, protease inhibitors were added in every buffer used during purification to optimize the integrity of purified protein complexes (cOmplete protease inhibitor cocktail (Roche) in the lysis buffer and leupeptine and pepstatine (Sigma) in every buffer).

After sonication, cell debris was pelleted by centrifugation and resulting supernatant (lysate) was incubated with Ni-NTA resin (Qiagen) for at least 1 h while shaking in the cold room (for details see Material & Methods chapter). Batch purification by incubation with the resin gave a better yield as compared to resin-filled columns operated by gravity flow or peristaltic pumps (results not shown). This suggests that AMPfret constructs require extended time periods to attach to the beads, possibly due to the high viscosity of the lysis buffer (0.5 M sucrose, 30% (w/v) glycerol) that limits diffusion. The batch mixture beads/supernatant was loaded into glass chromatography columns (Econo-Column® - BioRad). The resin was heavily washed (> 20 CV) with washing buffer and high salt buffer. The latter aims to limit nucleic acid contamination since it disrupts the electrostatic interactions between protein (AMPfret) and nucleic acids (DNA or RNA), but also between IMAC resin and nucleic acids. Protein contaminant sticking to the resin may also be eluted by this washing step. Once the protein eluted, resin was re-equilibrated with lysis buffer and flow-through from the first binding was re-incubated with the resin. This was repeated 2 or 3 times to pull out highest possible amount of AMPfret construct for further purification steps. Next steps were carried out on an Akta HPLC system and consisted in an anion exchange chromatography and a size exclusion chromatography. The first allows the separation of AMPfret from other proteins interacting with Ni-NTA resin and from remaining DNA-AMPfret complex and from non-stoichiometric AMPfret in which subunits are not present in a 1:1:1 ratio (data not shown). Size exclusion chromatography was finally used to obtain pure and homogenous proteins, in

particular to remove AMPfret oligomers. Addition of spermidine in sample and buffer during this last purification step seems to increase the portion of monomeric AMPfret after concentration (the same was observed in an earlier work, (Riek, 2006)) (results not shown). AMPfret constructs were eluted from the calibrated size exclusion chromatography column, Superose 6 10/300, as having an apparent molecular weight of ~290 kDa instead of the 180 kDa expected, suggesting that AMPfret is not globular but rather has an elongated shape (Figure 14). This elongated shape was reported already for the AMPK heterotrimer, especially by SAXS measurements (Riek et al., 2008), and more recently by X-Ray crystallography (Calabrese et al., 2014). All AMPfret constructs and derived mutants were obtained with a good purity as shown on SDS-PAGE gels (Figure 15), albeit with relatively low yield (between 500 µg and 1 mg per liter of bacterial culture). As AMPK was reported to not be stable when stored for a long time and to be sensitive to freeze-thaw cycles, AMPfret constructs were all stored at -20°C in 50% (v/v) glycerol containing buffer. No important degradation events were visible during AMPfret utilization over a long period.

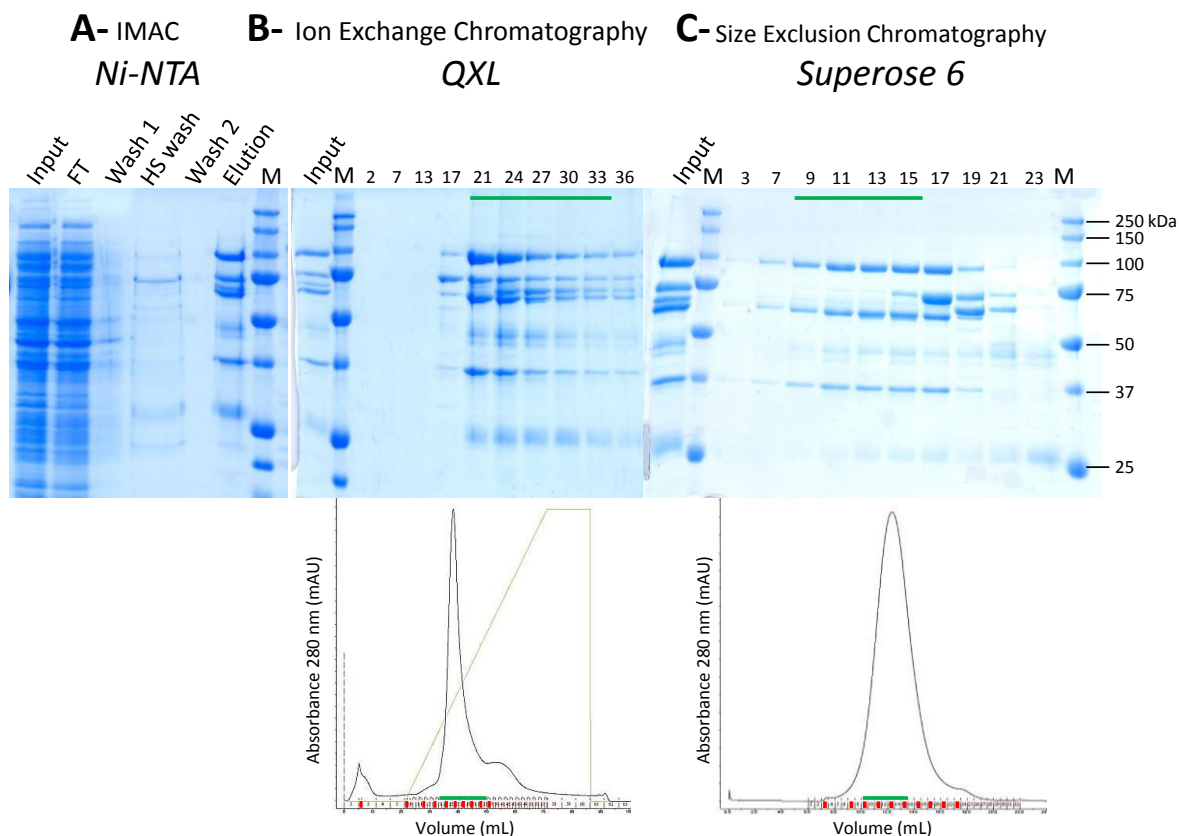


Figure 14: Purification of AMPfret constructs.

A- First purification step consisted in batch incubation of lysate containing AMPfret constructs (e.g. here AMPfret A) with Ni-NTA resin. Resin was washed with 20 column volumes (CV) of washing buffer (lysis buffer lacking sucrose and glycerol) (Wash 1), followed by 20 CV of high salt washing buffer (washing buffer + 1 M NaCl) and 20 CV of washing buffer (Wash 2). Attached proteins were finally eluted using 5 CV of elution buffer (washing buffer containing 400 mM Imidazole) (Elution). **B-** Eluted proteins were applied onto a QXL column and were separated by using a salt gradient (0.1 – 1 M NaCl; yellow line on the chromatogram). Fractions loaded onto 12% SDS-PAGE gels are labeled by red marks and pooled fractions are labeled by the green line. Note that (i) AMPfret constructs eluted at a salt concentration of 200 – 300 mM NaCl, (ii) the last broad peak had a 260 nm/280 nm equal to 30 suggesting that it contained mainly nucleic acids. **C-** Once concentrated, proteins were applied onto a Superose 6 10/300 column and were eluted according to their molecular size. Fractions loaded onto 12% SDS-PAGE gels are labeled by red marks and pooled fractions are labeled by the green line. Note that AMPfret eluted at a volume corresponding to higher molecular weight (~ 300 kDa instead of 180 kDa). Lanes containing molecular weight protein marker are indicated by M. Molecular weight of α 2-CFP is 93 kDa, β 2-YFP is 68 kDa and γ 1 is 37 kDa.

In SDS-PAGE of purified AMPfret constructs (Figure 15), the band at 30 kDa corresponds to AMPK β 2-subunit whereas lower molecular mass bands can be contaminants or degradation products of AMPK subunits. The band at 37 kDa corresponds to the AMPK γ 1, the \sim 57 kDa band corresponds to fluorescently tagged β 2, the 64 kDa band to AMPK α 2 tagged with a 10His-tag and the \sim 65 kDa band to fluorescently tagged γ 1. The latter three different bands are close to each other and are visible in the AMPfret I and J lanes. The higher band at \sim 90 kDa corresponds to fluorescently tagged α 2. The α 2 subunit tagged at its N-terminus with CFP appeared as less stable. More degradation products were visible when purifying AMPfret B, E, F and L. The main degradation product had a molecular mass (\sim 27 kDa) close to the one of CFP, suggesting that fluorescent proteins are sensitive to proteolytic cleavage when positioned at the α 2-N-terminus. As suggested by a recently deposited structure (PDB ID: 4CFE) the fifteen first α 2 amino acids are forming an unfolded stretch which, when becoming a linker to CFP, is sensitive to protease or other degradation processes.

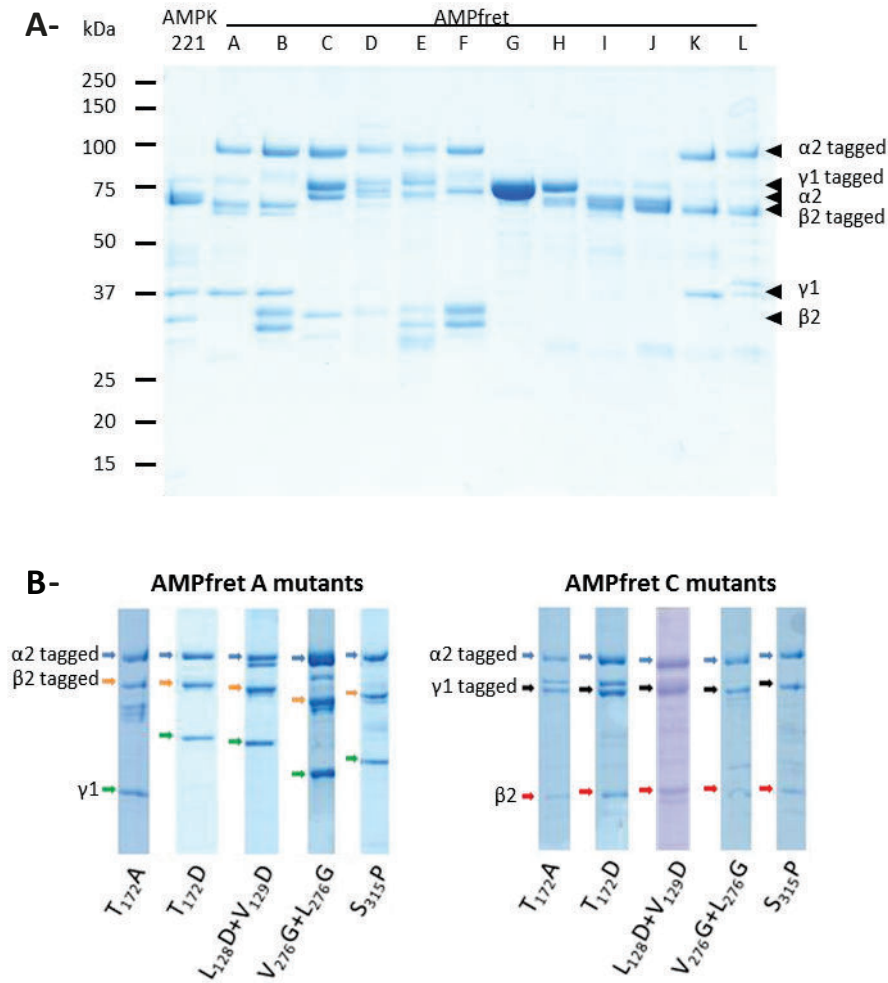


Figure 15: Purity of AMPfret constructs.

A- SDS-PAGE of purified initial 12 AMPfret constructs (1st generation). AMPK221 corresponds to untagged $\alpha 2\beta 2\gamma 1$ complex. AMPfret constructs A-L correspond to AMPfret variants coded by vectors listed in Table 1. $\alpha 2=65$ kDa, $\beta 2=30$ kDa, $\gamma 1=37$ kDa, eCFP= 27kDa and YFP= 27kDa. AMPK are indicated to the right. **B- SDS PAGE of purified AMPfret A mutants (left) and AMPfret C (1.0) mutants (right).** Mutations are mentioned under lanes showing purified AMPfret variants. The 3 most intense bands correspond to AMPK subunits tagged or not with fluorescent proteins. Different migration of same subunits is due to different gels and migrations (e.g. all bottom lanes in AMPfret A mutants are 37kDa and correspond to $\gamma 1$). Blue, orange and green arrows respectively represent $\alpha 2$ -CFP, $\beta 2$ -YFP and $\gamma 1$. Black and red arrows show $\gamma 1$ -YFP and $\beta 2$ respectively. The purity of CBS site mutants was estimated by different SDS-PAGE gels. Note that mutants derived from AMPfret A were not further used but are available.

3. Characterization of AMPfret 1.0

3.1. Enzymatic activity

We first tested the ability of each the 12 initial AMPfret constructs (A - L) to phosphorylate acetylCoA carboxylase (ACC), a substrate of AMPK widely used as a readout of total AMPK activity. Kinase activity of generated AMPfret constructs was assessed by pre-incubation with CamKK β for activation (in presence of 200 μ M ATP and 40 μ M AMP), followed by incubation with ACC domain in presence of AMP and radiolabeled 32 P-ATP. All 12 AMPfret WT constructs phosphorylated ACC and hence showed AMPK kinase activity, indicating that AMPfret constructs folded correctly (Figure 16 A-). AMPfret H was identified as the construct showing the lowest activity (\sim 70%) (Figure 16 A- lane H). The variations in phosphorylated ACC signal can be attributed to different experimental conditions (e.g. time contact with the storage phosphor screen, 32 P-ATP age or Typhoon settings during acquisition). Also the T172D and T172A mutants derived from AMPfret C (1.0) were analyzed (Figure 16 A-). As expected, T172A is not activatable. The T172D mutant has a less important activity compared to native AMPK. Indeed, this constitutively active AMPK mutant is about half as active compared to native AMPK (Stein et al., 2000).

Among the mutants of the γ -subunit CBS sites, only the site 3 mutant has a much lower activity than the other two CBS mutants, already indicating that it affects allosteric activation by AMP (further analyzed below, see Results chapter 4.) (Figure 16). To conclude, the AMPK enzymatic activities observed with AMPK substrate ACC suggest appropriate folding and assembly of the heterotrimeric complex tagged with fluorescent proteins.

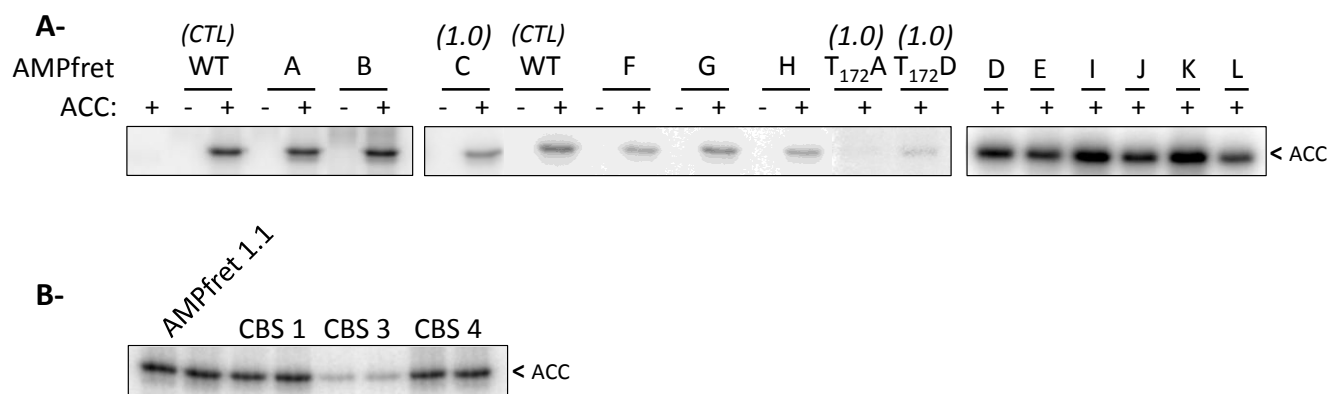


Figure 16: Enzymatic activity of AMPfret constructs.

A- Autoradiogram of ACC phosphorylated by native AMPK and initial AMPfret constructs in presence of 200 μ M ATP and 40 μ M AMP. AMPfret constructs (A-L) and AMPfret C derived mutants T172A and T172D. Differences of intensity are inherent to different activity test conditions (e.g. time contact with the storage phosphor screen). The first lanes are negative controls, either lacking AMPK (showing that phosphorylation is not due to CamKK β), or ACC. **B-** Kinase activities of AMPfret 1.1 and AMPfret 1.0 derived CBS site mutants.

3.2. FRET signal variations as a readout of AMP-induced conformational changes

We next looked at the effect of AMP and ATP binding to the AMPfret γ -subunit on the fluorescence properties of AMPfret constructs. The different versions of AMPfret (A-L) were separately incubated with 100 μ M AMP or 3 mM ATP (in buffers containing 5 mM MgCl₂). Then, using a spectrofluorimeter - PTI and an excitation wavelength set at 430 nm, their 450 to 600 nm emission spectra were recorded (Figure 17). FRET ratios were calculated as the ratios between the emission maxima of CFP (476 nm) and YFP (527 nm), taking into account 4 nm windows. We then determined which constructs exhibited a change in FRET ratio depending on the adenylate they were incubated with (Figure 17).

In view of their fluorescence emission spectra, constructs could be classified in three categories. First, constructs that do not show FRET in their emission spectrum (constructs E, F and L). Second, constructs which present a more or less pronounced FRET signal in their emission spectrum, but which is identical with AMP and ATP (constructs B, D, G, H, I and J). The third class contains constructs that show a FRET signal and a change in this signal in presence of AMP as compared to ATP (constructs A, C and K). AMPfret K, which exhibited

small FRET variation upon AMP addition ($\sim 4\%$) was discarded for further experiments. Thus, out of twelve realized constructs, two were selected, A (α_2 -CFP β_2 -YFP γ_1) and C and (α_2 -CFP β_2 γ_1 -YFP), further called positive constructs.

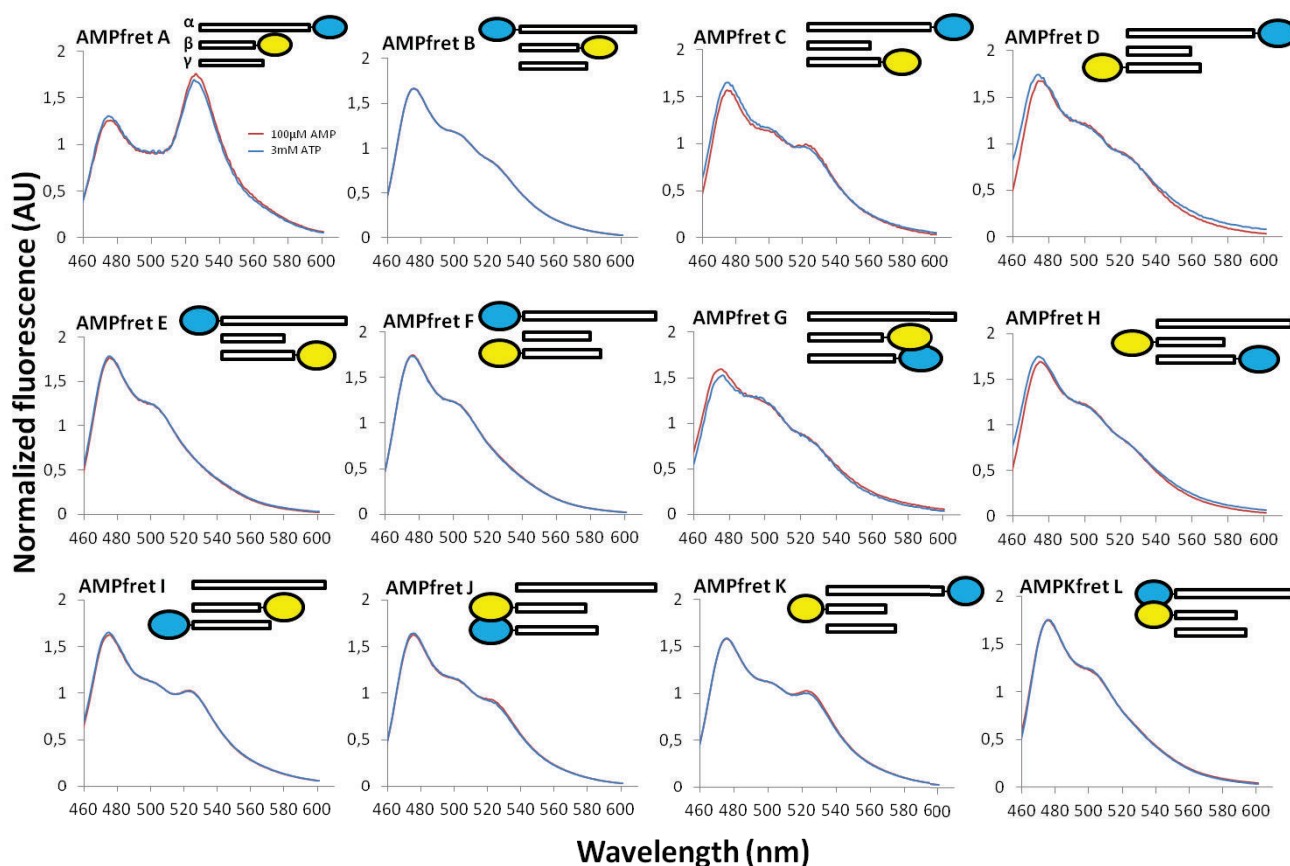


Figure 17: Emission spectra of AMPfret constructs A - L.

The small sketch above each spectrum represents the topology of the AMPfret fusion construct: CFP and YFP are respectively represented as blue and yellow circles respectively. Purified proteins were incubated in presence of 3 mM freshly prepared ATP (blue line), or in presence of 100 μ M AMP (red line). Peaks at 476 and 527 nm are the emission peaks of CFP and YFP, respectively. Spectra in presence of ATP or AMP were normalized using the CFP/YFP isosbestic point at 512 nm. The isosbestic point corresponds to a specific wavelength at which the absorbance and emission does not vary during considered experiment. In practice, when working with a FRET pair, the isosbestic point corresponds to the wavelength at which their emission spectra cross each other.

Properties of the two selected positive constructs A and C are summarized in Figure 18 and compared with the negative construct F. Both positive and negative constructs display similar kinase activity with ACC as substrate (Figure 16 and Figure 18). Their change in FRET ratios is 7% for A and 9% for C.

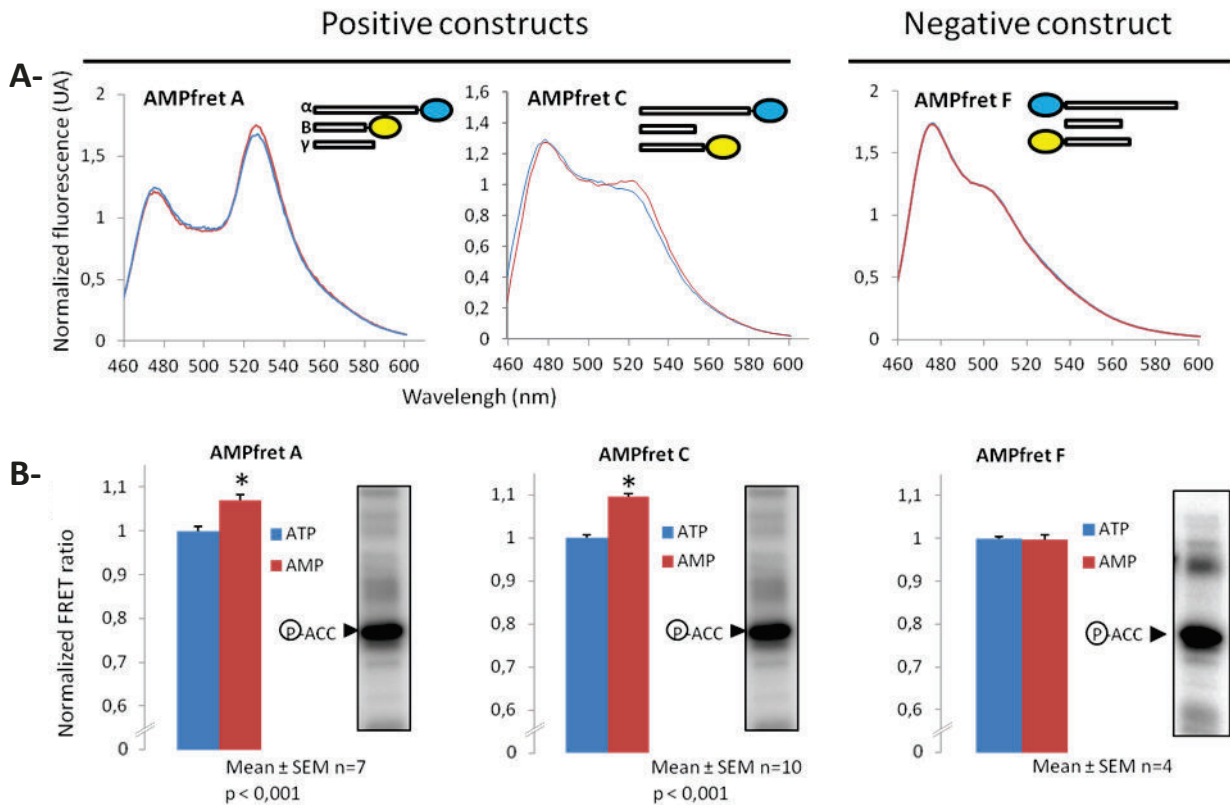


Figure 18: AMPfret A and AMPfret C (1.0) are the positive constructs that show significant FRET ratio difference upon AMP binding.

A- The small sketch above each spectrum represents the topology of the AMPfret fusion construct (same color code as in Fig. 17). Purified proteins were incubated in presence of 3 mM freshly prepared ATP (blue line), or in presence of 20 μ M AMP (red line) in buffer containing 5 mM $MgCl_2$. Peaks at 476 and 527 nm are the main emission peaks of CFP and YFP respectively. Spectra in presence of ATP or AMP were normalized using the CFP/YFP isosbestic point at 512 nm. AMPfret F serves as a negative control. **B** - FRET ratio of AMPfret constructs calculated from data in (A-) (same color code). FRET ratio (CFP/YFP) was normalized to the incubation in presence of ATP (blue bar). Autoradiograms of *in vitro* kinase activity assays with these constructs using acetyl-CoA carboxylase (ACC) as a substrate. Data correspond to mean \pm SEM and significance was assessed through a Student-Newman-Keuls test (AMPfret A: n=7; AMPfret C: n=4; AMPfret F: n=4; * $p < 0,001$). Note: All constructs exhibit similar activity as native AMPK (Figure 16).

FRET intensity, even if not affected by AMP addition, gives also information on the proximity of the two fluorophores in the construct. These values can be compared with those estimated from recently published crystal structures (Xiao et al., 2011, 2013) representing almost full length AMPK (Table 2).

As expected, shorter distances between fluorescent proteins generally yield a higher FRET signal. However, it has to be noted that several terminal residues have been removed for crystallization or are not visible in the electron density map (see legend to Table 2). In particular the β_2 N-terminal domain (about 50 amino acids) was not solved by any of these structural studies, given distances in constructs containing to β_2 N-terminally bound fluorescent protein (AMPfret H, J, K and L) are less precise. For example, given the absence of FRET in AMPfret L, a distance of 20,1 Å between the fluorophores is certainly largely under-estimated. Generally, FRET is seen in constructs where the tagged termini are up to about 60 Å apart in the crystal structure. Given the physical conditions needed for FRET it has to be assumed that many constructs have their real subunit termini somehow bend such to get into closer proximity. At around 80 Å, no FRET is observed anymore.

In the case of AMPfret A, the FRET pair is located at the C-termini of α_2 and β_2 , separated by only 14 Å. This closest distance correlates very well with the emitted spectrum observed which shows the most important FRET ratio. Concerning AMPfret C, CFP and YFP were positioned at the C-termini of α_2 and γ_1 respectively, which are ~ 60 Å apart, corresponding to a much lower FRET ratio. Some of the constructs show an only small emission peak at 527 nm (I,K) or at least a detectable shoulder in the spectrum (B, D, G, H). Despite presence of FRET in these constructs, no FRET variation is visible in all these constructs upon AMP addition (except for AMPfret K), suggesting that tagged termini do not move relatively to each other during AMPK allosteric activation. No FRET was detectable in few constructs (E, F, L). Except for construct L, FRET roughly correlates with the distance between tagged termini.

AMPfret construct	Organization	Peak at 527 nm visible	FRET ratio (YFP/CFP)	Distance between tagged termini (Å)
AMPK 221	$\alpha_2 - \beta_2 - \gamma_1$	/	/	/
AMPfret A	α_2 -CFP - β_2 -YFP - γ_1	+++	1.444	13.6
AMPfret B	CFP- α_2 - β_2 -YFP - γ_1	±	0.492	82.6
AMPfret C	α_2 -CFP - β_2 - γ_1 -YFP	+	0.639	62.4
AMPfret D	α_2 -CFP - β_2 - YFP- γ_1	±	0.513	62.9
AMPfret E	CFP- α_2 - β_2 - γ_1 -YFP	-	0.370	80.6
AMPfret F	CFP- α_2 - β_2 - YFP- γ_1	-	0.387	76.2
AMPfret G	α_2 - β_2 -YFP - γ_1 -CFP	±	0.524	51.4
AMPfret H	α_2 - YFP- β_2 - γ_1 -CFP	±	0.464	(66.4)
AMPfret I	α_2 - β_2 -YFP - CFP- γ_1	+	0.637	52.8
AMPfret J	α_2 - YFP- β_2 - CFP- γ_1	±	0.559	(62.7)
AMPfret K	α_2 -CFP - YFP- β_2 - γ_1	+	0.648	(66.3)
AMPfret L	CFP- α_2 - YFP- β_2 - γ_1	-	0.391	(20.1)

Table 2: Distance separating fluorescently tagged termini and corresponding FRET ratio of different AMPfret constructs.

Distances (Å) were measured in a solved AMPK crystal structure (PDB ID: 4CFF (Xiao et al., 2013)) using PyMOL. Peak at 527 nm is annotated using +++ when very strong, ++ when strong, + when detectable, ± when shoulder and – when absent. FRET ratios were calculated from CFP/YFP emission spectra recorded in presence of AMP (Figure 17) and correspond to ratios of fluorescence values at 527 nm (YFP) and 476 nm (CFP). It has to be noticed that in this crystal structure, which is one of the most complete, 8 residues are missing at α N-terminus, 77 at β N-terminus, 26 at γ N-terminus and 6 γ C-terminus. In addition, the AMPK isoform crystalized is $\alpha_2\beta_1\gamma_1$ and AMPfret is based on AMPK $\alpha_2\beta_2\gamma_1$.

For further interpretation of these data, it has to be considered that distances given here between subunit termini and those between chromophores of the fluorescent proteins may differ, and that the relative orientations the fluorescent proteins regarding each other also affect FRET. Within these limitations, some information regarding allosteric activation of

AMPK can be obtained. The correlation between the distance that separate the tagged subunit termini and the FRET ratio measured indicates that the fluorescence signal comes from AMPfret monomers (AMPK has been reported to also form oligomers (Riek et al., 2008; Zhu et al., 2011), but concentrations of AMPfret constructs used in the cuvette are much lower than the ones at which it may oligomerize). Moreover, the data indicates that during AMP- dependent allosteric activation the α_2 C-terminus is moving relatively to β_2 and γ_1 C-termini (constructs A and C) and also the β_2 N-terminus (construct K). An increase in FRET suggests a more compact conformation of AMPK heterotrimer when bound to AMP as also observed by SAXS, EM and crystallographic studies (Riek et al., 2008, Zhu et al., 2011, Chen et al., 2012). Comparable observations were made by Landgraf et al. when they analyzed AMP-induced conformational changes by hydrogen/deuterium exchange (Landgraf et al., 2013).

Except AMPfret K, none of the AMPfret constructs carrying a fluorescent tag on the β_2 N-terminus showed a difference in FRET upon AMP addition in solution. These constructs should be re-investigated regarding the activation mechanism by A-769662. Recent studies (Calabrese et al.; Xiao et al., 2013) published after our screening of AMPfret constructs with AMP showed that the β N-terminal domain containing the CBM module is participating in A-769662 activator binding at the α/β interface. Also, models for the A-769662 activation mechanism propose that the CBM module is highly mobile, sitting on top of the α -kinase domain in presence of A-769662. This probably triggers small rearrangement of the kinase domain leading to the activation of AMPK. It seems possible that A-769662-related activation at the α/β allosteric site can be investigated using AMPfret constructs other than identified here. Ultimately, it may be possible to report separately conformational changes and activation due to either AMP (or ADP) or to compounds binding at the α/β -interface.

The moderate amplitude of the changes in FRET observed with our constructs agrees well with previous structural studies on AMPK allosteric activation revealing only small changes in global shape within the heterotrimer (Riek et al., 2008; Zhu et al., 2011). The nature of the conformational changes reported by FRET cannot be defined more precisely. They may include movements between the subunits, but probably also local movements that trigger some displacement of domains (e.g. as Linker Sequence and Auto Inhibitory Domain) located between the two fluorescent proteins.

3.3. Salt and pH controls

The correlation between the above described AMP-dependent FRET changes and conformational changes linked to allosteric activation of the AMPK heterotrimer had to be validated through controls. As reported by Willemse et al. (Willemse et al., 2007), FRET signal variation can indeed be affected by pH fluctuations, especially when YFP is involved. The monitored FRET variations can also be altered due to variations in salt concentration. Although this is not problematic for the characterization of AMPfret *in vitro*, done under controlled conditions (pH, salt and temperature), problems may occur in cellular applications. AMPfret is aimed to be used in cells to monitor AMPK allosteric activation under metabolic stress, where ionic composition and pH would not be controlled. Thus the eCFP/YFP FRET pair was replaced in AMPfret C (AMPfret 1) to yield the improved version AMPfret 1.1 (Figure 8).

AMPfret 1.1 was incubated in presence of various amounts of salt (NaCl) or in buffers of different pH, and AMP-dependent FRET changes were measured. Salt variations did not alter the AMP-dependent FRET changes with AMPfret 1.1 except for the range above 800 mM (the difference between the two curves, Figure 19-A). As seen in Figure 19-B, the AMPfret 1.1 FRET signal appears to be also stable over a large pH range of 6,5 – 8,5. By comparing our results and the observations made by Willemse et al., it appears that the FRET pair replacement remarkably reduced AMPfret sensor pH sensitivity. Such pH sensitivity measurements are crucial controls because interpretations of biosensor results have to rely on their exclusive dependence on the single signal to be monitored. Thus, FRET variation of the mseCFP_{Δ11}/cpVenus FRET pair due to AMP binding on AMPfret did not vary in function of pH or salt concentration. We concluded that, in physiological range, our sensor is reporting only the AMP-induced conformational changes (Figure 19).

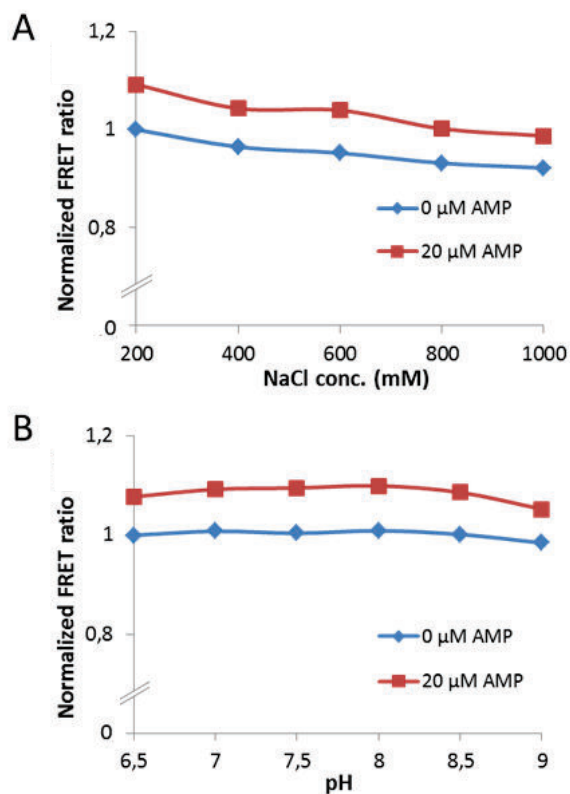


Figure 19: Salt and pH controls.

A- AMPfret 1.1 was incubated in buffers containing 50 mM Tris pH 8, 2 mM β -mercaptoethanol and various amounts of salt (200 mM – 1 M) (blue line). The FRET signal variation due to the addition of 20 μ M AMP was measured (red line). **B-** AMPfret 1.1 was incubated in solutions containing 200 mM NaCl, 2 mM β -mercaptoethanol and varying pH, 50 mM Tris (pH 6,5 – 9) (blue line). The FRET signal variation due to the addition of 20 μ M AMP was measured (red line). Note: The AMP-induced FRET variation is stable throughout the tested range of salt and pH.

From the initial characterization of AMPfret 1.0 it can be concluded that (i) recorded FRET variations report true conformational changes, (ii) recorded emission spectra originate from monomeric AMPfret sensors and (iii) conformational changes involve the α -subunit C-terminus. Hence, AMPfret 1.0 can be considered as a true sensor of AMP-dependent conformational changes happening in the AMPK heterotrimer.

3.4. AMPfret responds to AMP and ADP physiological concentrations.

For further experiments, we retained construct AMPfret 1.0, or when tagged with mseCFP_{Δ11}/cpVenus, AMPfret 1.1 (Figure 8).

3.4.1. The AMP-response

We next explored in more details how AMPfret responds to AMP. Physiological activation of AMPK is mediated by a gradual increase of AMP concentration. AMPfret 1.1 was titrated with increasing amounts of AMP and the FRET ratio was measured (Figure 20). FRET ratio increased with AMP concentration in a range from 0 to 20 μM corresponding to physiological AMP concentrations at the onset of energy stress. Hence, AMPfret appears as being a suitable reporter of AMP-dependent conformational changes as they happen within the AMPK heterotrimer during allosteric activation. Thus, AMPfret retains native AMPK functions and affinities for adenylates. The best curve fitting of the FRET data was achieved with a one site saturation ligand binding curve model ($FRET = \frac{FRET_{MAX} \times [AMP]}{K_d + [AMP]}$). The binding curve yielded an affinity constant for AMP (K_d) of 1.8 μM. This value reflects the affinity of AMPK for AMP in absence of other adenylates. In cells, ADP and ATP compete for γ-subunit binding, resulting in higher AMP concentration necessary for half-maximal activation. The precision of our data does not allow distinguishing binding to different CBS sites via multi-phase binding curves. More data points in the nanomolar range may be beneficial to validate a single site model of activation with more confidence. We cannot exclude that e.g. a dual site binding curve could fit to our data better if containing more and more precise data points. So far our data suggest that the conformational changes and the allosteric activation by AMP binding rely on a single CBS site. The same experiment performed with AMPfret 1.0 (data not shown) gave essentially the same results with an affinity constant for AMP (K_d) of 2 μM.

In these first experiments, only AMP was titrated, neglecting that the AMP/ATP ratio regulates AMPK *in vivo*. However, this allowed us to circumvent a major problem with ATP: its contamination with AMP and ADP. Spontaneous hydrolysis of ATP in aqueous solution releases AMP and ADP. At 3 mM ATP, already 0.1% hydrolyzed ATP yield 3 μM AMP (considering complete breakdown of produced ADP) which would trigger conformational changes and AMPK activation.

The correlation of the AMPfret response with physiological AMP concentrations represents a major advantage: this means that AMPfret could truly report cellular AMP variations (Figure 20 A-, B-). In addition, it confirms again that AMPfret and native AMPK share the same affinities for AMP (Gowans et al., 2013; Suter et al., 2006).

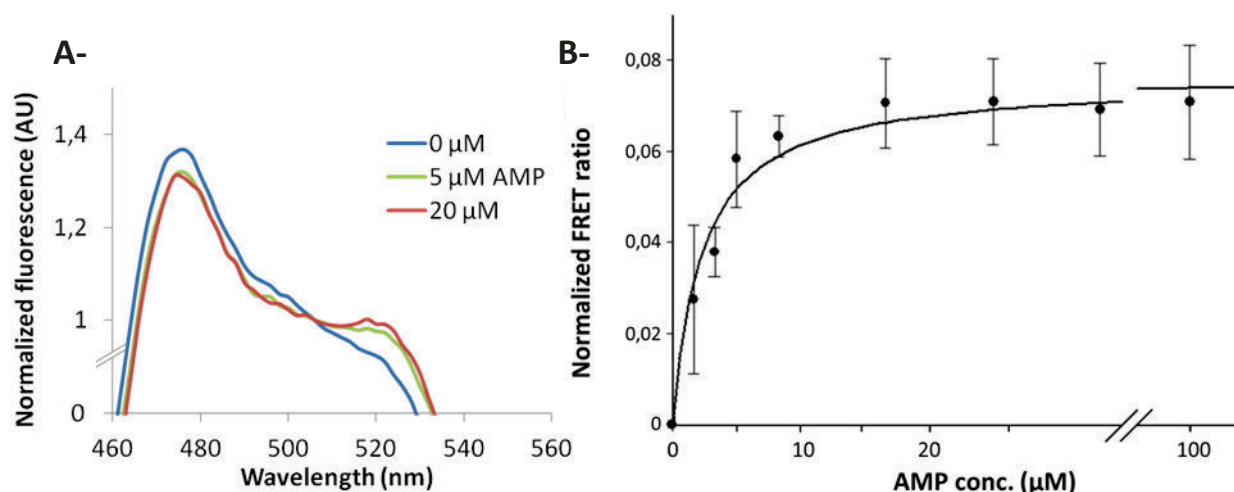


Figure 20: FRET response of AMPfret correlates with the concentration of AMPK activator AMP.

A - Fluorescence emission spectra of AMPfret 1.1 excited at 430 nm. AMPfret 1.1 fluorescence emission spectra reveal AMP-induced conformational changes through FRET variations. Spectra show fluorescence peaks of CFP (476 nm) and YFP (527 nm), and their variation upon AMP binding (blue, green and red lines: no AMP, 5 μM and 20 μM AMP respectively). **B** - Dependence of normalized FRET ratio on the concentration of AMP. AMPfret 1.1 FRET ratio variation correlates with AMP-induced conformational changes. The FRET ratio of AMPfret 1.1 was calculated from fluorescence emission spectra excited at 430 nm. Data were fitted with Sigma Plot 1.1 software to single site binding kinetics, yielding an affinity of 1,8 μM. Data points correspond to mean ± SEM (n=5).

Next we analyzed whether FRET changes correlate with AMP-dependent allosteric activation of AMPK (Figure 21). AMPfret 1.0 pre-activated by CamKKβ was incubated in presence of its substrate ACC and increasing concentrations of AMP (0-20 μM) and ATP (200 μM). Phosphorylation of ACC was quantified by immunoblotting using antibodies against P-ACC or ACC. The ratio between P-ACC and ACC was taken as a readout of total AMPfret activity. It was observed that increasing AMP to 20 μM triggers an about 2-fold rise in P-ACC signal and thus AMPK activity in agreement with previous studies using bacterially expressed AMPK (Suter et al., 2006, Sanders et al., 2007).

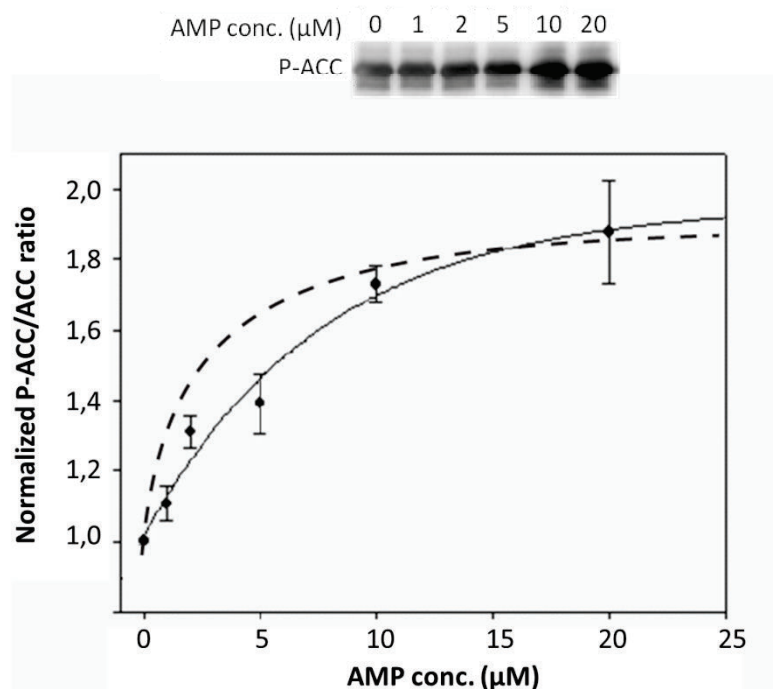


Figure 21: AMPfret is activated by a concentration range of AMP where FRET changes were observed.

Allosteric activation of preactivated AMPK in presence of 200 μM ATP, was followed by Western blot, showing increase of ACC phosphorylation with rising AMP concentration (0, 1, 2, 5, 10 and 20 μM). Western blot quantification is given below. Band intensities were quantified using ImageJ 1.4, normalized with the P-ACC value for 0 μM AMP and plotted against AMP concentration (black line). AMP-induced FRET response in absence of ATP from Figure 20 B- is represented as dashed line. Note that ATP shifts the curve to higher AMP concentrations. Traces of AMP related to ATP spontaneous hydrolysis were not taken in account.

AMP-dependent FRET variation and ACC phosphorylation do not fit perfectly. This is due to the presence of ATP in the in vitro kinase assay which i) might spontaneously hydrolyzed and produced AMP (and ADP), ii) is consumed during the kinase assay and iii) may compete AMP for γ 1 binding (see Results chapter 4.5).

We concluded that the data point corresponding AMPK activity at 0 μM was biased and therefore decided to superimpose the P-ACC/ACC signal (allosteric activation) onto the AMP-dependent FRET signal changes for more accuracy (Figure 22). Taken together, these results suggested that the kinase assay was contaminated with ~1.5 μM AMP, which is a rather high value that probably reflect both AMP and ADP contamination (see Results chapter 3.4.2). However, these initial results showed that AMPfret permit to examine the early phase of

AMPK allosteric activation that occurs at low AMP concentration, whereas it is hardly achievable through a conventional kinase assay involving nucleotides mixes.

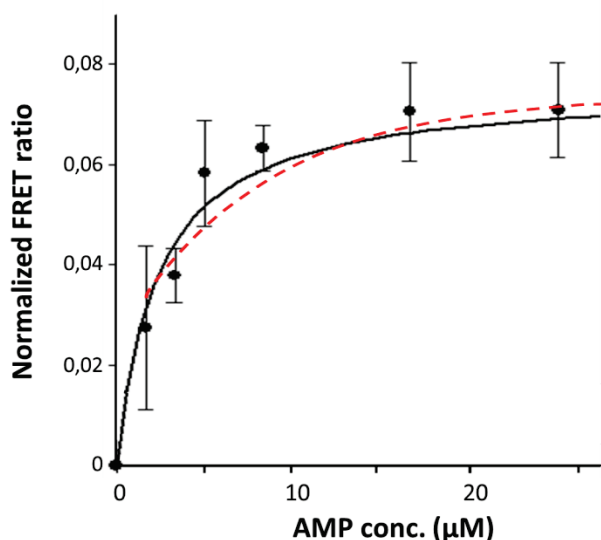


Figure 22: Fit of AMP-dependent allosteric activation of AMPK with AMP-dependent FRET changes. The red dashed curve, corresponding to the P-ACC/ACC variation showing the allosteric activation by AMP (black line in Figure 21), is superimposed to the AMP-induced FRET signal increase (from Figure 20 - B). The fit looks better when considering the portion covering the $\sim 1.5 \mu\text{M}$ to $25 \mu\text{M}$ range of the black line, suggesting that $1.5 \mu\text{M}$ AMP are contaminating the kinase assay. Note that ADP should also contaminate the kinase assay (see Results chapter 3.4.2).

Taken together all these data - concerning AMP-induced conformational changes and AMP-related allosteric activation - we concluded that the FRET ratio changes measured are directly linked to AMP-induced conformational changes and the allosteric activation of the kinase.

3.4.2. The ADP-response

Next we were interested in ADP that was reported to activate AMPK by protecting it from dephosphorylation (Gowans et al., 2013; Xiao et al., 2011). AMPfret 1.0 was incubated with increasing concentrations of ADP (0-200 μM) (Figure 23 A-). Like for AMP, we observed an increase of FRET ratio of AMPfret with rising ADP concentration. The FRET data showed, as for AMP, a hyperbolic shape reflecting binding of ADP to AMPK. The data could again be fitted to a single binding site equation using SigmaPlot. Like in the case of AMP, different

models were tested, but already a single binding site equation yielded a good fit. Here again, it is also possible to fit the data points with a two-sites binding equation considering two exchangeable nucleotide binding sites, but with the precision of our data we cannot provide evidence for this. Thus, the ADP-dependent mechanism either involves only a single CBS site, or both sites have similar affinity and do not show cooperative behavior.

The observed variation in FRET supports ADP-induced conformational changes of AMPK heterotrimer. These movements can be related to the protection against dephosphorylation and/or the promotion of phosphorylation (Gowans et al., 2013) by upstream kinases. Thus, to test this hypothesis, we analyzed whether FRET correlates with protection from dephosphorylation. AMPfret 1.0 was phosphorylated in presence of CamKK β and ATP, re-purified by size exclusion chromatography and incubated in the presence of PP2C α phosphatase and increasing concentrations of ADP (0-200 μ M). The resulting phosphorylation status of AMPfret was assessed by Western blot against phosphorylated Thr172 (Figure 23 B-). We found that ADP-dependent protection from dephosphorylation correlates with changes in FRET and thus ADP-induced conformational changes. The fitted binding curve yielded a K_d ADP of $\sim 5 \mu$ M. ADP does not allosterically activate AMPK (Gowans et al., 2013) thus only protection from dephosphorylation has been analyzed. Our results are consistent with ADP binding to γ -subunits protecting AMPK from dephosphorylation by a conformational change.

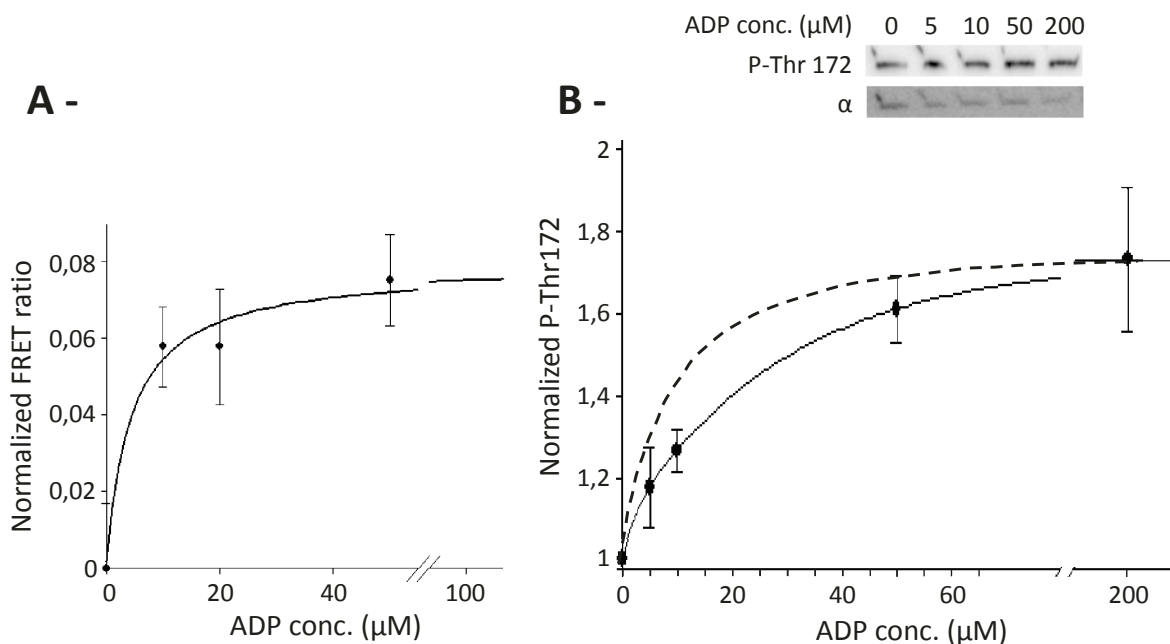


Figure 23: Dependence of normalized FRET ratio and Thr172 phosphorylation status after dephosphorylation on the concentration of ADP.

A- The FRET ratio of AMPfret 1.0 was calculated from fluorescence emission spectra excited at 430 nm. Data were fitted with Sigma Plot 1.1 software to single site binding kinetics, yielding an affinity of about 5 μM . Data points correspond to mean \pm SEM ($n \geq 3$). **B-** ADP effect on phosphorylated Thr172 protection was verified by Western blot, showing Thr172 phosphorylation for different ADP concentrations (0 – 200 μM) (black line). Band intensities were quantified using ImageJ 1.46. Data points corresponds to mean \pm SEM ($n=3$). ADP-induced FRET response from AMPfret is represented as dashed line. Note: AMPfret is sensitive to ADP concentration in a physiological range (0-50 μM).

Taken together AMPfret 1.0 / 1.1 are reporters of AMP- and ADP-induced conformational changes that occur in AMPK. The FRET variation allows the determination of affinity parameters that have physiological significance. In addition AMP- and ADP-dependent conformational changes, visualized through FRET variations, were respectively correlated to AMP- and ADP-dependent activation of AMPK, i.e. allosteric activation and protection from dephosphorylation. The latter finding is interesting, since the two activation mechanisms are most probably linked to different conformational changes. Thus, AMPfret signals are a readout for both activation processes, and it seems not possible to separate AMP- and ADP-dependent activation phenomena e.g. for future *in vivo* experiments.

4. Exploring molecular mechanisms of AMPK complex regulation by adenylates

4.1. AMPK CBS sites

The possibility to directly detect the conformational changes linked to allosteric activation by AMP and protection from dephosphorylation by ADP (and AMP), without the need of ATP for kinase activity assays allows for the first time direct analysis of the role of specific CBS site in the adenylate-sensing γ -subunit. The rationale for the mutations as outlined in chapter 2.1 aimed at disrupting adenylate interactions at specific sites in the γ -subunit, CBS 1, CBS 3 and CBS 4, the latter being commonly designated as non-exchangeable site.

AMPfret CBS site mutants were purified following the previously established protocol (Figure 15) and AMPK activity in presence of AMP and ATP measured as before (Figure 16). Except for CBS site 3 mutant, activities were similar to wild-type (Figure 16). Mutations at CBS site 3 have already been reported to suppress AMP-dependent allosteric activation of AMPK (Burwinkel et al., 2005; Chen et al., 2012; Scott et al., 2004).

We first performed preliminary nucleotide binding FRET assays with either 30 μ M AMP or 200 μ M ADP. Mutations of AMPfret CBS site 1 significantly diminished AMP-dependent FRET variations (Figure 24) as compared to WT, but did not affect ADP-dependent FRET changes. Mutations at the level of CBS site 3 abolished both AMP- and ADP-induced FRET response. These data confirm CBS 3 as the major site of AMP, but also ADP effects on AMPK. Site 1 seems to participate in conformational changes leading to AMP allosteric activation but to a lower extent than CBS site 3 as an AMP-induced FRET response was reduced but not completely abolished. When we then mutated the CBS site 4, the AMP-induced FRET signal variation was unchanged, but surprisingly, ADP-dependent FRET changes were lost (Chen et al., 2013). These results suggest that the CBS site 4 is not involved in AMP-dependent conformational changes leading to allosteric activation of AMPK, which would agree with site 4 being rather non-exchangeable. However why the ADP effect is lost? As previously noted in 2.1, it cannot be excluded that exchange of Ser315 by a Pro has some impact on the CBS site tandem 3 + 4. Hence, it may be that effect of CBS site 4 mutation on ADP-dependent FRET changes are indeed mediated by CBS site 3.

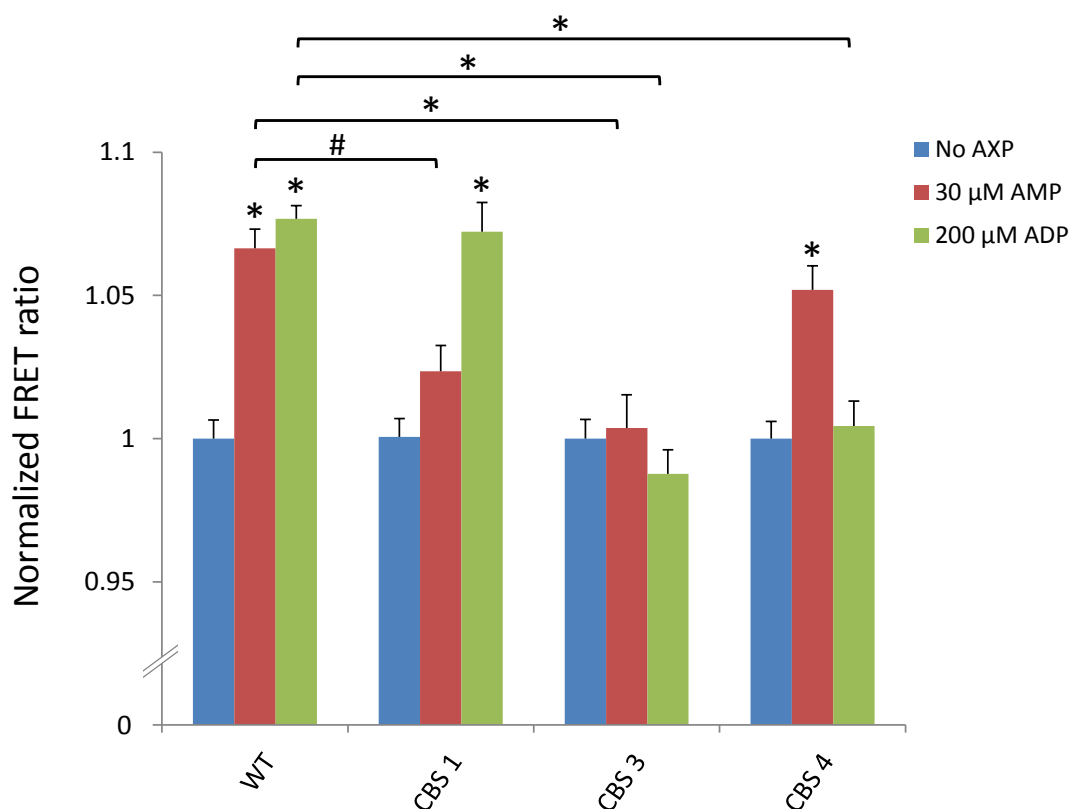


Figure 24 : Effects of CBS site mutations on FRET changes induced by AMP and ADP.

AMP- and ADP-induced conformational changes of AMPfret 1.0 and its γ_1 -subunit CBS site derived mutants. FRET ratios of AMPfret WT and its CBS sites mutants in absence of AMP or ADP (blue bars) or in presence of either 30 μ M AMP (red bars) or 200 μ M ADP (green bars) were normalized to the adenylate-free control. Bars represent mean \pm SEM ($n \geq 5$), significance was assessed through Students tests (*: $p < 0.002$ and #: $p < 0.01$). Similar results were obtained, in presence or in absence of 20 μ M AMP when using 1mM ATP and 1.5 mM Mg^{2+} (Mg-complexed ATP) (results not shown).

4.2. AMPK CBS sites and allosteric activation by AMP

We next analyzed in more detail whether the altered FRET responses observed in mutants with AMP correlate with changes in allosteric AMPK activation by AMP. We performed enzyme kinetic assay, in presence or absence of 20 μ M AMP, using the AMPK substrate ACC and 200 μ M ^{32}P -ATP (Figure 25).

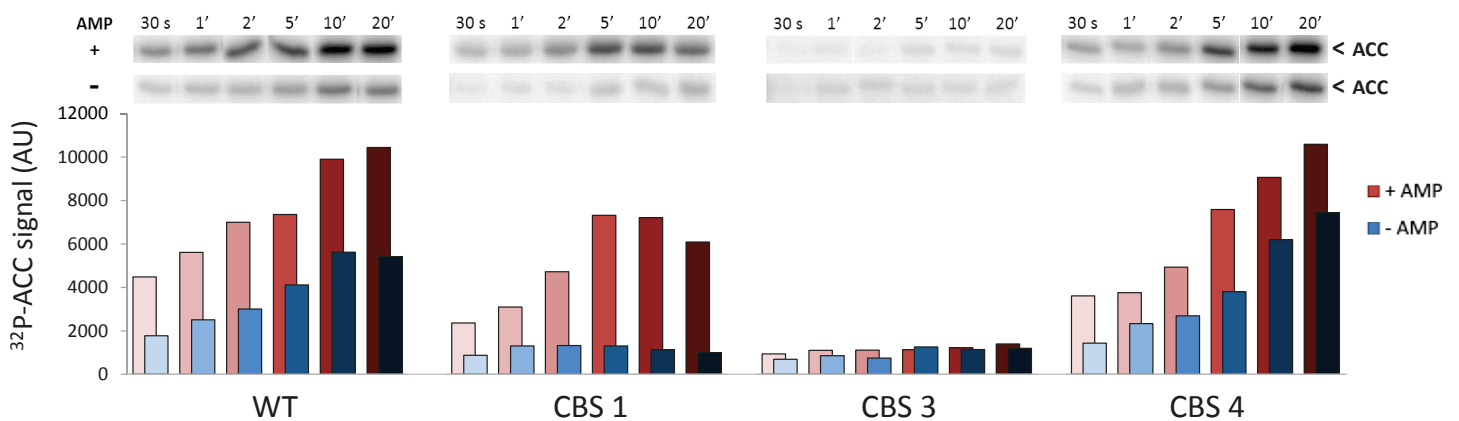


Figure 25 : Activity of AMPfret and its CBS site mutants.

Kinase assays of pre-activated AMPK with ACC as substrate, done for different time intervals (30 sec, 1 min, 2 min, 5 min, 10 min and 20 min), in presence or in absence of 20 μM AMP and radiolabeled 200 μM ^{32}P -ATP with all proteins in equal amount in each assay (3 pmol). Autoradiograms (top) and quantification of labeled ACC using ImageJ (bottom). ^{32}P -phosphorylation of ACC was revealed with Typhoon imager.

Figure 25 shows the time course of AMPK activities of AMPfret WT and mutants in presence and absence of AMP. Activities of AMPfret 1.1 and CBS site 4 mutant were almost doubled due to presence of AMP (Figure 25), showing that these two constructs responded to AMP. CBS site 1 mutant also increases activity due to the presence of AMP, although somewhat less than WT. CBS site 3 mutant showed a reduced activity as compared to WT and addition of AMP did not increase the ^{32}P -ACC signal. Taken together (i) CBS sites 1 and 3 mutants had a reduced basal activity (without AMP), but not site 4 mutant and (ii) CBS site 1 mutation slightly decreased activation by AMP, whereas mutations at site 3 abolished the activation by AMP correlating very well with AMP-induced changes in FRET (Figure 24). Once again, the data suggest that CBS site 3 mutant has a more important role in AMP-induced allosteric activation as compared to site 1.

For a more detailed analysis of CBS mutant, we titrated WT and mutants AMPfret with AMP (0 – 20 μM) (Figure 26). This time, we evaluated AMPK activation by immunoblotting for phosphorylated ACC.

Our results confirm that WT and site 4 mutant are allosterically activated by AMP with similar concentration dependence and extent (~ 2 -fold). The fitted binding curves, obtained by applying a single binding site model to our data using SigmaPlot, are very similar and half maximal activation is achieved for both constructs at ~ 5 μM . Kinase activity of site 3 mutant

is not enhanced by AMP. Site 1 mutant shows some intermediate response, with kinase activity only increased at AMP concentrations above 5 μM , suggesting that site 1 is involved in high affinity AMP binding during allosteric activation. The biphasic behavior of CBS site 1 mutant, with activation above 5 μM , correlates well with the FRET signal seen at 30 μM AMP (Figure 24) and ACC phosphorylation seen at 40 μM AMP (Figure 16). These results confirmed our preliminary data obtained in Figure 25 which showed AMP-sensitivity decreased in CBS site 1 mutant that even suppressed in CBS site 3 mutant.

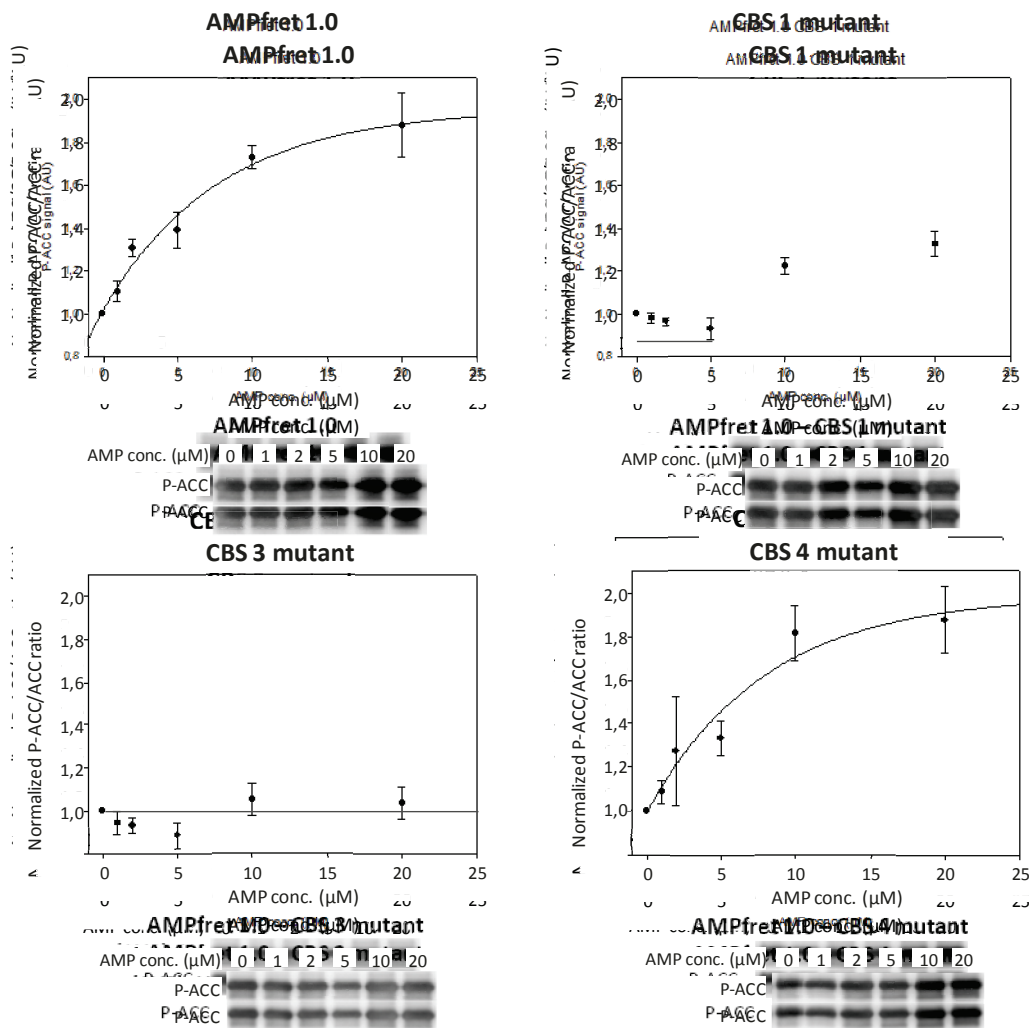


Figure 26 : AMP-induced allosteric activation of AMPfret WT and its CBS site mutants.

AMPfret 1.0 and mutants derivatives activities were examined in presence of increasing concentrations of AMP (0 – 20 μM) and fixed ATP 200 μM . AMPK activities were quantified by immunoblotting against P-ACC and ImageJ 1.46. Corresponding P-ACC bands are represented under their quantification. Activities were normalized according to kinase activity in absence of AMP. Data points represent the mean \pm SEM (n=3).

Results obtained with AMPfret WT and its derived CBS site mutants strongly suggest that CBS site 3 is essential for AMP-induced allosteric AMPK activation: this site should further be considered as the key site for the development of AMPK activators and drugs. CBS site 1 seems also to be involved, but in a more moderate way, so it might be involved for the proper propagation of the conformational changes along the heterotrimer in particular at low AMP concentrations.

As CBS site 3 was identified as being directly linked to AMP-dependent allosteric activation, a mutated version of AMPfret 2.1 (V275G + L276G) was also generated (Figure 8). It could later be used as a negative control for experiments in cells. Indeed, such control construct should not show any AMP-related variation in its FRET due to AMP-binding abolition, or at least alteration, on the γ -subunit.

4.3. AMPK CBS sites and protection against dephosphorylation by ADP.

We finally analyzed whether the altered FRET response seen in CBS mutants with ADP correlates with changes in AMPK activation by protection of AMPK from dephosphorylation.

The ability of ADP to protect WT and CBS sites mutants against dephosphorylation by protein phosphatase 2C α (PP2C α) was investigated. Re-purified after having been phosphorylated, AMPfret protein complexes were dephosphorylated *in vitro* by PP2C α in presence or in absence of increasing concentrations of ADP. The phosphorylation status of Thr172 was then examined by Western blot and quantified (Figure 27).

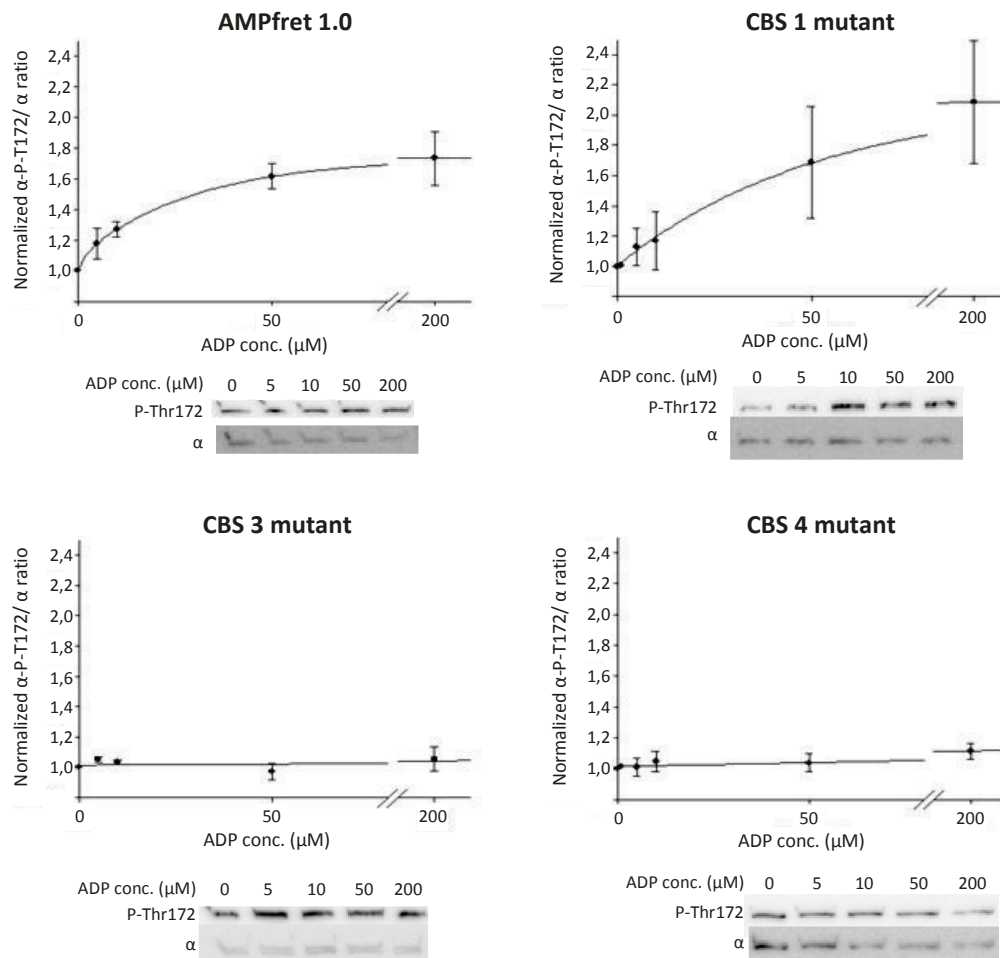


Figure 27: ADP-dependent protection against dephosphorylation by PP2C α .

Ability of AMPfret WT and its CBS site mutants to be protected against dephosphorylation in presence of increasing concentrations of ADP (0 – 200 μ M) were investigated by immunoblotting for P-Thr172 in the α -subunit. Quantification of the P-Thr172 bands was achieved using ImageJ 1.46. Corresponding bands are represented below their quantification. Phosphorylation status was normalized according to the value when dephosphorylated in absence of ADP. Data points represent the mean \pm SEM (n=3).

CBS site 1 mutant shows a similar ADP-dependent protection of its phosphorylated Thr172 as WT. This agrees with the similar FRET variations seen in WT and site 1 mutant at 200 μ M ADP (Figure 24).

In contrast in CBS site 3 and site 4 mutants, any protective effect of ADP was lost with AMPK remaining dephosphorylated even at 200 μ M ADP. Again, this agrees with the FRET data (Figure 24). These results support a mechanistic model in which ADP-dependent protection against dephosphorylation is directly linked to ADP binding at site 3. CBS site 4 is mostly

reported as a "non-exchangeable" site thus the effect of the site 4 mutation is surprising. However, the S315P mutation may slightly disrupt the structural organization of the neighboring site 3, an effect that may become obvious only with the more bulky ADP bound to CBS 3. Such suggestion supports a structural role of an occupied CBS site 4.

The involvement of different CBS sites of the AMPK γ -subunit in AMP-dependent allosteric activation (sites 1 and 3) or ADP-mediated protection from dephosphorylation (sites 3, possibly 4) suggests that both rely on different mechanisms for signal transduction within the heterotrimeric complex.

Taken together these results suggest: (i) conformational changes linked to allosteric activation by AMP depend on AMP binding at sites 1 and 3, and transfer of the activation signal to the α -kinase domain, (ii) conformational changes linked to and protection by ADP from dephosphorylation by phosphatases depend on ADP binding at CBS site 3. Also, CBS site 4 seems to be important for the ADP-mediated effect, but this may be through a structural role CBS impacting site 3 integrity rather than direct binding of ADP.

4.4. Thr172 phospho-status does not condition AMP-dependent conformational changes.

Activation of AMPK is determined by two factors, the phosphorylation status of Thr172, situated on the activation loop of the α -subunit and allosteric activation by AMP via binding to CBS site(s). Generally, FRET experiments performed in this thesis use non-phosphorylated AMPfret. Although, very low level of autophosphorylation may occur in recombinantly expressed AMPK, Thr172 is generally not phosphorylated (data not shown). Here we investigated whether prior covalent activation of AMPK affects the AMP-induced FRET signal occurring with allosteric activation (Figure 28). It is commonly assumed that AMPK activation occurs sequentially, with Thr172 phosphorylation preceding AMP-dependent allosteric activation. Thus, a full conformational change induced by AMP may require phosphorylation of Thr172. In addition, Thr172 phosphorylation itself may induce conformational changes. However, already a recent study showed that AMPK can be activated by AMP and A-769662 without the need of Thr172 phosphorylated (Scott et al., 2014).

First we used AMPfret mutant T172D, mimicking constitutively phosphorylated AMPK (Stein et al., 2000), and T172A mutant, an AMPK non-phosphorylatable at Thr172. When AMPfret T172A and T172D mutants were incubated in presence of 20 μ M AMP, they both exhibited the same change in FRET ratio as WT (Figure 28-A).

Instead of using mutants, we also tested AMPfret WT that was phosphorylated in vitro by CammKK β , and re-purified using size exclusion chromatography (verified by Western blot against P-Thr172). Phosphorylated AMPfret WT again exhibited similar AMP-dependent FRET variations as non-phosphorylated control (Figure 28-B). We conclude that AMP-induced conformational changes reported by AMPfret, occurring during allosteric activation, are independent of the phosphorylation status of α -Thr172. This does not exclude that P-Thr172 triggered structural effects that are not reported by AMPfret.

The independence of FRET-reported conformational changes from the AMPK phosphorylation state represents an advantage for using AMPfret for screenings of direct AMPK interactors, since no pre-phosphorylation with upstream kinases is required.

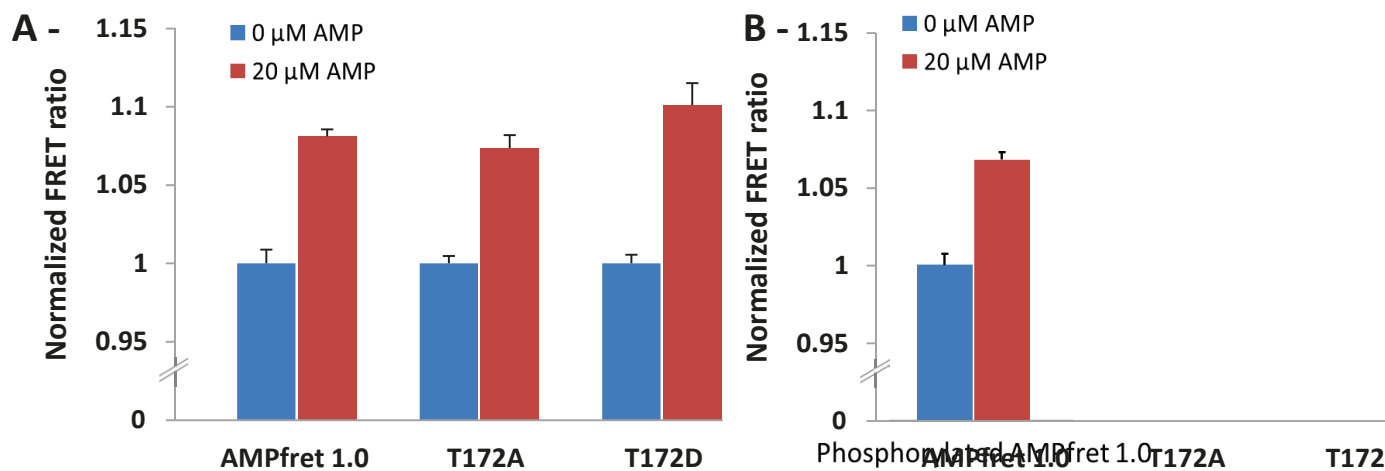


Figure 28: Conformational changes do not require Thr172 phosphorylation.

A - AMPfret 1.0 WT, T172A and T172D mutants were incubated in absence (blue bars) or in presence of 20 μ M AMP (red bars). **B** - Phosphorylated AMPfret 1.0 was incubated in absence (blue bar) or in presence (red bar) of 20 μ M AMP. AMP-induced FRET variation was measured. Bars represent mean \pm SEM (n \geq 3). Note: The status of Thr172 seems to not interfere with AMP-induced conformational changes.

4.5. Free- and Mg-complexed ATP in AMPK allosteric activation

In order to mimic a more physiological situation (where ATP competes AMP binding at γ -subunit) FRET change was induced by addition of 20 μ M AMP in a buffer containing 3 mM Mg^{2+} -complexed ATP (Figure 29). We determined that 97% ATP were complexed to magnesium in our buffer using the maxchelator software (<http://maxchelator.stanford.edu>). Presence of Mg^{2+} -complexed ATP in the *in vitro* FRET assay did not alter the AMP-induced FRET response of AMPfret WT and mutants, suggesting that Mg^{2+} -complexed ATP, at a concentration of 3 mM, may not compete AMP for the inhibition of the conformation changes.

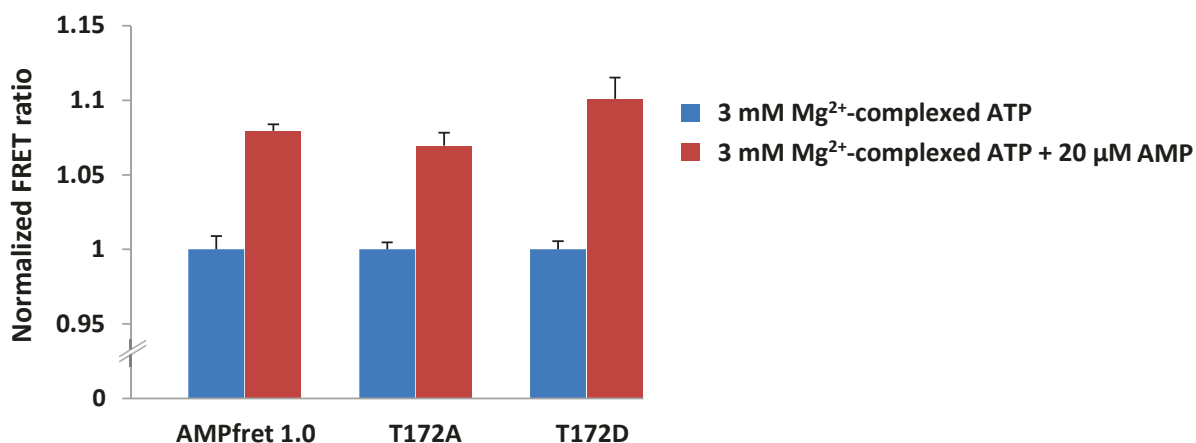


Figure 29: AMP-induced FRET changes still occur in presence of Mg^{2+} -complexed ATP.

AMPfret 1.0 WT, T172A and T172D mutants were incubated in presence of 3 mM ATP (blue bars) or 3 mM ATP+ 20 μ M AMP (red bars). Mg^{2+} -complexed ATP does not alter the AMP-induced FRET. Bars represent mean \pm SEM (n=3).

One important question concerning AMPK activation is how the kinase is capable to sense low micromolar concentration of AMP in presence of millimolar concentrations of ATP, a difference of three orders of magnitude. To solve this paradox, it has been proposed that only free ATP competes AMP (Hardie et al., 2012; Townley and Shapiro, 2007; Xiao et al., 2007). Free ATP is present in the cell only at micromolar concentrations, since most ATP is complexed with magnesium, while AMP does not complex Mg^{2+} . AMPfret allowed for the first time to directly test this hypothesis, since it does not require an Mg-ATP-dependent kinase assay as a readout (Figure 30 A-, B-). In our *in vitro* assay Mg^{2+} had no effect on the baseline FRET signal of AMPfret in absence of adenylates or increased FRET signal in

presence of 20 μM AMP. When AMPfret was incubated with 20 μM AMP and 3 mM ATP in absence of Mg^{2+} , this reduces the FRET ratio to adenylate-free baseline levels, clearly showing competition of AMP-induced changes by free ATP. When now excess Mg^{2+} was added, this entirely removed the inhibitory effect of ATP. These data show that it is only the free ATP that is competing with AMP for inhibiting conformational changes.

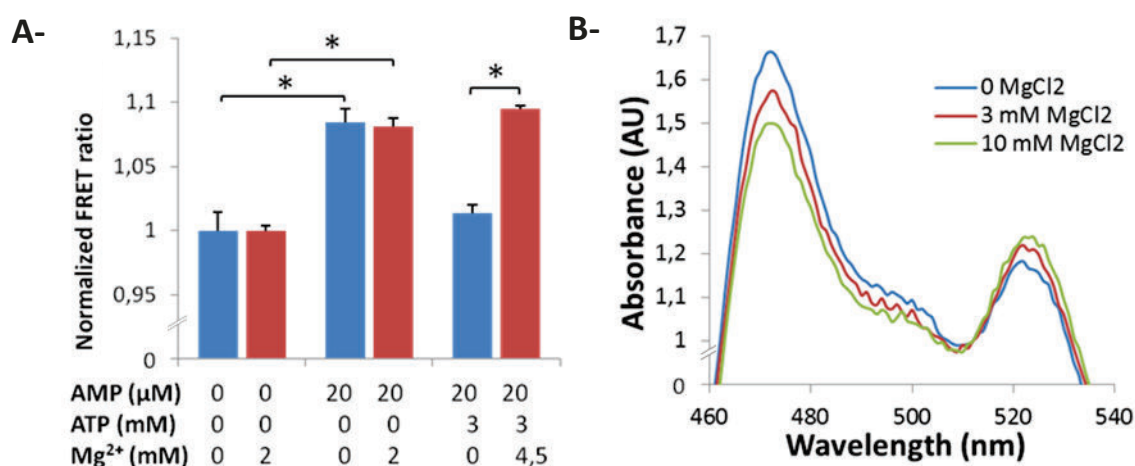


Figure 30: Only free ATP, not Mg^{2+} -complexed ATP, competes with AMP to inhibit FRET.

A – MgCl_2 does not affect baseline FRET and AMP-induced FRET, but prevents ATP-induced FRET inhibition. Blue and red bars respectively correspond to FRET signal measured in absence or in presence of Mg^{2+} . Data correspond to mean \pm SEM ($n \geq 3$) and significance was assessed through a Student-Newman-Keuls test ($* = p < 0,003$). **B** - Normalized FRET emission spectra of AMPfret incubated with 20 μM AMP and 3 mM ATP in absence (blue line) or in presence of 3 mM or 10 mM Mg^{2+} (respectively red and green lines). Using maxchelator software at <http://maxchelator.stanford.edu>, amounts of free ATP were calculated according to the magnesium concentration to be 400 μM (red line) and 30 μM ATP (green line).

Our results, using AMPfret sensor *in vitro*, showed for the first time direct evidence that free ATP but not Mg^{2+} -complexed ATP competes with AMP to bind the AMPK γ subunit, as has been previously suggested (Hardie et al., 2012; Townley and Shapiro, 2007; Xiao et al., 2007). This explains how AMPK can sense fluctuations in ATP, ADP and AMP concentrations despite their concentrations at different orders of magnitude.

4.6. ATP analogues

Non-hydrolysable ATP analogues could avoid the problem of spontaneous ATP hydrolysis, which leads to contamination with ADP and AMP and precluded systematic utilization of ATP in our *in vitro* assay. AMPfret was incubated in presence of 3 mM of different non-hydrolysable ATP analogs (ATP α S, ATP γ S, ApCpp, AppCp or AppNHp, Figure 31 A-), 3 mM Mg²⁺ and changes in FRET ratio by 20 μ M AMP were recorded. AMP-dependent FRET changes were antagonized by these analogues similar as with ATP (Figure 31 B-). However, this inhibition by ATP analogues could not be overcome by increasing AMP concentration, as it occurs with a rising ATP/AMP ratio (Figure 31 C-). Thus, these analogues do not easily exchange with AMP, and do not represent a suitable replacement of ATP for avoiding ADP and AMP contamination during *in vitro* experiments.

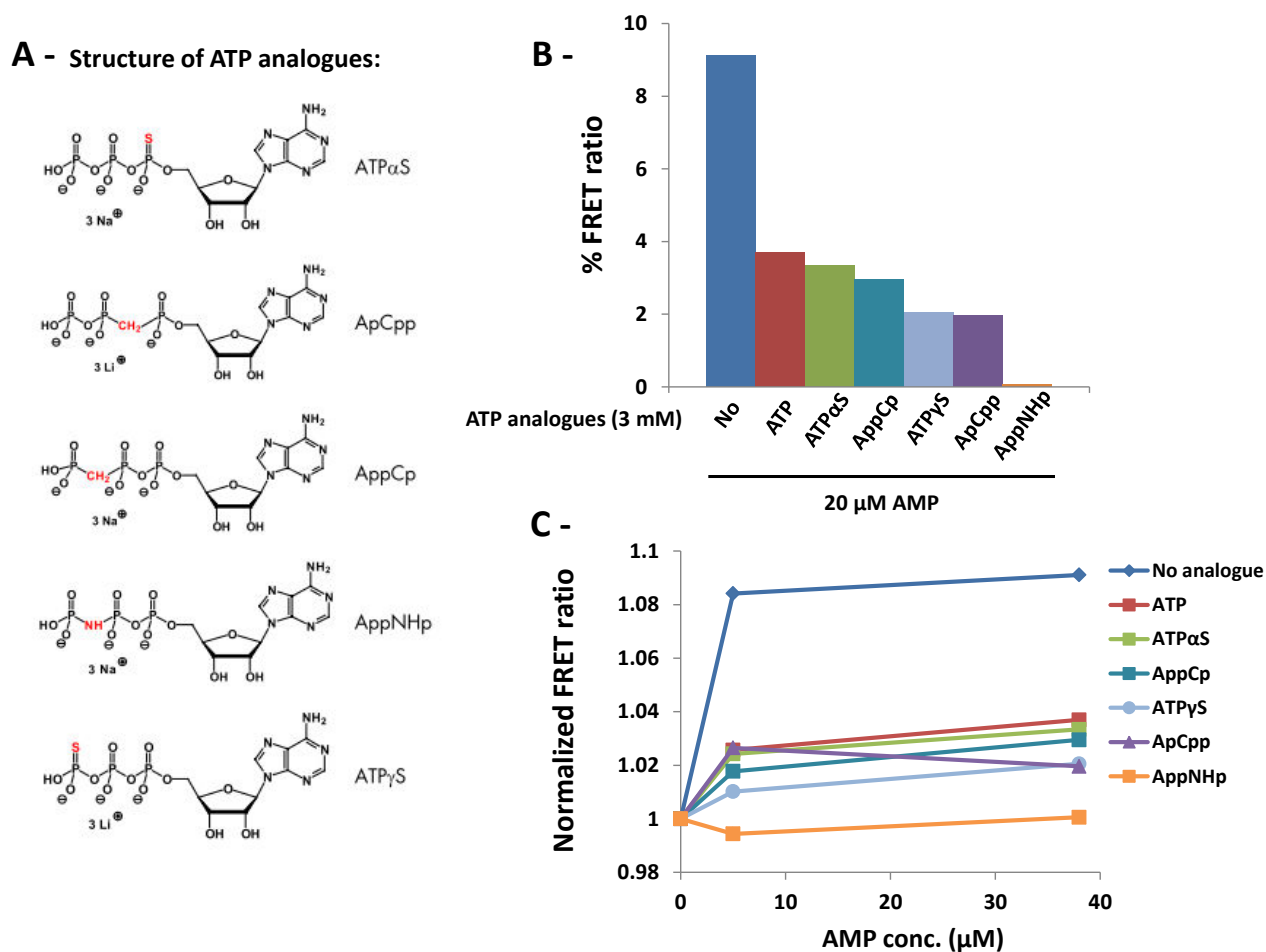


Figure 31: ATP analogues compete with AMP for binding to AMPK and inhibit AMP-induced conformational changes.

A - Structure of non-hydrolysable ATP analogs, differences with ATP structure are given in red and names are mentioned to the right. ATP α S: Adenosine-5'-(α -thio)-triphosphate; ApCpp: Adenosine-5'-[(α,β)-methylene]triphosphate; AppCp: Adenosine-5'-[(β,γ)-methylene]triphosphate; AppNHp: Adenosine-5'-[(β,γ)-imido]triphosphate; ATP γ S: Adenosine-5'-(γ -thio)-triphosphate **B** - Percentage of FRET ratio variation (with or without 20 μ M AMP) of AMPfret 1.0 in presence of 3 mM ATP analogs and 3 mM Mg²⁺. **C** - Effect of 3 mM ATP analogs on AMP-concentration dependent changes in FRET of AMPfret 1.0. Same color code in **B** - and **C** -.

These strong effects of ATP analogs are most probably due to their lower affinity for Mg²⁺ as compared to ATP which is important for the inhibitory effect of this nucleotide (see results chapter 4.5). They are carrying modifications located at the level of the phosphate chain where magnesium coordinates with ATP. Thus, in presence of 3 mM Mg²⁺, considerable amounts of these compounds are present under their free form and compete with AMP for binding of AMPK yielding reduced FRET changes.

ATP α S, owing to its structure (very close to ATP), may bind magnesium similarly to ATP and this is supported by similar inhibitions of AMP-induced FRET changes by ATP α S and ATP. AppNHp, which could be structurally considered as the least analogous to ATP, and may be expected to bind Mg²⁺ with a much lower affinity than ATP (different charge repartition), totally inhibits the AMP-dependent FRET changes.

Taken together, results obtained using free ATP and ATP analogues show that they can compete with AMP for allosteric activation. This suggests that inhibitors of AMPK allosteric activation could probably be identified within the ATP analog moieties.

5. An optimized AMPfret biosensor: AMPfret 2.0

5.1. Optimization: linker engineering

Using genetically encoded FRET biosensor, for cellular *in vivo* studies, requires reliability for the FRET signal, but also the maximal FRET signal amplitude for detection above background. FRET relies on the distance between the pair of fluorophores but also on their relative orientation and environment. Thus, efforts were done in order to engineer AMPfret in order to improve the nucleotide-induced FRET change. As mentioned above, reliability for the monitored signal was insured by the presence of the mseCFP_{Δ11}/cpVenus FRET pair. We then applied further molecular engineering to improve the amplitude of the FRET ratio using the two initial constructs identified as reporting AMP-dependent FRET changes (AMPfret A and C) (Figure 8).

To interfere with the distance between fluorophores and their orientation, we engineered the linkers between AMPK subunits and fluorescent proteins. In a first phase, we removed the flexible and non-folded part of the linker consisting of subunit termini. This was expected to improve the transmission of intramolecular movements to the fluorescent proteins positioned at the AMPK subunits termini. Then, in such constructs, an engineered linker in form of rigid α -helix was inserted between α 2-C-terminus and CFP. This was expected to lock the orientation of one fluorescent protein relatively to the remainder of the complex, which may increase the FRET signal changes occurring during conformational changes.

5.2. Reducing flexibility by linker shortening

In order to reduce the length and the flexibility of the interface between AMPK subunits and the fluorescent proteins, we performed small truncations in the AMPfret A and C constructs. Based on the available crystal structure at that time (PDB ID: 2Y94, Xiao et al., 2011), and secondary structure prediction, we identified those amino acids located at the termini of the AMPK subunits and of the fluorescent proteins which were not involved in any secondary structures. Secondary structure prediction was realized by a combining results issued from both PSIPRED and Network Protein Sequence Analysis (NPS@) servers. Once identified, unfolded residues located between AMPK subunits and the fluorescent proteins were

removed. In addition, we also deleted amino acids resulting from the initial cloning strategy of AMPfret constructs (restriction sites) that were still inserted between AMPK subunits and fluorescent proteins. In addition to reduce the linker length, this helped to identify the correct clones during cloning due to modified restriction patterns.

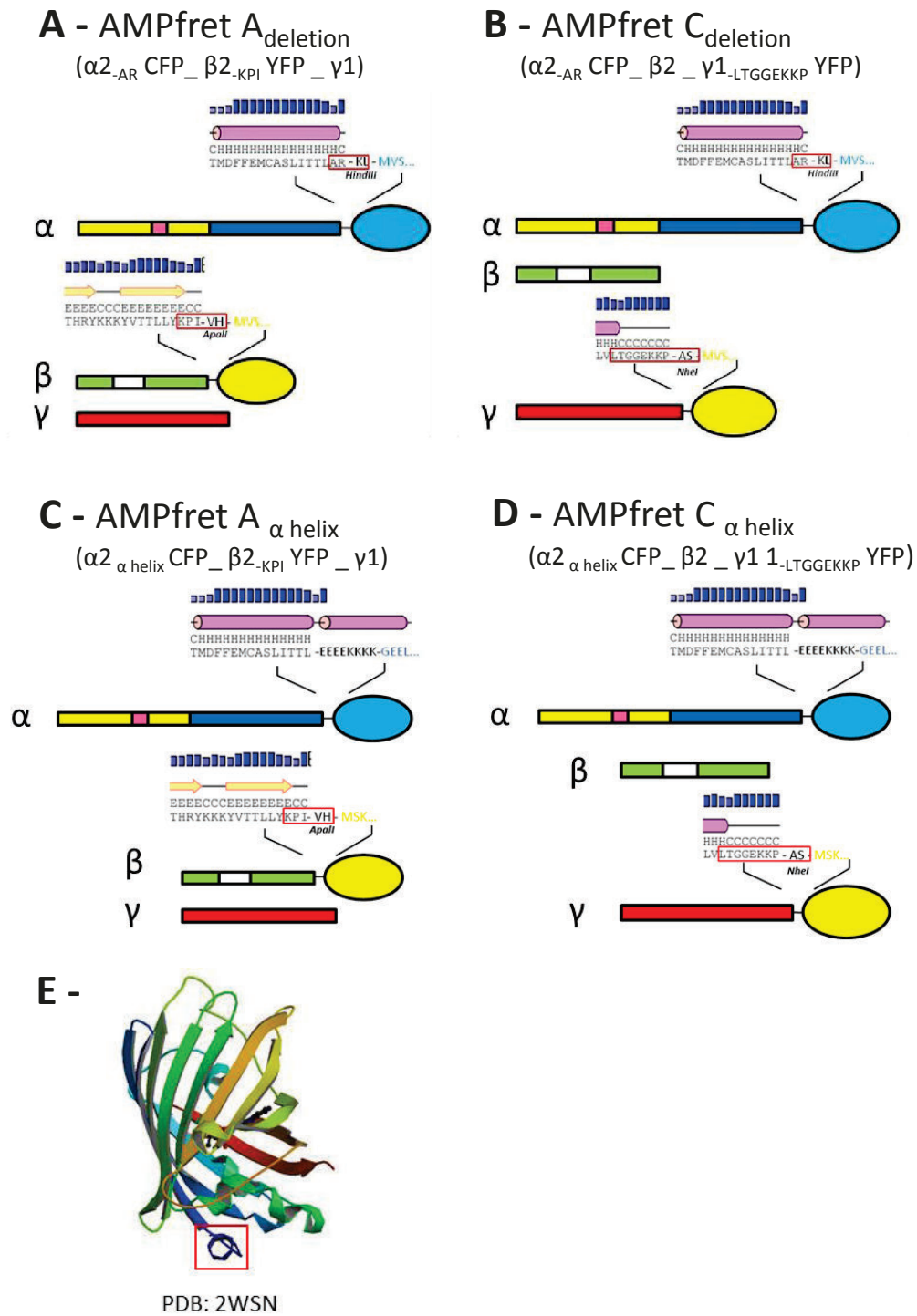


Figure 32: AMPfret optimization through shortening or engineering of the linker.

Optimization was done with AMPfret A (A- and C-) and AMPfret C (1.0) (B- and D-). α is depicted as the yellow (kinase domain) and blue (C-terminal domain) bar; in pink is showed the activation loop. β is represented as the green bar, its CBM domain is white. γ is represented as the red bar. CFP and YFP are respectively presented as blue and yellow circles. A- and B- Shortening of the linker consisted in the removal of unfolded amino acid stretches located between the most C-terminal secondary structure of AMPK subunits and the most N-terminal secondary structure of fluorescent proteins. This was done according to crystal structures and secondary structure prediction. Secondary structure prediction results are shown as following: blue bars represent the confidence a secondary structure is present at the level of a given residues. Secondary structures are shown under blue bars and helices (H) are depicted as pink cylinders and β -strands (E) are yellow arrows. Unfolded residues are annotated with C (coil). Amino acid sequence is shown. Residues in bold are encoded by the restriction site inserted during cloning between AMPK subunits and FPs. In blue or yellow are given the first residues of CFP or YFP respectively. Residues boxed un red were removed to create AMPfret A_{deletion} (A-) and AMPfret C_{deletion} (B-). C- and D- Same color code as above ; E/K repeat in bold represent the α -helix inserted between α subunit and CFP. First amino acids of the CFP sequence were deleted as they did not seem to be involved in any secondary structure and inserted 8AA helix should be prolonged by the small one present at CFP N-Ter boxed in red in E-. Amino acids boxed in red present between AMPK subunit and YFP were removed as well. This resulted in AMPfret A _{α -helix} (C-) and AMPfret C _{α -helix} (D-). E- represents the crystal structure of eCFP obtained at physiological pH (PDB ID: 2WSN). In red is boxed the small α -helix supposed to follow the putative inserted one.

As for AMPfret CBS sites and Thr172 mutants, cloning was done using the advanced self-SLIC method (see chapter Materials & Methods and Haffke et al., 2015). We removed Ala551 and Arg552 at the C-terminus of the α 2-subunit, as well as the lysine and leucine residues encoded by the HindIII restriction site previously located between the α 2 and CFP coding sequences (Figure 32 A-), yielding pACE α 2-_{AR}CFP. Using the same approach, Lys268, Pro269 and Ile270 were deleted from the β 2 C-terminus additionally to the valine and histidine residues encoded by the ApalI restriction site previously located between β 2 and YFP coding sequences, yielding pDC β 2-_{KPI}YFP (Figure 32 A-). Finally, Leu323, Thr324, Gly325, Gly326, Glu327, Lys328, Lys329 and Pro330 were removed from the γ 1 C-terminus, as well as the alanine and serine encoded by the NheI restriction site present between the γ 1 and YFP genes, yielding pDSy1-_{LTGGEEKP}YFP (Figure 32 B-).

Plasmids were then fused by Cre recombination in a way that new versions of AMPfret with shorter linkers were obtained. After expression and purification, AMPfret A_{deletion} and AMPfret C_{deletion} were obtained (Figure 32 A-, B- and Figure 8).

Based on the average peptide bond length (3.8 Å), linkers between $\alpha 2$ C-terminus and CFP N-terminus, $\beta 2$ C-terminus and YFP N-terminus or $\gamma 1$ C-terminus and YFP had their size reduced by 15.2 Å, 19 Å and 38 Å respectively. These are theoretical distances, since unfolded amino acid sequences could have been more or less packed and were most probably not extended as a rigid stretch. Values may be overestimated, but the applied modifications resulted in more compact AMPfret versions with shorter and more rigid linkers.

The new versions of AMPfret A and AMPfret C with shorter linkers were expressed and purified following the protocol previously established. Then, we tested their AMP-dependent FRET response in presence of 3 mM ATP or in presence of 100 μ M AMP (Figure 33).

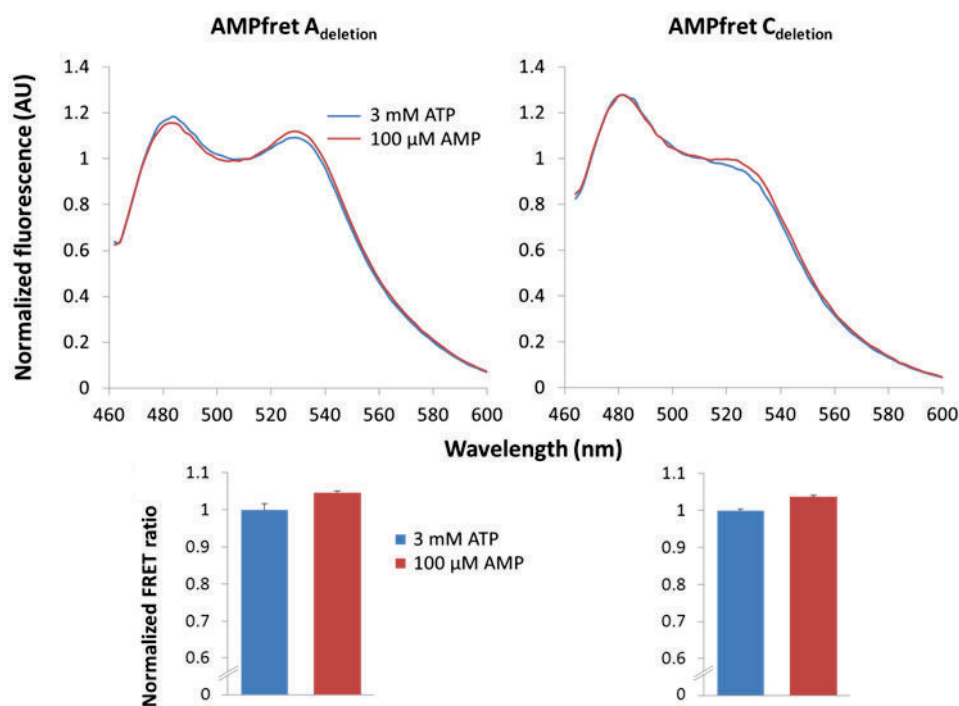


Figure 33: Shorter linkers in AMPfret.

(Upper panel) AMPfret constructs with shortened linkers between AMPK subunits and fluorescent proteins were incubated either in presence of 3 mM ATP (blue line) (freshly made solution containing 5 mM Mg^{2+}) or 100 μ M AMP (red line), as in Figure 17. Peaks at 476 nm and 527 nm are the emission peaks of CFP and YFP respectively. Spectra in presence of ATP or AMP were normalized using the CFP/YFP isosbestic point at 512 nm. (Lower panel) FRET ratio of truncated constructs calculated from data (upper panel). FRET ratio (YFP/CFP) was normalized to the incubation in presence of ATP (blue bars). Data correspond to mean \pm SEM (n = 3).

Despite shortening of linkers between AMPK subunits and fluorescent protein, AMPfret A_{deletion} and AMPfret C_{deletion} did not show improvement in their AMP-induced FRET changes. AMPfret C_{deletion} was even presenting lower FRET ratio change (~ 5%) than initial AMPfret C. Deletion of unfolded amino acids yield in more compact shape of AMPfret. This may i) inhibit the transmission of intramolecular movements towards fluorescent proteins or ii) alter the proper folding of the sensor due to steric hindrance and impact the native AMP-induced conformational changes. However, if compaction of the overall shape of AMPfret did not yield to any improvement in the AMP-dependent FRET ratio variations, it suggests that conformational changes happening in the whole AMPK heterotrimer are not of great scale and do not modify deeply the overall shape of AMPK. This agrees with previous studies made by SAXS (Riek et al., 2008), EM (Zhu et al., 2011) and crystallography (Chen et al., 2012) which reported conformational changes of a moderate extend.

5.3. Reducing flexibility with a putative rigid α -helix.

As part of the AMPfret optimization, we then introduced a rigid α -helix linker in previous constructs lacking unfolded amino acids at their termini. This rigid arm linker was introduced in-between α -subunit and CFP. This aimed to lock one fluorescent protein orientation relatively to the other. To avoid “locking” donor and acceptor at a distance from each other bigger than before, only the donor (CFP) was fixed using the rigid linker. Such rigid arm may also better transduce the conformational changes to the fluorescent protein. The rigid α -helix linker was engineered according to Sivaramakrishnan et al. work (Sivaramakrishnan et al., 2008) visible on Figure 34. It consisted in a putative 8 amino acids α -helix, made of ER/K repeats as side-chain interactions contribute to substantial bending rigidity in such repeat.

This round of optimization was realized on AMPfret A_{deletion} and AMPfret C_{deletion} , yielding AMPfret $A_{\alpha\text{-helix}}$ and AMPfret $C_{\alpha\text{-helix}}$ (Figure 8 and Figure 32 C-, D-).

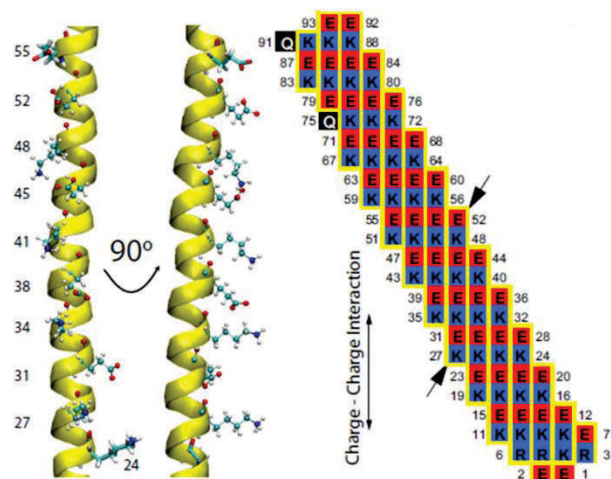


Figure 34: Charge interactions along the ER/K α -helix backbone.

Snapshot of two orthogonal views of a section of the ER/K α -helix (residues 24 –55) in mannosyltransferase from MD simulation, showing side-chain interactions and residue numbers. For reference, the backbone carbonyl oxygens corresponding to the illustrated side chains are also shown. (Right) The charge interaction map shown to the right illustrates the pattern of E<->R/K interactions along the vertical axis (see yellow boxed groups of residues in columns). Arrows show boundaries of the segment of the α -helix displayed in Left. From Sivaramakrishnan et al., 2008.

At the interface between the α 2 subunit and CFP, where the α -helix linker would be introduced, unfolded amino acid sequences at CFP N-terminus were removed. In addition to Ala551 and Arg225 deleted from the α 2 C-terminus, Met1, Val2, Ser3 and Lys4 from the CFP amino acid sequence had been removed too. Indeed, they were identified as not being involved in any secondary structure according to crystal structure (pdb: 2YDZ) (Figure 32 E-) and secondary structure predictions done with both PSIPRED and NPS@ servers. This aimed to reduce again the liberty of the donor relatively to the acceptor. Thus, we expected the rigid linker to be continued by the small α -helix localized at the N-Terminus of CFP and formed by Gly5, Glu6, Glu7, Leu8 and Phe9 (Figure 32 E-).

After having been produced and purified, AMPfret A $_{\alpha}$ -helix and AMPfret C $_{\alpha}$ -helix were both incubated in presence or not of 20 μ M AMP to validate whether the insertion of the putative rigid α -helix was beneficial regarding AMP-induced FRET response.

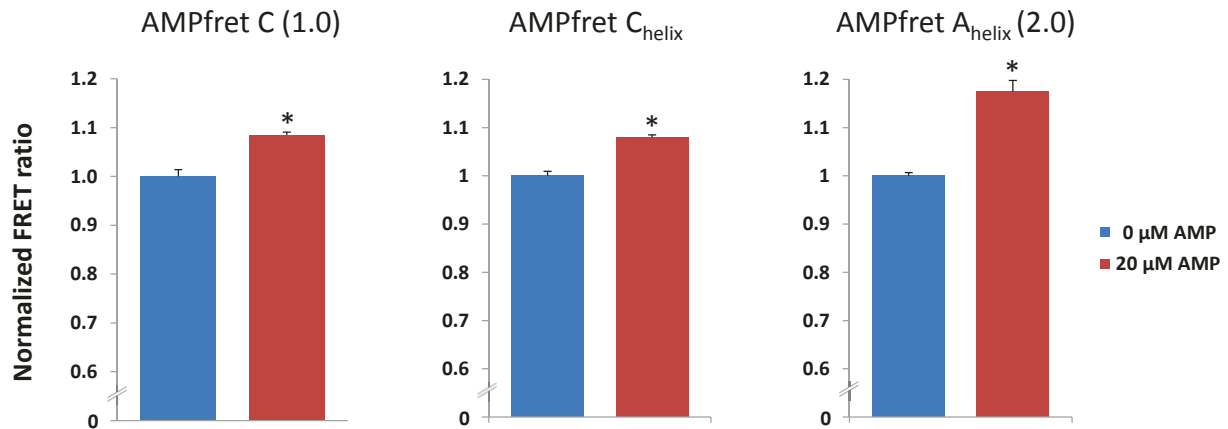


Figure 35: Beneficial effect of α -helix insertion in AMPfret A on AMP-dependent FRET response compared to AMPfret 1.0.

AMPfret 1.0 exhibited a FRET ratio variation of $\sim 10\%$ when incubated with in presence or in absence of $20 \mu\text{M}$ AMP. Introduction of the α -helix linker had no beneficial effect on AMP-dependent FRET signal changes of AMPfret C. By opposition, AMPfret A _{α -helix} (renamed 2.0) presented a FRET range twice greater than when non-optimized (see Figure 18). FRET ratio was normalized to the incubation in absence of AMP (blue bars). Data correspond to mean \pm SEM ($n \geq 3$; *: $p < 0.01$).

As a result, this optimization was beneficial and led to an increase of the FRET variation amplitude. Interestingly, insertion of this rigid linker in AMPfret A but not in AMPfret 1.0 (C) represented a 100% improvement of the FRET signal amplitude variation upon AMP binding (Figure 35). Despite, it was previously presented (Figure 18) that AMPfret A and 1.0 (C) were showing similar AMP-dependent FRET changes the insertion of the rigid linker only improved AMPfret A FRET response to AMP. AMPfret A_{helix} was renamed AMPfret 2.0 because it presented a different structure than AMPfret 1 series with fluorescent proteins located at different locations. Improvement between AMPfret series 1 and 2 is visible when comparing AMP-related FRET changes of AMPfret 1.0 and 2.0 on Figure 35. To further improve its environment stability for later *in cellulo* experiments, the mseCFP Δ 11/cpvenus FRET pair was inserted in AMPfret 2.0 yielding AMPfret 2.1.

5.4. AMPfret 2.0 presents an improved FRET signal variation

After the second round of optimization, a genetically encoded biosensor was obtained, AMPfret 2. It exhibited, like other published FRET-based biosensors (Imamura et al., 2009) (see Introduction chapter 2), an acceptable FRET ratio variation (~ 20%). Like for the AMPfret 1 constructs series, its biochemical properties were examined. Also, its AMP-dependent FRET changes allows to plan *in cellulo* experiments.

AMPfret 2.0 shows an increase of ~ 20% in its FRET signal when incubated with AMP compared to ~ 10% for AMPfret 1 constructs. However, AMPfret 1.0 and AMPfret 2.0 rely on two different AMPfret constructs on which the FRET pairs are positioned at different locations. Thus, it was crucial to show that the improved sensor AMPfret 2.0 also conserves native AMPK characteristics especially regarding adenylates concentration fluctuations. Even if both based on full length AMPK, we had to confirm that AMPfret 2 constructs series conserve the same native behavior than AMPfret 1.0.

After having shown that AMPfret 2.0 presented AMP-dependent FRET signal changes, we looked at the kinase activity of AMPfret 2.0 through the phosphorylation of ACC with ³²P-ATP (Figure 36).

In addition to the enhanced AMP-dependent FRET changes, results showed that AMPfret 2.0 has a comparable kinase activity to AMPfret 1 and to native AMPK WT. This, coupled to size exclusion chromatography elution profile, supported that AMPfret 2.0 was obtained properly folded, functional and monomeric after expression and purification.

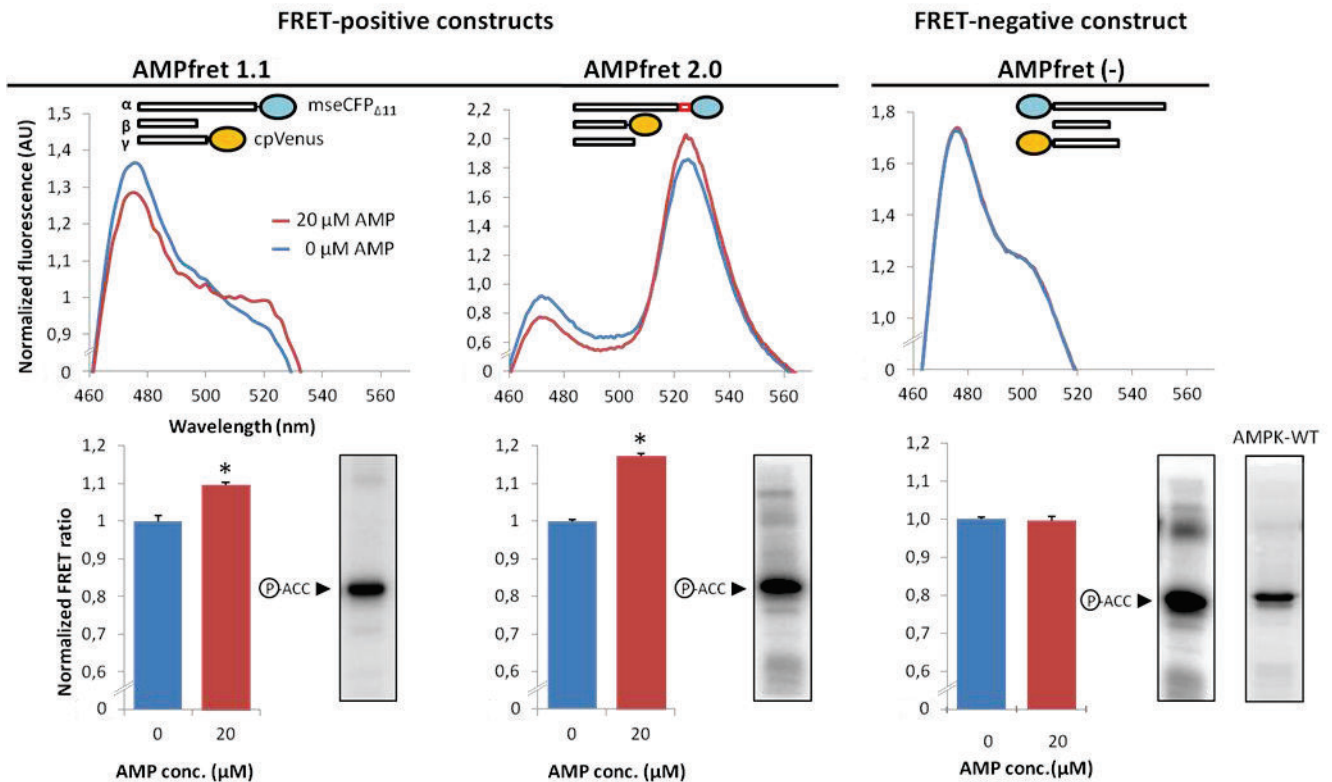


Figure 36: Optimized AMPfret constructs.

Positive AMPfret constructs 1.1 and 2.0 derived from constructs AMPfret C and A respectively (Figure 8) are compared to the negative construct AMPfret (-) (AMPfret F). Schemes on top represent AMPfret constructs topologies; blue circles represent CFP or mseCFP Δ 11 and yellow circles YFP or cpVenus. In the case of AMPfret 2.0, a putatively rigid helix (8AA) was inserted between the α -subunit C-terminus and CFP (see red box in scheme). (**Upper panel**) Fluorescence emission spectra of AMPfret constructs excited at 430 nm. Spectra show fluorescence peaks of CFP (476 nm) and YFP (527 nm), and their variation upon AMP binding (blue line: no AMP, red line: 20 μM AMP). (**Lower panel**) FRET variation of AMPfret constructs calculated from data in upper panel (same color code) and autoradiograms of *in vitro* kinase activity assays with these constructs using acetyl-CoA carboxylase (ACC) as a substrate. Data correspond to mean \pm SEM ($n \geq 7$) and significance was assessed through a Student-Newman-Keuls test (*: $p < 0,001$). Note: AMPfret constructs exhibit similar activity as native AMPK WT. AMPfret 2.0 reveals improved FRET variation range as compared to AMPfret 1.1, providing proof of principle that optimization of FRET based reporter is possible.

5.5. AMPfret 2.0 responds to AMP and ADP physiological concentrations

After having identified AMPfret 2.0 as being an optimized version of functional AMPfret, its affinities for AMP and ADP were investigated. This will validate whether AMPfret 2.0 conserves AMPfret 1 series (and AMPK) attributes. Using the larger FRET fluctuation range, we investigated AMPfret 2.0 sensitivities for AMP and ADP (Figure 37 and Figure 38).

5.5.1. The AMP response

Like AMPfret 1 construct series, AMPfret 2.0 FRET response to increasing amounts of AMP was examined. We incubated AMPfret 2.0 with various concentrations of AMP and recorded its fluorescence emission spectra using the PTI. It was previously observed that AMP-binding on the γ -subunit was still producing conformational changes in AMPfret 2.0 as visible through FRET changes (Figure 36). According to this, AMP was titrated and affinity constant was calculated from the FRET variation going along with the AMP rise in the assay (Figure 37).

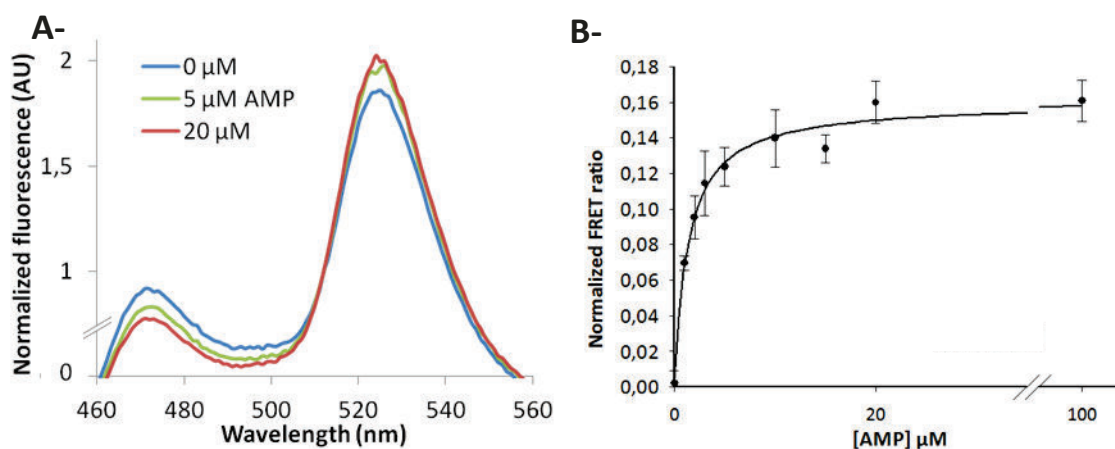


Figure 37: FRET response of AMPfret 2 correlates with the concentration of the AMPK activator AMP.

A – Fluorescence emission spectra of AMPfret 2.0 excited at 430 nm. AMPfret 2.0 fluorescent emission spectra reveal AMP-induced conformational changes through FRET variations. Spectra show peaks at 476 nm and 527 nm corresponding to CFP and YFP respectively, and their variation upon AMP binding (blue, green and red lines: no AMP, 5 μ M and 20 μ M AMP respectively). **B** – Dependence of normalized FRET ratio on the concentration of AMP. AMPfret 2.0 FRET ratio variation correlates with AMP-induced conformational changes visible when using AMPfret 1.0. The FRET ratio of AMPfret 2.0 was calculated from fluorescence emission spectra excited at 430 nm. Data were fitted with Sigma Plot 1.1 software to single site binding kinetics, yielding affinity of 1,5 μ M. Data points correspond to mean \pm SEM ($n \geq 3$).

As presented on Figure 37 A-, AMPfret 2.0 emission spectrum showed increasing FRET signal upon AMP addition, CFP peak at 476 nm diminishing and YFP peak at 527nm rising, reporting AMP-induced conformational changes. Gradual addition of AMP allowed the determination of affinity constant: AMPfret 2.0 K_d for AMP was calculated to be 1,5 μM (1,8 μM with AMPfret 1.1). The binding curve was obtained by fitting the data points using a single-ligand binding curve equation. Again, the precision of our data does not allow distinguishing binding to different CBS sites via multi-phase binding curves. We cannot exclude that e.g. a double component binding curve would have better fit to our data if containing more precise data points. However, our present data suggest that the conformational changes and the allosteric activation rely on AMP binding at the level of a single CBS site.

The obvious similarity between K_d for AMP obtained with AMPfret 1.1 and AMPfret 2.0 shows that both AMPfret constructs respond the same way to AMP despite a different positioning of fluorescent proteins within their structures. These results confirm, as with AMPfret 1 constructs set, that AMPfret retains native AMPK functions and affinities for adenylates. Such K_d value reflects the affinity AMPK has for AMP in absence of other adenylates and AMPfret 2.0 may have a lower affinity for AMP under physiological conditions as ATP and ADP compete for γ -subunit binding.

5.5.2. The ADP response

In turn, as for AMP, AMPfret 2.0 was incubated with increasing concentrations of ADP and its FRET signal variations were monitored. Thus, ADP was titrated and the resulting affinity constant was determined (Figure 38).

Incubation of AMPfret 2.0 with increasing concentrations of ADP allowed the determination of an affinity constant for ADP of 7,4 μM . Difference on K_d for ADP (7,4 μM against 5 μM with AMPfret 1.1) can be explained by different number of data points collected. Also, AMPfret 2.0 exhibits a higher FRET variations range than AMPfret 1.0, suggesting that its use is less prone to lead to misinterpretation.

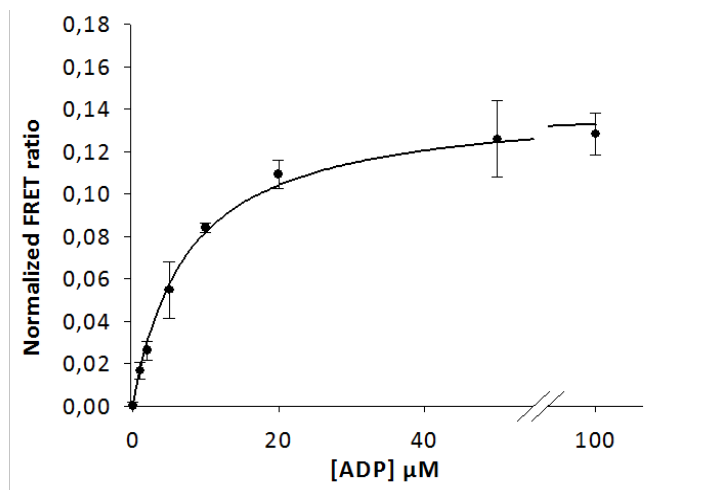


Figure 38: FRET response of AMPfret 2.0 correlates with the concentration of ADP.

Dependence of AMPfret 2.0 normalized FRET ratio on the concentration of ADP. The FRET ratio (CFP/YFP) of AMPfret 2.0 was calculated from fluorescence emission spectra excited at 430 nm. Data were fitted with Sigma Plot 1.1 software to single site binding kinetics, yielding affinity constant of about 7,4 μM . Data points correspond to mean \pm SEM ($n \geq 3$).

Again, the binding curve was obtained by fitting the data points using a single-ligand binding curve equation and the precision of our data does not allow distinguishing several bindings to different CBS sites via multi-phase binding curves. We cannot exclude that e.g. a double component binding curve would have better fit to our data if containing more precise data points. However, our data may suggest that the conformational changes monitored rely on ADP binding at the level of a single CBS site. However, the affinity constant obtained for ADP is comparable with EC_{50} value obtained by Xiao et al. in 2011 where they evaluated the power of ADP to protect Thr172 against dephosphorylation ($\sim 10 \mu\text{M}$).

We conclude that, optimizations carried on AMPfret biosensor, yielding AMPfret 2.0, had for only consequence to magnify by 2-fold the range of FRET variations triggered by conformational changes happening upon nucleotide binding on AMPK. In addition, despite various linker and FP positions, AMPfret 1 series and AMPfret 2.0 conserve native AMPK properties and can be considered as biosensors for nucleotides fluctuations which may represent a tool of choice to decipher AMPK regulation. With 20 % amplitude in FRET changes, AMPfret can be compared to some existing FRET-based biosensors (Imamura et al., 2009; Tsou et al., 2011) (see Introduction chapter 2).

5.6. AMPfret 2.0 reports physiological fluctuations of adenylates mixes

After having shown that AMPfret retained AMPK native functions, we planned to validate its use as a biosensor in cells. Under physiological conditions, AMPK activity is tightly regulated by nucleotides fluctuation. According to ATP, ADP and AMP basal concentrations *in vivo* and recycling existing reactions, when ATP is consumed it will trigger a rise in ADP and especially AMP concentration (via the AK reaction) (Figure 39).

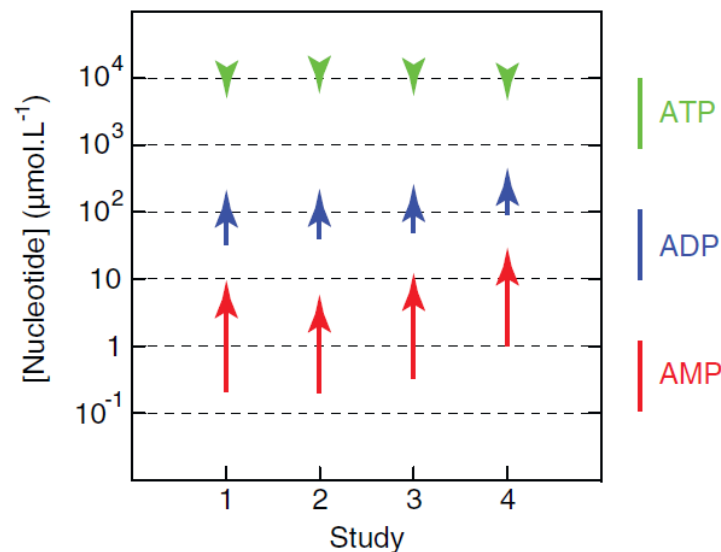


Figure 39: ADP and AMP are the energetic stress indicators *in vivo*.

Estimated changes in nucleotide concentration under metabolic stress during 4 independent studies are represented. ATP drop is represented by green arrows. ADP and AMP rises are respectively represented by blue and red arrows. Physiological basal concentration range of ATP, ADP and AMP are depicted by the green, blue and red line on the right. (ATP range: 1 - 10 mM; ADP: 10 - 100 μM and AMP: 0,1 - 1 μM). Their recorded fluctuations due to metabolic stress during four studies (1 - 4) are represented through the arrows (same color code). As visible, a light diminution in ATP concentration (due to its consumption) is followed by a large increase in ADP and especially AMP concentrations. (from Hardie et al. *TiBS*, 2011).

As shown in Figure 39 (Hardie et al., 2011), ADP and especially AMP are the indicators of energetic stress *in vivo*. However under basal conditions, AMP would already be present in the cell at low concentrations, and ATP and ADP would compete AMP for γ -subunit binding. AMPfret would probably not exhibit the same behavior than during *in vitro* characterization using single nucleotide. Thus, AMPfret has to be further characterized *in vitro* in presence of adenylates mixes as we wanted to estimate under which conditions it could be used in cells but also determine its usage limitation. We decided to evaluate the range of physiological

conditions that could be covered when using AMPfret, and examined AMPfret 2.0 response when incubated under conditions that mimic physiological realities (healthy, light or strong energetic stress). Thus, AMPfret 2.0 was incubated with various adenylates mixes supposed to resemble different physiological conditions (Figure 40).

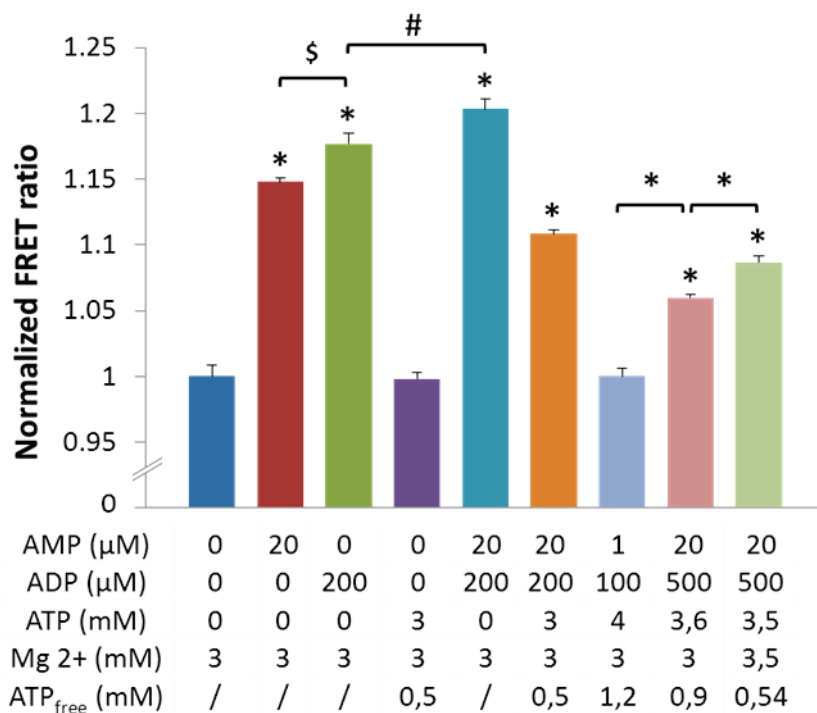


Figure 40: AMPfret 2.0 response to various nucleotides mix.

Comparison of AMPfret 2.0 FRET ratio changes when incubated in presence of one or several nucleotides. Four first bars show the FRET ratio exhibited by AMPfret 2.0 when incubated with single nucleotide. Five last bars show the FRET response of AMPfret 2.0 when incubated with nucleotide mixes. Orange bar represents a high energy deprivation state, light blue bar condition feigns healthy cellular state whereas the two last conditions mimic moderate energy stress. Signal is normalized according to FRET ratio without nucleotide = 1 and values are mean \pm SEM (n=6). Significance was assessed through T-Test (*: $p < 0.005$; \$: $p < 0.01$; #: $p < 0.05$).

First, AMPfret 2.0 was incubated without nucleotide or with 20 μM AMP, 200 μM ADP or 3 mM ATP in presence of 3 mM Mg^{2+} (blue, red, green and purple bar respectively). Such measurements were used as calibration, showing the complete specific AMPfret 2.0 response to these nucleotides. Again, it was visible that AMP, ADP but not ATP triggered FRET changes, themselves translating conformational changes occurring in AMPfret structure upon their binding. Both AMP and ADP were inducing significant different FRET signal changes. Then AMPfret 2.0 was put in presence of both AMP and ADP (20 and 200 μM

respectively) and we observed that it yield a significantly greater FRET ratio than when incubated only with AMP or ADP (cyan bar). Taken together these results supported that AMP and ADP triggered FRET signal changes of a different nature which could have additive effect on the FRET ratio of AMPfret 2.0.

The four other bars on the right of Figure 40 are showing how FRET ratio changes depending on AMPfret 2.0 incubation with various mixes of AMP, ADP and ATP concentrations. To feign an important energetic stress (Figure 40 - orange bar), it was decided to set AMP, ADP and ATP concentrations to 20 μM , 200 μM and 3 mM respectively. These values totally agree with adenylates concentration variations occurring during metabolic stress, as visible on Figure 39. ATP concentration non-complexed to Mg^{2+} was calculated to be 0,5 mM (Maxchelator server). These results showed that the maximum expected FRET signal changes when using AMPfret 2.0 in cells is $\sim 10\%$. The reduced amplitude of the FRET ratio ($\sim 10\%$ versus $\sim 20\%$) under this condition suggested that free ATP still slightly compete with AMP and ADP as related conformational changes did not fully occur. Then, we incubated AMPfret 2.0 with 1 μM for AMP, 100 μM for ADP and 4 mM for ATP (Figure 40 - pastel blue bar) to mimic basal healthy conditions which may be encountered in cells (Figure 39). Under such conditions no FRET signal variation are visible. These results suggested that free ATP (1,2 mM), which was present in a larger extent than AMP or ADP, could compete them to bind AMPK γ -subunits. We concluded that AMPfret 2.0 was under an ATP-bound form explaining why no FRET signal variation was measurable. To set up a realistic moderate energetic stress (Figure 40 - light red bar), we imagined that 10% of the 4 mM ATP were consumed by any anabolic processes, leading to AMP and ADP generation. According to such "ATP consumption" ADP and AMP may respectively increase by 5- and 20-fold setting their concentrations to 20 μM and 500 μM respectively. Under such conditions, AMPfret presented a FRET signal change of 7%. To validate our hypothesis consisting in linking the FRET signal variation to the competition between AMP, ADP and free ATP to bind the γ -subunit we decided to vary the free ATP concentration by increasing the Mg^{2+} concentration whereas AMP and ADP concentrations remained unchanged (Figure 40 - light green bar). As a result, the FRET ratio significantly increases from 7 % to $\sim 10\%$ supporting that free ATP is less competing with other adenylates and that monitored conformational changes rely on the equilibrium between free ATP and AMP/ADP for CBS sites binding. Also, this allowed

highlighting using AMPfret 2.0, that free ATP and not Mg^{2+} -ATP is competing with AMP and ADP to bind AMPK as previously underlined using AMPfret 1.0 (Figure 30).

Taken together these results showed that AMPK nucleotide-bound-state, i.e. its activation state, not only relies on nucleotide concentrations but also on the relative amounts of AMP, ADP and free ATP. Thus, AMPK is regulated by dynamic equilibriums of adenylates concentration during energy-consuming or -demanding processes. These results also suggest that important energetic stress (e. g. ischemia reperfusion) may be necessary to expect a 10% change in AMPfret 2 signal. This forced us to admit that *in cellulo* studies may not have been realistically conceivable using AMPfret 1 series constructs. However, these results (Figure 40) also suggested that AMPfret represents a biosensor which may be used, in correlation with calibration curves taking in account enzymatic equilibriums (e.g. Adenylate Kinase), for nucleotides quantifications.

6. AMPfret: a tool to screen and identify AMPK direct interactors

6.1. In vitro screening of AMPK interactors

AMPK is considered as a central cellular signaling hub and as a drug target of major importance for treatment of type 2 diabetes and other metabolic diseases (see Introduction chapter 1). Previously, we showed that AMPfret constructs (1 and 2 series) retain AMPK native properties: (i) affinities of the sensor for adenylates and (ii) kinase activity regulated through AMP- and ADP-induced conformational changes. Thus, our sensor based on full length AMPK may represent a promising tool to screen and identify direct AMPK activators. As a proof of principle, to illustrate that AMPfret may be useful in such application, we incubated AMPfret with various chemicals compounds reported to act on AMPK and monitored corresponding FRET response: AMP, A-769669 compound, salicylate, Metformin, Imeglimin (Poxel), and citrullin (Citrage).

As positive control, we incubated AMPfret with 20 μ M AMP (Figure 41 A-). A-769662 is binding AMPK at a different location as compared to AMP (Calabrese et al., 2014). However, recent model propose that A-769662 binding may trigger structural changes AMPK (Li et al., 2014). In order to examine whether these putative conformational changes could be visualized using AMPfret, it was incubated in presence of 20 μ M A-769662, but no FRET ratio changes were measured (Figure 41 B-). In addition, we tested the ancient drug salicylate that was reported to bind AMPK through the same mechanism as A-769662 (Calabrese et al., 2014), directly activating AMPK (Hawley et al., 2012). In a cell free assay it was shown that salicylate stimulates AMPK activity in the millimolar range (1 – 10 mM). Thus, we incubated AMPfret 2.0 with 5 mM salicylate and monitored the FRET ratio (Figure 41 C-) as compared to AMP (20 μ M). In our assay, salicylate triggered a small decrease in FRET ratio. In addition, the more salicylate was added the lower became the FRET signal (data not shown). Salicylate has a pKa equal to 2,9 mM and although the test was carried in a buffered solution, with pH-sensitive eYFP FRET changes could be due to a slight acidification of the medium. Likely, salicylate similar to A-769662 does not alter FRET ratio when used alone.

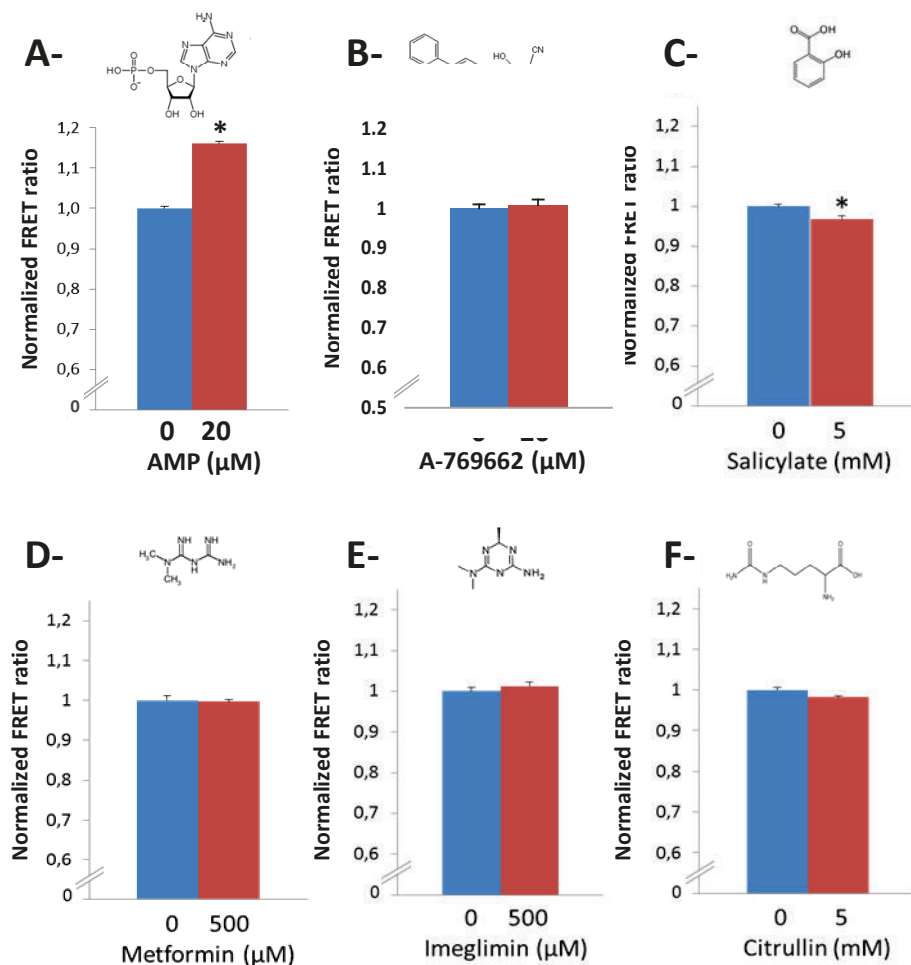


Figure 41: AMPfret sensor is a valuable tool to identify AMPK allosteric interactors.

AMPfret 2.0 is incubated in absence (blue) or in presence (red) of **A-** AMP (20 μM), **B-** A-769662 (20 μM), **C-** Salicylate (5 mM), **D-** Metformin (500 μM), **E-** Imeglimin (500 μM), **F-** Citrullin (5 mM) in order to validate their effect on AMPK allosteric mechanisms. Structures of tested moieties are mentioned above corresponding bars. Data correspond to mean ± SEM and significance was assessed through paired Student test (AMP: n=7; A-769662: n=6; Salicylate: n=4; Metformin: n=4; Imeglimin: n=4; Citrullin: n=4; * = p < 0,01).

Metformin and Imeglimin, two drugs widely used in type 2 diabetes treatment, were tested at a 500 μM concentration (Figure 41 D- and E-). Metformin is activating AMPK through alteration of adenylate ratios (complex 1 inhibition), but was proposed to also interact with the γ-subunit (Zhang et al., 2012). As expected, both Metformin and Imeglimin did not induce any FRET signal variation and may be interpreted as negative control.

Citrullin is an α-amino acid studied in the laboratory for its positive effect on protein metabolism. It has been reported that Citrullin has the ability to stimulate protein synthesis through the mTor pathway which is also regulated by AMPK. Citrullin (5 mM) did not induce

any FRET variation (Figure 41 F-), suggesting that Citrullin was not interacting directly with AMPK.

We also investigated the effect of the synthetic ligand A-769662 (0 - 20 μM) on AMPfret 2.0 FRET signal in absence or in presence of AMP to account for potential synergistic effects (Figure 42). Binding of A-769662 activates AMPK by binding at the α -KD / β -CBM interface, different from the adenylate binding site (Xiao et al., 2013).

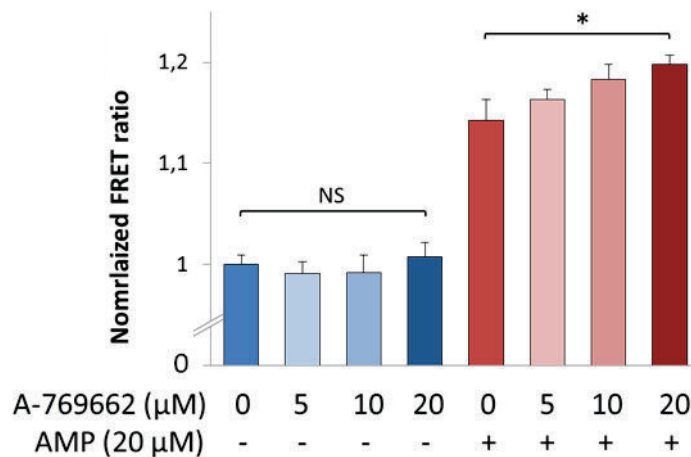


Figure 42: AMPfret is a specific reporter of adenylates binding on AMPK.

At lower concentration (5 - 20 μM), A-769662 has no effect on the FRET ratio (blue bars). However, it appears that A-769662 may potentiate AMP-dependent FRET changes. A cumulative effect on the FRET ratio is visible when AMPfret is with incubated with increasing amount of A-769662 and 20 μM AMP. Data correspond to mean \pm SEM and significance was assessed through T-test ($n = 6$; * = $p < 0,003$).

We did not observe FRET signal variation upon addition of A-769662 over the tested concentration range (0 - 20 μM). Although A-769662 has higher affinity to $\beta 1$ as compared to $\beta 2$ used here, it can be expected that at 20 μM binding occurs at both isoforms. Thus, AMPfret does not directly report A-769662-related structural rearrangements. Interestingly, when the same analysis was done in the presence of 20 μM AMP, A-769662 increased the FRET ratio further (Figure 42). This supports a cumulative effect of A-769662 and AMP for AMPK activation as previously reported (Scott et al., 2014).

Taken together, these results suggest that AMPfret 2.0 can be used for screening and identification of AMPK direct-activators interacting with the γ -CBS sites

6.2. NAD⁺ putative interaction with AMPK.

Nicotinamide adenine dinucleotides were reported to activate on AMPK activity had been formulated (Rafaeloff-Phail et al., 2004) and even suggested as a direct activator of the kinase. However, several follow-up studies showed that the observed AMPK activation is probably linked to an AMP contamination in the commercial NAD preparation. AMPfret 2.0 was incubated with increasing concentrations of NAD, NADH and NADP and the FRET signal was monitored (Figure 43).

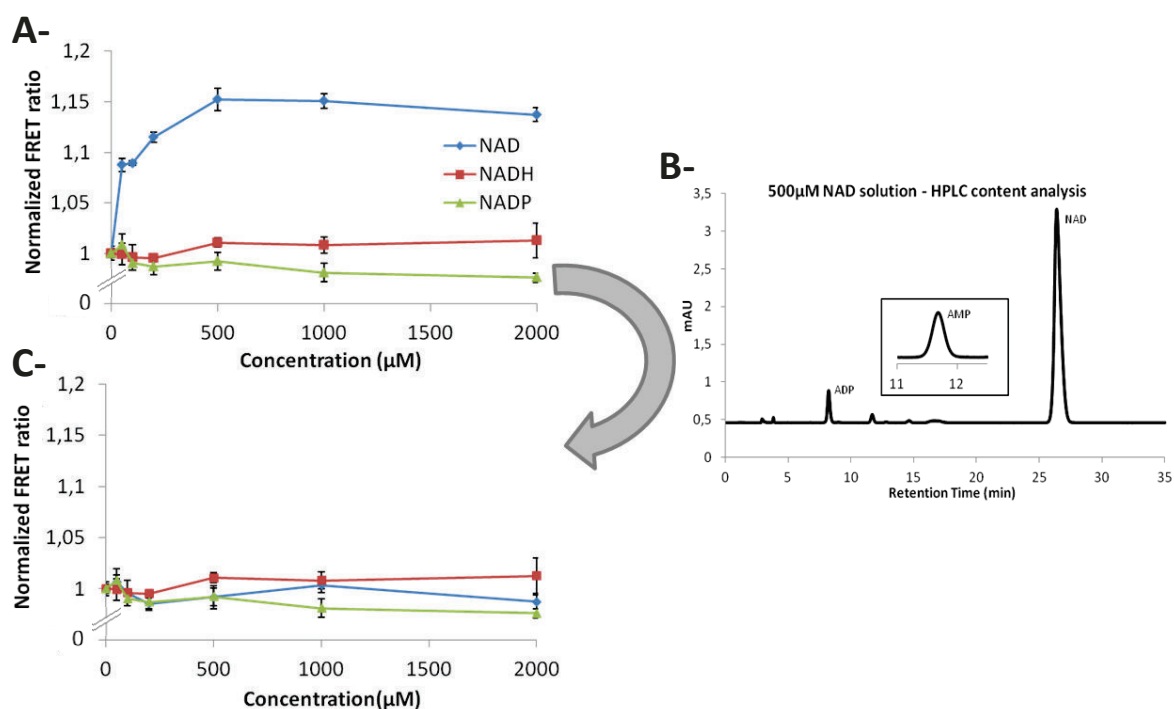


Figure 43: Nicotinamide adenine dinucleotides do not induce changes in FRET ratio.

A- AMPfret 2.0 was incubated with increasing amounts of nicotinamide adenine nucleotides, emission spectra (430 nm excitation) were recorded, and normalized FRET ratios were calculated. NAD: blue; NADH: red and NADPH: green. Mean \pm SEM (n=4). **B-** HPLC analysis of freshly-made 500 μ M NAD solution content on a C-18 column resulted in an elution profile which clearly shows that a 500 μ M NAD solution contains AMP (retention time = 10,9 min). According to a calibration curve, this peak correspond to 12,5 μ M AMP. **C-** The curves in **A-** are re-plotted taking into account the AMP contamination in NAD according to the HPLC analysis. Note that after correction NAD alone (like NADH and NADP) does not induce conformational changes in the AMPFret sensor.

AMPfret was incubated with various amounts of NAD (0 - 500 μ M) and a rise of the FRET ratio was observed. At first glance, unlike NADH and NADP, NAD seems to trigger FRET signal changes similar to AMPK activation reported in earlier studies (Figure 43 A-). Surprisingly,

NADH addition did not lead to FRET signal change despite its highly similar structure. However, HPLC analysis of the NAD solution revealed a considerable amount of AMP contamination (Figure 43 B-). After having quantified the AMP contaminating NAD solutions (12,5 μM AMP in a 500 μM NAD solution), we subtracted the FRET ratio increase signal due to this AMP and re-plotted data (Figure 43 C-), showing that the FRET signal increase was entirely due to AMP contamination.

Like NAD, NADH and NADP addition did not modify the FRET signal and therefore earlier reports supporting that NADH interacts with the γ -subunit could not be confirmed (Xiao et al., 2011). These results obtained using NAD^+ and NADH concentrations NADH above the physiological ones (70 μM and 100 nM respectively (Fjeld et al., 2003; Zhang et al., 2002)) suggest that, in cells neither NAD^+ or NADH may interact with AMPK triggering conformational changes.

These results confirmed that the supposed beneficial effect of NAD on AMPK activity is in fact due to important AMP contamination present in commercially available NAD powder (from Roche in this study) (Figure 43) (Suter et al., 2006). Therefore caution is necessary, e.g. by applying HPLC analysis (Figure 43 B-).

7. AMPfret in cellulo

After having successfully characterized the AMPfret 2.0 response to various adenylate mixes, we decided to investigate how it behaves when transfected into living cells. For this, AMPfret subunits were cloned into vectors of the MultiMam expression system in order to validate its putative application in cells. During this cloning step, the FRET pair was replaced by mseCFP Δ ₁₁/cpVenus (Figure 8) which confers stability of the FRET signal relative to environment variability as existing in cells. This yielded AMPfret 2.1.

7.1. AMPK activation by AICAR

One of the purposes of AMPfret design and construction consisted in the generation of a sensor that could report AMPK allosteric activation as occurring during energetic stress and directly linked to increasing AMP concentration. Addition of AICAR to cells is known to mimic an increase of the AMP/ATP ratio and to lead to allosteric activation, as AICAR is metabolized into ZMP, an AMP analogue and AMPK activator. As a proof of concept, we first validated AMPfret use for *in cellulo* studies through the monitoring of pharmacological activation of AMPK by AICAR.

First we decided to use the AMPfret biosensor in cells under conditions known to allosterically activate AMPK. HeLa and 3T3-L1 cell lines were selected according to the expertise of the laboratory: 3T3-L1 cells may be more sensitive to energetic stress and thus better system to characterize AMPfret. Cells were cultured (see chapter Material & Methods) and transiently transfected with the AMPfret 2.1 coding vector using Lipofectamine 2000 (see chapter Material & Methods). More than 24 hours after the transfection, cells were treated with AICAR (1 mM final) and observed for 1 hour using a Leica TCS SP2 AOBS confocal microscope under controlled temperature and O₂ concentration (37°C and 21% respectively).

Both “signature” spectra from mseCFP Δ ₁₁ and cpVenus were recorded through λ -scans using the Leica confocal software in order to validate transfection and proper cellular expression and processing of the AMPfret 2.1 coding vector. λ -scans record emission spectra through the scanning of fluorescence intensities emitted over a range of wavelength. Then,

AICAR (1 mM final concentration) was added to the medium to allosterically activate AMPfret. The monitoring of this activation was done by exciting the AMPfret 2.1 sensor using the 458 nm laser and by recording emission spectra (λ scans) from 463 nm to 600 nm every 15 min (Figure 44 B-). FRET ratios were quantified from these acquired spectra as before (Figure 44 C-, D-).

First, we visualized that AMPfret 2.1 was well transfected into HeLa and 3T3-L1 cells by recording its typical spectral signature. Transfection was more efficient in HeLa cells (~ 50%) than in 3T3-L1 cells (< 25%). AMPfret 2.1 FRET signal was increasing with time, significantly in HeLa cells, upon AICAR addition. This suggested that AMPfret 2.1 indeed monitored AMPK allosteric activation. According to these measurements, more than half-maximal response was already reached after about 10 min of treatment, and the maximal effect reached after about 30 min (Figure 44 C-, D-). These results also indicated that the FRET signal variations exhibited by AMPfret 2.1 may depend on the cell type used (Figure 44 C-, D-). This concerns the absolute signal, ~ 7% and ~ 10% for HeLa cells and 3T3 cells respectively, but also the variability of the results within the cell population. The later may also be affected by the different cell number taken into account for experiments done with each cell type. Indeed, 3T3-L1 cells have the ability to differentiate from fibroblasts into adipocytes. However, the amplitude of AMPfret response may also be explained by different AMP/ATP ratios at basal conditions in each cell type since our data have to be normalized to $t=0$ of the experiment. Thus, the basal AMP/ATP ratio would condition the AMPfret response range.

As a control experiment, 3T3-L1 cells were separately treated with 1 mM AICAR for different time intervals, lysed and AICAR-activation of AMPK was followed by immunoblotting against the AMPK-specific phosphosite in ACC (Figure 44 E-). The AICAR-dependent activation kinetics of AMPK monitored by Western blot correlated with the AMPfret FRET signal variations recorded under the same conditions (Figure 44 D-).

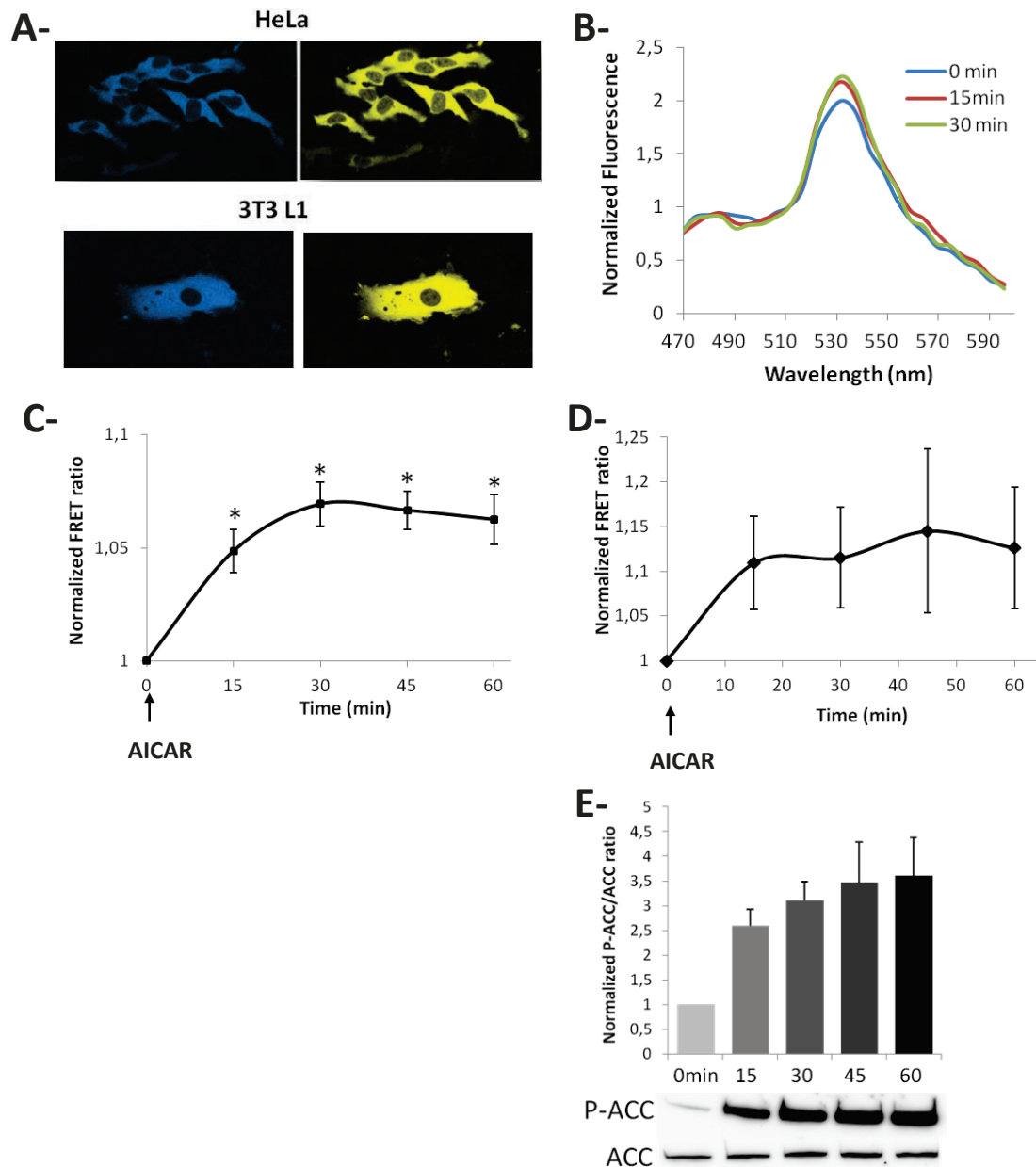


Figure 44: In cellulo studies using AMPfret 2.1.

A – Picture of HeLa (upper panel) and 3T3-L1 (lower panel) cells transfected with AMPfret 2.1 through blue and yellow channels (CFP and YFP respectively). **B** – Fluorescence emission spectra show an increase of the cpVenus peak (527nm) over time after addition of 1mM AICAR (Blue: 0min; red: 15min and green: 30min) in HeLa cells. **C** - **D** - Normalized AMPfret 2.0 FRET signal variation after incubation with 1 mM AICAR of HeLa (**C**-) and 3T3-L1 (**D**-) cells. FRET ratio was normalized to its value at T_0 of AICAR addition ($=1$). FRET ratios were measured on population of individual cells. (HeLa: mean \pm SEM; n=45; 3T3-L1: mean \pm SEM; n=9; * = $p < 0,001$ according to the performed Mann-Whitney Rank Sum Test). Note: FRET variation amplitude is lower than observed *in vitro*; this suggests that AMP is already present at $t=0$ at an amount triggering a FRET change. **E** – Kinetic of AICAR-dependent activation of AMPK was verified in 3T3-L1 cells by western blot (lower panel) and its quantification (upper panel). Data correspond to mean \pm SEM and significance was assessed through a Student-Newman-Keuls test (n=3; * = $p < 0,05$).

As visible on Figure 44 A-, AMPfret 2.1 is present only in the cytosol of both HeLa and 3T3-L1 cells. It has been reported (Viollet et al., 2010) that heterotrimers comprising $\alpha 2$ and $\beta 2$ isoforms have the ability to translocate, especially during hypoxia, into the nucleus notably through the nuclear localization signal – (NLS) sequence present in $\alpha 2$ (and not in $\alpha 1$). This suggested that the existing NLS of $\alpha 2$ could have become inaccessible (e.g. due to the fluorescent protein tags), and that another NLS should be introduced in AMPfret's coding sequence, if monitoring of AMPK allosteric activation in the nucleus is desired.

Taken together, these results showed that AMPfret reports AMPK allosteric activation by the pharmacological activator AICAR in cell lines and also allows for spatiotemporal analysis AMPK activation.

As AMPfret reports conformational changes happening in AMPK structure upon AMP (and ADP) binding independent of AMPK phosphorylation, its readout not only monitors allosteric AMPK activation, but rather the underlying nucleotides fluctuations (increases of AMP and ADP).

7.2. Ischemia-reperfusion

After having validated a preliminary *in cellulo* application of AMPfret when following AICAR-dependent activation of AMPK, we went on to apply AMPfret 2.1 for monitoring endogenous variation of adenylate pools and the allosteric AMPK activation during situations of energy stress such as ischemia-reperfusion.

Using an incubation flow-through chamber fitted to the confocal microscope which permits to control temperature as well as O_2 concentration, HepG2 cells were placed under ischemia-like conditions, comprising hypoxic conditions (2% O_2) and glucose free medium at 37°C. ATP pools may not be affected when hypoxia is applied in a high nutrient containing medium since cells can adapt to hypoxia by switching their energy metabolism through anaerobic pathways to compensate for aerobic ATP production. The deprivation period was followed by 1 hour of reperfusion with complete medium and O_2 (21%). During the 2 hours of the ischemia-reperfusion protocol, the FRET ratio was monitored every minute by recording simultaneously mseCFP $_{\Delta 11}$ and cpVenus fluorescence emitted within 4 nm

windows (corresponding to fluorescence emission) using two independent channels. Images were collected and processed using ImageJ in order to i) remove eventual background fluorescence and ii) isolate individual cells from acquired pictures. Then, we extracted the fluorescence intensities from single cell images using Volocity. Thus, we analyzed the effect of ischemia-reperfusion on the AMPfret 2.1 signal in single cells (Figure 45).

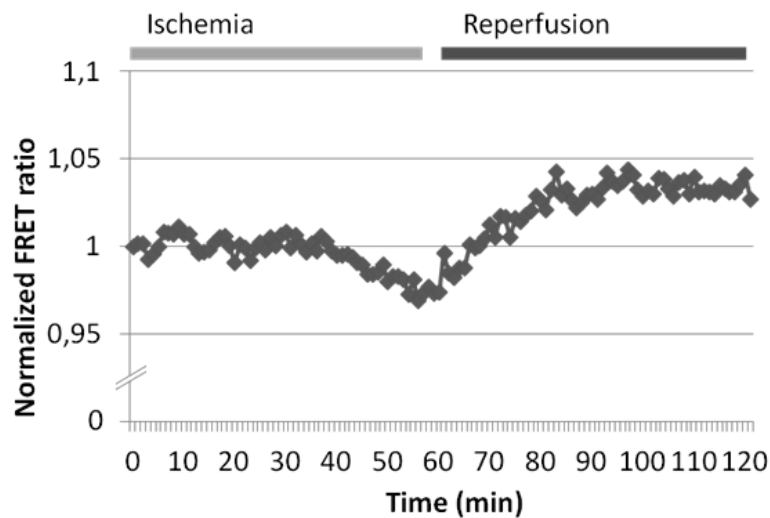


Figure 45: Effect of 1 hour ischemia followed by 1 hour reperfusion on HepG2 cell followed by AMPfret.

AMPfret 2.1 normalized FRET ratio evolution during 1h ischemia (light grey bar) and 1h reperfusion (dark grey bar). Transfected HepG2 cells were cultured on a glass slide mountable onto the incubation flow-through chamber of our Leica TCS SP2 AOBS confocal microscope. At $t=0$, the cell was placed under ischemia-like conditions: hypoxic conditions (2% O_2) and glucose-free medium at 37°C. Deprived medium was previously bubbled with N_2 for at least 10 minutes before its addition onto the cells. After 1hour of deprivation, started the 1 hour-reperfusion period with glucose-rich medium and O_2 (21%). FRET values were record every minute from a single isolated cell using the Leica confocal software. The FRET ratio was followed by recording simultaneously mseCFP Δ 11 (476 nm) and cpVenus (527 nm) fluorescence emitted within 4 nm windows using two independent channels, under excitation set at 458 nm. FRET ratio was normalized to 1 at $t=0$.

During ischemia in HepG2 cells, the FRET signal did not vary. It is unclear whether this indicates a lack of AMP/ATP fluctuation. Changes in AMP/ATP ratio under such conditions were proposed to happen in the liver (Churchill et al., 1994) and AMPK becomes activated, but a recent study suggested that AMPK was activated during ischemia through adenylate-independent pathways (Morrison et al., 2014). Figure 45 shows results of a single cell; globally, the response of the analyzed cell population was heterogeneous (not shown). Also

Tsou et al. observed that AMPK activation could differ from a cell to another when they characterized their AMPK activity reporter (AMPKAR) (Tsou et al., 2011).

During reperfusion of HepG2 cells, the FRET signal increased over the first 30 minutes indicating increased AMP and ADP concentrations. Subsequently, the FRET ratio remained at unchanged high values, suggesting that elevated AMP and ADP concentrations were maintained. In fact, AMPfret should revert the FRET ratio as soon as AMP and ADP levels drop again. These results suggest that in HepG2 cells, reperfusion represented a more drastic energy stress than ischemia regarding adenylate concentrations and AMPK allosteric activation.

Then, we considered the AMPfret 2.1 signal evolution during reperfusion in 3 different HepG2 cells (Figure 46). Again, results showed an increase of the FRET signal during first 30 minutes of reperfusion. However, over the following 30 minutes, the response became heterogeneous, as visible through error bars, with some cells decreasing FRET, while others maintaining it.

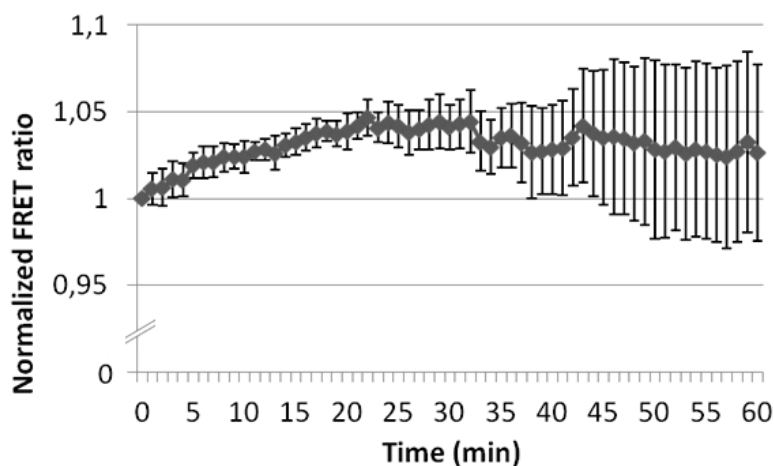


Figure 46: Normalized FRET signal emitted by AMPfret 2.1 during reperfusion.

Data points represent the normalized FRET ratio variation during 1 hour reperfusion after 1 hour of ischemia. Transfected HepG2 cells were cultured on a glass slide mountable onto the incubation flow-through chamber of our Leica TCS SP2 AOBS confocal microscope. At $t=0$, the cells were placed back under 21% O_2 and glucose rich medium conditions at 37°C. FRET values were recorded every minute from 3 single isolated cells using the Leica confocal software. The FRET ratio was followed by recording simultaneously mseCFP Δ 11 (476 nm) and cpVenus (527 nm) fluorescence emitted within 4 nm windows using two independent channels, under excitation set at 458 nm. FRET ratio was normalized to 1 at $t=0$. Data points are mean \pm SEM ($n=3$). Note that the increasing cell-to-cell variability, during the last 30 minutes, is visualized through the increasing size of error bars.

Through these experiments, using AMPfret 2.1 in HepG2 cells, we did not detect any FRET signal changes during ischemia, suggesting that AMP and ADP concentrations remained unchanged. However, we showed in different cells an increase of AMPfret FRET signal during reperfusion, suggesting an elevation of intracellular AMP and ADP and allosteric activation of AMPK. In addition, we showed that this response in the FRET became heterogeneous after 30 minutes of reperfusion. Thus, AMPK allosteric activation seems to be rather transient response of cells to reperfusion during the first 30 minutes, while the response shows high cell to cell variability in the following, as previously reported by Tsou et al., 2011.

To conclude, all these experiments achieved in living cells using AMPfret 2.1 showed that AMPfret 2.1 was properly transfected and its fluorescence monitored over time. In addition, we showed, through AMPK activation by AICAR, that AMPfret 2.1 provides a readout of AMP/ZMP concentrations and AMPK allosteric activation by reporting the related conformational changes. Experiments involving AICAR and particularly ischemia-reperfusion, showed that AMPfret 2.1 can monitor endogenous changes of adenylates and AMPK allosteric activation over time. Monitoring of transient events related to AMPK allosteric activation is promising to decipher or unravel new aspects of its regulation. However, experiments presented here also underline some difficulties. These are mainly: (i) the basal AMP/ATP ratio, which seems to depend on cell type and physiological conditions, and which diminishes the exploitable FRET signal of AMPfret 2.1 that is normally 20%. AMPfret sensors with higher FRET change between 0 and 20 μ M AMP may be necessary. (ii) In response to an endogenous energetic stress, there is intrinsic variability between cells. It remains to be unambiguously shown that this variability is due to different adenylate concentrations, and not to variability of AMPfret under these conditions.

8. References

- Bieniossek, C., Nie, Y., Frey, D., Olieric, N., Schaffitzel, C., Collinson, I., Romier, C., Berger, P., Richmond, T.J., Steinmetz, M.O., et al. (2009). Automated unrestricted multigene recombineering for multiprotein complex production. *Nat. Methods* 6, 447–450.
- Burwinkel, B., Scott, J.W., Bühner, C., van Landeghem, F.K.H., Cox, G.F., Wilson, C.J., Grahame Hardie, D., and Kilimann, M.W. (2005). Fatal congenital heart glycogenosis caused by a recurrent activating R531Q mutation in the gamma 2-subunit of AMP-activated protein kinase (PRKAG2), not by phosphorylase kinase deficiency. *Am. J. Hum. Genet.* 76, 1034–1049.
- Calabrese, M.F., Rajamohan, F., Harris, M.S., Caspers, N.L., Magyar, R., Withka, J.M., Wang, H., Borzilleri, K.A., Sahasrabudhe, P.V., Hoth, L.R., et al. (2014). Structural basis for AMPK activation: natural and synthetic ligands regulate kinase activity from opposite poles by different molecular mechanisms. *Structure* 22, 1161–1172.
- Calabrese, M.F., Rajamohan, F., Harris, M.S., Caspers, N.L., Magyar, R., Withka, J.M., Wang, H., Borzilleri, K.A., Sahasrabudhe, P.V., Hoth, L.R., et al. Structural Basis for AMPK Activation: Natural and Synthetic Ligands Regulate Kinase Activity from Opposite Poles by Different Molecular Mechanisms. *Structure*.
- Chen, L., Wang, J., Zhang, Y.-Y., Yan, S.F., Neumann, D., Schlattner, U., Wang, Z.-X., and Wu, J.-W. (2012). AMP-activated protein kinase undergoes nucleotide-dependent conformational changes. *Nat. Struct. Mol. Biol.* 19, 716–718.
- Chen, L., Xin, F.-J., Wang, J., Hu, J., Zhang, Y.-Y., Wan, S., Cao, L.-S., Lu, C., Li, P., Yan, S.F., et al. (2013). Conserved regulatory elements in AMPK. *Nature* 498, E8–E10.
- Churchill, T.A., Cheetham, K.M., and Fuller, B.J. (1994). Glycolysis and Energy Metabolism in Rat Liver during Warm and Cold Ischemia: Evidence of an Activation of the Regulatory Enzyme Phosphofructokinase. *Cryobiology* 31, 441–452.
- Fjeld, C.C., Birdsong, W.T., and Goodman, R.H. (2003). Differential binding of NAD⁺ and NADH allows the transcriptional corepressor carboxyl-terminal binding protein to serve as a metabolic sensor. *Proc. Natl. Acad. Sci. U. S. A.* 100, 9202–9207.
- Gowans, G.J., Hawley, S.A., Ross, F.A., and Hardie, D.G. (2013). AMP Is a True Physiological Regulator of AMP-Activated Protein Kinase by Both Allosteric Activation and Enhancing Net Phosphorylation. *Cell Metab.* 18, 556–566.
- Haffke, M., Marek, M., Pelosse, M., Diebold, M.-L., Schlattner, U., Berger, I., and Romier, C. (2015). Characterization and production of protein complexes by co-expression in *Escherichia coli*. *Methods Mol. Biol. Clifton NJ* 1261, 63–89.
- Hardie, D.G., Carling, D., and Gamblin, S.J. (2011). AMP-activated protein kinase: also regulated by ADP? *Trends Biochem. Sci.* 36, 470–477.
- Hardie, D.G., Ross, F.A., and Hawley, S.A. (2012). AMP-Activated Protein Kinase: A Target for Drugs both Ancient and Modern. *Chem. Biol.* 19, 1222–1236.
- Hawley, S.A., Ross, F.A., Chevtzoff, C., Green, K.A., Evans, A., Fogarty, S., Towler, M.C., Brown, L.J., Ogunbayo, O.A., Evans, A.M., et al. (2010). Use of cells expressing gamma subunit variants to identify diverse mechanisms of AMPK activation. *Cell Metab.* 11, 554–565.
- Hawley, S.A., Fullerton, M.D., Ross, F.A., Schertzer, J.D., Chevtzoff, C., Walker, K.J., Peggie, M.W., Zibrova, D., Green, K.A., Mustard, K.J., et al. (2012). The ancient drug salicylate directly activates AMP-activated protein kinase. *Science* 336, 918–922.
- Imamura, H., Nhat, K.P.H., Togawa, H., Saito, K., Iino, R., Kato-Yamada, Y., Nagai, T., and Noji, H. (2009). Visualization of ATP levels inside single living cells with fluorescence resonance energy transfer-based genetically encoded indicators. *Proc. Natl. Acad. Sci.* 106, 15651–15656.
- Landgraf, R.R., Goswami, D., Rajamohan, F., Harris, M.S., Calabrese, M.F., Hoth, L.R., Magyar, R., Pascal, B.D., Chalmers, M.J., Busby, S.A., et al. (2013). Activation of AMP-Activated Protein Kinase Revealed by Hydrogen/Deuterium Exchange Mass Spectrometry. *Structure* 21, 1942–1953.

- Li, X., Wang, L., Zhou, X.E., Ke, J., de Waal, P.W., Gu, X., Tan, M.H.E., Wang, D., Wu, D., Xu, H.E., et al. (2014). Structural basis of AMPK regulation by adenine nucleotides and glycogen. *Cell Res.*
- Matsuda, T., Miyawaki, A., and Nagai, T. (2008). Direct measurement of protein dynamics inside cells using a rationally designed photoconvertible protein. *Nat. Methods* 5, 339–345.
- Morrison, A., Chen, L., Wang, J., Zhang, M., Yang, H., Ma, Y., Budanov, A., Lee, J.H., Karin, M., and Li, J. (2014). Sestrin2 promotes LKB1-mediated AMPK activation in the ischemic heart. *FASEB J. Off. Publ. Fed. Am. Soc. Exp. Biol.*
- Nagai, T., Iбата, K., Park, E.S., Kubota, M., Mikoshiba, K., and Miyawaki, A. (2002). A variant of yellow fluorescent protein with fast and efficient maturation for cell-biological applications. *Nat. Biotechnol.* 20, 87–90.
- Nagai, T., Yamada, S., Tominaga, T., Ichikawa, M., and Miyawaki, A. (2004). Expanded dynamic range of fluorescent indicators for Ca(2+) by circularly permuted yellow fluorescent proteins. *Proc. Natl. Acad. Sci. U. S. A.* 101, 10554–10559.
- Oganesyan, N., Ankoudinova, I., Kim, S.-H., and Kim, R. (2007). Effect of Osmotic Stress and Heat Shock in Recombinant Protein Overexpression and Crystallization. *Protein Expr. Purif.* 52, 280–285.
- Rafaeloff-Phail, R., Ding, L., Conner, L., Yeh, W.-K., McClure, D., Guo, H., Emerson, K., and Brooks, H. (2004). Biochemical regulation of mammalian AMP-activated protein kinase activity by NAD and NADH. *J. Biol. Chem.* 279, 52934–52939.
- Riek, U. (2006). Biochemical and biophysical properties of heterotrimeric 5'-AMP-activated protein kinase (AMPK): molecular shape, function and regulation. ETH Zürich.
- Riek, U., Scholz, R., Konarev, P., Rufer, A., Suter, M., Nazabal, A., Ringler, P., Chami, M., Muller, S.A., Neumann, D., et al. (2008). Structural Properties of AMP-activated Protein Kinase: DIMERIZATION, MOLECULAR SHAPE, AND CHANGES UPON LIGAND BINDING. *J. Biol. Chem.* 283, 18331–18343.
- Sanders, M.J., Grondin, P.O., Hegarty, B.D., Snowden, M.A., and Carling, D. (2007). Investigating the mechanism for AMP activation of the AMP-activated protein kinase cascade. *Biochem. J.* 403, 139–148.
- Scott, J.W., Hawley, S.A., Green, K.A., Anis, M., Stewart, G., Scullion, G.A., Norman, D.G., and Hardie, D.G. (2004). CBS domains form energy-sensing modules whose binding of adenosine ligands is disrupted by disease mutations. *J Clin Invest* 113, 274–284.
- Scott, J.W., Ross, F.A., Liu, J.D., and Hardie, D.G. (2007). Regulation of AMP-activated protein kinase by a pseudosubstrate sequence on the γ subunit. *EMBO J.* 26, 806–815.
- Scott, J.W., Ling, N., Issa, S.M.A., Dite, T.A., O'Brien, M.T., Chen, Z.-P., Galic, S., Langendorf, C.G., Steinberg, G.R., Kemp, B.E., et al. (2014). Small Molecule Drug A-769662 and AMP Synergistically Activate Naive AMPK Independent of Upstream Kinase Signaling. *Chem. Biol.*
- Sivaramakrishnan, S., Spink, B.J., Sim, A.Y.L., Doniach, S., and Spudich, J.A. (2008). Dynamic charge interactions create surprising rigidity in the ER/K α -helical protein motif. *Proc. Natl. Acad. Sci.* 105, 13356–13361.
- Stein, S.C., Woods, A., Jones, N.A., Davison, M.D., and Carling, D. (2000). The regulation of AMP-activated protein kinase by phosphorylation. *Biochem. J.* 345 Pt 3, 437–443.
- Studier, F.W. (2005). Protein production by auto-induction in high density shaking cultures. *Protein Expr. Purif.* 41, 207–234.
- Suter, M., Riek, U., Tuerk, R., Schlattner, U., Wallimann, T., and Neumann, D. (2006). Dissecting the Role of 5'-AMP for Allosteric Stimulation, Activation, and Deactivation of AMP-activated Protein Kinase. *J. Biol. Chem.* 281, 32207–32216.
- Townley, R., and Shapiro, L. (2007). Crystal structures of the adenylate sensor from fission yeast AMP-activated protein kinase. *Science* 315, 1726–1729.
- Tsou, P., Zheng, B., Hsu, C.-H., Sasaki, A.T., and Cantley, L.C. (2011). A Fluorescent Reporter of AMPK Activity and Cellular Energy Stress. *Cell Metab.* 13, 476–486.
- Viollet, B., Horman, S., Leclerc, J., Lantier, L., Foretz, M., Billaud, M., Giri, S., and Andreelli, F. (2010). AMPK inhibition in health and disease. *Crit Rev Biochem Mol Biol* 45, 276–295.

- Willemse, M., Janssen, E., Lange, F. de, Wieringa, B., and Fransen, J. (2007). ATP and FRET—a cautionary note. *Nat. Biotechnol.* *25*, 170–172.
- Xiao, B., Heath, R., Saiu, P., Leiper, F.C., Leone, P., Jing, C., Walker, P.A., Haire, L., Eccleston, J.F., Davis, C.T., et al. (2007). Structural basis for AMP binding to mammalian AMP-activated protein kinase. *Nature* *449*, 496–500.
- Xiao, B., Sanders, M.J., Underwood, E., Heath, R., Mayer, F.V., Carmena, D., Jing, C., Walker, P.A., Eccleston, J.F., Haire, L.F., et al. (2011). Structure of mammalian AMPK and its regulation by ADP. *Nature* *472*, 230–233.
- Xiao, B., Sanders, M.J., Carmena, D., Bright, N.J., Haire, L.F., Underwood, E., Patel, B.R., Heath, R.B., Walker, P.A., Hallen, S., et al. (2013). Structural basis of AMPK regulation by small molecule activators. *Nat. Commun.* *4*, 3017.
- Zhang, Q., Piston, D.W., and Goodman, R.H. (2002). Regulation of corepressor function by nuclear NADH. *Science* *295*, 1895–1897.
- Zhang, Y., Wang, Y., Bao, C., Xu, Y., Shen, H., Chen, J., Yan, J., and Chen, Y. (2012). Metformin interacts with AMPK through binding to γ subunit. *Mol. Cell. Biochem.* *368*, 69–76.
- Zhu, L., Chen, L., Zhou, X.-M., Zhang, Y.-Y., Zhang, Y.-J., Zhao, J., Ji, S.-R., Wu, J.-W., and Wu, Y. (2011). Structural Insights into the Architecture and Allostery of Full-Length AMP-Activated Protein Kinase. *Structure* *19*, 515–522.

Discussion

1. AMPfret provides insight into AMP-induced conformational changes.....	221
2. AMPfret also provides insight into ADP-induced conformational changes.....	226
3. Unlike ATP-Mg ²⁺ , free ATP compete with AMP for binding at CBS sites.	226
4. Deciphering AMPK complex regulation with AMPfret.	227
4.1. CBS sites roles	227
4.2. AMPK allosteric activation is not linked to its phosphorylation status.	229
5. AMPfret as a new tool to screen and identify AMPK activators.....	230
6. Preliminary results obtained with AMPfret in cellulose	232
7. Optimization is possible.	235
8. Outlook	236
9. References.....	239

Discussion

Free cytosolic ADP, ATP and AMP concentrations are important parameters of interest when studying energy metabolism (Atkinson, 1968). They represent the energy pool available to supply the metabolism. In contrast, for the measurement of the total amount of adenylates in cell extracts, one has to consider compartmentalized and macromolecular-bound forms of adenylates which are not all available to participate in enzyme reactions in the cytosol. In brief, sensing adenylate pool variations *in cellulo* is in principle the best way to investigate the cellular energy state. Technically, this can be achieved through the use of genetically encoded fluorescent reporters like ATeam (Imamura et al., 2009), Frex (Zhao et al., 2011), peredox (Hung et al., 2011) or AMPfret, presented herein. However, caution has to be taken when working with such FRET reporters of adenylate concentration. It has to be shown that FRET only depends on the change in adenylate concentrations, in particular in cells *in vivo*, and that, *in vitro*, spontaneous ATP hydrolysis does not affect the measurement. The latter requires pH buffering and evaluation of ATP hydrolysis products (ADP, AMP) by HPLC.

1. AMPfret provides insight into AMP-induced conformational changes

AMPfret was designed to be a reporter of AMPK allosteric activation. AMPK is primarily activated in a systemic manner by upstream kinases, but its maximal degree of activity is achieved due to a rise of AMP and ADP in cells, which can be mimicked by pharmacological small activators like AICAR. Such a probe for the allosteric activation of AMPK may be considered as promising for the identification of new AMPK activators. In order to create AMPfret, we decided to choose an AMPK subunit isoform combination presenting the highest response to AMP-dependent allosteric activation: $\alpha 2\beta 2\gamma 1$ (Sanders et al., 2007).

After a first round of AMPfret construct generation, which positioned the FRET pair randomly through a matrix approach at all termini of the AMPK heterotrimer, we identified two positive constructs that exhibited AMP-dependent FRET changes, AMPfret A and C, the latter further characterized as AMPfret 1.0. Characterization of these AMPfret constructs led to the confirmation that the monitored FRET change triggered by AMP indeed correlated with to AMP-dependent allosteric activation of AMPK.

The fact that the two generations of AMPfret constructs (based on the initial constructs C and A) are tagged on the $\alpha 2$ C-terminus and either $\beta 2$ - or $\gamma 1$ - C-terminus, respectively, implies that these termini are moving relatively to each other upon AMP binding. Such changes in distance between α -C-terminus and β - or γ -C-terminus during AMP-induced allosteric activation is also supported by data of Landgraf et al. using hydrogen/deuterium exchange (Landgraf et al., 2013). This study is one of the few (together with SAXS measurements, Riek et al., 2008) that were interested in conformational changes that occur in full length AMPK heterotrimer in solution. Most structural studies on AMPK used truncated AMPK, crystallized or fixed on EM grids (Chen et al., 2012; Zhu et al., 2011). Landgraf et al. observed variations in the α -subunit in the accessibility for hydrogen/deuterium exchange upon AMP allosteric activation, but not particularly in the C-terminus. The observed changes were mainly located at the level of the active site, confirming that the allosteric activation triggers a reorganization of the active site. With the 221 heterotrimer, singular changes at the level of the $\beta 2$ C-terminus were observed upon AMP activation (Landgraf et al., 2013). This agrees with our data on the AMPfret A construct. The H/D exchange study also reported movements at the level of the $\gamma 1$ C-terminus, more important when $\gamma 1$ was in the context of the AMPK 221 heterotrimer as compared to other isoform combinations ($\alpha 1\beta 1\gamma 1$).

Surprisingly, no construct, in which the $\beta 2$ - and $\gamma 1$ -subunit pair was labeled, showed significant FRET signal variation when incubated with AMP, suggesting that these subunits do not move significantly relatively to each other. It can be that structural rearrangements linked to AMP binding occur mainly at the level of the core of β - and γ - subunits and not at the termini (Li et al., 2014). In this case, FRET fluorophores positioned at the termini would not report any significant structural variations. Another explanation would be that tagged termini are moving in the same direction, such that our sensor would not report this because the distance between FRET fluorophores remains constant. Such a hypothesis would favor a model in which β - and γ -subunits are moving as an entity relative to the α -C-terminus.

AMPfret contains full length AMPK and, despite the addition of fluorescent tags, we showed that the biosensor retains native properties of AMPK WT. Presence of the fluorescent proteins may have altered the attributes of the kinase but AMPfret conserves kinase activity and affinities for adenylates of AMPK WT. Nucleotides exchange occurring as in AMPK WT

makes AMPfret FRET signal readily reversible. In addition, similarly to AMPK, AMPfret is allosterically activated by AMP and protected from dephosphorylation by ADP.

Figure 1 represents a conceptual detailed diagram explaining the relationship between nucleotide concentration and FRET, as well as the different forms of AMPK activation. The readily-reversible FRET signal, triggered by the exchange of nucleotide, can be followed using AMPfret being phosphorylated or not. Under a non-phosphorylated form, AMPfret reports transitions between conformations varying in their ability to be phosphorylated and dephosphorylated. When phosphorylated, AMPfret gives a readout of allosteric activation which corresponds to the conformational state having the maximal activity in addition of being protected by dephosphorylation.

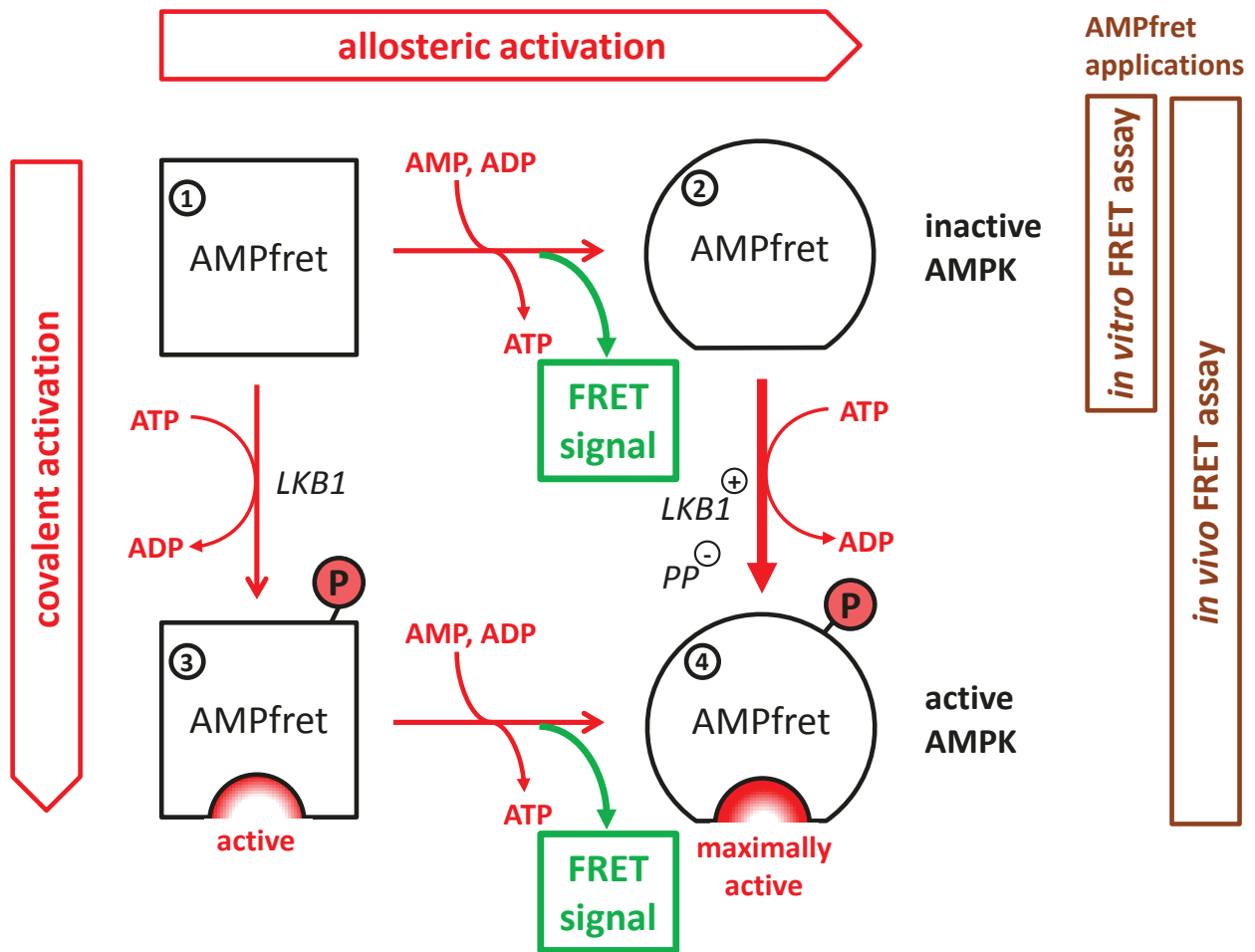


Figure 1: Relationship between nucleotide (AMP, ADP) concentrations and FRET, as well as the different forms of AMPK activation.

AMPfret reports conformational changes induced by AMP and ADP binding (green box). These changes can happen within AMPK being covalently activated (3 to 4) or not (1 to 2). AMPfret is represented as a square when bound to ATP (1 and 3) and as a circle when bound to AMP and/or ADP (2 and 4). Binding of AMP and ADP promotes the covalent activation through phosphorylation by upstream kinases (LKB1) and also the protection from dephosphorylation by phosphatases (PP) (2 to 4). Phosphorylation yielding covalently activated AMPfret is depicted (P) (3 and 4). Note that only AMP triggers allosteric activation of AMPfret, yielding maximally activated AMPfret (4) and that every step is reversible, i.e. FRET signal is also generated when AMPfret returns to conformations 1 or 3. *In vitro*, AMPfret can be used under its non-phosphorylated form to study the nucleotide-dependent conformational changes. AMPfret signal *in vivo* is a readout of conformational changes happening prior (1 to 2) or after (3 to 4) the phosphorylation by AMPKK.

Having at our disposal a reporter of AMP-dependent conformational changes, which are at the origin of AMP-triggered allosteric activation of AMPK and ADP-triggered protection of

dephosphorylation, without using ATP, it became possible for the first time to characterize this type of regulation of AMPK. The affinity constant of AMP was calculated.

According to the monitored FRET changes as a function of AMP concentration, binding of AMP occurs at one or several binding sites having the same affinity. However, at the given precision of the FRET data, we cannot exclude two binding sites with slightly different affinities. Indeed, AMPK can bind AMP at the level of two different exchangeable CBS sites (Hardie et al., 2012a). However AMP concentration range fluctuation *in vivo* is included in the tested range. The calculated affinity for AMP of 1.5 μM is well in the expected range estimated for AMPK, and the binding curve covering 0 to 20 μM covers the range of physiological fluctuations of AMP concentration. *In vivo*, competition with free ATP would shift half-maximal binding and the entire binding curve to higher concentrations, as seen in the kinase activity assays.

Thus AMPfret is indeed providing for the first time a readout of AMPK allosteric activation independently of other adenylates present. Until now, the only way to follow AMPK allosteric activation involved kinase activity measurements that require ATP and produce ADP and AMP (Davies et al., 1989) thus perturbing measurements of allosteric activation. We showed that the AMP-dependent FRET changes correlate with AMP-induced allosteric activation of AMPK. Differences observed here are explained by the mentioned presence of different adenylates. In particular due to ATP contamination by AMP, activity measured through the phosphorylation of ACC could be achieved at 0 μM AMP. In addition, this experiment confirmed that AMPfret retains the native kinase activity of AMPK (Frederich and Balschi, 2002). Indeed, Frederich and Balschi calculated $A_{0.5} = 1.8 \mu\text{M}$ for AMP on AMPK activity using cytosolic extracts containing at least 0.2 μM AMP. We obtained a very similar value from the FRET ratio measurements (1.5 - 1.8 μM). Importantly, AMPfret allowed to examine specifically the effect of single nucleotides on AMPK allosteric activation.

2. AMPfret also provides insight into ADP-induced conformational changes.

AMPfret reported conformational changes not only for AMP but also for ADP. Such ADP-related movements in AMPK were not observed so far by any structural study. They support the general model that AMPK senses AMP/ATP and also ADP/ATP ratio.

ADP does not directly activate AMPK but acts through protection of AMPK from dephosphorylation (Gowans et al., 2013). Our results support the latter model in which binding of ADP to the γ -subunit protects AMPK from dephosphorylation, thus keeping it activated. Indeed ADP is the first signal emerging in cells when the balance between ATP synthesis and its consumption is disrupted. When ATP is consumed, ADP concentration increases immediately. However, if the ATP deficit increases, ADP is consumed through the adenylate kinase (AK) reaction to form ATP and AMP, a reaction used by cells to quickly and transiently restore ATP (Noda, 1973). Thus AMPK may respond sequentially to ADP and AMP. Our results strongly support such a concept, since ADP binding to AMPK, like AMP, triggers conformational changes. A single affinity binding site was calculated for ADP, similar to AMP, and binding to the γ -subunit was shown to yield protection against dephosphorylation of the Thr172. Since ADP does not allosterically activate AMPK, AMP- and ADP-dependent conformational changes have to differ in nature within the whole AMPK heterotrimer, at least partially.

Taken together, results obtained with AMPfret in presence of AMP or ADP showed that AMPfret represents a powerful and easy-to-use tool to decipher activation mechanisms of AMPK. As previously mentioned AMPfret allows to study AMPK regulation mechanisms independently of any kinase activity readout permitting to work with individual nucleotides.

3. Unlike ATP-Mg²⁺, free ATP compete with AMP for binding at CBS sites.

ATP is present in the cell mainly bound to magnesium, and kinases use ATP under its Mg²⁺-complexed form as co-substrate. However, it was suggested that free ATP which is present in cells at a much lower concentration than ATP-Mg²⁺ could be a competitor of AMP in the cell (Hardie et al., 2012b; Townley and Shapiro, 2007; Xiao et al., 2007). For the first time, results

from the present study provide strong evidence showing that only free ATP competes with AMP for binding to AMPK and thus regulates its activity. Such observations support a new role for free ATP in cell signaling. With AMPfret we succeeded in examining the effect the different forms of ATP (bound vs. free) on AMPK activity showing that free ATP, but not ATP complexed to magnesium, competes with AMP to bind AMPK. ATP-Mg²⁺ represents the major part of ATP, when ATP is incubated with excess of Mg²⁺ at physiological pH (~ 90%) (Storer and Cornish-Bowden, 1976), as it should be in cells. Thus, free ATP is present at micromolar concentration.

A role of free ATP has been postulated before (Hardie et al., 2012b; Townley and Shapiro, 2007; Xiao et al., 2007) but never proven. Our findings suggest the need to precisely analyze adenylates but also magnesium concentrations when studying AMPK regulation mechanisms.

4. Deciphering AMPK complex regulation with AMPfret.

4.1. CBS sites roles

AMPfret represents a new readout of AMPK allosteric activation that does not require the use of ATP. It thus allows to analyze the binding of the single type of nucleotide and its effect on AMPK conformation. To study mechanisms of AMPK allosteric activation, CBS site mutants of AMPfret were generated.

CBS site 1 and CBS site 3 were identified as responsible for the AMP-dependent allosteric activation. The CBS site 3 appeared as the crucial one for allosteric activation and also protection from dephosphorylation. This is supported by mutational (Chen et al., 2012) and structural studies (Calabrese et al.; Xiao et al., 2013), in particular the crystallographic structure showing that CBS site 3 is in contact with two other subunits that is, α -hook and the β subunit, but also by naturally occurring γ -subunit mutants involved in cardiac pathologies (e.g. R531G/Q) (Burwinkel et al., 2005; Scott et al., 2004). Mutations at CBS site 1 do not abolish AMP effects, but shift the AMPK allosteric activation to higher AMP concentrations. This supports a model in which the overall conformational changes are mediated by CBS site 1 (Chen et al., 2013; Li et al., 2014) but require the binding of AMP at

CBS site 3 for full allosteric activation. We postulate that AMPK allosteric activation with increasing AMP concentrations begins by the binding of AMP at CBS site 3, but that the conformational changes require additional binding of AMP to CBS site 1.

Using AMPfret we also showed that ADP have the ability to protect P-Thr172 against dephosphorylation (Gowans et al., 2013) by PP2C α , suggesting that the mechanism requires AMP or ADP binding at the same site. Again CBS site 3 was identified as the site essential to trigger conformational changes leading to protection from dephosphorylation, while CBS site 1 seems to have no role in this type of activation.

In our hands, also mutation of Ser315 at the level of CBS site 4 abolished the ADP-induced conformational changes. This result first appeared surprising because CBS site 4 has been reported as being a non-exchangeable AMP-binding site. However, the ADP-induced conformational changes may require an adenylate-bound CBS site 4. In recombinant protein as used here, site 4 is normally to a large degree (> 50%) occupied by AMP (or ADP). Mutation of this site eliminates this binding, and this apparently does not disturb the AMP-dependent conformational changes and the allosteric activation via site 3 (and site 1). However, the ADP-dependent conformational changes may require an occupied site 4, without this site necessarily being an exchangeable site. That site 4 may even exchange adenylates, although under particular conditions, has been demonstrated (Chen et al., 2012). Alternatively, replacement of Ser315 by a proline may disorganize the CBS site tandem (site 3+4), interfering specifically with binding of ADP at CBS site 3. However, this is less likely, since AMP effects are not changed by this mutation. Further mutations at CBS site 4 should be realized to clarify the function of this site.

Our data suggested that AMP- and ADP- dependent conformational changes are different: each is involving a specific set of CBS sites. However, AMPfret may present limitations to solve this question unequivocally. Co-crystallization of the full-length heterotrimer in presence of AMP or ADP or the use of an optimized version of AMPfret with greater FRET variation magnitude will be very informative in this respect. Next generation of AMPfret sensors will be able to report more precisely the nature of movements occurring during allosteric activation and protection from dephosphorylation.

4.2. Conformational changes do not require phosphorylation.

As previously mentioned, allosteric activation of AMPK can be studied using AMPfret while avoiding AMPK kinase activity measurements. Thus, using the AMPfret sensor, we were able to evaluate the impact of AMPK phosphorylation status on conformational changes leading to allosteric activation.

During the characterization of AMPfret, it was shown that AMP-dependent conformational changes correlate with AMP-induced allosteric activation. This supports the AMPK activation model suggested by us (Riek et al., 2008) and others, proposing that AMP binding at the γ -subunit resulted in conformational changes in the whole heterotrimer, leading to the allosteric activation of AMPK most probably due to a final rearrangement of the kinase domain. Recent studies (Scott et al., 2014) showed that AMPK can be activated by combined use of AMP and A-769662, but not AMP alone, independently of covalent activation by upstream kinases. This supports the presence of independent mechanisms that can synergistically cooperate to activate AMPK. In AMPfret, Thr172 phosphorylation status has no influence on AMP-dependent conformational changes. Movements occurring in the heterotrimer upon AMP binding do not require AMPK phosphorylation, suggesting that AMP-allosteric activation may in principle happen independently. As AMP alone does not activate non phosphorylated AMPK, Thr172 phosphorylation triggers some conformational changes at the active site necessary for activation. In cases where activation occurs without phosphorylation, the second allosteric site at the α/β interface may trigger these changes. Thus, AMPK may be quickly and transiently activated only by AMP plus a ligand that binds at the α/β interface, bypassing the upstream kinases signaling.

These findings add a new layer of complexity to AMPK activation regulation. Although allosteric and covalent activation mechanisms could occur independently, they are generally tightly connected. Indeed, the γ -subunit nucleotide binding status (to AMP, ADP or ATP) has an essential role in modulating the phosphorylation status of Thr172. Possibly, an primary/ancestral role of AMPK in multicellular organisms consisted in restoring a “healthy” energetic status in the cell by sensing nucleotide availability. Then, during evolution, AMPK signal input was extended as AMPK activation became linked to several other upstream pathways, including those linked to upstream kinases, and extracellular signals like endocrine

signaling etc. It was proposed that ancestral AMPK functions consisted in sensing the carbon source availability as it is the case in yeast (Celenza and Carlson, 1986; Hardie et al., 2011) and present day AMPK may have preserved different ancestral functions.

For pharmacological approaches, AMPK activity may be modulated through the use of combined drugs interacting with AMPK (allosteric activators or inhibitors) without consideration about its phosphorylation state. Since nucleotide-based drugs would affect all types of nucleotide regulated processes, efforts are required to identify more specific AMPK modulators (acting through the α/β binding site).

AMPfret represents a new *in vitro* tool to decipher AMPK complex regulation mechanism and beyond. We were able to gain new insight into regulation by adenylates (role of CBS sites, AMP-induced conformational changes independent of phosphorylation status) by studying the effect of single nucleotides on AMPK allosteric activation. It can be envisaged to extend analysis now to the effect of other nucleotides such as GMP or GTP. Do they also bind AMPK on γ -subunit? Does GMP have the ability to compete with AMP for allosteric activation?

5. AMPfret as a new tool to screen and identify AMPK activators.

Very few AMPK activity modulators are available, given its key regulating role in energy metabolism, and the related metabolic diseases that affect millions of humans (type 2 diabetes, obesity and others) (Viollet et al., 2009). One application AMPfret was designed for consists in the screening of AMPK direct activators. AMPfret reports by simple fluorescence changes the direct binding of a molecule to AMPK. Indirect activators of AMPK, as expected, do not trigger AMPfret signal changes. Metformin was recently claimed to interact with gamma subunit (Zhang et al., 2012) but our results confirm that Metformin activates AMPK through an indirect mechanism. AMPfret versions based on the initial constructs A and C allowed the identification of activators binding AMPK at the level of its γ -CBS sites, AMP and ZMP. However, A-769662 did not result in a modified FRET signal. The binding site of synthetic ligands, such as the A-769662 compound, was recently identified at the α/β interface and it was proposed that its attachment triggers conformational changes, i.e. the

capping of the α -KD by the β -CBM (Calabrese et al., 2014; Li et al., 2014; Xiao et al., 2013). AMPfret may not be suitable, in principle, for monitoring conformational changes related to the attachment of A-769662 to AMPK. Heterotrimers containing β 2 isoform may also have too low affinity for A-769662. Recent studies indicate that different activators may act synergistically to activate AMPK. This suggests that AMP-bound AMPfret may be used to monitor the attachment of synthetic ligands at the α/β interface. These data reveal different binding sites for AMP and A-769662 (Calabrese et al., 2014; Xiao et al., 2013) and activation modes that can occur independently or with synergistic effects on AMPK activity (Ducommun et al., 2014; Scott et al., 2014). Indeed, in our study, in presence of AMP, A-769662 induced an additional FRET signal despite that A-769669 was proposed to interact preferably with β 1 subunit isoform (Ducommun et al., 2014; Sanders et al., 2007). Our data are consistent with a higher affinity of A-769669 for β 1 as compared to β 2 (Scott et al., 2008). Alternatively to using AMP-bound AMPfret, other AMPfret constructs may be more sensitive to conformational changes induced by synthetic ligands binding at the α/β -site. The original constructs A-L can be re-screened with such ligands, and new constructs can be generated containing β 1 subunit, having higher affinity to at least A-769662. Both approaches are currently on going.

These preliminary results showed that AMPfret is a promising tool for AMPK activator screening. As compared to other screening tools, a method targeting allosteric activation only is particularly relevant in the light of recent work from Scott et al. (Scott et al., 2014). They showed that AMPK can be entirely activated allosterically by combining AMP and A-769669, independently of phosphorylation by upstream kinases. Thus, AMPK covalent activation can be bypassed through the combined use of ligands, opening the possibility to manipulate AMPK activation entirely by directly binding pharmacological ligands.

AMPfret not only contains AMPK subunits but also fluorescent proteins. As a control, the affinity that a positively identified moiety may have for fluorescent proteins and the potential effect on FRET has to be tested. Such effects can be investigated using a FRET construct in which donor and acceptor are connected through only a small linker. Such construct (CFP-linker-YFP) was produced during the presented work, containing a TEV cleavage site in the linker to shut down the FRET signal by proteolytic cleavage.

To summarize, based on AMPK ability to undergo conformational changes depending on relative adenylates concentration (sensing of adenylates), AMPfret was developed as a reporter of these structural changes through FRET. Because AMPfret conserves AMPK native features, it represents a promising tool to screen and identify AMPK direct activators that specifically attach to the γ -CBS adenylate binding sites and possibly also to the novel α/β -site.

6. Preliminary results obtained with AMPfret in cellulo

Using AMPfret sensor *in cellulo*, were produced preliminary data supporting that the developed sensor would be suitable to monitor the allosteric activation of AMPK and the energy status of a living cell. Despite various transfection efficiencies, AMPfret was successfully transfected in HeLa, 3T3-L1 and HepG2 cell lines and the spectral signature of AMPfret (carrying CFP and YFP variants) could be detected.

We showed that AMPfret permits the monitoring of AMPK activation by AICAR in HeLa and 3T3-L1 cells. Once imported into the cytoplasm, AICAR is converted into ZMP, an AMP analog that allosterically activates AMPK. Our results thus validate AMPfret as a FRET reporter for AMPK allosteric activation. Tsou et al., using their AMPK activity reporter (AMPKAR) observed maximal AICAR effect on AMPK after around 1h (Tsou et al., 2011). Possibly, AMPfret-reported conformational changes occur more rapidly than the AMPK activity monitored by AMPKAR, an artificial AMPK substrate which carries a phosphorylation-motif for AMPK. In this case, AMPfret would allow the monitoring of the allosteric activation of AMPK in a more direct manner than AMPKAR. In addition, AMPfret would have the advantage of monitoring transient events, since the FRET signal readily reverts when AMP declines, while AMPK substrates remain phosphorylated for an undetermined period.

After this proof of principle, that AMPfret can detect AMP and report AMPK allosteric activation, we analyzed a physiological energy stress such as ischemia-reperfusion. Ischemia-reperfusion injury is a pathophysiological event causing tissue injury through complex and not entirely understood mechanisms. During ischemia (1h at 2 % O₂), we did not observe any increase in the FRET signal exhibited by AMPfret. Similar results were obtained by Mungai et

al. when they measured adenylate concentrations in 143B osteosarcoma cells under hypoxia (2% O₂) (Mungai et al., 2011). They showed, in contrast to previously proposed models, that AMPK was not activated by accumulation of AMP during hypoxia, since no changes in adenylate concentrations occurred ([AMP], [ADP] and [ATP]). AMPK was activated during hypoxia, but probably through an adenylate-independent mechanism that rather involves ROS signaling, calcium release from ER and extracellular stores, CamKK β activation and finally the covalent activation of AMPK.

In our hands AMPfret did not show FRET signal variation over 1 hour of ischemia, suggesting that AMPK is not activated allosterically when cells are cultured with 2% O₂. However, true ischemia consisting of nutrient deprivation combined with hypoxia activated AMPK in different models (Baron et al., 2005; Lopaschuk, 2008), probably not only due to covalent activation by AMPKK, since other studies have reported increased nucleotide-monophosphate concentrations (Chouchani et al., 2014; Onodera et al., 1986). However, as raised by Lopaschuk, elucidating the role of AMP in the control of AMPK is hampered by the complexity of accurately measuring cytoplasmic AMP concentration (Lopaschuk, 2008).

According to our observation, it may be that the rich medium (5 mg/mL glucose) was not properly exchanged by the depleted one when using the syringes linked to the flow-through chamber, allowing the cells to maintain adenylates at concentrations that do not trigger AMPK allosteric activation. In addition, discrepancy between the literature and our results may be explained by the cell type used. Most studies were carried on cardiac cells and tissue whereas we used hepatic cell lines. Heart disposes of very little energy reserves (Lopaschuk, 2008) and developed specific mechanisms to maintain energy homeostasis. Finally, in tissue, it has been shown that ischemia triggers pH decrease that in turn activates AMPK (Ponticos et al., 1998), although this might not be observed when working with cells cultured in pH buffered medium.

At reperfusion, complete medium was added onto the cells and O₂ was restored to 21 %. We observed an increase of the FRET ratio of AMPfret during the first 30 minutes as a common feature between tested cells, suggesting a rise in the AMP/ATP ratio. This is consistent with known damage occurring during reperfusion, especially at the level of the respiratory chain in mitochondria due to a sudden burst of reactive oxygen species (Chouchani et al., 2014). It

has been reported in the heart, that the most important damage due to ischemia-reperfusion occurs at reperfusion (Verma et al., 2002). Bolli et al. showed that potent oxidant radicals, such as superoxide anion and hydroxyl radical, are produced within the first few minutes of reflow and play a crucial role in the reperfusion injury (Bolli et al., 1989). Our results, showing a quasi-immediate FRET increase at reperfusion, support a parallel allosteric activation of AMPK due to such burst of reactive oxygen species and their detrimental effect on the ATP/AMP ratio. Transient activation of AMPK at reperfusion was already observed (Paiva et al., 2010), although the underlying mechanism (covalent and allosteric activation of AMPK) remained unknown. Here, our AMPfret data provide additional insight.

The FRET-response monitored at reperfusion, through FRET increase, shows higher cell-to-cell variability the longer reperfusion goes on. This reveals, at least in certain cells, a transient AMPK response detected by AMPfret. Does this mean that the cellular energy state starts to be restored within less than 1hour? Does activation of AMPK at reperfusion re-orient the cellular metabolism toward apoptosis (Kefas et al., 2003)? AMPK allosteric activation due to reperfusion may indeed last length less than 1 hour in some cells, supporting that either the ATP/AMP ratio was restored or that apoptosis-oriented pathways are already engaged. However, Kefas et al. observed AICAR-induced apoptosis on MIN6 cells after a longer time span than 30 minutes. In contrast, in cardiac cells, AMPK activation was linked to protection against apoptosis (Shibata et al., 2005). Thus, more investigations have to be done to better characterize the AMPK response to ischemia-reperfusion and its consequences on the cellular metabolism, using AMPfret as a tool.

Some limitations of AMPfret for cellular applications have to be mentioned. AMPfret was characterized *in vitro* as reporting AMP- but also ADP-induced conformational changes. Thus, AMPfret reports not exclusively AMPK allosteric activation but also ADP-dependent protection against dephosphorylation. However, both activation mechanisms are directly linked to ATP depletion (rise of AMP and ADP concentrations), and thus AMPfret is indeed a biosensor for energy stress. Further, the 20% difference in the FRET signal exhibited by AMPfret 2.0 *in vitro* may be insufficient for observations in cells under a physiological stress. Cells already have a baseline level of ADP and AMP that leads to a baseline FRET signal, with less than 20% increase left for the physiological response. Thus, the basal AMP/ATP (and ADP/ATP) ratio would condition the AMPfret response range.

7. Optimization is possible.

The range of the FRET change occurring during a full conformational switch may be increased by optimization through molecular engineering. During the present work, we have already proved that optimization of biosensor parameters is possible: i) insertion of a putative small α -helix linker between the α -subunit and CFP increased the FRET ratio by $\sim 100\%$ and ii) the sensitivity of AMPfret to undesired environment fluctuations such as pH was reduced by exchanging the FRET pair iii) affinities for nucleotides were tuned by site directed mutagenesis. An advantage of protein-based biosensors is that in principle any parameter can be fine-tuned by molecular engineering.

Obviously, optimization of AMPfret to improve the FRET range should be pursued. Despite limitations of the current versions of AMPfret, it has proven suitable for most experiments in this study, and further optimization by molecular engineering may correct its present defaults. A further increase of the FRET range could be achieved through additional deletions/insertions within the AMPK sequence based on recently published “quasi-full-length” crystal structures (Calabrese et al., 2014; Xiao et al., 2013). The engineering strategy for the linker could also be examined again. Additionally, FP could be inserted somewhere within the structure of the 3 subunits of AMPK under the condition that they do not alter proper folding (e.g. flexible loop). Several existing biosensors were engineered in respect to their affinities for the detected ligand and although the AMPfret biosensor could also be tuned for different adenylates out strategy has been to preserve the native affinities. However AMPfret could be optimized toward a version which specifically reports AMP-induced conformational changes and vice versa concerning ADP-related ones. Other mutations may further reduce the pH sensitivity (Hung et al., 2011).

Through a mutational approach, we generated AMPfret derivatives that cannot be phosphorylated anymore or that have their affinities for adenylates abolished at specific CBS site. AMPfret CBS site 3 mutants can serve as negative control during *in cellulo* experiments.

The result of optimization attempts is difficult to predict. For example the benefits linked to α -helix linker insertion on FRET variation amplitude were not observed when inserted in AMPfret 1.0, only in AMPfret 2.0. There are several explanations: (i) the rigid α -helix brings CFP closer to YFP during AMP-dependent FRET changes, only in the case of AMPfret 2.0, (ii) it

might rather trigger the orientation of CFP relative to YFP, more favorable for FRET only in the case of AMPfret 2.0, (iii) possibly the α -helix, due to its length and its rigidity, amplifies the conformational changes occurring in AMPK upon AMP binding: CFP is moving with a greater range than previously. Numerous optimizations applied to existing biosensors are presented in chapter 2.

8. Outlook

Optimizations can be envisaged for different properties of the genetically encoded biosensor: at the level of its fluorescent tags or its recognition element. In the case of AMPfret the recognition element consists in full length AMPK and thus retains all its native properties. Molecular engineering can be applied to report the binding of synthetic ligand at the α/β interface, to sense the two distinct mechanisms through which AMPK can be allosterically activated by two classes small molecules: the synthetic compounds A-769662 and its analogues (e.g. 991 compound), or AMP and its analogues (Ducommun et al., 2014; Scott et al., 2014). Synthetic ligands were shown to bind at the interface of the α - subunit kinase domain (KD) and the carbohydrate binding module (CBM) of β -subunit. As the CBM module is followed in the sequence by a long unfolded stretch it has been proposed that this domain may be highly mobile regarding to the heterotrimer (Calabrese et al., 2014; Xiao et al., 2013). Mechanistically, it has been postulated that it may exist equilibrium between the free- or “flying”- form of the CBM module and its α -KD bound form which can be shifted through the KD-attached form in presence of synthetic ligands (Li et al., 2014). This model is supported by evidence which showed that A-769662 mediates and helps the α - and β -subunits to come closer (Li et al., 2014; Calabrese et al., 2014; Xiao et al., 2013). Such putative great conformational changes of the CBM should be exploitable for a new version of AMPfret that specifically reports AMPK activation by synthetic ligands. Ultimately, by positioning specifically the FRET pair, various versions of AMPfret could be obtained, dedicated to the monitoring of particular AMPK activation modes. Indeed, the current versions of AMPfret (1.0 and 2.0) would provide a readout of AMP-induced conformational changes and another version fluorescently tagged in a different way could be a specific indicators of A-769662 (and analogues)-binding and of the subsequent activation. Such

versions of AMPfret, reporting the attachment of synthetic ligand at the α/β interface, are actually under construct and investigation. As synthetic ligands preferentially activates β 1-containing complex (Scott et al., 2008), we are currently studying the response of β 1-containing AMPfret constructs. Again, movements going along with synthetic ligand-dependent allosteric activation are not fully characterized, thus we are working with AMPfret comprising β 1-fluorescently tagged but also other combinations. Recently, a new molecule activating AMPK similarly than A-769662 but with greater affinity, was identified (Xiao et al., 2013). This compound, 991, shows so high affinities for AMPK that even β 2-containing complex are activated at rather low concentration of the activator. Therefore, AMPfret candidate constructs will be screened using such compound in order to identify one that positively responds. According to its great efficiency to activate all AMPK heterotrimers, the 991 compound will also be used to test pre-existing constructs (AMPfret A-L).

AMPfret has proven suitable for deciphering mechanisms of AMPK activation. However these mechanisms remain not fully elucidated and AMPfret would further lead to better understand them. The generated CBS site mutants will be used soon to explore the mechanism of AMP-dependent protection from phosphorylation. In addition, the recently identified synergistic activation of AMPK, occurring when both AMP and synthetic ligands are combined, could also be examined with a construct reporting synthetic ligand binding.

A-769662 compound preferentially binds and activates β 1-containing complex (Scott et al., 2008), underlining different specificities each combinational-isoforms-heterotrimer may have. As presented in the introduction (chapter 1), AMPK is differentially distributed among tissues and cell type depending on its isoform combination. By switching the subunits isoforms within AMPfret it can be imagined to dispose of various AMPfret versions, consisting of different isoforms combinations, in order to follow their individual response to energy stress. Such a panel of sensors would provide new insight concerning the response of different AMPK heterotrimers to metabolic stress. This would be an advantage face to existing AMPKAR that gives a readout of global AMPK activity and which can be phosphorylated by all different heterotrimers. A salient feature of genetically encoded FRET reporter is that they can be targeted to defined locations by appending the corresponding subcellular localization signals. Such tuning was already widely applied on existing biosensors for energy metabolism (Miyawaki et al., 1997; Forkink et al., 2014; Zhao et al., 2011;

Miyamoto et al., 2015) and, could be also applied to AMPfret for the specific monitoring of AMPK allosteric activation at defined subcellular compartments.

It may also be beneficial to generate an AMPfret sensor carrying other FRET pair than CFP/YFP. For example, AMPfret tagged with red and green fluorescent proteins could be applied in combination with ATeam or AMPKAR (carrying CFP/YFP based FRET pair) without any spectral issue due to overlapping of their excitation and emission spectra. This would allow to monitor in parallel and in real time and space, several parameters of interest of cellular metabolism.

In addition, the broad applications have to be considered in which AMPfret may be useful *in vitro* as well as *in cellulo*. As previously mentioned, AMPfret will be helpful for the screening and the identification of drugs interacting with AMPK. High throughput screens based on multi-well plates would permit the identification of AMPK interactors using fluorescence readout. Change in the FRET signal would indicate that AMPfret was incubated with a moiety that induces conformational changes within AMPK. As previously mentioned, controls using a FRET construct that does not contain any AMPK subunit would be required as a control for background FP interactors. *In vitro* characterization (affinity constant determination, competition assay, etc...) of the positively identified compound could also be achieved through a fluorescence assay as we did for AMP and ADP. By transfecting AMPfret onto cells, it might become a tool of choice to further evaluate the effect of the previously identified compound within a single living cell comparing AMPK activation by metabolic stress with the compound's ability to modulate AMPK activity.

To summarize, many optimization strategies can be further applied to AMPfret, notably due its genetically encoded nature. Also, because AMPfret is a reporter of AMPK allosteric activation, that occurs under metabolic stress and that can be engaged by synthetic ligands, applications are realistic to identify new potent AMPK modulators. Taking these two aspects into consideration makes AMPfret a promising tool to follow, in real time and space within a cell, the effects of energy stress or drugs.

9. References

- Atkinson, D.E. (1968). The energy charge of the adenylate pool as a regulatory parameter. Interaction with feedback modifiers. *Biochemistry (Mosc.)* 7, 4030–4034.
- Baron, S.J., Li, J., Russell, R.R., 3rd, Neumann, D., Miller, E.J., Tuerk, R., Wallimann, T., Hurley, R.L., Witters, L.A., and Young, L.H. (2005). Dual mechanisms regulating AMPK kinase action in the ischemic heart. *Circ Res* 96, 337–345.
- Bolli, R., Jeroudi, M.O., Patel, B.S., DuBose, C.M., Lai, E.K., Roberts, R., and McCay, P.B. (1989). Direct evidence that oxygen-derived free radicals contribute to postischemic myocardial dysfunction in the intact dog. *Proc. Natl. Acad. Sci. U. S. A.* 86, 4695–4699.
- Burwinkel, B., Scott, J.W., Buhner, C., van Landeghem, F.K., Cox, G.F., Wilson, C.J., Grahame Hardie, D., and Kilimann, M.W. (2005). Fatal congenital heart glycogenesis caused by a recurrent activating R531Q mutation in the gamma 2-subunit of AMP-activated protein kinase (PRKAG2), not by phosphorylase kinase deficiency. *Am J Hum Genet* 76, 1034–1049.
- Calabrese, M.F., Rajamohan, F., Harris, M.S., Caspers, N.L., Magyar, R., Withka, J.M., Wang, H., Borzilleri, K.A., Sahasrabudhe, P.V., Hoth, L.R., et al. (2014). Structural basis for AMPK activation: natural and synthetic ligands regulate kinase activity from opposite poles by different molecular mechanisms. *Structure* 22, 1161–1172.
- Calabrese, M.F., Rajamohan, F., Harris, M.S., Caspers, N.L., Magyar, R., Withka, J.M., Wang, H., Borzilleri, K.A., Sahasrabudhe, P.V., Hoth, L.R., et al. Structural Basis for AMPK Activation: Natural and Synthetic Ligands Regulate Kinase Activity from Opposite Poles by Different Molecular Mechanisms. *Structure*.
- Celenza, J.L., and Carlson, M. (1986). A yeast gene that is essential for release from glucose repression encodes a protein kinase. *Science* 233, 1175–1180.
- Chen, L., Wang, J., Zhang, Y.-Y., Yan, S.F., Neumann, D., Schlattner, U., Wang, Z.-X., and Wu, J.-W. (2012). AMP-activated protein kinase undergoes nucleotide-dependent conformational changes. *Nat. Struct. Mol. Biol.* 19, 716–718.
- Chen, L., Xin, F.-J., Wang, J., Hu, J., Zhang, Y.-Y., Wan, S., Cao, L.-S., Lu, C., Li, P., Yan, S.F., et al. (2013). Conserved regulatory elements in AMPK. *Nature* 498, E8–E10.
- Chouchani, E.T., Pell, V.R., Gaude, E., Aksentijević, D., Sundier, S.Y., Robb, E.L., Logan, A., Nadtochiy, S.M., Ord, E.N.J., Smith, A.C., et al. (2014). Ischaemic accumulation of succinate controls reperfusion injury through mitochondrial ROS. *Nature* 515, 431–435.
- Davies, S.P., Carling, D., and Hardie, D.G. (1989). Tissue distribution of the AMP-activated protein kinase, and lack of activation by cyclic-AMP-dependent protein kinase, studied using a specific and sensitive peptide assay. *Eur J Biochem* 186, 123–128.
- Ducommun, S., Ford, R.J., Bultot, L., Deak, M., Bertrand, L., Kemp, B.E., Steinberg, G.R., and Sakamoto, K. (2014). Enhanced activation of cellular AMPK by dual-small molecule treatment: AICAR and A769662. *Am. J. Physiol. - Endocrinol. Metab.* 306, E688–E696.
- Forkink, M., Manjeri, G.R., Liemburg-Apers, D.C., Nibbeling, E., Blanchard, M., Wojtala, A., Smeitink, J.A.M., Wieckowski, M.R., Willems, P.H.G.M., and Koopman, W.J.H. (2014). Mitochondrial hyperpolarization during chronic complex I inhibition is sustained by low activity of complex II, III, IV and V. *Biochim. Biophys. Acta* 1837, 1247–1256.
- Frederich, M., and Balschi, J.A. (2002). The relationship between AMP-activated protein kinase activity and AMP concentration in the isolated perfused rat heart. *J Biol Chem* 277, 1928–1932.
- Gowans, G.J., Hawley, S.A., Ross, F.A., and Hardie, D.G. (2013). AMP Is a True Physiological Regulator of AMP-Activated Protein Kinase by Both Allosteric Activation and Enhancing Net Phosphorylation. *Cell Metab.* 18, 556–566.
- Hardie, D.G., Carling, D., and Gamblin, S.J. (2011). AMP-activated protein kinase: also regulated by ADP? *Trends Biochem Sci* 36, 470–477.

- Hardie, D.G., Ross, F.A., and Hawley, S.A. (2012a). AMPK: a nutrient and energy sensor that maintains energy homeostasis. *Nat Rev Mol Cell Biol* *13*, 251–262.
- Hardie, D.G., Ross, F.A., and Hawley, S.A. (2012b). AMP-Activated Protein Kinase: A Target for Drugs both Ancient and Modern. *Chem. Biol.* *19*, 1222–1236.
- Hung, Y.P., Albeck, J.G., Tantama, M., and Yellen, G. (2011). Imaging cytosolic NADH-NAD(+) redox state with a genetically encoded fluorescent biosensor. *Cell Metab.* *14*, 545–554.
- Imamura, H., Nhat, K.P.H., Togawa, H., Saito, K., Iino, R., Kato-Yamada, Y., Nagai, T., and Noji, H. (2009). Visualization of ATP levels inside single living cells with fluorescence resonance energy transfer-based genetically encoded indicators. *Proc. Natl. Acad. Sci.* *106*, 15651–15656.
- Kefas, B.A., Heimberg, H., Vaulont, S., Meisse, D., Hue, L., Pipeleers, D., and Van de Casteele, M. (2003). AICA-riboside induces apoptosis of pancreatic beta cells through stimulation of AMP-activated protein kinase. *Diabetologia* *46*, 250–254.
- Landgraf, R.R., Goswami, D., Rajamohan, F., Harris, M.S., Calabrese, M.F., Hoth, L.R., Magyar, R., Pascal, B.D., Chalmers, M.J., Busby, S.A., et al. (2013). Activation of AMP-Activated Protein Kinase Revealed by Hydrogen/Deuterium Exchange Mass Spectrometry. *Structure* *21*, 1942–1953.
- Li, X., Wang, L., Zhou, X.E., Ke, J., de Waal, P.W., Gu, X., Tan, M.H.E., Wang, D., Wu, D., Xu, H.E., et al. (2014). Structural basis of AMPK regulation by adenine nucleotides and glycogen. *Cell Res.*
- Lopaschuk, G.D. (2008). AMP-activated protein kinase control of energy metabolism in the ischemic heart. *Int. J. Obes.* *32 Suppl 4*, S29–S35.
- Miyamoto, T., Rho, E., Sample, V., Akano, H., Magari, M., Ueno, T., Gorshkov, K., Chen, M., Tokumitsu, H., Zhang, J., et al. (2015). Compartmentalized AMPK Signaling Illuminated by Genetically Encoded Molecular Sensors and Actuators. *Cell Rep.*
- Miyawaki, A., Llopis, J., Heim, R., McCaffery, J.M., Adams, J.A., Ikura, M., and Tsien, R.Y. (1997). Fluorescent indicators for Ca²⁺ based on green fluorescent proteins and calmodulin. *Nature* *388*, 882–887.
- Mungai, P.T., Waypa, G.B., Jairaman, A., Prakriya, M., Dokic, D., Ball, M.K., and Schumacker, P.T. (2011). Hypoxia triggers AMPK activation through reactive oxygen species-mediated activation of calcium release-activated calcium channels. *Mol Cell Biol* *31*, 3531–3545.
- Noda, L. (1973). 8 Adenylate Kinase. In *The Enzymes*, P.D. Boyer, ed. (Academic Press), pp. 279–305.
- Onodera, H., Iijima, K., and Kogure, K. (1986). Mononucleotide metabolism in the rat brain after transient ischemia. *J. Neurochem.* *46*, 1704–1710.
- Paiva, M.A., Goncalves, L.M., Providencia, L.A., Davidson, S.M., Yellon, D.M., and Mocanu, M.M. (2010). Transitory activation of AMPK at reperfusion protects the ischaemic-reperfused rat myocardium against infarction. *Cardiovasc Drugs Ther* *24*, 25–32.
- Ponticos, M., Lu, Q.L., Morgan, J.E., Hardie, D.G., Partridge, T.A., and Carling, D. (1998). Dual regulation of the AMP-activated protein kinase provides a novel mechanism for the control of creatine kinase in skeletal muscle. *EMBO J* *17*, 1688–1699.
- Riek, U., Scholz, R., Konarev, P., Rufer, A., Suter, M., Nazabal, A., Ringler, P., Chami, M., Muller, S.A., Neumann, D., et al. (2008). Structural Properties of AMP-activated Protein Kinase: DIMERIZATION, MOLECULAR SHAPE, AND CHANGES UPON LIGAND BINDING. *J. Biol. Chem.* *283*, 18331–18343.
- Sanders, M.J., Ali, Z.S., Hegarty, B.D., Heath, R., Snowden, M.A., and Carling, D. (2007). Defining the mechanism of activation of AMP-activated protein kinase by the small molecule A-769662, a member of the thienopyridone family. *J Biol Chem* *282*, 32539–32548.
- Scott, J.W., Hawley, S.A., Green, K.A., Anis, M., Stewart, G., Scullion, G.A., Norman, D.G., and Hardie, D.G. (2004). CBS domains form energy-sensing modules whose binding of adenosine ligands is disrupted by disease mutations. *J Clin Invest* *113*, 274–284.
- Scott, J.W., van Denderen, B.J., Jorgensen, S.B., Honeyman, J.E., Steinberg, G.R., Oakhill, J.S., Iseli, T.J., Koay, A., Gooley, P.R., Stapleton, D., et al. (2008). Thienopyridone drugs are selective activators of AMP-activated protein kinase beta1-containing complexes. *Chem Biol* *15*, 1220–1230.

- Scott, J.W., Ling, N., Issa, S.M.A., Dite, T.A., O'Brien, M.T., Chen, Z.-P., Galic, S., Langendorf, C.G., Steinberg, G.R., Kemp, B.E., et al. (2014). Small Molecule Drug A-769662 and AMP Synergistically Activate Naive AMPK Independent of Upstream Kinase Signaling. *Chem. Biol.*
- Shibata, R., Sato, K., Pimentel, D.R., Takemura, Y., Kihara, S., Ohashi, K., Funahashi, T., Ouchi, N., and Walsh, K. (2005). Adiponectin protects against myocardial ischemia-reperfusion injury through AMPK- and COX-2-dependent mechanisms. *Nat Med* *11*, 1096–1103.
- Storer, A.C., and Cornish-Bowden, A. (1976). Concentration of MgATP₂-and other ions in solution. Calculation of the true concentrations of species present in mixtures of associating ions. *Biochem J* *159*, 1–5.
- Townley, R., and Shapiro, L. (2007). Crystal structures of the adenylate sensor from fission yeast AMP-activated protein kinase. *Science* *315*, 1726–1729.
- Tsou, P., Zheng, B., Hsu, C.-H., Sasaki, A.T., and Cantley, L.C. (2011). A Fluorescent Reporter of AMPK Activity and Cellular Energy Stress. *Cell Metab.* *13*, 476–486.
- Verma, S., Fedak, P.W.M., Weisel, R.D., Butany, J., Rao, V., Maitland, A., Li, R.-K., Dhillon, B., and Yau, T.M. (2002). Fundamentals of Reperfusion Injury for the Clinical Cardiologist. *Circulation* *105*, 2332–2336.
- Viollet, B., Lantier, L., Devin-Leclerc, J., Hebrard, S., Amouyal, C., Mounier, R., Foretz, M., and Andreelli, F. (2009). Targeting the AMPK pathway for the treatment of Type 2 diabetes. *Front Biosci* *14*, 3380–3400.
- Xiao, B., Heath, R., Saiu, P., Leiper, F.C., Leone, P., Jing, C., Walker, P.A., Haire, L., Eccleston, J.F., Davis, C.T., et al. (2007). Structural basis for AMP binding to mammalian AMP-activated protein kinase. *Nature* *449*, 496–500.
- Xiao, B., Sanders, M.J., Carmena, D., Bright, N.J., Haire, L.F., Underwood, E., Patel, B.R., Heath, R.B., Walker, P.A., Hallen, S., et al. (2013). Structural basis of AMPK regulation by small molecule activators. *Nat. Commun.* *4*, 3017.
- Zhang, Y., Wang, Y., Bao, C., Xu, Y., Shen, H., Chen, J., Yan, J., and Chen, Y. (2012). Metformin interacts with AMPK through binding to γ subunit. *Mol. Cell. Biochem.* *368*, 69–76.
- Zhao, Y., Jin, J., Hu, Q., Zhou, H.-M., Yi, J., Yu, Z., Xu, L., Wang, X., Yang, Y., and Loscalzo, J. (2011). Genetically encoded fluorescent sensors for intracellular NADH detection. *Cell Metab.* *14*, 555–566.
- Zhu, L., Chen, L., Zhou, X.M., Zhang, Y.Y., Zhang, Y.J., Zhao, J., Ji, S.R., Wu, J.W., and Wu, Y. (2011). Structural insights into the architecture and allostery of full-length AMP-activated protein kinase. *Structure* *19*, 515–522.

Annexes

1. Molecular cloning	245
1.1. List of primers used for PCR during AMPfret constructs creation.....	245
1.1.1. List of primers used to create 1st AMPfret generation	245
1.1.2. List of primers used for fluorophores replacement	246
1.1.3. List of primers used to create 2nd AMPfret generation:	246
1.1.4. List of primers used to create AMPfret mutants:	246
1.1.5. List of primers used to clone AMPfret 1.1 and AMPfret 2.1 in the MultiMam expression system.....	247
1.2. Vector Maps.....	247
1.2.1. pACE1-based constructs	248
1.2.2. pDC-derived constructs.....	249
1.2.3. pDS-derived constructs.....	251
1.3. Secondary structure prediction	254
1.3.1. Legend of symbols for secondary structure prediction	254
1.3.2. AMPK α2-subunits.....	254
1.3.3. AMPK β2 subunit.....	256
1.3.4. AMPK γ1-subunit.....	257
2. Crystallization assay	258

1. Molecular cloning

DNA sequences were visualized, translated and modified *in silico* with the plasmid editor *APE* (<http://biologylabs.utah.edu/jorgensen/wayned/ape/>). Cre-LoxP fusion plasmids from individual Acceptor and Donor plasmids were generated with *Cre-ACEMBLER* (http://www.embl.fr/multibac/multiexpression_technologies/cre-acemblem/).

1.1. List of primers used for PCR during AMPfret constructs creation

All oligonucleotides used in this study were synthesized by Life Technologies and supplied in desalted quality at a 25 nmol synthesis scale. Oligonucleotides were dissolved in ultrapure water and stored at -20 °C until use.

1.1.1. List of primers used to create 1st AMPfret generation

- *AMPK α-subunit*:

5HindIIIeCFP: ttataaagcttatggtgagcaagggcgaggag
 3eCFPXhoI: aatatctcgagttatcagtgagctcgatctgagtc
 5His10TEVNde1eCFP: gaaaacctgtatcttcaggggcatatggtgagcaagggcgaggag
 3eCFP2Gly2: cgtgcttctgcttctcagccataccgctgagctcgatctgagtc

- *AMPK β-subunit*:

5ApalIYFP: ttatagtgacatggtgagcaagggcgaggag
 3YFPSphI: aatatgcatgcttatcatctagatccggtggatcccggg
 5NdeIYFP: ttatacatggtgagcaagggcgaggag
 3YFPStuI: aatatagccttctagatccggtggatcccggg

- *AMPK γ-subunit*:

5pDSNde1g1: gtttaactttaagaaggagatatacatatggagtcggttgctgcagag
 3g1Nhe1eCFP: tcctcgccttgctcaccatgctagcgggcttcttctccacctgtg
 5Nhe1eCFP: aaaaagctagcatggtgagcaagggcgaggag
 3eCFPSpe1pDS: ggcacatgggtttaaacggaactagttatcagtgagctcgatctgagtc
 5eCFPNhe1g1: tcagatctcgacgagctcacgctagcatggagtcggttgctgcagag
 3g1Spe1pDS: ggcacatgggtttaaacggaactagttatcagggcttcttctccacctgtg
 5pDSNde1eCFP: aactttaagaaggagatatacatatggtgagcaagggcgaggag
 3eCFPNhe1: aaaaagctagcgtgagctcgatctgagtc
 3g1Nhe1YFP: gctcctcgccttgctcaccatgctagcgggcttcttctccacctgtg
 5Nhe1YFP: aaaaagctagcatggtgagcaagggcgaggag
 3YFPSpe1pDS: ggcacatgggtttaaacggaactagttatcatctagatccggtggatcccggg
 5YFPNhe1g1: cgggatccaccgatctagagctagcatggagtcggttgctgcagag
 5pDSNde1YFP: aactttaagaaggagatatacatatggtgagcaagggcgaggag

3YFPNhe1: aaaaagctagctctagatccggtggatcccggg

1.1.2. List of primers used for fluorophores replacement

5Apal1cpVenus ttatagtgacatgggCGGCGTgcagctcg
 3cpVenusSph1: aatatgcatgctcattactcgatggttgGCGGATcttgaagttgg
 5Nde1cpVenus: ttatacatatgggCGGCGTgcagctcg
 3cpVenusStu1: aatataggcctctcgatggttgGCGGATcttgaagttgg
 5Nhe1cpVenus: attatagctagcatgggCGGCGTgcagctcg
 3Pme1cpVenus: ttatagtttaaacctattactcgatggttgGCGGATcttgaagttgg
 3Nhe1cpVenus: tattagctagcctcgatggttgGCGGATcttgaagttgg
 5HindIII CFPtrunc: atattaagcttatggtgagcaagggCGAGGAGctg
 3Xho1CFPtrunc: ttatactcgagctattaggCGGCGGTcACGAactccag
 5SLICCFPtruncNde1: aacctgtatTTTCAGGGCATatggtgagcaagggCGAGGAGctg
 3SLICCFPtrunc2gly: cgtgcttctgcttctcagccataccgCGGCGGCGGTcACGAactccag
 5Nhe1CFPtrunc: atatagctagcatggtgagcaagggCGAGGAGctg
 3Pme1CFPtrunc: atatagtttaaacctattaggCGGCGGTcACGAactccag
 5Nde1CFPtrunc: atatacatatggtgagcaagggCGAGGAGctg
 3Nhe1CFPtrunc: atatagctagCGGCGGCGGTcACGAactccag

1.1.3. List of primers used to create 2nd AMPfret generation:

5a2-_{AR}CFP: ccagtcttactactgctttaaTGGTGAGcaagggCGAGGAG
 3a2-_{AR}CFP: taaagcagtgataagactggcgCACATttc
 5b2-_{KPI}YFP: atgttactactctgctatacatggtgagcaagggCGAGGAG
 3b2-_{KPI}YFP: gtatagcagagtagtaacatacttcttctgtagcgatgg
 5g1-_{LTGGEEKP}YFP: acatcttacaggctctggtgatggtgagcaagggCGAGGAG
 3g1-_{LTGGEEKP}YFP: caccagagcctgtaagatgtcagacagc
 5a2-8AAhelix-CFP: gaggaggaagagaagaaaaagaaagggCGAGGAGctgttcaccgg
 3a2-8AAhelix-CFP: ttttcttctctcctcctctaaagcagtgataagactggcgCACATttc

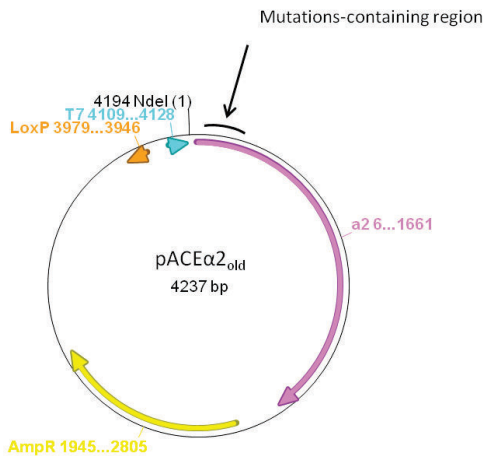
1.1.4. List of primers used to create AMPfret mutants:

5L128D+V129D: gatgattgcatttctccaaatgccagcttgttcgatg
 3L128D+V129D: ttggagaaatgcaatcatctggcttaaaggagtcctgcaggtagacctc
 5V275GL276G: ggaggtaaagtgctacctacatgagactctcaggcaatcatcaatagactg
 3V275GL276G: ttaggttagcacttacctccacctcgaagtagtgaccggtgc
 5S315P: cccgatatcttacaggctctggtgctcacaggtgg
 3S315P: agagcctgtaagatatcgggcagcgatacaatgcccttgaccacgtcatg
 5T172A: gctagctgtggatcgccaaattatgc

fused vectors by Cre recombination that encode for AMPfret heterotrimeric constructs are not depicted herein.

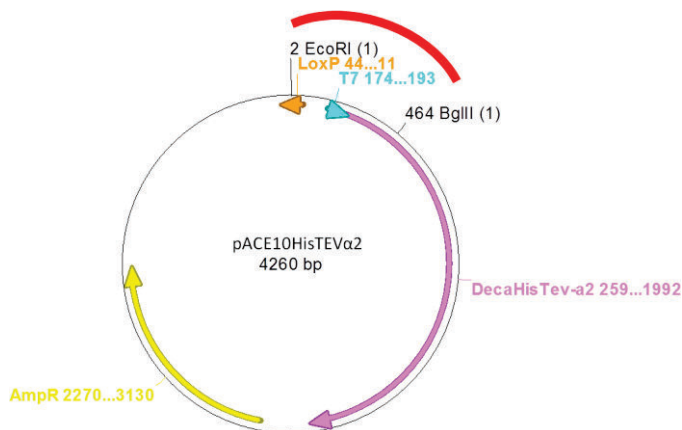
1.2.1. pACE1-based constructs

- pACE α 2_{old}:

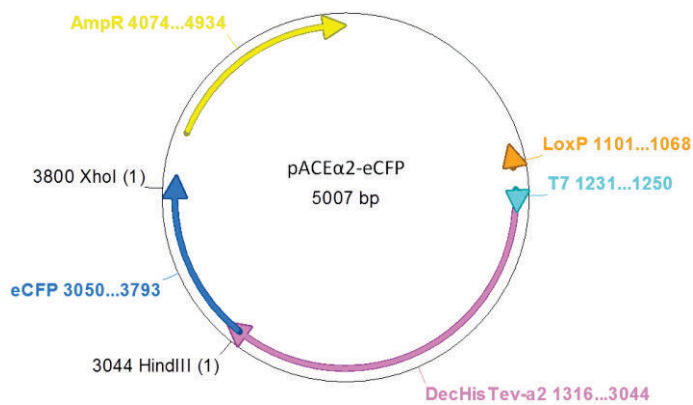


Faulty pACE α 2_{old} vector map: the NdeI restriction site (CA TATG) represents the undesirable ATG start codon located between the T7 pro (light blue arrow) and the start of the incorrect α 2 coding sequence (purple arrow). Such extra ATG results into the beginning of an extra ORF. 5' region of α 2 gene containing mutations is mentioned through the black curve. Antibiotic resistance gene (here AmpR) and LoxP site are respectively represented as yellow and orange arrow.

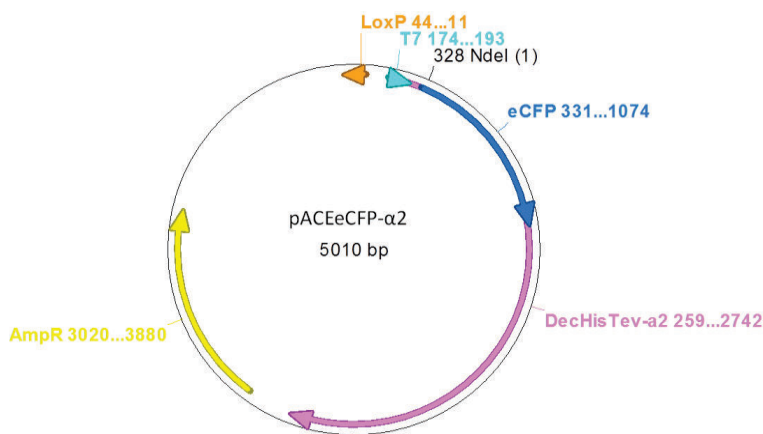
- pACE10HisTEV α 2 (pACE α 2)



Repaired pACE α 2: the DNA piece ordered to fix defective sequence and to insert a 10 His tag covers the region located under the red arch and was cloned using the EcoRI and BglII restriction sites.

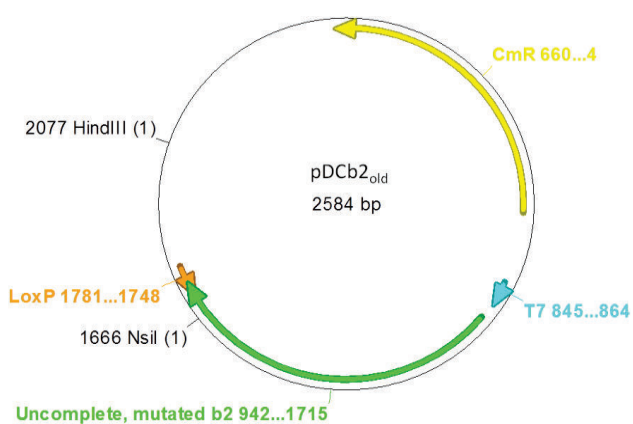
- pACE α 2eCFP

The eCFP coding sequence (blue arrow) was inserted in the pACE α 2 using HindIII and XhoI restriction sites.

- pACEeCFP α 2

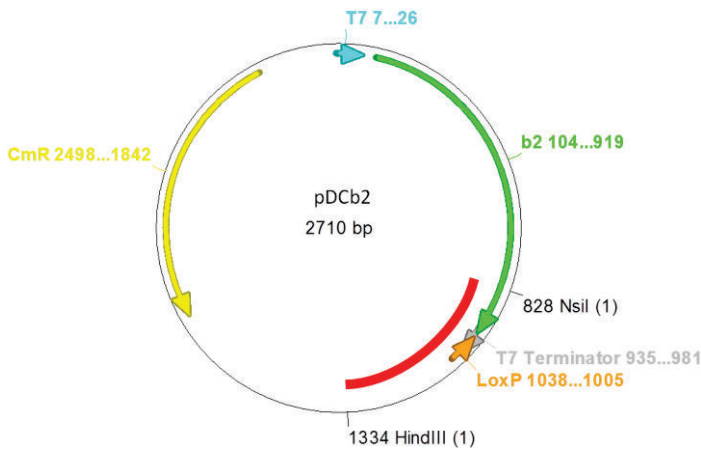
The eCFP coding sequence (blue arrow) was inserted in the pACE α 2 via the SLIC method after opening of pACE α 2 using NdeI restriction enzyme.

1.2.2. pDC-derived constructs

- pDC β 2_{old}:

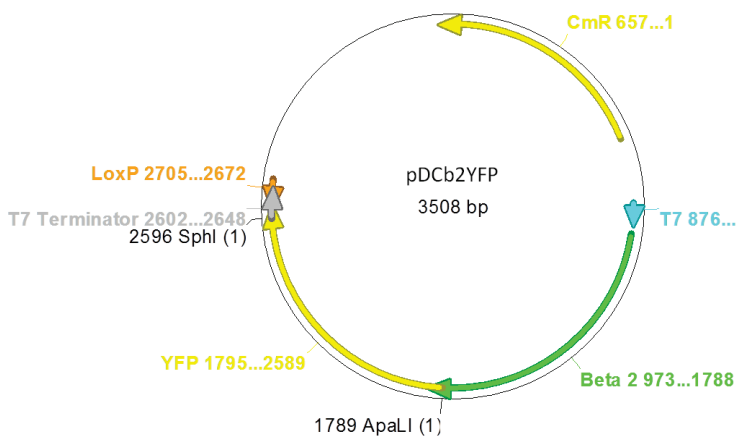
Unrepaired pDC β 2 vector presented, downstream the T7 promoter (light blue arrow) a coding sequence for the AMPK β 2 subunit which carried mutations and lacking 14 amino acids at the C-Ter. In addition no terminator was present on the vector backbone. Antibiotic resistance gene (here CmR) and LoxP site are respectively represented as yellow and orange arrow.

- pDCβ2:



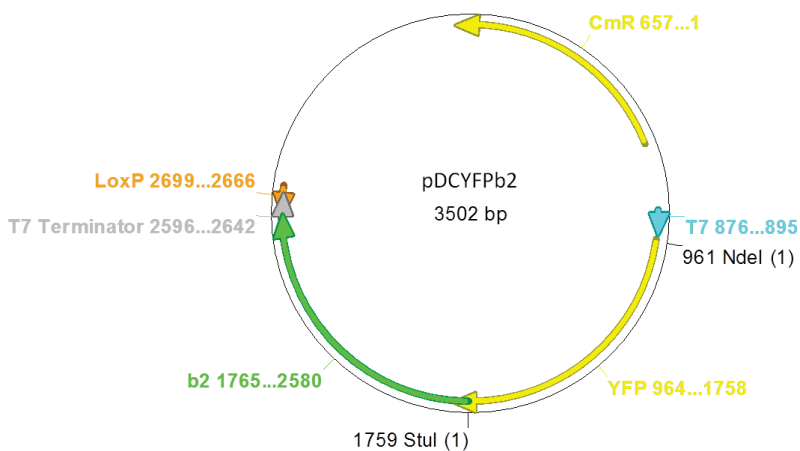
Fixed pDCβ2: the DNA piece ordered to fix defective sequence and to insert a T7 terminator (grey arrow) covers the region located under the red arch and was cloned using the NsiI and HindIII restriction sites.

- pDCβ2YFP:



The YFP gene (yellow arrow) was cloned into the pDCβ2 using the ApaLI and SphI restriction sites.

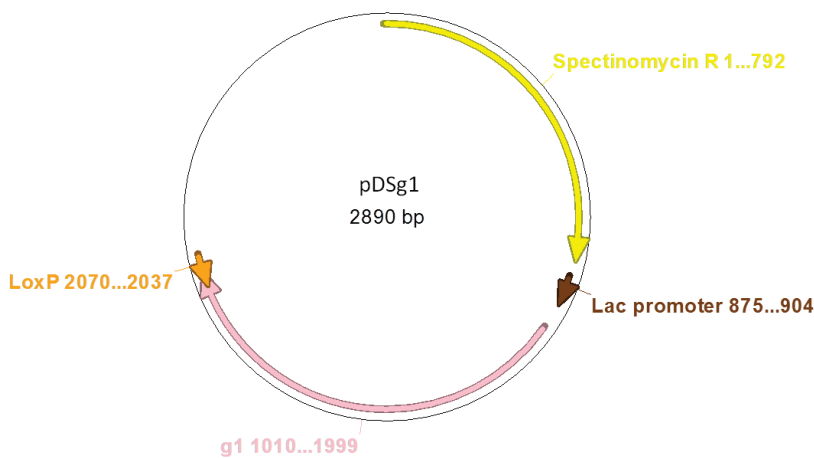
- pDCYFPβ2:



The YFP gene (yellow arrow) was cloned into the pDCβ2 using the NdeI and StuI restriction sites.

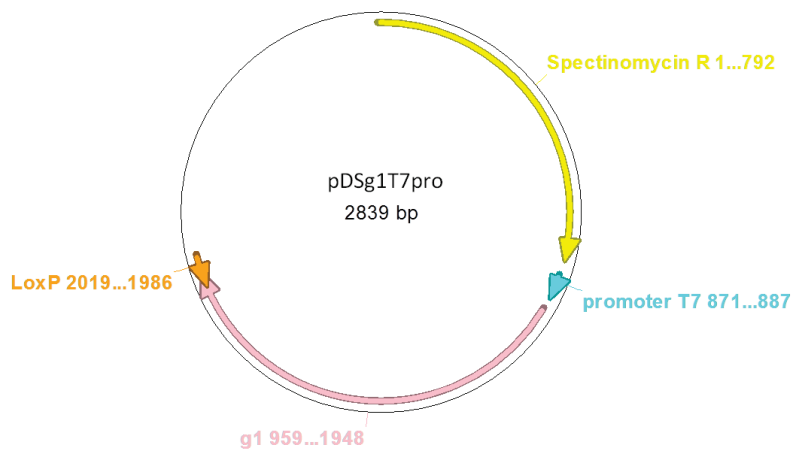
1.2.3. pDS-derived constructs

- pDSy1:



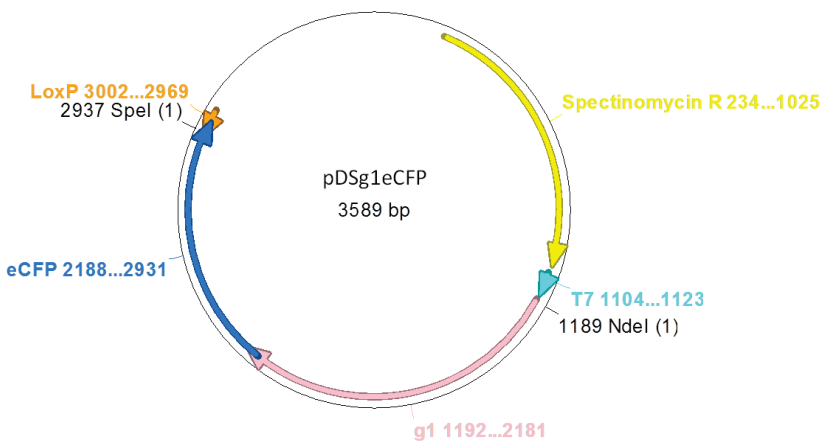
The $\gamma 1$ coding sequence (pink arrow) was cloned after the Lac promoter (brown arrow) into the pDS vector from the *MultiColi* expression system using SLIC. Antibiotic resistance gene (here SpectinomycinR) and LoxP site are respectively represented as yellow and orange arrow.

- pDSy1T7pro:

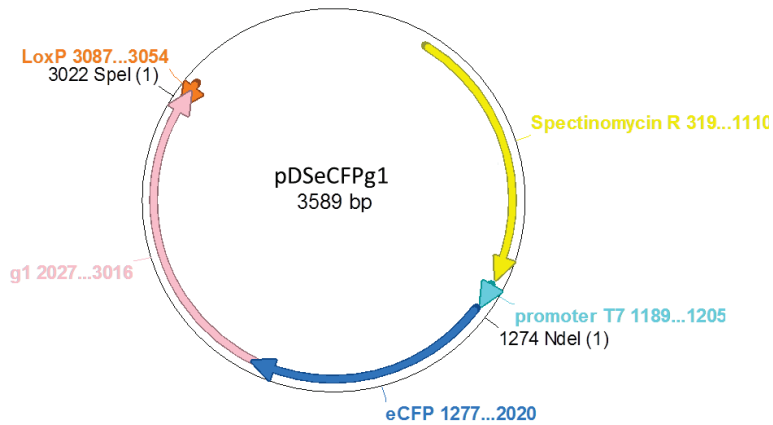


As presented in Fig. 4, the Lac promoter was replaced by the T7promoter (light blue arrow) in order to have available all plasmids coding for AMPK subunits that contains the same promoter. This was aim to get subunits stoichiometry during expression.

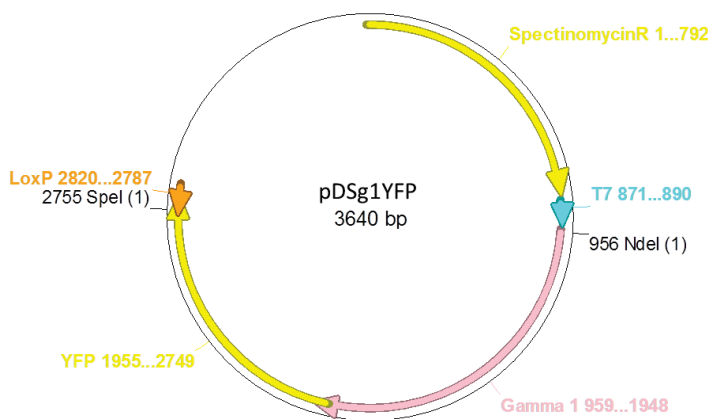
All following plasmids, carrying the $\gamma 1$ -subunit tagged with a fluorescent protein, also exists under a version containing the Lac Promoter. However, corresponding maps are not presented as they were not used in the presented work. During the thesis work Lac promoter was exchanged by T7 promoter to get stoichiometric expression of AMPK subunits (as $\alpha 2$ and $\beta 2$ are both under the control of the T7 promoter) and the strategy was presented in the results chapter.

- pDSy1eCFP:

γ 1 and eCFP coding sequences (respectively represented as pink and blue arrows) were simultaneously cloned by SLIC into the pDS vector previously opened with NdeI and SpeI restriction enzymes.

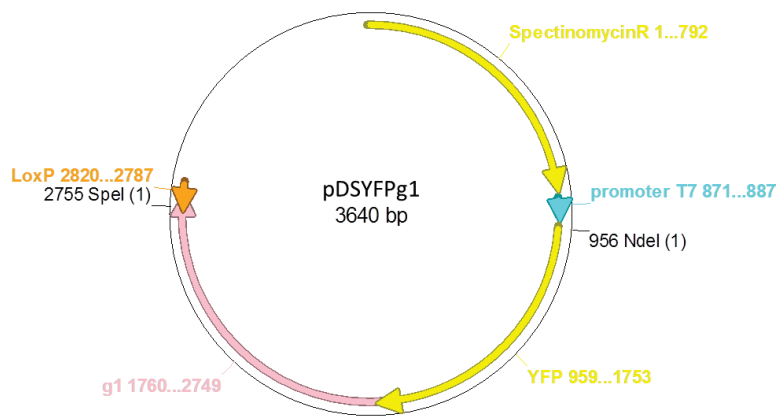
- pDSeCFPy1:

eCFP and γ 1 genes were simultaneously cloned by SLIC into the pDS vector previously opened with NdeI and SpeI restriction enzymes.

- pDSy1YFP:

γ 1 and YFP coding sequences (respectively pink and yellow arrow) were simultaneously cloned by SLIC into the pDS vector previously opened with NdeI and SpeI restriction enzymes.

- pDSYFP γ 1:

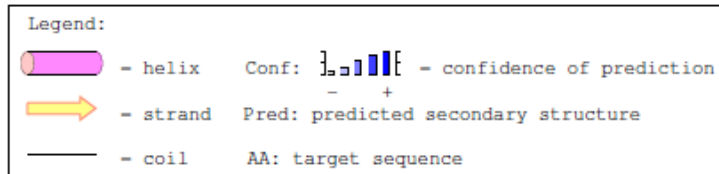


YFP and γ 1 genes were simultaneously cloned by SLIC into the pDS vector previously opened with NdeI and Spel restriction enzymes.

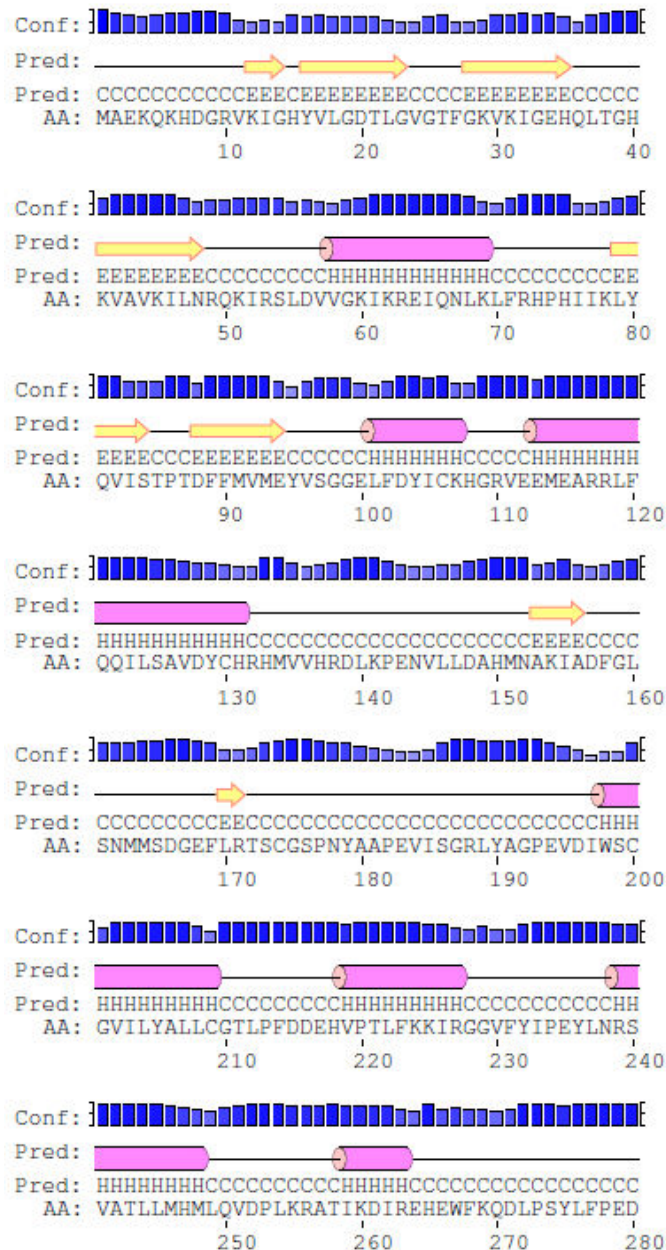
1.3. Secondary structure prediction

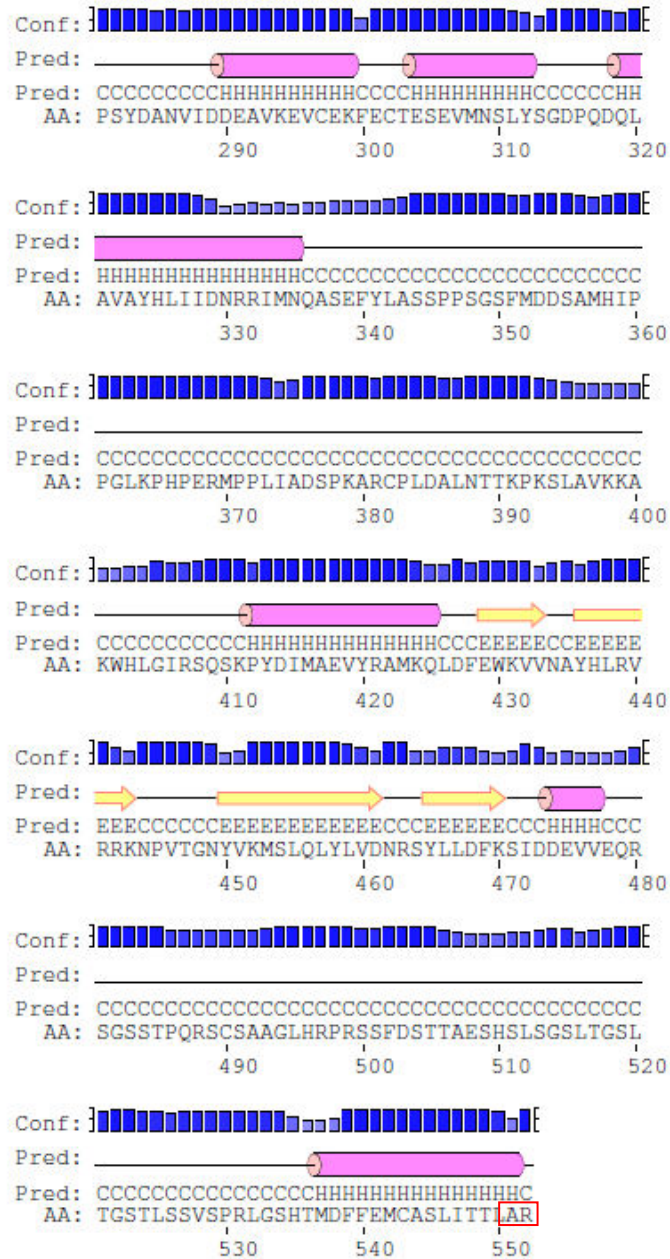
Predicted unfolded aminoacids deleted from α_2 , β_2 and γ_1 subunits C-termini are boxed in red.

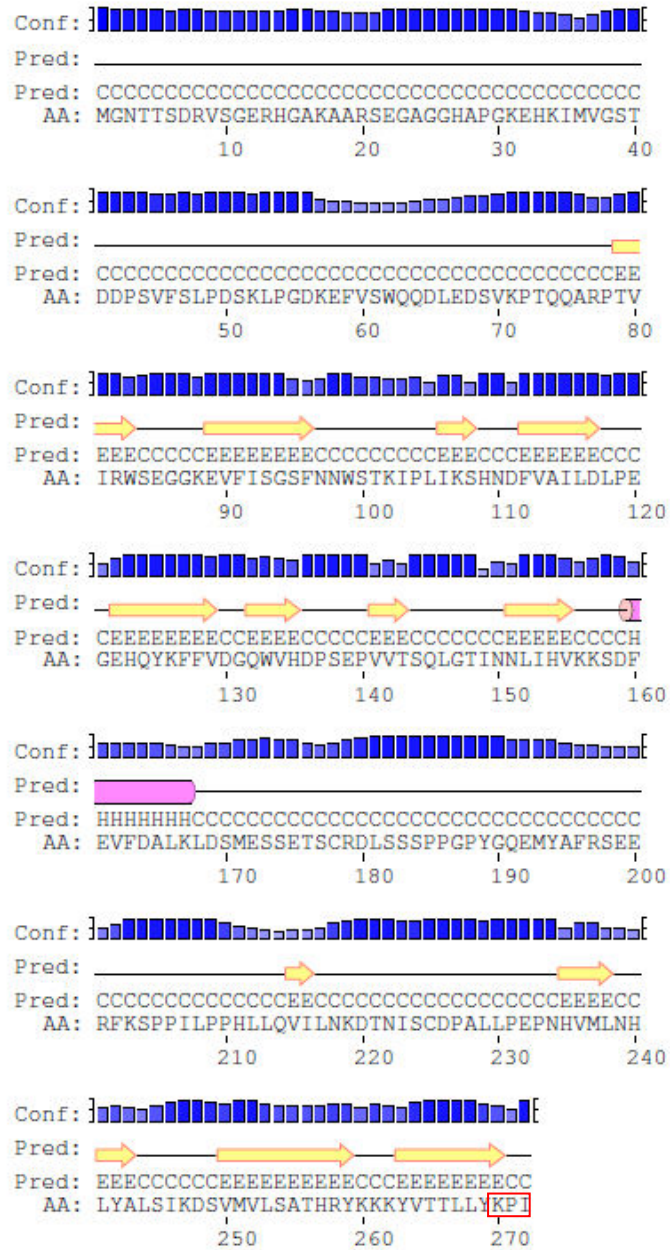
1.3.1. Legend of symbols for secondary structure prediction

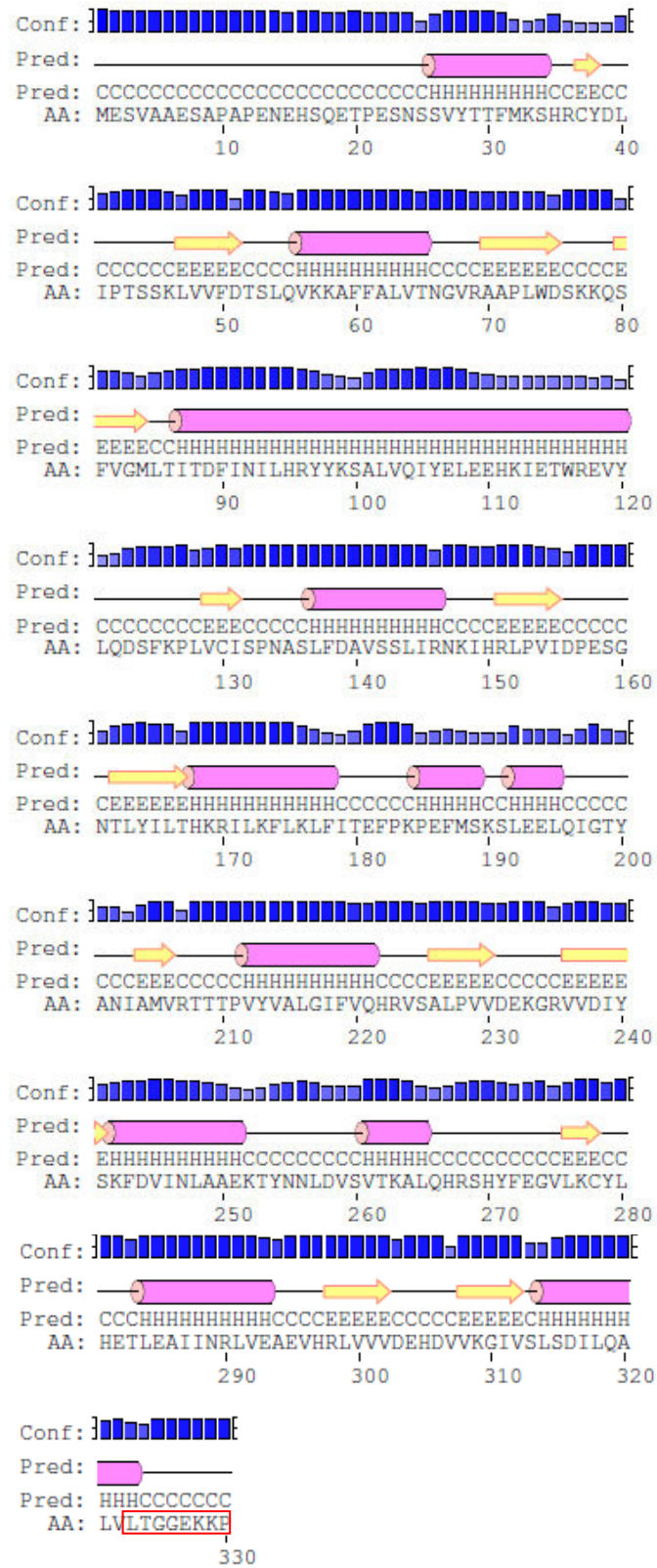


1.3.2. AMPK α_2 -subunits





1.3.3. AMPK β 2 subunit

1.3.4. AMPK γ 1-subunit

2. Crystallization assay

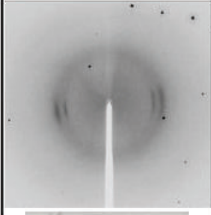
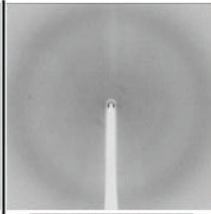
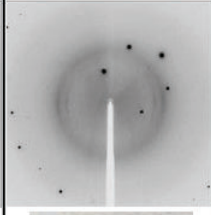
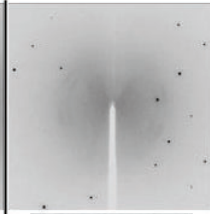
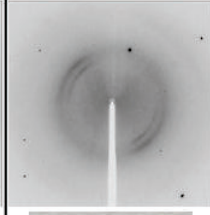
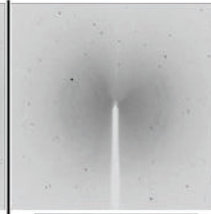
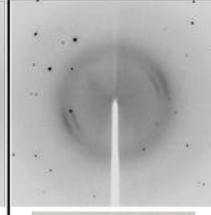
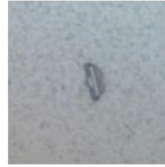
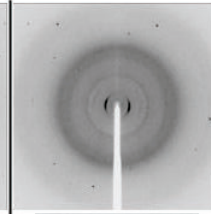
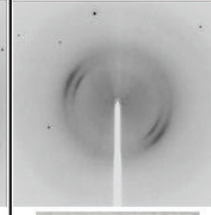
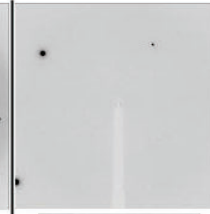
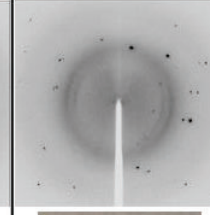
After TALON resin and S200 16/600, AMPfret 2.0 was obtained pure with a relatively good yield compared to other AMPfret constructs (>10mg). Right after size exclusion chromatography (SEC), the protein complex in SEC buffer (50mM Tris pH 8, 200mM NaCl, 2mM Spermidine, 2mM MgCl₂, 2mM β-ME) was concentrated until 8mg/mL using Amicon centrifugal filter unit. AMPfret 2.0 was then flash-freeze in liquid nitrogen and stored at -80°C for less than a week. Samples were thawed and centrifuged 10min at 16'000g before being sent to the crystallization robot the HTXlab, EMBL Grenoble. The crystallization experiments were set up with a Cartesian PixSys 4200 crystallization robot (Genomic Solutions, U.K.) using as standard plate Greiner CrystalQuick plates (flat bottom, untreated). Sitting drops of 200nL were made in 96-wells plates for crystallization by mixing 100nL of protein solution with 100nL of precipitant contained in the reservoir. Plates' reservoirs composition corresponded to commercially available screens for crystallization conditions. A total of 6 plates were set up, stored and examined by the imaging system Formulatrix RockImager (Formulatrix, Inc., U.S.) at 4°C. After one day, crystals were visible in some of the drops. Even if they were from different shapes, most of them were looking like "coffin-lid", "paper-boat" and "double-edged razor blade" crystals. Such crystals are often reported as being salt crystals made of magnesium, ammonium and phosphate. As the protein buffer contained 2mM MgCl₂ and view to the fact that precipitants of the crystallization solutions, in which crystals appeared, were almost always containing ammonium and phosphate, salt crystals could have been expected. More encouraging were the small needles growing after 8 days in 0.2M NaCl, 0.1M Na/K phosphate pH 6.2, 50% (v/v) PEG200. Despite this, crystals issued from different drops were fished using micro-loops under an optic microscope at 4°C. Glycerol mixed at 50% with solution contained in the reservoir, was used as cryoprotectant. Frozen crystals were then tested under single-wavelength anomalous dispersion (SAD) experiment at the ESRF, on the microfocus beamline: ID 23-2. This beamline is fixed energy and dedicated to perform experiment with very small protein crystals. Energy and wavelength respectively had values of 14.209 keV and 0.8726 Å. Results are summarized in table 1 where pictures of small obtained crystals are presented and their corresponding diffraction pattern. I concluded that crystals were salt because their diffraction pattern

showed strong and sporadic spots especially located at the mid high resolution (distant from the center of the diffraction image).

The high-throughput crystallization (HTX) laboratory at EMBL Grenoble supplied all commercial crystallization screens. Other crystallization grade reagents and crystal handling tools were obtained from Hampton Research Inc. or Molecular Dimensions, if not otherwise stated.

Table 1: Summary of AMPfret 2.0 crystallization trials.

For each hit, for which a crystal grew and was successfully fished, the crystallization conditions are mentioned accompanied with a crystal picture and its corresponding diffraction pattern.

Crystallization reagent	Crystal	Diffraction pattern	Crystallization reagent	Crystal	Diffraction pattern
0.1M Tris HCl pH 8.5, 0.1M ammonium phosphate, 0.5M sodium phosphate, 0.5M potassium phosphate			0.1M acetate pH 4.5, 1M ammonium phosphate.		
0.1M Tris HCl pH 8.5, 0.1M ammonium phosphate, 12% (w/v) PEG 6000			0.1M imidazole pH 8, 1M ammonium phosphate		
0.1M HEPES pH 7.5, 0.1M ammonium sulfate, 0.5M sodium phosphate, 0.5M potassium phosphate			0.1M Tris pH 8.5, 1M ammonium phosphate		
0.1M Na/K phosphate pH 6.2, 0.2M NaCl, 50% (v/v) PEG200			0.1M Tris pH 8.5, 0.2M ammonium phosphate, 25% (w/v) PEG3350		
0.1M Sodium acetate pH 4.5, 1M ammonium phosphate			0.1M ADA pH 6.5, 1M ammonium phosphate		
0.1M Tris pH 8.5, 0.2M ammonium phosphate, 50% (v/v) MPD			0.1M Tris pH 8.5, 0.2M ammonium acetate, 25% (w/v) PEG3350		

Abbreviations

Å	Angstrom	E	Glutamic acid
A	Alanine	EDTA	Ethylene diamine tetraacetic acid
AA	Amino acid		
ACC	AcetylCoA carboxylase	F	Phenylalanine
ADP	Adenosine-5'-monophosphate	FP	Fluorescent protein
Ala	Alanine	FPLC	Fast protein liquid chromatography
Amp	Ampicillin	FLIM	Fluorescence-lifetime imaging microscopy
AMP	Adenosine-5'-diphosphate	FRET	Fluorescence resonance energy transfer
AMPK	AMP-activated protein kinase		
Arg	Arginine	G	Glycine
Asn	Asparagine	Gent	Gentamycin
Asp	Aspartic acid	GFP	Green fluorescent protein
ATP	Adenosine-5'-triphosphate	Gln	Glutamine
		Glu	Glutamic acid
bp	Base pairs	Gly	Glycine
β-ME	β-mercaptoethanol		
BSA	Bovine serum albumin	H	Histidine
		His	Histidine
C	Cysteine	h	Hour
Camp	Chloramphenicol	HPLC	High performance liquid chromatography
CamKKβ	Calcium/calmodulin-dependent protein kinase β	HTX	High-throughput crystallization
CBM	carbohydrate binding module		
CBS	Cystathionine β-synthase	I	Isoleucine
CFP	Cyan fluorescent protein	IEX	Ion exchange chromatography
cpVenus	circularly permuted Venus	Ile	Isoleucine
CV	Column volume	IMAC	Immobilized metal affinity chromatography
Cys	Cysteine	IPTG	Isopropyl β-D-1-thiogalactopyranoside
D	Aspartic acid	K	Lysine
Da	Dalton	K _a	acid dissociation constant
dCTP	Deoxy cytosine triphosphate	Kan	Kanamycin
dNTP	Deoxynucleoside triphosphate	K _d	Dissociation constant
DTT	Dithiothreitol	kDa	Kilodalton

L	Leucine	Pro	Proline
LB	Luria broth		
Leu	Leucine	Q	Glutamine
LKB1	Liver kinase B1		
Lys	Lysine	R	Arginine
		rpm	Rotation per minute
M	Methionine		
mA	milliampere	S	Serine
MCS	Multi cloning site	SAXS	Small angle X-ray scattering
Met	Methionine	SEC	Size exclusion chromatography
mg	milligram		
MgCl ₂	Magnesium chloride	sec	Seconds
min	Minute	Ser	Serine
mM	millimolar	SLIC	Sequence and ligation independent cloning
mRNA	Messenger RNA		
MS	Mass spectrometry	SN	Supernatant
mseCFP	Monomeric super enhanced cyan fluorescent pritein	SNP	Supernatant+pellet
		T	Threonine
MW	Molecular weight	TEMED	N,N,N',N'-Tetra methyl ethylene diamine
		Tet	Tetracycline
N	Asparagine	TEV	Tobacco etch virus
NaCl	Sodium chloride	Thr	Threonine
NaOH	Sodium hydroxide	Trp	Tryptophan
ng	nanogram	TSS	Transcription start site
nm	nanometer		
NMR	Nuclear magnetic resonance	U	Units
nt	nucleotide	UV	Ultraviolet
NTD	N-terminal domain		
		V	Valine
OD	Optical density	V	Volt
		(v/v)	Volume per volume
P	Proline	Val	Valine
PAGE	Polyacrylamide gel electrophoresis		
PCR	Polymerase chain reaction	W	Tryptophan
PDB	Protein data bank	(w/w)	Weight per weight
pl	Isoelectric point	(w/v)	Weight per volume
pg	picogram	WT	Wild type
PKA	Protein kinase A		
PKB	Protein kinase B	Y	Tyrosine
		YFP	Yellow fluorescent protein

Side project

Inhibition of HBV replication through AMPK: involvement of nucleotide analogues reverse-transcriptase inhibitors

Collaborative project with Mouzannar K., Ramiere C. and Andre P. at the Centre International de Recherche en Infectiologie (CIRI) U1111/UMR5308 Inserm-CNRS-UCBL-ENS de Lyon.

1. Introduction.....	265
2. Results.....	268
2.1. Effect of adefovir, tenofovir and AICAR on viral replication (Lyon)	268
2.2. Effect of adefovir and tenofovir on AMPK activation (Grenoble)	270
2.3. Adefovir and AMPfret (Grenoble)	274
3. Discussion.....	276
4. Materials and Methods	278
4.1. Cell culture.....	278
4.2. Confocal microscopy.....	278
4.3. Image treatment	279
4.4. Immunoblotting	279
4.4.1. Cell culture and treatment.....	279
4.4.2. Protein extraction	279
4.4.3. SDS-PAGE and immunoblot.....	279
5. References.....	281

Abstract. This chapter presents the collaborative work achieved with Mouzannar K., Ramiere C. and Andre P. on nucleotide analogues used in the treatment of hepatitis B virus and their putative ability to modulate AMPK activity. Nucleotide analogues are widely used in the treatment of viral infection as they have the ability to inhibit viral reverse-transcriptase. Two adenine analogues, Adefovir (ADV) and Tenofovir (TNF), are widely used against HBV. Inside the cell, these drugs are metabolized into analogues of AMP, ADP and ATP. AMPK has the ability to sense adenylates and thus the cellular energy charge, and to respond by its kinase activity to fluctuations in adenylate concentration. Our data suggest that Adefovir and Tenofovir differ in their effect on AMPK. While TNF did not alter AMPK activity, ADV activated AMPK, but only in presence of AMPK activator AICAR in a synergistic manner. However, no direct interaction between ADV, ADV under its AMP-analogue form, and AMPK was seen when we used AMPfret, a genetically encoded fluorescent biosensor reporting adenylate-induced conformational changes in AMPK.

Résumé. Dans ce chapitre sont présentés les travaux collaboratifs réalisés avec Mouzannar K., Ramiere C. et Andre P. portant sur les analogues nucléotidiques utilisés dans le traitement contre le virus de l'hépatite B et leur capacité supposée à moduler l'activité de l'AMPK. Les analogues nucléotidiques sont utilisés dans le cadre de traitement contre les infections virales car ils ont la capacité d'inhiber la reverse transcriptase virale. Deux analogues de l'adénosine, Adefovir (ADV) et Tenofovir (TNF), sont largement utilisés contre HBV. Une fois dans la cellule, ces molécules sont métabolisées sous la forme d'analogues de l'AMP, de l'ADP et de l'ATP. L'AMPK est capable de sentir les différentes formes phosphorylées de l'adénosine, représentant l'état énergétique de la cellule, et de répondre par son activité kinase à des changements de leurs concentrations. Nos données suggèrent que l'Adefovir et le Tenofovir ont différents effets sur l'AMPK. Alors que le TNF ne modifie pas l'activité de l'AMPK, l'ADV active l'AMPK mais seulement en présence de l'activateur de l'AMPK AICAR et selon une manière synergique. Cependant aucune interaction directe entre l'AMPK et ADV, sous sa forme analogue de l'AMP n'a pu être vu en utilisant AMPfret, un biosenseur fluorescent rapporteur des changements de conformation de l'AMPK induits par les adenylates.

1. Introduction

Nucleotide analogs are widely used as antiretroviral drugs due to their potent inhibition of reverse transcriptase, a viral DNA polymerase essential for replication of retroviruses. Typical examples of nucleotide analog reverse-transcriptase inhibitors (NtARTIs) are Adefovir and Tenofovir (Figure 1), used for treating chronic infection with hepatitis B virus (HBV) or human immunodeficiency virus 1 (HIV-1). These drugs are administered in the so-called pro-drug forms, adefovir dipivoxyl (ADV) and tenofovir disoproxil fumarate (TDF). Pro-drugs are more hydrophobic derivatives that can cross biomembranes and are more stable. Within the cell, they are phosphorylated by cellular kinases like adenylate kinase or nucleoside diphosphate kinase to yield monophosphate and finally diphosphate forms, adefovir-diphosphate and tenofovir-diphosphate. These represent analogues of dATP that can inhibit DNA synthesis by reverse transcriptase (or polymerase). Once integrated by the enzyme in a newly synthesized viral DNA strand, further prolongation of the DNA strand is inhibited because these analogues lack a deoxyribose moiety with the necessary 3'-hydroxyl group to bind the next nucleotide (Figure 1).

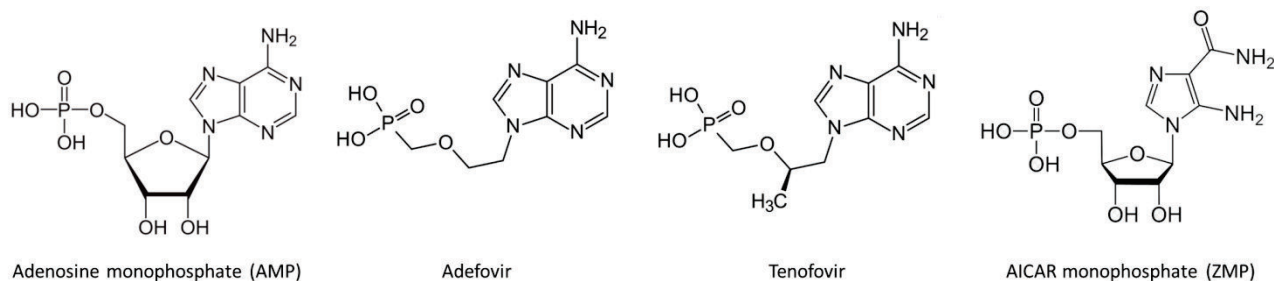


Figure 1: Structure of AMP, Adefovir, Tenofovir and ZMP. All molecules are carrying an adenine ring (except AICAR) and a phosphate group. ZMP is the bioreactive cellular derivative of AICAR.

The structural similarity of NtARTIs with adenylates, allowing them to serve as substrates for viral polymerases, can potentially interfere with adenylate-dependent processes of the host cell, in particular within energy metabolism. Indeed, their clinical use is linked to numerous side effects such as weakness (asthenia), fever, headache, nausea or even lactic acidosis (Zhao et al., 2011), and higher doses of NtARTIs are toxic. Although Adefovir and Tenofovir only differ by a methyl group, they have divergent therapeutic effects. ADV was reported to

be more toxic than TDF, notably due to severe and frequent kidney toxicity at high doses, and is not used for HIV treatment in contrast to TNF (Cihlar et al., 2002). Studies on HBV showed that daily doses of 300 mg TDF had superior antiviral efficacy with a similar safety profile as compared to a daily dose of 10 mg ADV (Marcellin et al., 2008).

This divergent ratio between antiviral efficacy and side effects of ADV and TDF may be due to interference/interaction with different components of the host cell. We hypothesized that Adefovir and/or Tenofovir, as a side effect, could also modulate AMPK activity. Both drugs and their mono- and diphosphate derivatives can act as AMP, ADP and ATP analogues, respectively, and could thus bind to the AMPK CBS sites at the gamma-subunit and directly interfere with allosteric AMPK regulation. This is entirely conceivable, since already small fluctuations in AMP and ADP in the micromolar range can activate AMPK. Nucleotide analogues could interfere with this activation by either having the same type of effect (allosteric activator) or by inhibiting binding of natural adenylates (competitive inhibition). Any dysregulation of AMPK activation would then translate into crucial alterations of cellular metabolism (Hardie et al., 2011), but could also affect HBV replication independent of polymerase inhibition.

AMPK directly regulates activity of nuclear receptors that act as key transcription factors for regulating central carbon metabolism, but can also affect viral replication. Among others, AMPK directly phosphorylates the peroxisome proliferator-activated receptor-gamma coactivator 1alpha (PGC-1 α ; Shlomai et al., 2006) and the farnesoid X receptor (FXR; Lien et al., 2014), highly expressed in the liver. As reported by Lien et al. (2014), activated AMPK interacts with, phosphorylates, and represses ligand-induced FXR transcriptional activity. This inhibition is achieved by decreasing FXR interaction with its transcriptional coactivators, and finally precipitates liver injury under conditions favoring cholestasis. While AMPK phosphorylation of FXR seems to be inhibitory, phosphorylation of PGC-1 α at Thr177 and Ser538 rather activates transcription from the PGC-1 α promoter.

Gene transcription and replication of the HBV genome are also controlled by nuclear receptors such as HNF-4 α , PPAR α , FXR α or LRH-1. They can bind to different sites within the regulatory promoter and activator regions of the HBV genome. For example, two putative FXR binding sites are present at the level of the enhancer 2 and the core promoters and they

can control transcription of pregenomic RNA and HBV genome replication (Ramière et al., 2008). Since FXR and PGC-1 α have important roles for both nutrient signaling of the host cell and transcription/replication of the HBV genome, the host cell metabolism could directly affect viral gene expression and life cycle, thus playing a key role for virus-host interactions (Jäger et al., 2007).

By potentially interfering with AMPK kinase activity, Adefovir and Tenofovir would alter the activity of nuclear receptors/transcription factors and affect HBV replication. As outlined above, these NtARTIs could in principle act as activators or inhibitors of AMPK, and AMPK activation at the cellular level could affect the activity of nuclear receptors in different ways. We propose here to study the potential effect of AMPK activation on viral replication and a putative direct effect of Adefovir and Tenofovir on AMPK activity.

2. Results

2.1. Effect of Adefovir, Tenofovir and AICAR on viral replication (Lyon)

To investigate the effect of antiviral drugs and of the allosteric AMPK activator AICAR on HBV replication, a reporter system for HBV replication was used that is based on HepaRG cells (Figure 2). These cells were infected with HBV at day 0 and maintained in culture for 11 days post-infection (Hantz et al., 2009). At day 11 medium was harvested and amounts of secreted antigens (HBsAg) and (HBeAg) and DNA (rcDNA) were quantified. HBeAg is the extracellular form of HBeAg (core antigen), a viral protein, and HBsAg is the surface antigen of the virus and both when, circulating in infected blood, indicate active replication of the virus. Relaxed circular DNA (rcDNA) corresponds to the DNA of the circulating virus, in contrast to the covalently closed circular DNA (cccDNA) which serves as the template for the transcription of viral RNAs (Guo et al., 2007).

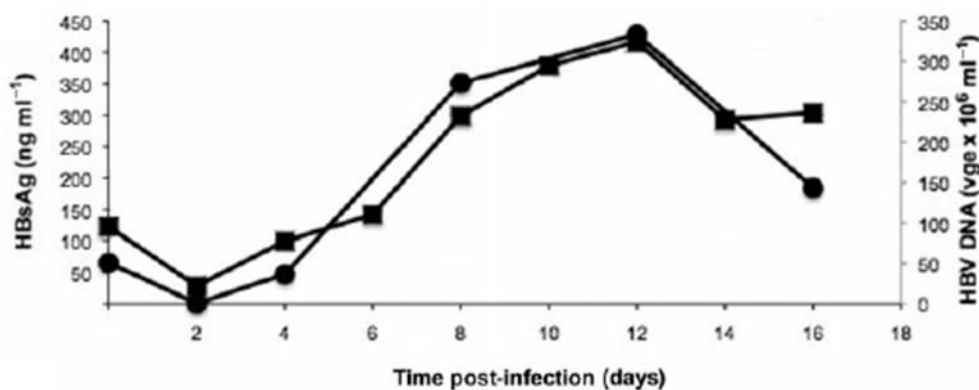


Figure 2: Infection of HepaRG cells by HBV. After infection with HBV, HepaRG cells were maintained in culture for the indicated days post-infection. Production of HBsAg (square) and HBV DNA (circle) in cell supernatants were detected by ELISA and by dot-blot hybridization, respectively. From (Hantz et al., 2009).

Infected HepaRG cells were treated with ADV alone, AICAR alone, or both combined for 24h to 48h before harvesting (day 8 or 9). At day 11, the culture medium was harvested and the contained viral-protein and -DNA concentrations were measured.

The results revealed that viral replication is inhibited in infected cells when treated by ADV, much less by TNF (Figure 2). Interestingly, the AMPK activator AICAR inhibited viral replication even more efficiently than the two NtARTIs, and inhibition by AICAR and ADV was additive. Already low concentrations of ADV (below 1 μ M) were able to further increase the

inhibition provided by 1 mM AICAR. Thus, AMPK activation appears to reduce viral replication, and a combination of both AICAR and ADV seems to be even more efficient than ADV or AICAR alone.

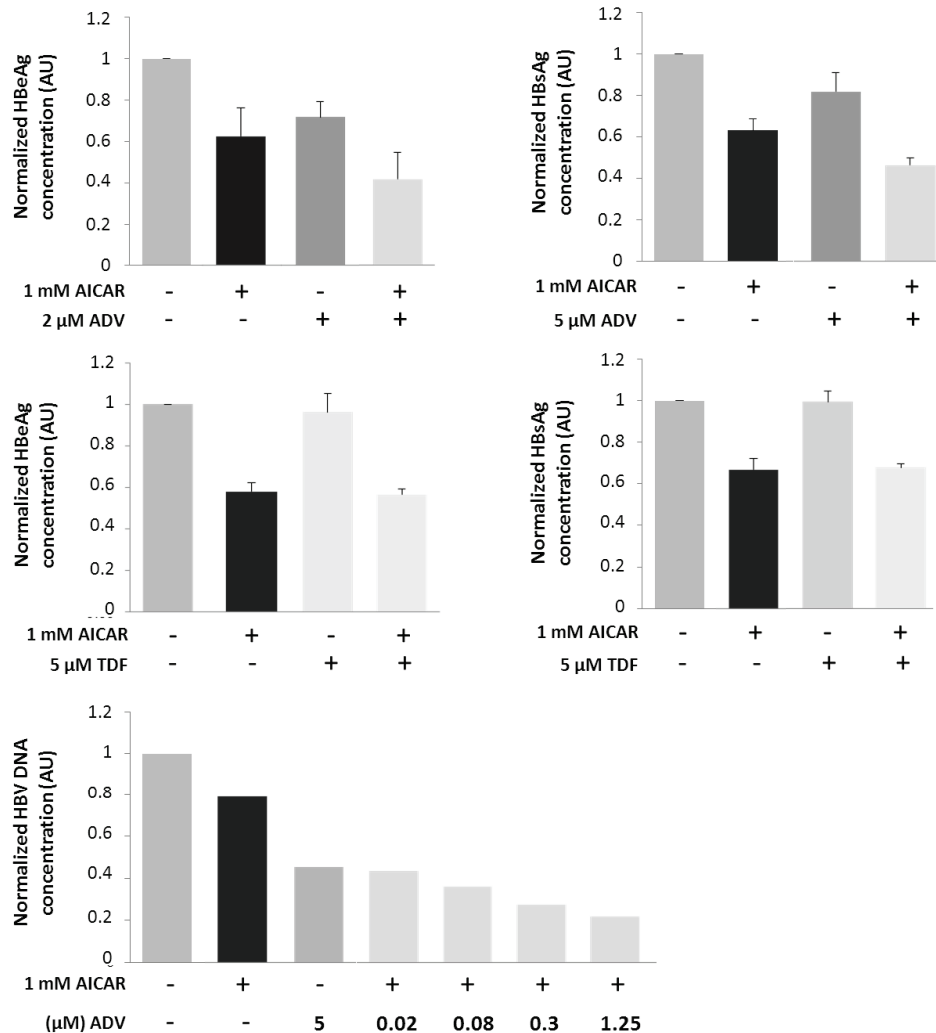


Figure 3: Content analysis of HBV-infected HepaRG cells culture medium

Cells were treated for at least 24h with either 1 mM AICAR, 2 or 5 μ M ADV, 2 or 5 μ M TDF and indicated combinations. Concentrations of antigens and rcDNA present in the medium of untreated cells were normalized to 1. Data are given as mean \pm SEM (at least duplicate experiments). Note that ADV, in contrast to TNF, has an additive effect with AICAR to inhibit HBV replication.

2.2. Effect of Adefovir and Tenofovir on AMPK activation (Grenoble)

Since AMPK is allosterically activated by low micromolar concentrations of AMP and ADP, and active AMPK seems to inhibit viral replication, we investigated whether NtRTIs could also act directly via regulation of AMPK. Since NtRTIs could have activatory or inhibitory effects on AMPK activity, we decided to use a competition setup. Here, AMPK is exposed to the pharmacological activator AICAR, and the effect of pre-incubation with the two prodrugs ADV or TDF on AMPK activation is studied. We used two different readouts: the AMPK-FRET sensor AMPKAR in living cells (Tsou et al., 2011), and immunoblotting of phosphorylated acetyl-CoA carboxylase (ACC), a reference AMPK substrate, in cell extracts.

AMPKAR is an artificial AMPK substrate that generates a FRET signal when phosphorylated. It consists of a target peptide sequence carrying the substrate motif of AMPK fused to the phospho-threonine-binding domain (FHA1), flanked with the FRET pair mseCFP_{Δ11} and cpVenus. When covalently and/or allosterically activated, AMPK phosphorylates the substrate motif within the reporter. This drives intramolecular interaction between P-Thr and FHA1, leading to close approximation of donor and acceptor fluorophores which finally yields a FRET signal. HuH7 cells were cultivated and transfected with AMPKAR using Lipofectamine 2000. Cells were then pre-treated with increasing concentrations of either ADV or TDF for 24 hours, followed by incubation with 1 mM AICAR for 45 minutes to trigger AMPK activation (Figure 4). The FRET response and thus AMPK activation in TDF pre-treated cells was the same as in cells without drug (only receiving AICAR), while with increasing ADV concentration an additive activatory effect was observed. Thus, in contrast to TNF, ADV is capable to activate AMPK on top of AICAR, suggesting an additive effect.

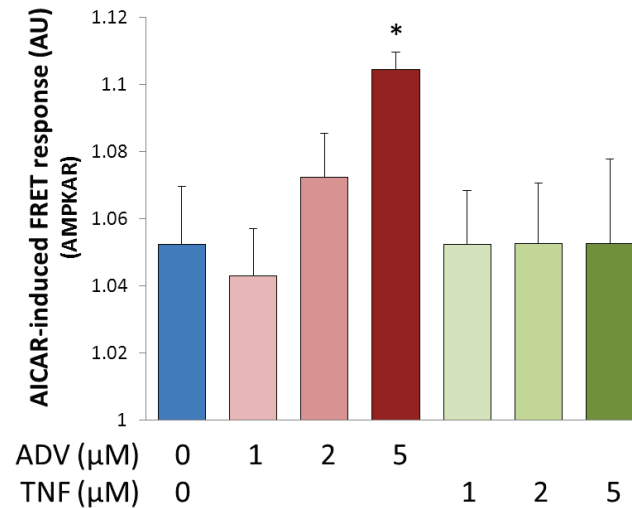


Figure 4: ADV and TDF effects on AICAR-activated AMPK activity determined by AMPKAR-FRET.

Quantification of FRET signals from pictures acquired prior to AICAR addition (blue; signal normalized to 1) and after 45 minutes of incubation with AICAR. Cells pre-incubated with 1 μM, 2 μM or 5 μM ADV (red) or TDF (green). Data are given as mean ± SEM (n=4-6). Statistics were done by T-test (*p<0,02). Note that cells exhibiting anomalous FRET ratios exceeding thresholds were not taken into account.

AMPK activation was then verified in HuH7 cell extracts by classical immunoblot detection of phosphorylated ACC (Figure 5). Cells were pre-treated with increasing concentrations of ADV and TDF for 24 hours, followed by incubation with 1 mM AICAR for 45 minutes.

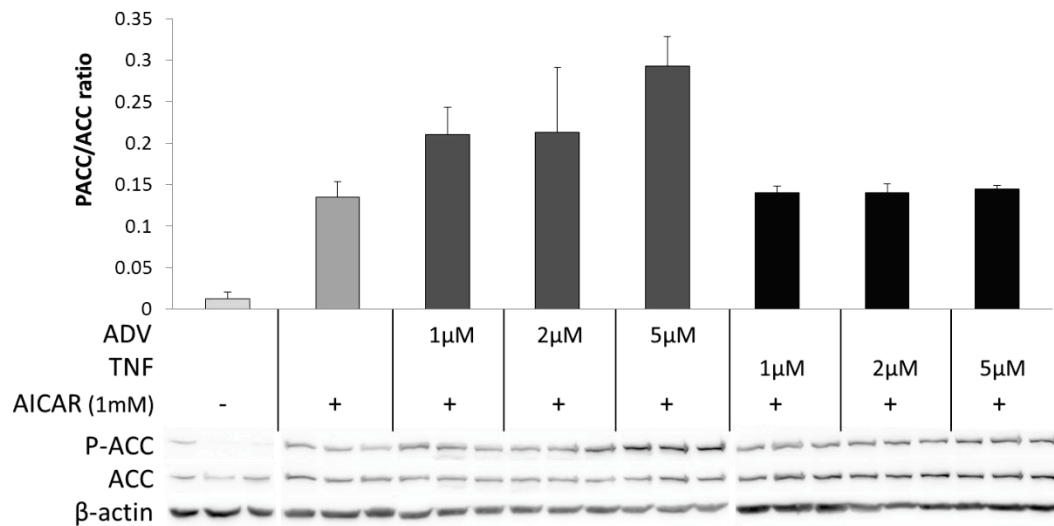


Figure 5: ADV and TDF effects on AICAR-activated AMPK determined by immunoblotting.

Immunoblots for ACC and P-ACC and corresponding quantification (bar graphs) given as the P-ACC/ACC ratio (readout for AMPK activity). Cells were pre-incubated with 1 μ M, 2 μ M or 5 μ M ADV and TDV as in Figure 2. Data are given as mean \pm SEM of 3 independent experiments.

The results entirely supported our observations with the AMPKAR-FRET sensor. ADV pre-treatment increased AMPK activity above the level obtained without drug (AICAR only), while TNF had no additive effect on AMPK activity.

The AMPK activity increase seen with ADV may have two reasons: either ADV is activating (also independent of AICAR), or ADV potentiates only the activating effect of AICAR. We therefore did a control experiment with ADV, where we included ADV treatments in absence of AICAR (Figure 6). The results showed that ADV pre-treatment itself has no apparent effect on AMPK basal activity (or even decreases it), but always potentiates activation by AICAR.

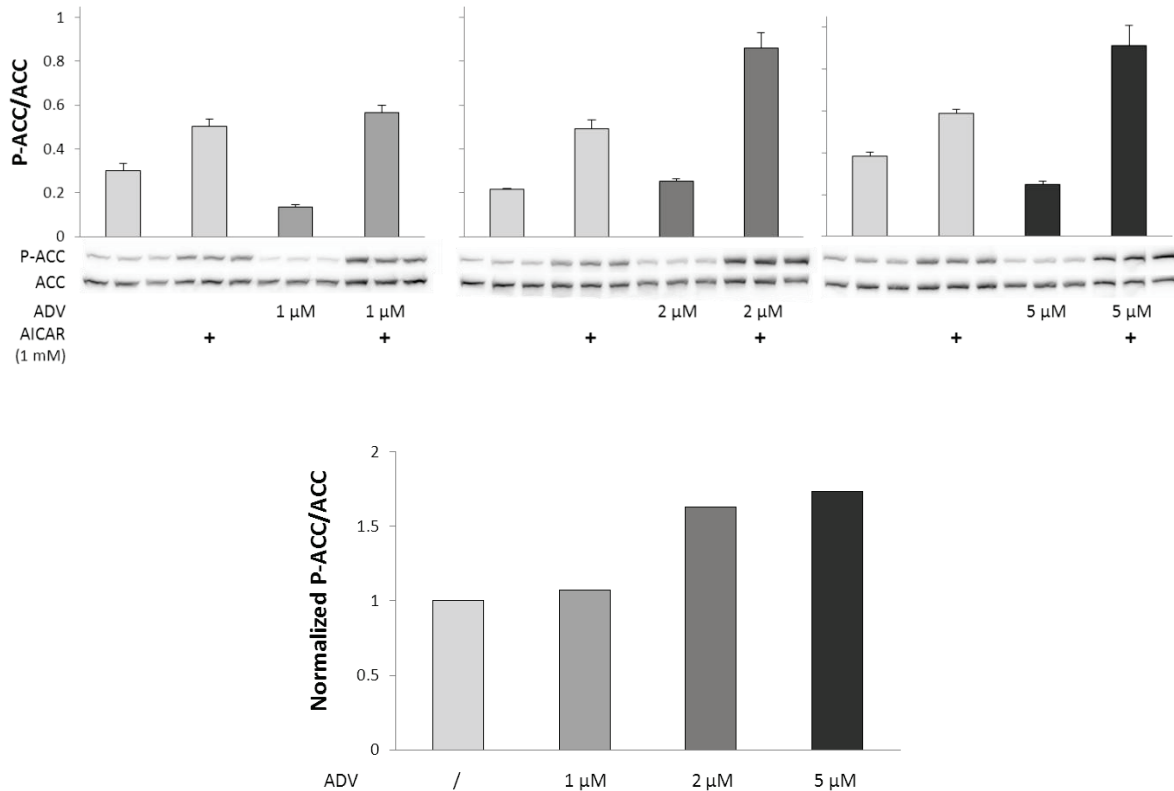


Figure 6: ADV effects on AMPK determined by immunoblotting.

Top – Immunoblots for ACC and P-ACC and corresponding quantification (bar graphs) given as the P-ACC/ACC ratio (readout for AMPK activity). Cells were pre-incubated with 1 μM, 2 μM or 5 μM ADV, followed by incubation without or with 1 mM AICAR addition for 45min (+). Data are given mean ± SEM of 3 independent experiments.

Bottom – Normalized AICAR-dependent increase of P-ACC/ACC ratio due to ADV (normalized data calculated from data in top panel).

Our study reveals that ADV and TNF have different effects on AMPK activation in HuH7 cells. Both do not activate AMPK on their own. However, ADV can potentiate the effect of an allosteric AMPK activator like AICAR. These data correlate well with our results on viral replication, where ADV but not and TNF could potentiate the inhibitory action of the AMPK activator AICAR for viral replication.

2.3. Adefovir and AMPfret (Grenoble)

Having shown that Adefovir potentiates AMPK activation by AICAR, we investigate the putative direct interaction between AMPK and Adefovir using AMPfret. We decided to incubate AMPfret with various amount of Adefovir (0 - 10 μ M) and to monitor its FRET signal. Adefovir was not shown to directly activate AMPK in cells, thus we also incubated AMPfret in presence of various amount of AMP in presence or in absence of Adefovir to examine whether it potentiates the AMP-induced FRET response. During these experiments the AMP analogous form of Adefovir was used.

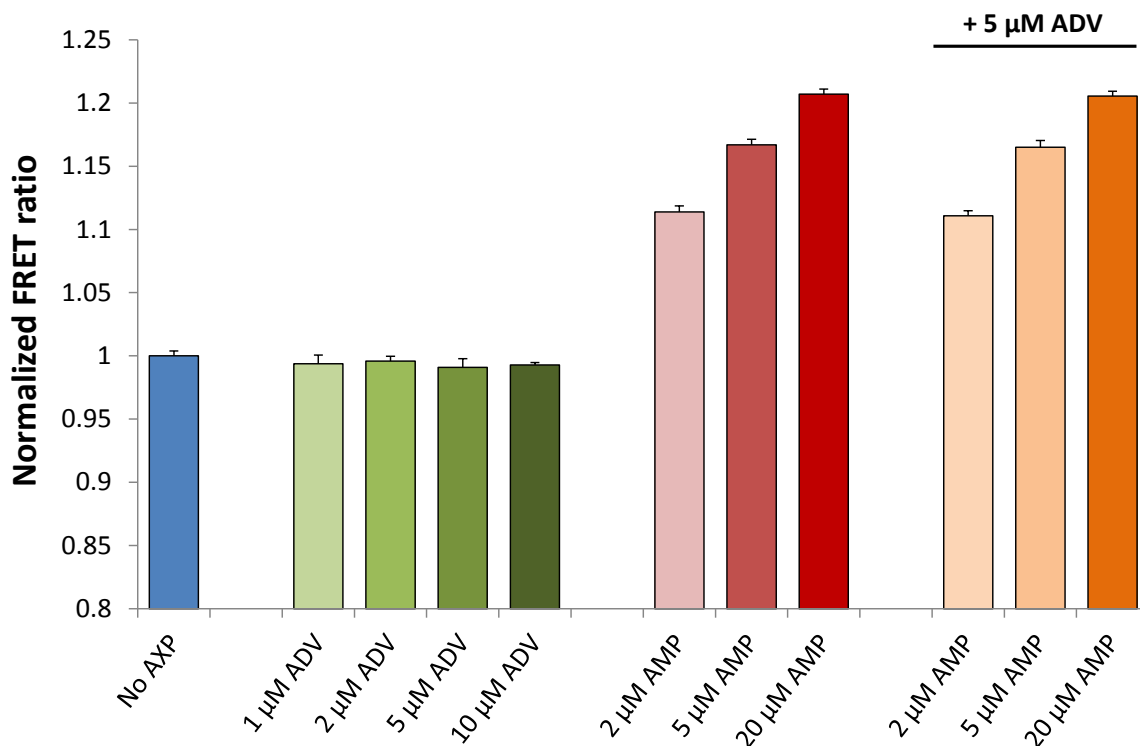


Figure 7: AMPfret does not report the direct interaction between Adefovir and AMPK.

AMPfret was incubated in absence (blue bar) or in presence of various amount of Adefovir (0 - 10 μ M) (green bars). AMPfret was also incubated with various amount of AMP (2 - 20 μ M) in absence (red bars) or in presence of 5 μ M Adefovir (orange bars). Bars correspond to mean \pm SEM, n=3.

It appears that incubation of AMPfret with Adefovir does not alter the FRET response suggesting that Adefovir is not interacting with AMPK as AMP does (Figure 7). Also, in contrast to results previously obtained with cells, our data did not show any beneficial effect of Adefovir on the AMP-induced response. The AMP-induced FRET response in presence or in absence of Adefovir is of same magnitude, thus suggesting that Adefovir does not potentiate the AMP-induced conformational changes. Despite Adefovir seems to have a non-analogous behavior face to AMPK as compared to AMP, these data do not exclude a direct interaction between Adefovir and AMPK.

3. Discussion

The study shows that ADV and AICAR both inhibit HBV replication, and that in presence of AICAR, ADV has additive effects on viral replication and potentiates AMPK activation. In contrast, TNF has no significant effect on HBV replication, and does not potentiate AICAR-dependent AMPK activation. These data suggest a dual role of ADV in inhibiting viral replication: (i) suppression of viral DNA synthesis by reverse transcriptase/polymerase, and, more indirectly, (ii) increased AMPK activation leading to reduced availability of active nuclear receptors/transcription factors like FXR, necessary for viral replication.

The presented data suggest that ADV and AICAR reduce HBV replication through a similar, AMPK-related mechanism. Lien et al. showed that the indirect AMPK activator metformin has the ability to reduce the activity of the FXR nuclear receptor by inducing its phosphorylation via AMPK. FXR is importantly expressed in the liver, where HBV propagates, and the HBV genome presents putative FXR binding sites which may control the transcription of the pregenomic DNA and HBV genome replication.

The prodrugs ADV and TNF are metabolized in the cell into Adefovir and Tenofovir, which have very similar structures, differing only by a methyl group. Their divergent therapeutic efficiency on viral replication may thus not only depend on inhibition of DNA synthesis, but may involve other nucleotide-dependent enzymes. AMPK is a very good candidate for two reasons: First, AMPK is allosterically activated by AMP, the structural analog of Adefovir. Thus, no further phosphorylation of Adefovir into the mono- and diphosphate forms as for DNA synthesis inhibition is necessary. Second, allosteric activation of AMPK occurs in the range of 1-10 μM AMP (or ZMP), so even with a probably lower affinity, Adefovir may bind to these allosteric sites in the μM range.

An unsolved puzzle, however, is the mechanism by which Adefovir increases the effect of AICAR (or its intracellular active metabolite ZMP), without directly acting as an activator. It can be envisaged that not all CBS binding sites on the γ -subunit can bind Adefovir with equal affinity. Under conditions where Adefovir would bind to CBS sites 1 and 4, but not to the crucial CBS site 3, it would only increase AMPK activity if site 3 is occupied by AMP or ZMP (the AICAR metabolization product). However, other models of Adefovir/ZMP synergy are certainly possible. The AMPKAR reporter used in the study only provides a global readout of

AMPK activity and does not allow discerning a molecular mechanism. Our data obtained using AMPfret, do not highlight a direct interaction between Adefovir and AMPK. However, despite its similar structure, it cannot be excluded that Adefovir binds AMPK in a different way than adenylates (e.g. active site, α/β interface) to potentiate its further activation by ZMP. In addition our experiments were done with the AMP-analogous form of Adefovir and it may be that in cells, the metabolized forms - phosphorylated - are more potent regarding AMPK activation.

Further experiments should be realized in order to elucidate the mechanism(s) involved. For example, it should be examined whether ADV or Adefovir directly interact with AMPK to potentiate AICAR activation, and what could be the role of PGC1 α in this model. PGC1 α is a downstream target of AMPK and it has been shown that down-regulation of this metabolic coactivator inhibits HBV (Mouler Rechtman et al., 2013). Mouler Rechtman et al. showed that curcumin triggers down-regulation of PGC1 α and reduces HBV mRNA (Mouler Rechtman et al., 2010). Interestingly, it was proposed that curcumin also activates AMPK by increasing its phosphorylation (Kim et al., 2009). Zhang et al. showed that PGC-1 α has the ability to activate the nuclear receptor FXR (Zhang et al., 2004) which may be important for HBV replication. AMPK can phosphorylate PGC1 α that in turn increases FXR activity by increasing FXR mRNA levels and by interacting with the FXR DNA-binding domain to enhance the transcription of FXR target genes (Kanaya et al., 2004). HBV replication may be regulated by a subnetwork of metabolic factors and transcription of HBV and metabolic genes may be similarly controlled and interrelated (Curtill et al., 2014).

The results presented herein, in the context of the essential role of AMPK in regulating cellular metabolism, suggest a model where AMPK is involved in regulating HBV tropism by modulating the activity of transcription factors such as PGC1 α and FXR, required for its replication. It is tempting to speculate that AMPK activators currently developed by pharmaceutical industry may have applications for treating viral infections. Certainly, the putative host-virus signaling pathway involving NtRTIs and AMPK deserves further investigation.

4. Materials and Methods

4.1. Cell culture

HuH-7 cells (130'000) were seeded in 8 well Labtek plates (1 cm² / well) and immediately transfected with the vector coding for AMPKAR using Lipofectamine 2000 following established procedures (250 ng plasmid pcDNA3.1 AMPKAR and 0,5 µL Lipofectamine 2000 per well in OptiMEM medium). Transfection was stopped after 6h by replacement of the medium by 500 µL of complete cell culture medium. To treat HuH7 cells we used prodrug forms of retrovirals: adefovir dipivoxil (ADV-DP) and tenofovir disoproxyl (TNF-DP) (respectively commercialized under name as Hepsera or Preveon and Viread). After 16 h, medium was replaced by complete medium containing 0, 1 µM, 2 µM or 5 µM ADV-DP (stock solution dissolved in 100% DMSO; corresponding amounts of DMSO were added to control cultures). Same medium replacement was done with medium containing 0, 1 µM, 2 µM or 5 µM TNF-DP. Treatment was applied for 24 hours before cells observation.

4.2. Confocal microscopy

After 24h of treatment, cells were observed with a Leica TCS SP2 AOBS confocal microscope after having been placed in an incubation chamber in which the temperature and O₂ concentration were maintained at 37 °C and 21%, respectively. Pictures were acquired using the Leica Confocal Software (LCS) using the following confocal microscope settings: excitation wavelength 458 nm, and two channel fluorescence emission set at 476 and 527 nm both presenting a 6nm width. FRET was measured through the record of fluorescence at these two peaks. Emission spectra showing FRET signal were monitored through λ scans from 463 nm to 600 nm to validate the proper transfection and expression of AMPKAR. Without moving the Labtek, 250 µL medium were replaced by the same volume of complete medium containing 2 mM AICAR (1 mM final) and appropriate amount of anti-HBV drugs. Pictures were acquired at t₀, prior AICAR addition and 45 min later (t₄₅). This was done for cells treated with 0, 1 µM, 2µM or 5µM ADV-DP or TNF-DP. Each condition was tested through at least 3 independent experiments.

4.3. Image treatment

Using ImageJ a background correction was applied to pictures acquired with the confocal microscope. Using same software, pictures were cropped in a way that each individual cell can be treated independently. CFP and YFP emitted fluorescence, acquired simultaneously through 2 channels using the microscope, were quantified using Volocity. Under Excel, the FRET ratios (emission at 527 nm / emission at 476 nm) and the resulting mean and standard error were calculated. In total, fluorescence was recorded for 149 cells. Data issued from cells exhibiting abnormal basal AMPKAR emission spectra were discarded.

4.4. Immunoblotting

4.4.1. Cell culture and treatment

Huh7 cells were grown in Petri dishes (\varnothing 35mm) containing complete medium until ~90% confluence. Cells were treated with 1 μ M, 2 μ M or 5 μ M of either ADV-DP or TNF-DF (stock solution dissolved in 100% DMSO) for 24h (corresponding amounts of DMSO were added for control). After about 24h of anti-HBV drug treatment, 1mM AICAR (final concentration) was added to the medium for 45 min. After the removal of the media, Petri dishes containing adherent Huh7 cells were immediately flash-frozen in liquid nitrogen.

4.4.2. Protein extraction

On ice, 200 μ L of buffer containing 50mM Tris pH8, 200mM NaCl and 2mM β -mercaptoethanol were added per petri dish and cells were scratched using a scraper. The 200 μ L of buffer containing the cells were transferred in Eppendorf tubes which were frozen in liquid Nitrogen. After thawing, cells were sonicated 4x5 seconds (80% power) using a sonicator equiped with a microtip. Lysates were centrifuged in a cooled table top centrifuge for 10 min and 16'000 xg at 4°C and the supernatant was kept.

4.4.3. SDS-PAGE and immunoblot

Proteins were quantified using the Bradford reagent. Sample volumes with identical protein content (60 μ g) were added to Laemmli sample buffer, heated at 90 °C for 1 min, and loaded onto 7,5% acrylamide SDS-PAGE gels. Proteins migrated for 1 hour at 180 V and were then

transferred onto a nitrocellulose membrane using the wet transfert method for 1 h 30 at 100 V. Membranes were saturated 1h at room temperature with TBS-Tween 0,1%, milk 5%, incubated overnight at 4 °C with antibodies diluted in TBS-Tween 0,1%, milk 5% (anti-acetyl-CoA carboxylase from rabbit (1:1000, Cell Signaling), anti phospho-Acetyl-CoA carboxylase from rabbit (1:1000, Cell Signaling) and anti- β -actin from rabbit (1:1000, Cell Signaling)). After three washing steps of 15 min each using TBS-Tween 0,1%, secondary antibody (donkey anti-rabbit IgG, 1:3000, GE Healthcare) conjugated with horseradish peroxidase and diluted in TBS-Tween 0,1%, milk 5% were applied to the membrane for 1 hour at room temperature. After three washing steps of 15 min each using TBS-Tween 0,1%, revelation solution was added on top of the membrane and bands were visualized using a digital imager. After having been used for P-ACC signal revelation, membranes were stripped for 20 min at 50 °C and re-used for immunoblotting against total ACC (stripping buffer: 2% SDS, 10 mM Tris pH 6,8, 50 mM β -mercaptoethanol). P-ACC, ACC and β -actin bands were quantified using ImageJ 1.46.

5. References

- Cihlar, T., Birkus, G., Greenwalt, D.E., and Hitchcock, M.J.M. (2002). Tenofovir exhibits low cytotoxicity in various human cell types: comparison with other nucleoside reverse transcriptase inhibitors. *Antiviral Res.* *54*, 37–45.
- Curtil, C., Enache, L.S., Radreau, P., Dron, A.-G., Scholtès, C., Deloïre, A., Roche, D., Lotteau, V., André, P., and Ramière, C. (2014). The metabolic sensors FXR α , PGC-1 α , and SIRT1 cooperatively regulate hepatitis B virus transcription. *FASEB J.* *28*, 1454–1463.
- Guo, H., Jiang, D., Zhou, T., Cuconati, A., Block, T.M., and Guo, J.-T. (2007). Characterization of the Intracellular Deproteinized Relaxed Circular DNA of Hepatitis B Virus: an Intermediate of Covalently Closed Circular DNA Formation. *J. Virol.* *81*, 12472–12484.
- Hantz, O., Parent, R., Durantel, D., Gripon, P., Guguen-Guillouzo, C., and Zoulim, F. (2009). Persistence of the hepatitis B virus covalently closed circular DNA in HepaRG human hepatocyte-like cells. *J. Gen. Virol.* *90*, 127–135.
- Hardie, D.G., Carling, D., and Gamblin, S.J. (2011). AMP-activated protein kinase: also regulated by ADP? *Trends Biochem Sci* *36*, 470–477.
- Jäger, S., Handschin, C., St-Pierre, J., and Spiegelman, B.M. (2007). AMP-activated protein kinase (AMPK) action in skeletal muscle via direct phosphorylation of PGC-1 α . *Proc. Natl. Acad. Sci. U. S. A.* *104*, 12017–12022.
- Kanaya, E., Shiraki, T., and Jingami, H. (2004). The nuclear bile acid receptor FXR is activated by PGC-1 α in a ligand-dependent manner. *Biochem. J.* *382*, 913–921.
- Kim, T., Davis, J., Zhang, A.J., He, X., and Mathews, S.T. (2009). Curcumin activates AMPK and suppresses gluconeogenic gene expression in hepatoma cells. *Biochem Biophys Res Commun* *388*, 377–382.
- Lien, F., Berthier, A., Bouchaert, E., Gheeraert, C., Alexandre, J., Porez, G., Prawitt, J., Dehondt, H., Ploton, M., Colin, S., et al. (2014). Metformin interferes with bile acid homeostasis through AMPK-FXR crosstalk. *J Clin Invest* *124*, 1037–1051.
- Marcellin, P., Heathcote, E.J., Buti, M., Gane, E., de Man, R.A., Krastev, Z., Germanidis, G., Lee, S.S., Flisiak, R., Kaita, K., et al. (2008). Tenofovir Disoproxil Fumarate versus Adefovir Dipivoxil for Chronic Hepatitis B. *N. Engl. J. Med.* *359*, 2442–2455.
- Mouler Rechtman, M., Har-Noy, O., Bar-Yishay, I., Fishman, S., Adamovich, Y., Shaul, Y., Halpern, Z., and Shlomai, A. (2010). Curcumin inhibits hepatitis B virus via down-regulation of the metabolic coactivator PGC-1 α . *FEBS Lett.* *584*, 2485–2490.
- Mouler Rechtman, M., Burdelova, E.O., Bar-Yishay, I., Ben-Yehoyada, M., Fishman, S., Halpern, Z., and Shlomai, A. (2013). The metabolic regulator PGC-1 α links anti-cancer cytotoxic chemotherapy to reactivation of hepatitis B virus. *J. Viral Hepat.* *20*, 34–41.
- Ramière, C., Scholtès, C., Diaz, O., Icard, V., Perrin-Cocon, L., Trabaud, M.-A., Lotteau, V., and André, P. (2008). Transactivation of the Hepatitis B Virus Core Promoter by the Nuclear Receptor FXR α . *J. Virol.* *82*, 10832–10840.
- Shlomai, A., Paran, N., and Shaul, Y. (2006). PGC-1 α controls hepatitis B virus through nutritional signals. *Proc. Natl. Acad. Sci. U. S. A.* *103*, 16003–16008.
- Tsou, P., Zheng, B., Hsu, C.-H., Sasaki, A.T., and Cantley, L.C. (2011). A Fluorescent Reporter of AMPK Activity and Cellular Energy Stress. *Cell Metab.* *13*, 476–486.
- Zhang, Y., Castellani, L.W., Sinal, C.J., Gonzalez, F.J., and Edwards, P.A. (2004). Peroxisome proliferator-activated receptor- γ coactivator 1 α (PGC-1 α) regulates triglyceride metabolism by activation of the nuclear receptor FXR. *Genes Dev.* *18*, 157–169.
- Zhao, S.-S., Tang, L.-H., Dai, X.-H., Wang, W., Zhou, R.-R., Chen, L.-Z., and Fan, X.-G. (2011). Comparison of the efficacy of tenofovir and adefovir in the treatment of chronic hepatitis B: A Systematic Review. *Virol. J.* *8*, 111.

Abstract. AMP-activated protein kinase (AMPK) is a heterotrimeric protein complex (130kDa), conserved from yeast to plants and mammals, and functions as a central signaling hub and master regulator of energy metabolism and beyond. AMPK emerged as a suitable target to develop novel drugs for various metabolic pathologies (e.g. type II diabetes). Once activated AMPK restores the energy homeostasis, among others by down-regulating ATP-demanding pathways (anabolism) and up-regulating ATP-producing ones (catabolism). *In vivo*, the AMPK activity is finely regulated by incompletely understood complex mechanisms. First, AMPK activity is systemically modulated via activating phosphorylation at the α -subunit which is increased upon AMP and ADP binding to the γ -subunit. Second, AMPK is allosterically activated by AMP binding to the γ -subunit when the ATP/AMP ratio is falling. All these mechanisms require close communication between the γ - and α subunits, but a complete consensus model for AMPK activation is still lacking. We and others have proposed an AMP-induced conformational switch within the full-length heterotrimeric AMPK complex based on different, complementary structural studies. In this work, we have exploited the conformational switch for designing and engineering an AMPK complex that allows a direct, real-time readout of the AMPK conformational state by fluorescence resonance energy transfer (FRET). A definite bottleneck is engineering and expression of such multiprotein complexes, which could be achieved by using site-specific and homologous recombination techniques within the ACEMBL technology. From an array of engineered constructs, those with AMP-sensitive FRET changes were selected and named AMPfret. The sensor can report conformational changes within the AMPK heterotrimer, independent of its phosphorylation state, that are induced by AMP or ADP binding, and the monitored FRET signal correlates with AMPK allosteric activation or protection of AMPK dephosphorylation, respectively. AMPfret responds to physiologically low, micromolar concentrations of AMP and ADP, provides final proof for the exclusive ability of ATP, but not Mg-ATP, to compete with AMP for binding to the γ -subunit, and allows novel insight into the role of CBS domains for allosteric AMPK activation. Proof of principle experiments are provided for using AMPfret as a tool for AMPK-targeted drug screening and for reporting the intracellular energy state.

Résumé. La protéine kinase activée par AMP (AMPK) est un complexe hétérotrimérique (130kDa), ubiquitaire chez les eucaryotes, fonctionnant comme un hub central de la signalisation cellulaire et un régulateur du métabolisme énergétique et au-delà. L'AMPK émerge comme étant une cible de choix pour développer de nouveaux médicaments contre de nombreuses maladies métaboliques (ex: diabète de type 2). Une fois activée, l'AMPK va restaurer l'homéostasie énergétique, notamment en diminuant le métabolisme demandeur d'ATP (anabolisme) et en stimulant le métabolisme produisant l'ATP (catabolisme). *In vivo*, l'activité de l'AMPK est finement régulée par des mécanismes complexes encore partiellement inconnus. Premièrement, l'activité de l'AMPK est modulée de manière systémique par phosphorylation de la sous unité α , elle-même augmentée par l'attachement d'AMP et d'ADP à la sous unité γ . Deuxièmement, l'AMPK est activée de manière allostérique par liaison de l'AMP à la sous unité γ lors de chutes du ratio ATP/AMP. Tous ces mécanismes requièrent une communication étroite entre les sous unités α et γ , mais un modèle consensus complet de l'activation de l'AMPK est toujours manquant. Se basant sur différentes études structurales, d'autres et nous-mêmes avons proposé un changement de conformation induit par AMP au sein de l'hétérotrimère AMPK. Lors de ce travail, nous avons exploité ces changements conformationnels pour imaginer et créer un hétérotrimère d'AMPK permettant de suivre directement et en temps réel l'état de conformation de l'AMPK par FRET. La création et la production de tels complexes multi protéiques sont de réelles difficultés, qui ont pu être réalisées par l'utilisation de la technologie ACEMBL qui exploite notamment, des techniques de recombinaisons homologues. A partir d'un éventail de constructions, celles présentant des changements de FRET induit par AMP ont été sélectionnées et renommées AMPfret. Indépendamment de son degré de phosphorylation, le senseur a la propriété de rapporter les changements de conformation de l'AMPK étant induits par l'AMP ou l'ADP et ces changements de signal FRET corrélaient respectivement avec l'activation allostérique de l'AMPK ou sa protection contre la dephosphorylation. Le senseur répond à des concentrations physiologiques en AMP et ADP (micromolaire) et a finalement démontré la capacité exclusive qu'a l'ATP, et non l'ATP-Mg, à concurrencer l'AMP. De plus, son utilisation a permis une meilleure compréhension du rôle des sites CBS lors de l'activation allostérique. Des preuves qu'AMPfret peut aussi être considéré comme un outil de choix pour le criblage de molécules ciblant l'AMPK, et pour le monitoring de l'état énergétique intracellulaire sont aussi présentées.